

**DEVELOPMENT OF PRODUCTION GUIDELINES AND
GREEN WATER USE ESTIMATION OF UNDERUTILISED
INDIGENOUS CROPS USING AVAILABLE MODELS WITHIN
SELECTED BIO-CLIMATIC REGIONS OF SOUTH AFRICA**

**Volume 2:
Climate change atlas for rainfed production
of selected underutilised crops**

Report to the
WATER RESEARCH COMMISSION

by

RP Kunz¹ and T Mabhaudhi²

¹Centre for Water Resources Research

²Centre for Transformative Agricultural and Food Systems
School of Agricultural, Earth and Environmental Sciences
University of KwaZulu-Natal, Pietermaritzburg, South Africa

WRC Report No. 2717/2/23

ISBN 978-0-6392-0273-0

April 2023



Obtainable from

Water Research Commission
Bloukrans Building, 2nd Floor
Lynnwood Bridge Office Park
4 Davenry Road
Lynnwood /manor
PRETORIA

orders@wrc.org.za or download from www.wrc.org.za

This report forms part of a series of two reports. The other report is *Developing a Guideline for Rainfed Production of Underutilised Indigenous Crops and Estimating Green Water Use of Indigenous Crops Based on Available Models Within Selected Bio-Climatic Regions of South Africa. Volume 1.* (WRC Report No 2717/1/23)

DISCLAIMER

This report has been reviewed by the Water Research Commission (WRC) and approved for publication. Approval does not signify that the contents necessarily reflect the views and policies of the WRC, nor does mention of trade names or commercial products constitute endorsement or recommendation for use.

EXECUTIVE SUMMARY

BACKGROUND AND MOTIVATION

The focus of this project (K5/2717), funded by the Water Research Commission (WRC), was guided by recommendations made in a research agenda developed by Modi and Mabhaudhi (2016). This agenda was designed to promote the production of underutilised indigenous crops, with the goal of upscaling production from subsistence to commercial scale. It highlighted 13 drought tolerant and nutrient-dense crops that should be targeted and prioritised for future research, development and innovation (Modi and Mabhaudhi, 2016).

Underutilised indigenous crops have an important role in improving agro-biodiversity in South Africa. Their suitability for low input agricultural systems and tolerance to drought and heat stress could improve the sustainability of rainfed cropping systems, especially in rural communities. Furthermore, underutilised indigenous crops are nutrient-dense and can provide essential minerals and vitamins required for healthy living. Thus, the promotion of underutilised indigenous crops under rainfed production will contribute to efforts to improve food and nutrition security in South Africa and build the resilience of rural farming communities to climate change impacts.

In order to promote the sustainable inclusion and production of underutilised indigenous crops in rainfed cropping systems, production guidelines are required by both small- and largescale farmers. Such guidelines should consider the potential impacts of climate change on crop production. Rising temperatures will substantially increase evaporative demand, translating into higher transpiration rates and increased crop yields, if water availability is not limited. Higher temperatures will enhance crop development and result in shorter crop cycles.

However, water availability mostly influences crop production, and projected changes in rainfall are less certain, with some parts of the country expected to become drier. Furthermore, elevated levels of ambient CO₂ concentration can increase the rate of photosynthetic carbon assimilation in plants and thus, stimulate plant growth. However, the magnitude of this CO₂ “fertilisation effect” remains uncertain, but is likely to be more beneficial for C3 than C4 crops. Higher CO₂ levels can also induce stomatal closure, resulting in lower transpiration, decreased crop water use, and increased crop water use efficiency. Hence, it is difficult to assess if climate change may result in higher or lower crop yields in the future.

One approach involves using mechanistic crop models to assess the integrated effects of changing rainfall combined with increased temperatures and CO₂ levels on biomass growth, water use and yield. Results from crop simulations are useful for planning agricultural interventions that include underutilised indigenous crops and contributing to efforts to broaden crop choice options for farmers. This should help increase farmers' preparedness and increase their capacity to adapt to climate change impacts by improving their resilience to climate shocks.

PROJECT OBJECTIVE AND AIMS

This project was titled “Developing a guideline for rainfed production of underutilised indigenous crops and estimating green water use of indigenous crops based on available models within selected bioclimatic regions of South Africa”, with total funding of R2 million. The 5-year project (April 2017 to March 2022) aimed to promote the rainfed production of underutilised indigenous crops in South Africa by:

1. developing production guidelines and land suitability maps for underutilised indigenous crops grown under rainfed conditions, and
2. mapping climate change impacts on yield, water use and water productivity for selected underutilised crops under rainfed growing conditions.

Based on this, the final project report was produced in two volumes, with this report representing **Volume 2** that highlights the potential impacts of climate change on four underutilised indigenous crops, viz. amaranth, bambara groundnut, sorghum and taro. These impacts were assessed using a crop water productivity model as described next.

METHODOLOGY

In this project, a crop simulation model called AquaCrop was selected and run to estimate the yield, water use efficiency and season length of the four underutilised crops under rainfed conditions. The model was run for the present period to represent historical conditions and two future periods. The reason for using AquaCrop is given next, together with a brief model description.

Crop model selection and description

AquaCrop was developed by the Food and Agricultural Organisation (FAO) of the United Nations to simulate the daily growth, productivity and water use of 16 herbaceous crops. The model was selected to meet the objective of this research project because it:

- is well suited for assessing crop response to different climate change scenarios in terms of altered soil water content, temperature regimes and elevated atmospheric CO₂ concentration (Steduto et al., 2012), and
- has been extensively used in other WRC-funded projects to estimate various crops' yield and water use across southern Africa.

AquaCrop's growth engine is water-driven and is particularly suited to simulating yield response to water availability. The model estimates biomass production via a conservative, crop-specific water productivity parameter (WP) and accumulated crop transpiration (Tr). Crop yield is calculated using the harvest index approach (i.e. the harvestable portion of biomass).

The WP parameter represents the rate of biomass production per unit of transpired water. It is normalised (as WP*) using reference evapotranspiration (ET₀) to improve the model's robustness and applicability across different climates. Adjustments are also made to WP that account for CO₂ effects on plant growth.

AquaCrop uses growing degree-days (GDD) as the thermal clock to account for the effects of temperature on phenology and crop growth. Stress coefficients (ranging from 0 to 1) account for water and temperature stress effects on plant growth. Therefore, minimum and maximum air temperatures are required as input to simulate cold and heat stress. Like most crop models, AquaCrop cannot account for the effects of pests and diseases on crop growth. In addition, it indirectly simulates the effects of fertility on crop growth.

Kunz et al. (2015b) noted that Version 4 of AquaCrop was particularly sensitive to soil moisture availability in the first plant growth stage. This issue was addressed in Version 6, which now assumes that sufficient reserves are available in the seed for leaf expansion to occur at its maximum rate just after germination. Therefore, crop yields simulated by Version 6 are typically higher than those produced by Version 4 of the model. In addition, the results from this study supersede those presented in past reports that used Version 4 (e.g. Mabhaudhi et al., 2016a; 2016b).

AquaCrop input files

As noted above, AquaCrop requires daily values of rainfall, maximum and minimum temperature, and ET_0 data as determined using the FAO56 or Penman-Monteith method (Allen et al., 1998). The model also requires the volumetric water contents (at saturation, field capacity and permanent wilting point) and depth for each soil horizon. This input data was obtained from the climate and soils databases Schulze et al. (2011) developed for each of the 5838 quinary catchments (called altitude zones in this document). Recently, the climate database was modified as described by Kunz et al. (2020). The model also requires saturated hydraulic conductivity, which was estimated from volumetric water content equations provided by Saxton and Rawls (2006).

AquaCrop was then run at the national scale of all 5838 altitude zones with 50 years of input climate data (1950-1999) to estimate crop yield, water use efficiency and season length for historical conditions. The model was also run for three 30-year periods representing present (1961-1990), near future 2015-2044), and distant future (2070-2099) conditions. These climate projections were derived from six GCMs that were dynamically downscaled and bias-corrected (against observed data) forced by two representation concentration pathways (RCPs), viz. RCP4.5 and RCP8.5. The dynamic downscaling was undertaken by the CSIR using their regional climate model (called CCAM).

A representative planting date and plant density were selected for each of the four underutilised indigenous crops. Since crop parameters were not developed in this project, they were obtained from previous studies that undertook calibration and validation of AquaCrop for specific crops. The availability of existing parameters largely determined which underutilised indigenous crops were focused on in this study.

Reducing computational expense

Owing to the computational expense of running AquaCrop multiple times with 30-50 years of daily input data, considerable effort was spent on minimising model run time. These efforts built on work originally described by Kunz et al. (2015c; 2020) and are described in detail in this report to assist others in improving model performance. This allows model users to consider additional modelling scenarios, since less time is spent waiting for model runs to complete.

Mapping of results

AquaCrop was run for all 5838 altitude zones using input climate projections for six CMIP5 GCMs that were dynamically downscaled and bias-corrected. Crop yield (Y), water use efficiency (WUE) and season length (i.e. crop cycle) were simulated for three 30-year periods, viz. present (PR; 1961-1990), near future (NF; 2015-2044) and distant future (DF; 2070-2099). The present period is deemed to accurately represent the historical period due to bias correction of GCM climate projections. The average and coefficient of variation (CV in %) were determined for each period and other useful statistics (e.g. standard deviation, range, etc.). To reduce the number of maps that can be shown, the mean seasonal values from each GCM were also averaged. This implies that equal weighting was given to each GCM. Maps highlighting the change in average value from 1) present to near future, 2) near future to distant future, and 3) present to distant future period were generated for each of the four underutilised indigenous crops, viz. amaranth, bambara groundnut, grain sorghum and taro (amadumbe). For example, the change in yield from PR to NF was expressed as 1) a percentage change $(100 \cdot (Y_{NF} - Y_{PR}) / Y_{PR})$, and 2) ratio (Y_{NF} / Y_{PR}) . For altitude zones where averaged values for the present (or near future) period are zero, the change cannot mathematically be determined. Such areas appear white on the maps and are labelled as "Undefined".

For each period, Confidence Index (CI) maps were also produced by calculating and analysing the ratio (not %) of change for each GCM (e.g. Y_{NF}/Y_{PR}). The percentage CV was then calculated from the six ratios. A low CV (< 5%) implies that the individual GCMs give similar ratios and thus, implies a very high CI. On the other hand, a high CV (> 50%) implies a large discrepancy among the ratios and hence, a very low CI. Whilst the categories are somewhat subjective; they indicate relative confidence in terms of the agreement between the six GCMs. A similar approach has been used in other studies (e.g. Schütte et al., 2021a).

RESULTS AND DISCUSSION

To better understand the impacts of climate change on agricultural response, it is important to first consider the projected changes in rainfall and temperature expected over the country and highlight the importance of bias correcting GCM projections.

Bias correction

The dynamically downscaled climate projections from six GCMs were bias-corrected against observed (i.e. historical) data. A comparison of observed mean annual precipitation and temperature data with projected (average of six GCMs) values for the present period (1961-1990) showed strong correlations. Surprisingly, the correlation was stronger for bias correction of rainfall using a multiplicative correction factor when compared to bias correction of temperature involving an additive factor. These results highlight the success of the bias correction method and show that the present period can be used to represent historical conditions.

Climate change projections

In general, greater confidence (lower uncertainty) is associated with temperature projections than future rainfall scenarios. The highest increases in future temperatures are expected in the northern parts of the country near the Botswana border, with maximum temperatures increasing more than minimum values. Projected increases in maximum temperatures exceed 6°C, which will result in a substantial increase in evaporative demand. However, this will not translate into higher transpiration rates and increased crop yields simply because rainfall in the northern regions of the North West and Limpopo provinces is limiting, which is expected to worsen into the future due to decreasing projected rainfall.

Rainfall in the Western and Northern Cape provinces is projected to decrease by 30% or more in the distant future, particularly along the border with Namibia and Botswana. In contrast, a 20% increase in rainfall is expected in the central interior region, especially to the west and south-west of Lesotho. Furthermore, current predictions also suggest that South Africa may experience decreasing rainfall in some areas and increased rainfall variability and frequency of extremes such as drought and floods. This could have a negative impact on current crop production areas.

Issues with RCP4.5

The climate change projections used in this study were derived as part of another WRC-funded project (K5/2833; Schütte et al., 2021a), which found that the rainfall maps produced for RCP4.5 were inconsistent with those produced in previous studies. It was concluded that the CSIR supplied the incorrect RCP4.5 dataset to project K5/2833. There was insufficient time and resources needed to correct this error, and thus, climate projections representing RCP8.5 were only used to assess the impact of climate change on crop response. Since RCP8.5 represents the “business as usual” scenario, it is important to note that the results obtained in this study do not span all possible future outcomes.

Climate change and crop yield

Results for the potential impact of climate change on crop yield showed the following general trends:

- For amaranth, yields in most areas north of the Free State and KZN borders are expected to decline by up to 30% in the near future, whilst a 10% yield increase may occur for most other areas.
- Yield declines exceeding 50% for bambara groundnut may be expected across most Limpopo and eastern Mpumalanga and the north-eastern parts of KwaZulu-Natal and North West provinces.
- Sorghum yields are expected to decline for most growing areas along the country's eastern seaboard, with the highest yield losses (> 50%) predicted for the Limpopo and eastern Mpumalanga provinces.
- In contrast, taro yields should improve for most areas in Limpopo, North West and KwaZulu-Natal (except in the north-east and along the coast) provinces.
- The CO₂ fertilisation effect may offset the negative impacts of climate change on crop production in southern Africa.
- The Limpopo province appears to be least favourable for crop production in the near future, except for taro production.

Expansion of cropping areas

The present to distant future maps do not show the potential expansion in crop growing areas that may result from climate change. Furthermore, based on the low confidence (i.e. high uncertainty) associated with climate projections towards the end of the 21st century, the present to distant maps should not be used for decision-making purposes. Therefore, the CV of yield maps for present and near-future conditions were compared to assess the likely expansion in crop growing areas, which showed the following general trends:

- Since the model simulated averaged non-zero yields for amaranth across all altitude zones, it was not possible to assess an expansion in growing areas.
- For bambara groundnut, the expansion in growing areas occurs mainly in western Mpumalanga, southern Free State and in the Eastern Cape (northern regions).
- No noticeable expansion in suitable growing areas for sorghum was simulated by the model from present to near future.
- Taro exhibits a large expansion in areas deemed suitable for growth in the central interior. This is mainly due to a substantial reduction in areas deemed too cold to grow the crop in the present period.
- Expansion of crop production from present to near future is most likely to occur in the Mpumalanga province.

Climate change and WUE

Relative to the present climate, amaranth's WUE is expected to increase in both the near future and distant future. For the other three crops, changes in WUE mimicked the expected changes in yield, i.e. both increases and decreases for bambara groundnut, mostly decreases for sorghum and mainly increases for taro.

Climate change and season length

A warmer future climate will result in accelerated accumulation of heat units (i.e. growing degree-days), thus shortening the time to reach physiological maturity (i.e. shorter growing season). Adaptation

strategies include shifting to earlier planting dates and growing early-maturing cultivars with shorter season lengths. Crop season length is expected to shorten from the present to the near future, except in some altitude zones for bambara groundnut and taro. Towards the distant future, taro may experience the largest reduction (> 30%) in season length across most areas, compared to a 10-30% reduction for the other three crops.

Confidence index

The variability in simulations between the six GCMs is lowest (i.e. highest confidence) for season length, since it is mostly affected by temperature only. In contrast, confidence is lowest for crop yield and WUE (i.e. higher CVs), since these variables are mostly affected by rainfall. As noted earlier, greater confidence (lower uncertainty) is associated with temperature projections than future rainfall scenarios.

CONCLUSIONS AND RECOMMENDATIONS

Limitations of study

Maps based on distant future projections should not be used for decision-making purposes due to the low confidence in rainfall and temperature projections towards the end of the 21st century. Furthermore, results presented in this study must be interpreted on the understanding that no GCM provides “perfect” future climate scenarios. Furthermore, the results do not span all possible future outcomes due to the following:

- Results were based on RCP8.5 climate projections only, as RCP4.5 scenarios were not used.
- Six GCMs cannot fully represent the entire CMIP5 ensemble of over 70 GCMs.
- The CMIP6 ensemble of GCMs project slightly drier conditions in the central part of the country, which none of the CMIP5 GCMs used in this study show.
- The CO₂ fertilisation effect may offset the negative impacts of climate change on crop production. However, crop response to elevated CO₂ is not well-understood.
- Soil fertility was assumed nonlimiting to growth, and the impact of weed growth was not considered.
- AquaCrop cannot account for pest and disease incidence, which is expected to increase due to rising temperatures in the future, thus causing yield declines.

Future research recommendations

The approach developed and implemented in this study is by no means considered “exhaustive”. Therefore, this study should be repeated in the near future to include the following recommendations, to show a wider range of possible future outcomes:

- at least two planting dates per crop,
- two plant densities representing both commercial and smallholder farming environments,
- climate projections for the RCP4.5 mitigation scenario, and
- more than six representative GCMs from the CMIP6 ensemble.

Due to the uncertainty of crop response to elevated CO₂, climate change impact assessments should be conducted with and without the CO₂ fertilisation effect. In addition, AquaCrop’s sensitivity to the f_{SINK} parameter should be determined to justify additional research to obtain representative values for each crop.

In April 2020, the WRC funded a project to update the altitude zone climate database, which involves extending the daily record by an additional 20 years. In addition, the spatial accuracy of the soils data

assigned to each altitude zone was recently improved. AquaCrop should be re-run with these latest input datasets to improve the accuracy and reliability of the simulated output.

These recommendations will certainly increase computational expense, and thus, additional effort is required to further improve AquaCrop's performance. It is suggested that the model is re-coded in the FORTRAN programming language to facilitate the development of a multi-threaded version, which should further improve performance.

The size and scale of the maps presented in this report limit their usefulness and applicability. Therefore, it is recommended that the output files be disseminated to end users via an online data portal (e.g. Water Research Observatory). This will allow end-users to generate additional maps not presented in this study that better suit their specific needs.

ACKNOWLEDGEMENTS

The research reported here formed part of an unsolicited project initiated, funded and managed by the Water Research Commission (WRC) in Key Strategic Area 4 (Water Utilisation in Agriculture). The project team is sincerely grateful to the WRC for funding and managing the project. The project team also wishes to sincerely thank the following members of the Reference Group for their valuable contributions and guidance:

Prof. S Mpandeli	Water Research Commission (Chairman)
Dr L Nhamo	Water Research Commission
Dr S Hlophe-Ginindza	Water Research Commission
Prof. W van Averbek	Tshwane University of Technology
Prof. K Ayisi	University of Limpopo
Dr G Ceronio	University of Free State
Dr C Mutengwa	University of Fort Hare
Dr K Tshikolomo	Department of Agriculture
Prof. S Walker	Agricultural Research Council

We would also like to thank the following individuals:

- Dr Sege Kiala (CTAFS) for creating all the maps presented in this document.
- Drs C Masemola, M Sibanda and VGP Chimonyo for supporting the development of maps.
- Dr David Clark (CWRR, UKZN) for his valuable contribution towards 1) converting the CSIR's downscaled climate projections from NetCDF to ASCII format, and 2) bias correcting the rainfall and temperature scenarios.
- Dr Piotr Wolski (CSAG, UCT) for checking the CSIR climate scenarios against other CMIP5 GCMs.

TABLE OF CONTENTS

EXECUTIVE SUMMARY	III
ACKNOWLEDGEMENTS	X
TABLE OF CONTENTS	XI
LIST OF FIGURES	XIII
LIST OF TABLES	XVI
LIST OF ABBREVIATIONS	XVII
LIST OF SYMBOLS	XIX
REPOSITORY OF DATA	XX
1 INTRODUCTION	1
1.1 Background and rationale	1
1.2 Project aim and objectives	2
1.3 Scope of the report	2
1.4 Structure of report	3
2 METHODOLOGY	5
2.1 AquaCrop model	5
2.1.1 Model overview	5
2.1.2 Crop response to stress	7
2.1.3 Crop response to elevated CO ₂	8
2.2 AquaCrop model improvements	9
2.2.1 Simulations in dry environments	10
2.2.2 Water thresholds for stomatal closure	10
2.3 AquaCrop input files	10
2.3.1 Planting date and plant density	10
2.3.2 Soils data	11
2.3.3 Observed climate	11
2.3.4 Future climate projections	14
2.3.5 Extraction of CSIR climate projections	18
2.3.6 Bias correction to station level	19
2.3.7 Generation of climate files	23
2.3.8 Issues with RCP4.5	24
2.4 Crop parameter files	27
2.4.1 Amaranth	28
2.4.2 Bambara groundnut	29
2.4.3 Sorghum	30
2.4.4 Taro	31
2.5 Minimising computational expense	31
2.5.1 Background	31
2.5.2 Desktop PC vs laptop	32
2.5.3 Derivation of smaller tasks	32
2.5.4 Grouping of tasks	32
2.5.5 Load balancing	32
2.5.6 Ram drive size	33
2.5.7 Automation procedure	33
2.5.8 Model run time	34
2.6 Mapping of results	34
2.6.1 Change maps	34
2.6.2 Confidence maps	35
3 RESULTS AND DISCUSSION	37
3.1 Bias correction	37
3.2 Climate change projections	38

	3.2.1	Rainfall	38
	3.2.2	Temperature.....	39
3.3		Climate change and crop yield.....	40
	3.3.1	Present to near future	40
	3.3.2	Near to distant future	43
	3.3.3	Present to distant future.....	46
	3.3.4	Confidence index	49
3.4		Expansion of cropping areas	54
3.5		Climate change and WUE.....	55
	3.5.1	Present to near future	55
	3.5.2	Near to distant future	57
	3.5.3	Present to distant future.....	59
	3.5.4	Confidence index	63
3.6		Climate change and season length.....	67
	3.6.1	Present to near future	68
	3.6.2	Near to distant future	70
	3.6.3	Present to distant future.....	72
	3.6.4	Confidence index	75
4		SUMMARY, CONCLUSIONS AND RECOMMENDATIONS	80
	4.1	Summary of approach.....	80
	4.2	Summary of main findings	80
	4.3	Limitations of study	82
	4.3.1	Distant future projections	82
	4.3.2	Rejection of RCP4.5 scenarios	82
	4.3.3	CMIP5 six-member GCM ensemble	82
	4.3.4	CMIP5 vs CMIP6 GCM projections.....	83
	4.3.5	CO ₂ fertilisation effect	83
	4.3.6	Biotic and abiotic stresses	83
	4.4	Recommendations and future research.....	84
5		REFERENCES	86
6		APPENDIX_A: DATA STORAGE	93
	6.1	Data storage.....	93
	6.1.1	AquaCrop input files.....	93
	6.1.2	AquaCrop output files	93
7		APPENDIX_B: PROJECTED CHANGES IN CLIMATE FOR RCP8.5	96
8		APPENDIX_C: CHANGES IN RAINFALL FROM PRE- TO POST-2005	98
9		APPENDIX_D1: MAPS OF CHANGE IN YIELD EXPRESSED AS A RATIO	100
10		APPENDIX_D2: MAPS OF CHANGE IN WUE EXPRESSED AS A RATIO	106
11		APPENDIX_D3: MAPS OF CHANGE IN SEASON LENGTH EXPRESSED AS A RATIO	112
12		APPENDIX_E1: VARIATION IN DISTANT FUTURE YIELD BETWEEN THE GCMS	118
13		APPENDIX_E2: VARIATION IN DISTANT FUTURE WUE BETWEEN THE GCMS	120
14		APPENDIX_E3: VARIATION IN DISTANT FUTURE SEASON LENGTH BETWEEN THE GCMS.....	122
15		APPENDIX_F: CMIP6-BASED CLIMATE PROJECTIONS	124

LIST OF FIGURES

Figure 2.1	The structural components of AquaCrop, including stress responses and the functional linkages among them (Steduto et al., 2012).....	6
Figure 2.2	Atmospheric CO ₂ concentration measured at Mauna Loa in Hawaii from 1950 to 2020, together with projected values from 2020 to 2100 as per RCP8.5.....	9
Figure 2.3	Projected CO ₂ emissions per decade for each Representative Concentration Pathway or RCP (IPCC, 2014).....	15
Figure 2.4	Global average surface temperature increases from 2006 to 2100, relative to 1986-2005, as determined from the mean of multi-model simulations for RCP2.6 (blue line) and RCP8.5 (red line), including the range (shading) as a measure of uncertainty (IPCC, 2014).....	16
Figure 2.5	Example of a portion of a .CSV file containing data extracted for a representative GCM grid point (Wolski et al., 2021).....	19
Figure 2.6	Example of a portion of a .CSV file containing observed rainfall, raw GCM rainfall and bias corrected GCM rainfall (Wolski et al., 2021).....	20
Figure 2.7	Comparison of daily rainfall distribution (raw and bias corrected) for the calibration period (1961-1999) obtained from ACCESS1-0 GCM (RCP8.5) compared to observed rainfall for rain gauge 0002069W (Wolski et al., 2021).....	21
Figure 2.8	Comparison of daily temperature (maximum and minimum) distributions for the calibration period (1961-1999) obtained from ACCESS1-0 GCM (RCP8.5) compared to observed values for station 0002069W (Wolski et al., 2021).....	22
Figure 2.9	Comparison of annual mean temperatures (raw and bias corrected) for the calibration period (1961-1999) obtained from ACCESS1-0 GCM (RCP8.5) as compared to observed values for station 0002069W (after Wolski et al., 2021).....	23
Figure 2.10	Designated Water Management Areas of South Africa.....	25
Figure 2.11	Comparison of annual rainfall totals derived for six CCAM-CRU datasets (RCP8.5) against the 21-member CMIP5 envelope and spatially averaged across each WMA (Wolski et al., 2021).....	25
Figure 2.12	Comparison of annual rainfall totals derived for six CCAM-CRU datasets (RCP4.5) against the 21-member CMIP envelope and spatially averaged across each WMA.....	26
Figure 2.13	(a) Mean daily rainfall and (b) number of rain days calculated on days with rainfall above 1 mm for station 0512481 W using the CCS derived projections for RCP4.5 (blue) compared to RCP8.5 (orange).....	26
Figure 2.14	The ratio of UKZN- to CSIR-bias corrected total annual rainfalls for a selected location (0512481W) and GCM (CCS).....	27
Figure 3.1	A comparison of mean annual precipitation derived from historical (i.e. observed) data (left) and that averaged from six dynamically downscaled and bias corrected GCMs (right) for the present period 1961-1990, together with a correlation between the two datasets (bottom) (Schütte et al., 2021b).....	37
Figure 3.2	A comparison of annual means of daily maximum temperature derived from historical (i.e. observed) data (left) and that averaged from six dynamically downscaled and bias corrected GCMs (right) for the present period 1961-1990, together with a correlation between the two datasets (bottom) (Schütte et al., 2021b).....	38
Figure 3.3	A comparison of annual means of daily minimum temperature derived from historical (i.e. observed) data (left) and that averaged from six dynamically downscaled and bias corrected GCMs (right) for the present period 1961-1990, together with a correlation (Schütte et al., 2021b).....	38
Figure 3.4	Averaged change in projected mean annual precipitation in absolute (mm on left) and relative (% on right) terms from present to near future (top row), present to distant future (middle row) and near to distant future (bottom row) (Schütte et al., 2021b).....	39

Figure 3.5	Averaged change in projected annual means of daily maximum (left) and minimum (right) temperatures (°C) from present to near future (top row), present to distant future (middle row) and near to distant future (bottom row) (Schütte et al., 2021b).....	40
Figure 3.6	Change in mean dry yield (as %) from present to near future for (a) amaranth, (b) bambara groundnut, (c) sorghum and (d) taro	43
Figure 3.7	Change in mean dry yield (as %) from near to distant future for (a) amaranth, (b) bambara groundnut, (c) sorghum, and (d) taro	46
Figure 3.8	Change in mean dry yield (as %) from present to distant future for (a) amaranth, (b) bambara groundnut, (c) sorghum, and (d) taro	49
Figure 3.9	Coefficient of variation (CV in %) in mean yield for amaranth obtained from the six GCMs for the (a) present and (b) near future periods	51
Figure 3.10	Coefficient of variation (CV in %) in mean yield for bambara groundnut obtained from the six GCMs for the (a) present and (b) near future periods	52
Figure 3.11	Coefficient of variation (CV in %) in mean yield for sorghum obtained from the six GCMs for the (a) present and (b) near future periods	53
Figure 3.12	Coefficient of variation (CV in %) in mean yield for taro obtained from the six GCMs for the (a) present and (b) near future periods	54
Figure 3.13	Change in mean water use efficiency (WUE; as %) from present to near future for (a) amaranth, (b) bambara groundnut, (c) sorghum and (d) taro	57
Figure 3.14	Change in mean water use efficiency (WUE; as %) from near to distant future for (a) amaranth, (b) bambara groundnut, (c) sorghum, and (d) taro	59
Figure 3.15	Change in mean water use efficiency (WUE; as %) from present to distant future for (a) amaranth, (b) bambara groundnut, (c) sorghum, and (d) taro	62
Figure 3.16	Responses (o average; – range) of (a) crop yield and (b) evapotranspiration (ETP) to elevated CO ₂ (550 ppm) for optimal (ample water) and water stressed (low water) conditions (after Kimball, 2016).....	63
Figure 3.17	Coefficient of variation (CV in %) in mean water use efficiency for amaranth obtained from the six GCMs for the (a) present and (b) near future periods	64
Figure 3.18	Coefficient of variation (CV in %) in mean water use efficiency for bambara groundnut obtained from the six GCMs for the (a) present and (b) near future periods	65
Figure 3.19	Coefficient of variation (CV in %) in mean water use efficiency for sorghum obtained from the six GCMs for the (a) present and (b) near future periods	66
Figure 3.20	Coefficient of variation (CV in %) in mean water use efficiency for taro obtained from the six GCMs for the (a) present and (b) near future periods	67
Figure 3.21	Change in mean season length (as %) from present to near future for (a) amaranth, (b) bambara groundnut, (c) sorghum and (d) taro	70
Figure 3.22	Change in mean season length (as %) from near to distant future for (a) amaranth, (b) bambara groundnut, (c) sorghum, and (d) taro	72
Figure 3.23	Change in mean season length (as %) from present to distant future for (a) amaranth, (b) bambara groundnut, (c) sorghum, and (d) taro	74
Figure 3.24	Coefficient of variation (CV in %) in mean season length for amaranth obtained from the six GCMs for the (a) present and (b) near future periods	76
Figure 3.25	Coefficient of variation (CV in %) in mean season length for bambara groundnut obtained from the six GCMs for the (a) present and (b) near future periods	77
Figure 3.26	Coefficient of variation (CV in %) in mean season length for sorghum obtained from the six GCMs for the (a) present and (b) near future periods.....	78
Figure 3.27	Coefficient of variation (CV in %) in mean season length for taro obtained from the six GCMs for the (a) present and (b) near future periods.....	79
Figure 4.1	Rainfall signal for past, present and future conditions obtained from different generations of GCMs (CMIP5 vs CMIP6) for the Western Cape province	83

Figure 7.1	Projected changes in annual average temperatures (°C) over southern Africa for the time period 2080-2099 relative to 1971-2000 under RCP8.5, based on CCAM (50 km resolution) downscaling of six GCMs (Archer et al., 2018)	96
Figure 7.2	Projected changes in annual average rainfall (10*m m day ⁻¹) over southern Africa for the time period 2080-2099 relative to 1971-2000 under RCP8.5, based on CCAM (50 km resolution) downscaling of six GCMs (Archer et al., 2018)	97
Figure 8.1	Ratio of mean daily rainfall per year in the post-2005 period (2005-2099) to the pre-2005 period (1961-2004)	98
Figure 8.2	Ratio of mean rain days per year in the post-2005 period (2005-2099) to the pre-2005 period (1961-2004)	99
Figure 9.1	Change in mean dry yield (as ratio) from present to near future for (a) amaranth, (b) bambara groundnut, (c) sorghum, and (d) taro	101
Figure 9.2	Change in mean dry yield (as ratio) from near to distant future for (a) amaranth, (b) bambara groundnut, (c) sorghum, and (d) taro	103
Figure 9.3	Change in mean dry yield (as ratio) from present to distant future for (a) amaranth, (b) bambara groundnut, (c) sorghum, and (d) taro	105
Figure 10.1	Change in mean water use efficiency (WUE; as ratio) from present to near future for (a) amaranth, (b) bambara groundnut, (c) sorghum, and (d) taro	107
Figure 10.2	Change in mean water use efficiency (WUE; as ratio) from near to distant future for (a) amaranth, (b) bambara groundnut, (c) sorghum, and (d) taro	109
Figure 10.3	Change in mean water use efficiency (WUE; as ratio) from present to distant future for (a) amaranth, (b) bambara groundnut, (c) sorghum, and (d) taro	111
Figure 11.1	Change in mean season length (as ratio) from present to near future for (a) amaranth, (b) bambara groundnut, (c) sorghum, and (d) taro	113
Figure 11.2	Change in mean season length (as ratio) from near to distant future for (a) amaranth, (b) bambara groundnut, (c) sorghum, and (d) taro	115
Figure 11.3	Change in mean season length (as ratio) from present to distant future for (a) amaranth, (b) bambara groundnut, (c) sorghum, and (d) taro.....	117
Figure 12.1	Coefficient of variation (CV in %) in distant future yield obtained from the six GCMs for (a) amaranth, (b) bambara groundnut, (c) sorghum, and (d) taro	119
Figure 13.1	Coefficient of variation (CV in %) in distant future water use efficiency (WUE) obtained from the six GCMs for (a) amaranth, (b) bambara groundnut, (c) sorghum, and (d) taro	121
Figure 14.1	Coefficient of variation (CV in %) in distant future season length obtained from the six GCMs for (a) amaranth, (b) bambara groundnut, (c) sorghum, and (d) taro	123
Figure 15.1	Projected changes in annual maximum (TXx) and minimum (TNn) temperatures, total annual precipitation and maximum daily precipitation (Rx1day) at 1.5, 2 and 4°C of global warming compared to 1851-1900, based on CMIP6 multi-model ensemble means	124

LIST OF TABLES

Table 2.1	Adjustment coefficient (f_{CO_2}) applied to the normalised water productivity value within the AquaCrop model for RCP8.5 emission scenario.....	9
Table 2.2	Planting date selected for each underutilised indigenous crop modelled in this study	10
Table 2.3	Custodian of rain gauges selected for each quaternary catchment (Kunz et al., 2020) ..	12
Table 2.4	Adjustments made to extreme rainfall values that existed in the quaternary catchments rainfall database (Kunz et al., 2020).....	13
Table 2.5	Histogram of altitude difference from each rain gauge to the selected (best) temperature station (Kunz et al., 2020).....	14
Table 2.6	The RCP scenarios adopted by the IPCC (Moss et al., 2010).....	15
Table 2.7	Details of the six GCMs selected for this study (Wolski et al., 2021)	16
Table 2.8	Largest daily rainfall value (uncorrected and corrected) obtained in each selected period for each GCM (RCP8.5)	21
Table 2.9	Summary of number of files read and written in generating ACRU and AquaCrop climate input files.....	24
Table 2.10	Source of existing crop parameter files for underutilised indigenous crops.....	28
Table 2.11	Load balancing of 5838 altitude zones, allowing 18 concurrent runs of AquaCrop to finish at the same time	33
Table 2.12	File size of input and output files required to run AquaCrop for the historical (baseline) and future climates	33
Table 2.13	Average (ave), standard deviation (std. dev.) and coefficient of variation (CV) calculated from ratios of near future to present mean annual precipitation (MAP) from six GCMs for altitude zone 1, i.e. quinary catchment A10A1 (Schütte et al., 2021b)	35
Table 2.14	Confidence index derived from the coefficient of variation (Schütte et al., 2021b)	35
Table 3.1	Percentage change in biomass (B), yield (Y), water use (ET) and water use efficiency (WUE) for bambara groundnut, relative to the past (1961-1990) period (after Mabhaudhi et al., 2018).....	62

LIST OF ABBREVIATIONS

ACC	Australian Community Climate and Earth System Simulator
ACRU	Agricultural Catchments Research Unit
APSIM	Agricultural Production Systems sIMulator
AR	Assessment Report
ARC	Agricultural Research Council
AVX	Advanced Vector Extensions
AZ	Altitude Zone
BIN	Binary
CABLE	CSIRO Atmosphere Biosphere Land Exchange model
CCAM	Conformal-Cubic Atmospheric Model
CCS	Community Climate System Model
CDF	Cumulative Density Function
CHPC	High-Performance Computing
CI	Confidence Index
CMIP	Climate Model Inter-comparison Project
CNR	National Centre for Meteorological Research Coupled GCM
CORDEX	Coordinated Regional Climate Downscaling Experiment
CPU	Central Processing Unit
CRU	Climate Research Unit
CSAG	Climate System Analysis Group
CSIR	Council for Scientific and Industrial Research
CSIRO	Commonwealth Scientific and Industrial Research Organisation
CSV	Comma Separated Value
CTAFS	Centre for Transformative Agricultural and Food Systems
CV	Coefficient of Variation
CWP	Crop Water Productivity
CWRR	Centre for Water Resources Research
DAFF	Department of Agriculture, Forestry and Fisheries (now DALRRD)
DALRRD	Department of Agriculture, Land Reform and Rural Development (former DAFF)
DARD	Department of Agriculture and Rural Development (now DALRRD)
DALT	Altitude difference between rainfall and temperature station
DF	Distant Future
DHSWS	Department of Human Settlements, Water and Sanitation (former DWS)
DPP	Directorate Plant Production
DSSAT	Decision Support System for Agrotechnology Transfer
DWS	Department of Water and Sanitation (now DHSWS)
ENSO	El Niño-Southern Oscillation
ET	Evapotranspiration
FACE	Free Air CO ₂ Enrichment
FAO	Food and Agricultural Organisation of the United Nations
FAO56	Food and Agriculture Organisation, Paper No. 56
GCM	Global Climate Model
GDD	Growing Degree-Day
GFD	Geophysical Fluid Dynamics Laboratory Coupled Model
GIS	Geographic Information System
HI	Harvest Index
IPCC	Intergovernmental Panel on Climate Change
KZN	KwaZulu-Natal
MAP	Mean Annual Precipitation
MAPE	Mean Absolute Percentage Error

ME	Model Efficiency
MPI	Max Planck Institute Coupled Earth System Model
NetCDF	Network Common Data Form
NF	Near Future
NOR	Norwegian Earth System Model
NWP	Nutritional Water Productivity
PC	Personal Computer
ppm	Parts Per Million
PR	PResent
QC	Quaternary Catchment
QDM	Quantile Delta Mapping
QnC	Quinary Catchment
QnCDB	Quinary Catchment Climate DataBase
QM	Quantile Mapping
RAM	Random Access Memory
RCM	Regional Climate Model
RCP	Representative Concentration Pathway
RMSE	Root Mean Square Error
RSR	RMSE Standard deviation Ratio
SASA	South African Sugar Association
SAWS	South African Weather Service
SIMD	Single Instruction, Multiple Data
SOM	Self Organising Map
SSE	Streaming SIMD Extensions
SST	Sea Surface Temperature
UCT	University of Cape Town
UKZN	University of KwaZulu-Natal
UWIN	Unix for WINdows
WMA	Water Management Area
WRO	Water Research Observatory
WP	Water Productivity
WRC	Water Research Commission
WSL	Windows Subsystem for Linux
WUE	Water Use Efficiency

LIST OF SYMBOLS

B	Accumulated biomass (g m^{-2})
CN	Curve number(integer)
CO ₂	Atmospheric carbon dioxide concentration (ppm)
CV	Coefficient of variation (%)
d	Willmott's d Index
DALT	Altitude difference between rainfall and temperature station (m)
E	Soil water evaporation (mm)
ET _O	Reference crop evaporation (mm)
f _{CO2}	CO ₂ factor for atmospheric CO ₂ normalisation (fraction)
f _{WPS}	WP* adjustment factor (fraction)
f _{SINK}	Crop sink strength coefficient (fraction)
f _{TYPE}	Correction factor for crop type (fraction)
GDD	Growing degree-days accumulated for the month ($^{\circ}\text{C d}$)
HI	Harvest Index (%)
I _a	Initial abstraction (% or fraction)
K _S	Water stress index (fraction)
MAP	Mean annual precipitation (mm)
obs_rfl	Observed daily rainfall (mm)
PWP	Permanent wilting point (volume %)
R ²	Coefficient of determination (fraction)
rhmaxscr	Maximum screen relative humidity (%)
rhminscr	Minimum screen relative humidity (%)
rnd24	Daily precipitation (mm)
rnd24_BC	Bias corrected daily precipitation (mm)
rx1day	1-day maximum rainfall (mm)
S	Potential maximum storage (mm; $S = 1000/\text{CN} - 10$)
tmaxscr	Maximum screen temperature ($^{\circ}\text{K}$ or $^{\circ}\text{C}$)
tminscr	Minimum screen temperature ($^{\circ}\text{K}$ or $^{\circ}\text{C}$)
T _n	Daily minimum air temperature ($^{\circ}\text{C}$)
T _{Nn}	Annual minimum temperature ($^{\circ}\text{C}$)
Tr	Transpiration (mm)
T _x	Daily maximum air temperature ($^{\circ}\text{C}$)
TX _x	Annual maximum temperature ($^{\circ}\text{C}$)
u ₁₀	Wind speed at height 10 meters (m s^{-1})
u ₂	Wind speed at height 2 meters (m s^{-1})
WP	Water productivity (kg m^{-3} or g m^{-2})
WP*	Normalised water productivity (kg m^{-2})
WUE	Water use efficiency of crop production (kg m^{-3})
Y	Dry crop yield (g m^{-2} or t ha^{-1})

REPOSITORY OF DATA

For details related to the project's data, please contact:

Richard Kunz (principal researcher)
Centre for Water Resources Research
School of Agricultural, Earth and Environmental Sciences
University of KwaZulu-Natal
Private Bag X01, Scottsville 3209
Pietermaritzburg, South Africa
Email: kunzr@ukzn.ac.za

1 INTRODUCTION

1.1 Background and rationale

Underutilised indigenous crops have an important role in improving agro-biodiversity in South Africa. Their suitability for low input agricultural systems and tolerance to abiotic stresses such as drought and heat stress could improve the sustainability of rainfed cropping systems in rural communities. The promotion of underutilised indigenous crops under rainfed production will contribute to efforts to improve food and nutrition security and build the resilience of rural farming communities to climate change impacts. Priority should be given to developing guidelines for the rainfed production of selected underutilised indigenous crops. These guidelines would go a long way in promoting the sustainable inclusion and production of underutilised indigenous crops in rainfed rural cropping systems. In developing these guidelines, consideration should also be given to the potential impacts of climate change on crop production.

There is a high degree of certainty that temperature will increase with climate change, which will result in a substantial increase in evaporative demand. This should translate into higher maximum transpiration rates and increased crop yields if water availability is nonlimiting. Higher temperatures also infer that growing degree-days will accumulate faster, and thus, crop development will be enhanced, thus resulting in shorter crop cycles. However, projected changes in rainfall are less certain, with some parts of the country becoming drier in the future, whilst others are expected to be wetter. Hence, it is difficult to assess if climate change may result in higher or lower crop yields in the future. However, impacts of changing rainfall and increasing temperature on crop yield and water use do not consider the crop's response to elevated CO₂ levels. Crop response to elevated CO₂ is dependent on changes in rainfall and temperature and changes in other variables such as soil moisture content and soil nutrient availability.

Evidence from free-air CO₂ enrichment (or FACE) experiments has shown that elevated levels of ambient CO₂ concentration can increase the rate of photosynthetic carbon assimilation in plants and thus, stimulate plant growth. Although such benefits have been reported for both C3 and C4 crops (e.g. Leakey et al., 2009), this CO₂ "fertilisation effect" is more beneficial for C3 (e.g. trees, forbs and temperate grasses) than C4 crops (e.g. tropical grasses) (Harle et al., 2007). However, the magnitude of the CO₂ fertilisation effect remains uncertain (Ainsworth et al., 2008). This is due to variations in experimental design (e.g. free air enrichment vs semi-closed systems) and various environmental factors affecting crop response to elevated CO₂. For example, water stress can increase the CO₂ growth stimulation, whilst limited nitrogen availability usually decreases the response to elevated CO₂ (Sun et al., 2009). In addition, higher CO₂ levels can also induce stomatal closure (i.e. decrease stomatal conductance), resulting in lower transpiration, which decreases crop water use and increases crop water use efficiency, as well as improves soil water content. This increased efficiency in converting water into dry matter has been shown to raise above-ground and, in some cases, below-ground plant biomass.

In water-limited conditions, such as those experienced in virtually all rainfed cropping systems in South Africa, the main benefit of increased CO₂ levels is derived through the interaction of plant water use efficiency and soil moisture availability. In general, enhanced CO₂ levels will improve the plant's ability to withstand the stresses associated with reduced rainfall, although this will vary with species and soil conditions. In the more arid regions of the country where annual rainfall varies between 300 and 500 mm, further decreases in rainfall due to climate change may offset the positive effects of enhanced CO₂ levels on plant growth. Low nutrient availability can further limit the response of plant productivity to raised CO₂ levels (Harle et al., 2007). For these reasons, the potential impacts of climate change on crop production should be assessed using mechanistic crop models. Such models can assess the

integrated effects of changing rainfall combined with increased temperatures and CO₂ levels on crop growth, yield and water use.

The application of available crop models can aid in assessing the potential impacts of climate change on the rainfed production of underutilised indigenous crops in South Africa. Such information will be useful for planning agricultural interventions that include underutilised indigenous crops and contributing to efforts to broaden crop choice options for farmers. This should help increase the level of preparedness of rural farmers and hence, increase their capacity to adapt to climate change impacts by improving resilience.

1.2 Project aim and objectives

In November 2016, the Crop Science discipline within the School of Agricultural, Earth and Environmental Sciences at the University of KwaZulu-Natal in Pietermaritzburg was awarded a research project initiated and funded by the Water Research Commission (WRC). This project (K5/2717) was titled “Developing a guideline for rainfed production of underutilised indigenous crops and estimating green water use of indigenous crops based on available models within selected bi-climatic regions of South Africa”, with total funding of R2 million. This 5-year project commenced in April 2017 and terminated in March 2022 and aimed to develop production guidelines and land suitability maps for underutilised indigenous crops grown under rainfed conditions. Another aim of this project was to map climate change impacts on yield, water use and water productivity for selected underutilised crops under rainfed growing conditions. Based on this, the final project report was produced in two volumes:

1. Land suitability mapping and production guidelines to promote the rainfed production of underutilised indigenous crops in South Africa.
2. Climate change atlas highlighting potential impacts of climate change on the productivity of selected underutilised indigenous crops.

Over the five years, ten reports were produced for the WRC, which have been integrated and synthesised to produce these two volumes. This report represents **Volume 2** and highlights the potential impact of climate change on four underutilised crops, *viz.* amaranth, bambara groundnut, sorghum and taro. The specific objectives of the project related to this report are as follows:

- To parameterise/calibrate and test/validate available crop models for selected underutilised crops under rainfed conditions in South Africa (**Aim 2**)
- To use available crop models and climate change data to map climate change impacts on yield, water use and water productivity of selected underutilised crops for rainfed production under South African conditions (**Aim 4**)

The information presented in this report (**Volume 2**) should help improve the resilience of rural farming communities to climate change impacts. Hence, the climate change maps will facilitate strategic decision making at all levels for crop choice and climate change adaptation strategies. It is envisaged that the climate change maps will also help to promote the sustainable inclusion and production of underutilised indigenous crops in rainfed cropping systems.

1.3 Scope of the report

In the past, underutilised indigenous crops were neglected (i.e. forgotten) by policymakers, researchers, breeders, producers and traders. Hence, these crops received little research attention, which prevented their full potential from being recognised. These crops have not been classified as major crops and are currently grown within traditional farming systems by subsistence and small-scale growers using

informal seed systems. Consequently, they have poorly developed and understood value chains. However, this situation is changing, albeit slowly. Over the past 25 years, increasing research attention has been afforded to underutilised crops through the vision and funding efforts of the WRC. In addition, agricultural-related policies have broadened their scope to include underutilised crops (DAFF, 2014). These efforts should help transform indigenous crops from underutilised to being produced at a commercial farming scale.

Underutilised crops that exhibit high potential for expanding agricultural production in South Africa have already been identified (Modi and Mabhaudhi, 2016). The 13 identified crops have been targeted and prioritised for future research, development and innovation. Hence, underutilised indigenous crops are receiving increasing recognition because of their drought and heat tolerance. Thus, their potential role in mitigating risk in agricultural production systems and promoting food security (Mabhaudhi et al., 2017). The maps presented in this report highlight the potential impacts of the changing climate on four underutilised indigenous crops. The main beneficiaries of the research represented in this report are as follows:

- Small- and large-scale farmers,
- Department of Agriculture, Land Reform and Rural Development (a merger between the Department of Agriculture, Forestry and Fisheries and the Department of Rural Development and Land Reform), in particular agricultural extension officers within the National Extension Support Services section,
- Department of Human Settlements, Water and Sanitation (a merger between the Department of Human Settlements and the Department of Water and Sanitation), and
- Department of Science and Innovation (former Department of Science and Technology).

It is envisaged that the maps will support strategic decision making at all levels for choice of crop enterprise and climate change adaptation strategies. In addition, the maps should improve the service provided by agricultural extension officers to rural farming communities and emerging farmers regarding where indigenous crops can be cultivated (**Volumes 1 and 2**), how best to produce these crops under rainfed conditions (**Volume 1**), what yields can be expected as well as understanding the possible impacts of climate change (**Volume 2**).

1.4 Structure of report

Chapter 2 (methodology) of this report (**Volume 2**) discusses the methodology used to run the crop productivity model (AquaCrop) at a national scale. The section begins with a description of the crop model (**Sections 2.1 and 2.2**), how the input files required to run the model were developed (**Sections 2.3 and 2.4**) and includes a detailed description of the necessary steps taken to reduce computational expense, i.e. minimise the time required to complete national model runs (**Section 2.5**). In **Section 2.6**, the approach used to develop the series of maps shown in this report is discussed.

In essence, AquaCrop was run with one planting date and plant density deemed appropriate for each of the four underutilised crops. This was done using 50 years of observed input climate data representing historical conditions. In addition, the model was run using 30 years of projected climate data representing three time periods (present, near future and distant future) derived from six dynamically downscaled and bias-corrected GCMs. The GCMs were forced with two CO₂ mitigation scenarios for Representative Concentration Pathways (RCP) 4.5 and 8.5. However, RCP4.5 was not used for modelling after problems were found with the dataset (cf. **Sections 2.3.8 and 4.3.2**, including **Chapters 7 and 8**).

In **Chapter 3** (results and discussion), the success of bias correcting the climate projections is given in **Section 3.1**, followed by expected trends in rainfall and temperature that may affect crop yield response to climate change (**Section 3.2**). Maps showing impacts of climate change on crop yield, WUE and

season length are given in **Sections 3.3, 3.5 and 3.6**, respectively. The maps highlight the percentage change from present to near future, near to distant future and present to distant future.

Similar maps expressing the change as ratios (i.e. present/near future) are given in **Chapters 9, 10 and 11** for yield, WUE and season length, respectively. The coefficient of variation among the ratios of change for the six GCMs was calculated to give a confidence index that reflects GCM agreement. These results are presented in **Sections 3.3.4, 3.5.4 and 3.6.4** and **Chapters 12 to 14**. A brief discussion on how areas deemed suitable for crop production may expand in the future is given in **Section 3.4**. This project has generated a wealth of data to quantify the potential impacts of climate change on four underutilised crops, as discussed in **Chapter 6** (data storage). Finally, the main findings of this study and its limitations are presented in **Chapter 4**, together with recommendations and future work.

2 METHODOLOGY

In this project, AquaCrop Version 6 was run to simulate crop yields, water use efficiency and season length under rainfed conditions. An overview and a brief description of the model is given in **Section 2.1**. Version 6 of the model underwent significant improvements compared to version 4, as explained in **Section 2.2**. The model was run at the national scale of all 5838 altitude zones. The derivation of historical and future climate files is discussed in **Section 2.3**, followed by a description of the crop parameter files used in this study (**Section 2.4**).

Kunz et al. (2020) developed a more efficient method for running simulation models at a national scale. This means that model users spend less time waiting for model runs to complete, which allows them to consider additional modelling scenarios. A detailed outline of the performance enhancements made to achieve this efficiency is summarised in **Section 2.5**, which should allow others to implement (and benefit from) a similar approach. The section ends with a discussion of the approach used to develop the maps shown in this report (**Section 2.6**).

2.1 AquaCrop model

2.1.1 Model overview

Kephe et al. (2021) identified most crop models that have been applied widely in agricultural management, viz. ACRU, DSSAT, SWB, EPIC, APSIM and AquaCrop. They noted that most studies assessing crop response in South Africa used the AquaCrop model. In addition, AquaCrop has been extensively used in other WRC-funded projects to estimate the yield and water use of commercial crops (e.g. canola, soybean, sugarcane and sugarbeet). Furthermore, the model has been successfully linked to the climate and soils databases that Schulze et al. (2011) developed for each of the 5838 quinary catchments (Kunz et al., 2015a; 2020). For these reasons, AquaCrop was chosen to meet the aims of this project.

The FAO developed AquaCrop to simulate the daily growth, productivity and water use of 16 herbaceous crops, as affected by changing water availability and environmental conditions. According to Steduto et al. (2012), AquaCrop can be used to perform the following:

- assess the effect of water deficits on crop production,
- compare the results of several water allocation plans,
- optimise irrigation scheduling,
- enhance management strategies for increased water productivity and water savings, and
- assess crop response to different climate change scenarios in terms of altered soil water content, temperature regimes and elevated atmospheric CO₂ concentration.

AquaCrop is particularly suited to simulating yield response to water availability as it is a water-driven model. Hence, AquaCrop is an engineering-type water productivity model that represents a simplified interpretation of water stress effects on crop productivity. The structural components of the model are shown schematically in **Figure 2.1**. The basic concepts and fundamental calculation procedures are briefly described next.

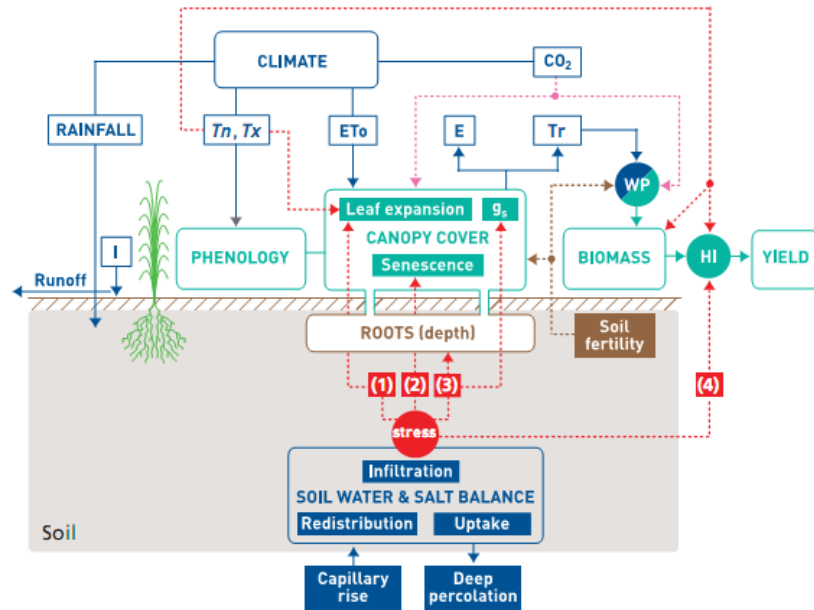


Figure 2.1 The structural components of AquaCrop, including stress responses and the functional linkages among them (Steduto et al., 2012)

AquaCrop’s growth engine is water-driven and estimates biomass production (B in g m^{-2}) via a conservative, crop-specific water productivity parameter (WP) and accumulated crop transpiration ($\sum Tr$) and as follows:

$$B = WP \cdot \sum Tr \quad \text{Equation 1}$$

AquaCrop is based on the dual crop coefficient method, separating K_{cb} (basal crop coefficient) and K_e (soil water evaporation coefficient). In other words, the model differentiates non-productive consumption of water (soil water evaporation or E) from productive consumption, i.e. transpiration. Thus, AquaCrop segregates evapotranspiration into two components: Tr and soil water evaporation (E). This approach is especially useful during periods of incomplete ground cover when E is high.

WP represents the biomass produced ($\text{g m}^{-2} \text{mm}^{-1}$) per unit of transpired water (mm). Both Tr and WP are normalised using ET_0 to improve the model’s robustness and applicability across different climates. ET_0 is determined using the FAO56 (or Penman-Monteith) method described by Allen et al. (1998). The normalised WP is designated as WP^* within the model as follows:

$$B = WP^* \cdot \sum (Tr/ET_0) \quad \text{Equation 2}$$

WP^* behaves conservatively, remaining virtually constant over a range of environments and is not affected by water stress (Steduto et al., 2009). According to Vanuytrecht et al. (2011), WP^* is higher for C4 crops (typical range: $30\text{-}35 \text{ g m}^{-2}$) than C3 crops (typical range: $15\text{-}20 \text{ g m}^{-2}$). WP^* is also a function of the ambient CO_2 level and is expected to increase over time (due to rising CO_2 levels).

For most crops, only part of the biomass is partitioned to the harvested organs to give yield. Yield is correlated to biomass production (and photosynthesis) and, thus, is directly and indirectly affected by environmental conditions (Challinor et al., 2009). The yield (Y in g m^{-2}) is the harvestable portion of the biomass (B), which is calculated using the harvest index (HI) as follows:

$$Y = B \cdot HI \quad \text{Equation 3}$$

The harvest index is estimated on a day-by-day basis over the yield formation period, which also enhances the robustness of the model. No other partitioning among the various plant organs occurs, thus avoiding the complexity of partitioning processes that are the most difficult to model (Steduto et al., 2009).

However, like most crop models, it cannot account for the effects of pests and diseases. AquaCrop does not directly simulate the effects of fertility on crop growth, nor can it simulate intercropping, which the APSIM model can (Kephe et al., 2021). Instead, it allows adjustment of default values pertaining to pivotal crop parameters (e.g. WP^* and canopy cover) based on fertility categories that range from near-optimal to poor. Compared to other crop models, AquaCrop requires a relatively small number of input crop parameters and readily available climate data [rainfall, maximum (T_x) and minimum (T_n) temperature, reference crop evapotranspiration (ET_o) and ambient CO_2 concentration], as indicated in **Figure 2.1**. Other inputs relate to soil characteristics and management practices that define the environment in which the crop will develop (Steduto et al., 2012).

2.1.2 Crop response to stress

Abiotic environmental stresses related to water and temperature can negatively impact canopy development, biomass production, and yield. The impact depends on the timing of occurrence, severity and duration.

Water stress

Water stress reduces transpiration which then decreases biomass production. The impact of water stresses on harvest index (and thus yield) can also be pronounced (either negative or positive), depending on the timing and extent of stress during the crop cycle (Steduto et al., 2009). **Figure 2.1** also shows the functional linkages between different stress responses in the model. The numbers represent water stress response functions for (1) leaf expansion, (2) senescence, (3) stomatal conductance and (4) harvest index. In AquaCrop, stress is described by means of a stress coefficient (K_s). In essence, K_s modifies its target model parameter and ranges from one (no stress) to zero (full stress). The shape of the stress curve is typically convex (but can be linear or concave), and the degree of curvature is set during model calibration.

Temperature stress

Franke (2021) reviewed the effects of increased temperature on crop growth and development, such as, *inter alia*, reduced photosynthesis, increased respiration, reduced net assimilation, higher evapotranspiration (assuming water is nonlimiting), shorter growing and grain filling periods. These combined effects typically result in reduced yields. Deterministic crop models generally have algorithms to simulate temperature impacts on net assimilation and phenological development, which is why such models are useful in assessing climate change impacts on crop growth. A review by Franke (2021) showed that DSSAT was used in half of the 20 climate change studies over southern Africa, followed by AquaCrop (20%) and LINTUL (10%).

AquaCrop uses growing degree-days (GDD) as the thermal clock to account for the effects of temperature on phenology and crop growth. Minimum and maximum air temperatures are used to account for cold and heat stress, respectively. For example, biomass production is affected by cold temperature stress, whereas hot or cold temperature stress inhibits pollination, which then reduces the HI. In addition, temperature stress modifies the water productivity parameter, and thus, both biomass production and yield formation are affected by temperature stress (Vanuytrecht et al., 2014).

2.1.3 Crop response to elevated CO₂

To estimate crop response to elevated CO₂, crop models utilise different simple and semi-complex methods. The majority of crop models assess atmospheric CO₂ levels on (i) photosynthesis/production, and (ii) stomata/transpiration, whilst some also consider (iii) nitrogen dynamics (Vanuytrecht and Thorburn, 2017). More importantly, APSIM has been validated against FACE experiments for three crops (wheat, rice and pasture). However, other crops (e.g. barley, potato, maize, sorghum and cotton) have not been validated, despite the availability of FACE data. On the other hand, AquaCrop has been tested for a range of crops using data from several FACE experiments (Vanuytrecht et al., 2011).

To account for plant response to rising CO₂ levels, version 4.0 of AquaCrop was modified to include:

- a downward adjustment of transpiration (due to increased stomatal conductance), and
- an upward adjustment of WP* (due to the CO₂ fertilisation effect).

Hence, WP* in **Equation 2** is adjusted by two dimensionless coefficients (f_{TYPE} and f_{CO_2}) as follows:

$$\text{WP}^*_{\text{adj}} = (1 + f_{\text{TYPE}} \cdot f_{\text{CO}_2} - f_{\text{TYPE}}) \cdot \text{WP}^* \quad \text{Equation 4}$$

The coefficient f_{TYPE} ranges from 0 to 1 and accounts for the response to elevated CO₂ levels being smaller for C4 crops than for C3 crops as follows:

$$f_{\text{TYPE}} = (40 - \text{WP}^*) / (40 - 20) \quad \text{Equation 5}$$

For C3 crops with a typical WP* of 15-20 g m⁻², f_{TYPE} is 1. For C4 crops, WP* ranges from 30 to 35 g m⁻², and thus, f_{TYPE} is 0.50 and 0.25, respectively.

The equation given by Vanuytrecht et al. (2011; Equation 6 on p 1755) to calculate f_{CO_2} is different to that given by Raes et al. (2018; cf. Equation 3.11c on p 3-100), with the latter equation incorporating a weighting factor (w). This weighting factor ranges from 0 to 1 for CO₂ concentrations below 369.71 ppm and above 550 ppm, respectively. The threshold of 369.71 ppm represents the averaged atmospheric CO₂ concentration measured at Mauna Loa Observatory, Hawaii, in the year 2000. The threshold of 550 ppm represents the CO₂ level typically maintained in the FACE experiments.

The f_{CO_2} coefficient adjusts WP* when the atmospheric CO₂ concentration (read in from the .CO2 file) differs from the reference value. **Figure 2.2** shows measured ambient CO₂ levels from 1950 to 2020, together with the RCP8.5 CO₂ trajectory. A CO₂ concentration of 550 ppm may be reached around 2052, increasing to over 900 ppm by 2100. The coefficient is dependent on the crop's sink strength coefficient (f_{SINK}), which varies from 0 (low CO₂ responsiveness) to 100% (high CO₂ responsiveness) depending on crop characteristics and field management. Vanuytrecht et al. (2011) provided specific values for certain crops, which are high (0.4-0.6) for root and tuber crops and low (0.0-0.2) for cereals.

Vanuytrecht et al. (2011) referred to the adjustment factor $(1 + f_{\text{TYPE}} \cdot f_{\text{CO}_2} - f_{\text{TYPE}})$ given in **Equation 4** as f_{WPS} . For C3 crops where WP* < 20 g m⁻², f_{TYPE} is 1 and $f_{\text{WPS}} = f_{\text{CO}_2}$, f_{WPS} increases steadily from 0.85 in 1950 to 1.00 for the reference year and up to 1.11 in 2020 (**Table 2.1**). From 2020 onwards, f_{WPS} increases steadily up to 1.85 towards the end of the 21st century. Therefore, WP* is adjusted upwards by a factor of 1.85 for C3 crops in the year 2100. For C4 crops where WP* is 30-35 g m⁻², f_{WPS} in 2100 is lower (1.43 and 1.21). The f_{WPS} values shown in **Table 2.1** are based on an f_{SINK} value of 50%, which is AquaCrop's default value.

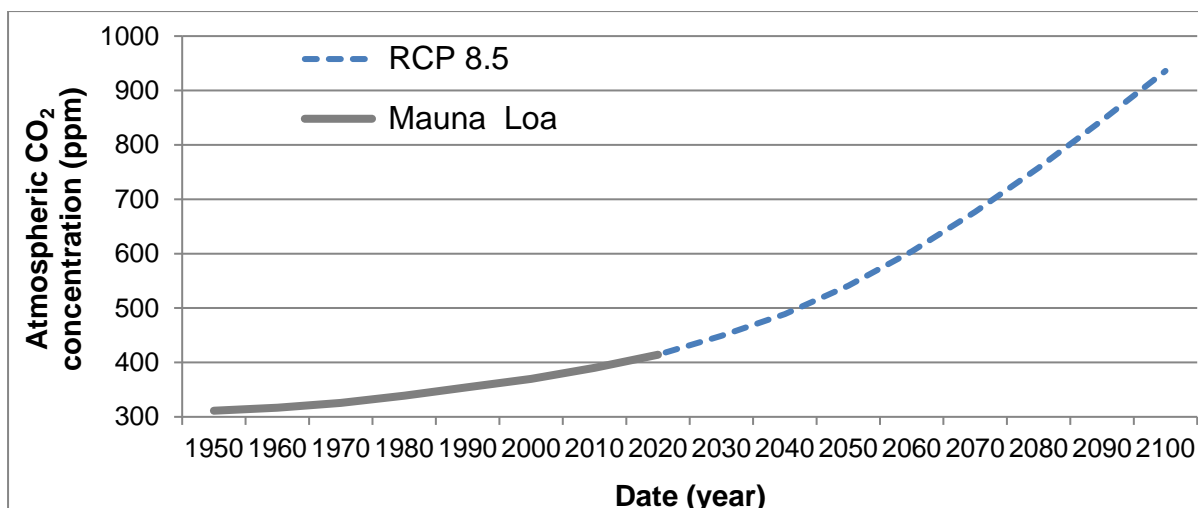


Figure 2.2 Atmospheric CO₂ concentration measured at Mauna Loa in Hawaii from 1950 to 2020, together with projected values from 2020 to 2100 as per RCP8.5

WP* is also adjusted downward to account for the production of lipids or proteins synthesised during yield formation, as these products require considerably more energy per unit dry weight than for the synthesis of carbohydrates. In addition, WP* is adjusted downwards when soil fertility or soil salinity limits plant growth (Raes et al., 2018). For a similar assessment on how the APSIM model assesses crop response to elevated CO₂, the reader is referred to Vanuytrecht and Thorburn (2017).

Table 2.1 Adjustment coefficient (f_{CO_2}) applied to the normalised water productivity value within the AquaCrop model for RCP8.5 emission scenario

Year	CO ₂ concentration (ppm)		WP* adjustment factor (f_{wps})		
	Observed (Mauna Loa)	Projected (RCP8.5)	WP* < 20	WP* = 30	WP* = 35
1950	311.30		0.849	0.924	0.962
1960	316.91		0.863	0.932	0.966
1970	325.68		0.886	0.943	0.972
1980	338.76		0.920	0.960	0.980
1990	354.45		0.961	0.980	0.990
2000	369.71		1.000	1.000	1.000
2010	390.10		1.051	1.025	1.013
2020	414.24		1.107	1.054	1.027
2030		449	1.180	1.090	1.045
2040		489	1.251	1.126	1.063
2050		541	1.322	1.161	1.080
2060		604	1.417	1.209	1.104
2070		677	1.526	1.263	1.131
2080		758	1.636	1.318	1.159
2090		845	1.745	1.373	1.186
2100		936	1.849	1.425	1.212

2.2 AquaCrop model improvements

In AquaCrop Version 6, the following improvements and new features have been made to the model:

- Improved simulation of crop performance in dry environments
- Improved water thresholds for stomatal closure for certain crops

- Effects of gravel in the soil profile
- Simulation of weed infestation on crop production
- Inclusion of dry beans as a new crop

In addition to the above, the ratio of initial abstraction (I_a) to potential maximum storage (S) has been decreased from 20% to 5%. Hence, AquaCrop Version 6 produces more runoff than Version 4. The default curve numbers have also been updated in Version 6, due to the coefficient of initial abstraction changing from 20 to 5%. However, only the first two updates listed above are discussed next in more detail. This is due to their greater impact on simulated output from AquaCrop in this study.

2.2.1 Simulations in dry environments

Kunz et al. (2015b) noted that AquaCrop Version 4 was particularly sensitive to soil moisture availability in the first growth stage. They found that water stress at the start of the second growth stage reduced leaf expansion to such an extent that the crop died, and thus, no biomass or yield was produced. A workaround was to set the initial soil water level to field capacity, which is the default option in AquaCrop. However, this is unrealistic for rainfed farming conditions in South Africa.

This issue has been addressed in Version 6, which assumes that sufficient reserves are available in the seed for leaf expansion to occur at its maximum rate just after germination. Any reduction of leaf expansion due to water stress is not considered until canopy cover is 25% above the initial value (CC_0). This protection of the seedling avoids an instantaneous killing of the seedling too soon after germination (FAO, 2017).

The main motivation to use Version 6 of the model in this project was the improvement in simulating the early development of the canopy cover under water stress. It is expected that the number of crop failures (i.e. zero yield) simulated by Version 6 of the model will be somewhat less than that outputted by Version 4.

2.2.2 Water thresholds for stomatal closure

FAO (2017) reported updates to crop parameters related to soil water thresholds for soybean, sorghum, potato and cotton. In particular, changes were made to the upper threshold for soil water depletion at which the stomata start to close and the shape factor for the stress-depletion relationship.

2.3 AquaCrop input files

2.3.1 Planting date and plant density

Table 2.2 provides the planting window and the ideal planting date utilised for each underutilised indigenous crop. Plant densities of 33 333, 166 667, 44 444 and 20 000 plants ha^{-1} were selected for amaranth, bambara groundnut, sorghum and taro, respectively. For further information, the reader is referred to **Volume 1** of this report

Table 2.2 Planting date selected for each underutilised indigenous crop modelled in this study

Crop	Planting window	Ideal planting date	Source
Amaranth	1 st Sep-30 Nov	15 th Sep	DAFF (2010a)
Bambara groundnut	1 st Oct-15 th Dec	15 th Oct	DAFF (2011)
Sorghum	15 th Oct-15 th Dec	15 th Oct	DPP/ARC (2006)
Taro	15 th Oct-15 th Jan	15 th Nov	DAFF (2010b)

2.3.2 Soils data

The minimum soil input parameters required by AquaCrop are depths of the A- and B-horizon (in m), the volumetric water contents (as %) at saturation, field capacity and permanent wilting point, as well as saturated hydraulic conductivity (in mm d⁻¹). The latter was calculated from equations provided by Saxton and Rawls (2006). For each altitude zone, the area-weighted and averaged volumetric water contents, together with the soil depths, were derived by Schulze and Horan (2008) using the AutoSoils decision support tool (Pike and Schulze, 1995 and updates) applied to the ISCW soils database (SIRI, 1987 and updates) for each of the land types that cover South Africa.

2.3.3 Observed climate

In this section, the development of the 1) historical and 2) future climate databases used in this study are described. For more detail on these two climate databases, the reader is referred to Kunz et al. (2020) and Wolski et al. (2021), respectively. The section begins with a brief description of the base datasets used to develop the historical climate database for the quaternary catchments and their altitude zones.

2.3.3.1 Description of base datasets

A comprehensive daily rainfall database for southern Africa was compiled by Lynch (2004) using data from 12153 daily rainfall stations. Extensive error checking of the dataset and infilling of missing data was done by Smithers and Schulze (2000) and refined by Lynch (2004). Some stations exhibit 152 years of record (from January 1850 to December 2001), whilst others have only a few months of reliable data. Kunz (2004) developed a useful utility to extract daily, monthly and annual data from the rainfall database.

Similarly, a daily temperature database for South Africa was compiled by Schulze and Maharaj (2004), which comprises daily data from 1950 to 2000 for 973 recording stations that were infilled and quality controlled. This base dataset was then used to derive interpolated daily temperatures for each minute of a degree across the country, i.e. 437038 grid points. This was achieved by selecting two temperature stations that best represent each grid point, then applying a distance weighting factor (i.e. from the station to the grid point). Thereafter, a lapse rate adjustment was applied to account for the altitude difference between the temperature station and each grid point.

2.3.3.2 Quaternary catchments climate database

Rainfall

The Department of Human Settlements, Water and Sanitation (DHSWS) delineated South Africa into a set of nested Primary, Secondary, Tertiary and Quaternary Catchment boundaries. At the quaternary level, there exist 1946 catchments. A representative driver rainfall station from the Lynch (2004) dataset was selected for each Quaternary Catchment (QC) to develop the Quaternary Catchments Climate Database (QnCDB). In total, 1240 stations were selected to represent the 1946 QC, of which the majority are owned by SAWS (**Table 2.3**).

As reported by Schulze et al. (2011), several criteria were used to select the rainfall driver stations as follows: mean annual precipitation (MAP), altitude, reliability of record, end year of record and distance of rainfall station from the centroid of each QC. Daily rainfall data for each selected driver station was extracted from the Lynch (2004) dataset using the Kunz (2004) utility from 1950-1999.

Table 2.3 Custodian of rain gauges selected for each quaternary catchment (Kunz et al., 2020)

Custodian	SAWS ID	Number	Percentage of total
SAWS	W	1158	93.4
ARC	A	34	2.7
SASA	S	22	1.8
SAWS/ARC	AW	15	1.2
Total		1240	100.0

For each QC, monthly adjustment factors were derived to estimate catchment rainfall from driver station rainfall. This was done by comparing the driver station’s median monthly rainfall to that derived for each QC using spatial estimates of median monthly rainfall developed by Lynch (2004). The monthly adjustment factors are used to derive rainfall estimates deemed more representative of each catchment.

Temperature

A software utility was developed to automate the selection of a suitable temperature dataset for each QC, which used the mean altitude and centroid location of each QC. The utility selected a grid data point that was 1) within the same catchment boundary (if possible), 2) of similar altitude to the catchment mean, and 3) closest to the catchment centroid. For the grid data point (1’ by 1’ pixel) selected for each QC, daily temperature data was extracted from the Schulze and Maharaj (2004) dataset.

Reference evapotranspiration

Using the method described by Schulze et al. (2011), which is based on the FAO56 equation (Allen et al., 1998), reference grass evapotranspiration (ET_0) was calculated from daily temperature and a default wind speed of 1.6 m s^{-1} . Hence, the QnCDB consists of 50 years (1950-1999) of daily rainfall, temperature and ET_0 for each of the 1946 QCs.

2.3.3.3 Altitude zones climate database

Delineation of altitude zones

For some purposes, even the QC boundaries are deemed too coarse, and thus, a finer delineation was deemed useful. Hence, three regions (upper, middle and lower) of similar altitude were delineated within each QC by Schulze and Horan (2011), based on natural breaks in altitude using Jenk’s optimisation method. As the regions are delineated by natural breaks in altitude, the upper region may comprise one or more discrete spatial units (i.e. polygons). For modelling, altitudinal regions consisting of more than one polygon are conceptualised as a single entity.

Runoff from the upper region flows into the middle region, with the latter flowing into the lower region. The lower region typically flows into the lower region of the downstream QC. Since the altitude zones do not represent true quinary catchments, they are now referred to as altitude zones (AZs) and not Quinary Catchments (QnCs), as was adopted by Schulze and Horan (2011).

Rainfall

The rain gauge selected to drive each quaternary was again chosen for each of the three AZs. For each of the 1 240 rainfall driver stations, daily rainfall from January 1950 to December 1999 was re-extracted from the rainfall database developed by Lynch (2004). This was done to obtain the data quality code, which indicates if the daily rainfall value is observed (code=" "), infilled (P for "patched") or missing (M). Missing daily values were set to zero after comparison with data from neighbouring rain gauges.

A total of 13 extreme daily rainfall events ($> 400 \text{ mm}$) were identified, with the worst case being 900.5 mm . A method was developed to automatically extract daily rainfall for the ten neighbouring stations

from the Lynch (2004) rainfall database. A manual comparison was then performed to validate each rainfall event, resulting in four extreme rainfalls being adjusted downward (**Table 2.4**). The rainfall code was changed to F, i.e. “fixed”.

Table 2.4 Adjustments made to extreme rainfall values that existed in the quaternary catchments rainfall database (Kunz et al., 2020)

SAWS ID	Date	Daily rainfall (mm)	
		Original	Adjusted
0150620 W	1997/02/22	900.5	0.0
0304446 W	1980/12/14	585.5	85.5
0214485 W	1953/02/23	520.0	0.0
0022148 W	1991/06/23	440.0	44.0

For each AZ, monthly adjustment factors were then derived by comparing the driver station’s median monthly rainfall to that derived for each AZ using spatial estimates of median monthly rainfall developed by Lynch (2004). The monthly adjustment factors are applied to each daily rainfall value to improve the representativeness of the AZ.

Temperature

Recently, observed temperature data was determined for each AZ (Kunz et al., 2020). A summary of the procedure used is described next for the reader’s convenience:

- The Schulze and Maharaj (2004) temperature database was screened to remove 275 “duplicate” stations (at similar locations and altitudes), which reduced the number of stations from 973 to 698.
- The distance from each rainfall driver station to surrounding temperature stations was computed with the altitude difference between the two locations (i.e. stations).
- An algorithm then used these two metrics to determine the best temperature station to represent each rain gauge. In other words, a “pseudo” temperature station was assigned to each rain gauge.
- Of the 698 unique temperature stations, 543 were chosen to represent all 1240 driver rain gauges. This means that the same temperature station was selected for up to 10 rain gauges.

Ideally, 114 temperature stations had the same SAWS ID as the rain gauge, meaning that both rainfall and temperature were measured at the same weather station. Similarly, a total of 184 temperature stations were within 1 minute (~1.7 km) of the rain gauge, with altitude differences ranging from 1 to 338 m. Approximately 95% of the selected temperature stations were situated within 30 minutes (~51 km) of the rainfall driver stations, with the furthest station being 52.5 minutes (~89 km) away.

Lapse rate adjustment

The altitudinal differences between the temperature station selected to represent a particular driver rain gauge (DALT) are shown in **Table 2.5**, with the worst-case exceeding 950 m for two stations. A lapse rate adjustment was applied to account for the altitude difference between the pseudo temperature station selected for each rain gauge. This dataset was used for bias correction of GCM climate projections. Thereafter, a second lapse rate adjustment was applied to account for the altitude difference between the selected temperature station and the average altitude across each AZ it represents. This dataset was used to develop the Altitude Zones Climate Database, which was called the Quinary Catchments Climate Database in the past.

Table 2.5 Histogram of altitude difference from each rain gauge to the selected (best) temperature station (Kunz et al., 2020)

DALT (m)	Count	Percentage of total	Accumulated percentage
< 50	524	42.26	42.26
50-100	256	20.65	62.90
100-150	148	11.94	74.84
150-200	91	7.34	82.18
200-250	65	5.24	87.42
250-300	43	3.47	90.89
300-350	25	2.02	92.90
350-400	24	1.94	94.84
400-450	20	1.61	96.45
450-500	6	0.48	96.94
500-550	14	1.13	98.06
550-600	9	0.73	98.79
600-650	4	0.32	99.11
650-700	4	0.32	99.44
700-750	4	0.32	99.76
> 750	3	0.24	100.00
Total	1240	100.00	

Reference evapotranspiration

Daily solar radiation and relative humidity (maximum and minimum) values were then generated from the lapse-rate adjusted temperatures using the method described by Schulze et al. (2011). Due to the lack of wind speed data, a daily default value of 2 m s^{-1} was used, as suggested by Allen et al. (1998). Daily reference evapotranspiration values (ET_0) were then calculated using the FAO56 version of the Penman-Monteith equation (Allen et al., 1998).

Summary

Therefore, the recently revised AZDB consists of 50 years of daily rainfall, temperature (maximum and minimum), reference evapotranspiration (FAO56 and A-pan equivalent), solar radiation, and wind run for each of the 5838 AZs. To date, this climate database has been used extensively in WRC Project No. K5/2491 (Kunz et al., 2020), K5/2833 (Schütte et al., 2021a) and more recently, this project (K5/2717).

These AZs represent areas of similar topography within each QC and are not equal in area. They can be considered as relatively homogeneous response zones, with minimal variation in climate and soils across each region. Therefore, the AZs are particularly useful for agricultural-related assessments involving crop simulation models to determine, amongst others, crop water use, crop yield, water use efficiency and nutritional water productivity.

2.3.4 Future climate projections

2.3.4.1 CO₂ concentrations

The Intergovernmental Panel on Climate Change (IPCC) adopted the Representative Concentration Pathways (RCPs), which represent plausible pathways to reaching a specific radiative forcing trajectory over time. Four RCPs were chosen, as shown in **Table 2.6**, that map a broad range of climate outcomes as they span a range of radiative forcing scenarios into the future (Moss et al., 2010).

Table 2.6 The RCP scenarios adopted by the IPCC (Moss et al., 2010)

RCP name	Radiative forcing (W m ⁻²)	CO ₂ concentration (ppm)	Pathway
2.6	~3	~490	Peak before 2100, then declines
4.5	~4.5	~650	Stable after 2100
6.0	~6	~850	Stable after 2100
8.5	> 8.5	> 1370	Rises after 2100

The RCPs range from RCP2.6 to RCP8.5, where RCP2.6 is the scenario with low radiative forcing that begins to decline after 2100, while RCP4.5 and RCP6.0 show a stabilisation of radiative forcing after 2100. RCP8.5 is based on continuing increases in radiative forcing due to rising GHG emissions, despite the declines in emissions in the second half of the 21st century (IPCC, 2014), as shown in **Figure 2.3**.

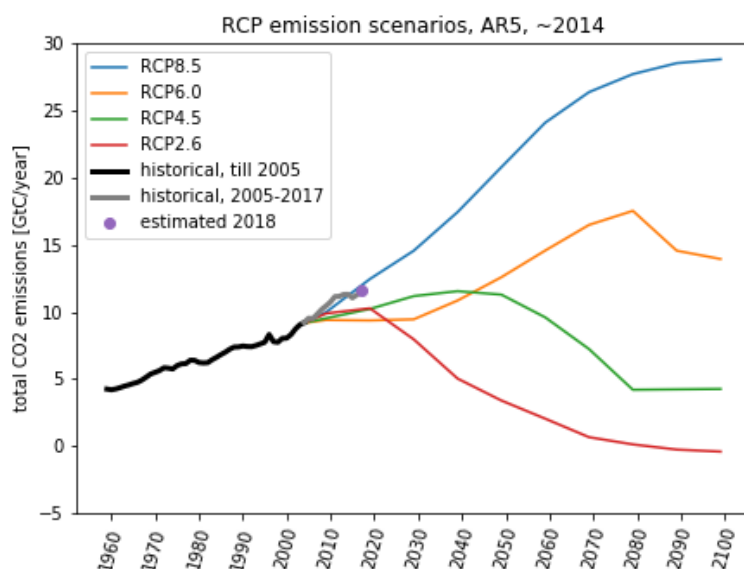


Figure 2.3 Projected CO₂ emissions per decade for each Representative Concentration Pathway or RCP (IPCC, 2014)

When these RCP pathways are used as input to multiple Global Climate Models (GCMs), the projected increase in global mean surface temperature for the period 2081-2100, relative to the period 1986-2005, is likely to be 1.1-2.6°C under RCP4.5 and 2.6-4.8°C under RCP8.5. The divergence in projected changes in temperature is only strongly evident from about 2050 onwards, as shown in **Figure 2.4** (IPCC, 2014). For this study, RCP4.5 and RCP8.5 (“business as usual” scenario) were initially selected to assess climate change’s potential impacts on future crop production.

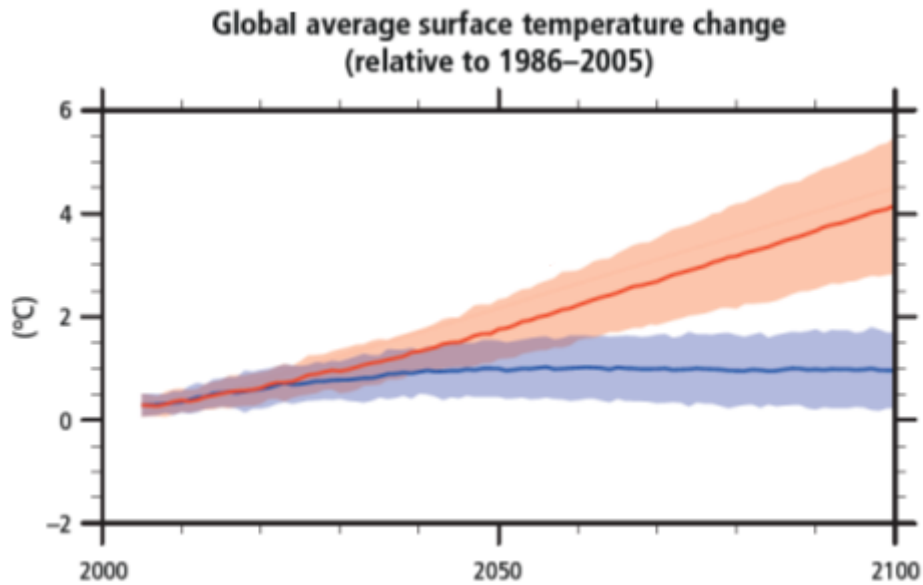


Figure 2.4 Global average surface temperature increases from 2006 to 2100, relative to 1986-2005, as determined from the mean of multi-model simulations for RCP2.6 (blue line) and RCP8.5 (red line), including the range (shading) as a measure of uncertainty (IPCC, 2014)

2.3.4.2 GCM selection

GCMs provide predictions (or projections) of various climate variables over time. Currently, there are a plethora of future climate projections generated using a multi-model, multi-method and multi-scenario approach. Developing future climate scenarios begins with global simulations of future climates using GCMs under various scenarios of greenhouse gas concentrations (as described in **Section 2.3.4.1**). These global simulations are made available in the Climate Model Inter-comparison Project (CMIP) archives, which form the basis of the IPCC assessment reports (e.g. AR5).

This study selected six GCM simulations from the CMIP5 archive, as described in the IPCC Assessment Report AR5 (IPCC, 2014). As shown in **Table 2.7**, the selection was based on their ability to provide a reasonable representation of the region's El Niño-Southern Oscillation (ENSO) phenomenon. The simulations span the period 1961-2100.

Table 2.7 Details of the six GCMs selected for this study (Wolski et al., 2021)

Abbr.	GCM details
ACC	Australian Community Climate and Earth System Simulator (ACCESS1-0)
CCS	Community Climate System Model (CCSM4)
CNR	National Centre for Meteorological Research Coupled GCM v5 (CNRM-CM5)
GFD	Geophysical Fluid Dynamics Laboratory Coupled Model (GFDL-CM3)
MPI	Max Planck Institute Coupled Earth System Model (MPI-ESM-LR)
NOR	Norwegian Earth System Model (NorESM1-M)

For this study, GCMs forced by RCP4.5 and RCP8.5 were initially selected to assess the impacts of climate change on crop response. As noted previously, the RCP scenarios only diverge significantly in their projections after approximately 2050. Until 2050, the variation between the available GCM projections is greater than the difference between the RCP scenario considered.

2.3.4.3 Downscaling techniques

Many GCMs fail to adequately capture the detailed spatial gradients and strong topographical forcing that influence South Africa's climate (Hewitson and Tadross, 2011). In response to this weakness, downscaling techniques were introduced to translate changes in the atmospheric circulation from the large scale to finer scales, which would be more suitable for local climates (Tadross et al., 2011). Hence, downscaling bridges the disparity between the spatially coarse-scaled GCM output and the finer-scaled input needs of hydrological and agricultural simulation models. The advantages of using downscaled climate projections are well recognised, but it is important to note that downscaling introduces additional uncertainties, which are sometimes not adequately quantified. There are two types of downscaling techniques performed in South Africa: dynamical downscaling (with Regional Climate Models or RCMs) and statistical (or empirical) downscaling. These two techniques are discussed next in more detail.

2.3.4.4 Statistical downscaling

The Climate System Analysis Group (CSAG), based at the University of Cape Town, has produced statistically downscaled climate projections applicable to South Africa. In the past, CSAG used an approach based on Self Organising Maps (SOM) to perform statistical downscaling. The SOM approach classifies observed synoptic drivers of weather into different states and then characterised local station responses (observed rainfall or temperature) for each of the states. These statistical relationships were then applied to GCM projected fields to develop the downscaled projections. However, results emerging from recent projects (e.g. VALUE-COST) focusing on assessing the value of statistical downscaling have highlighted limitations and constraints of the SOM approach.

Given the above, CSAG has temporarily moved away from the SOM approach and now uses a stochastic delta factor method, which is considered more conservative and more robust. This involves using a stochastic rainfall generator to modify observational time series of weather variables according to changes in means, variances, autocorrelations and spatial correlations between climate stations. The approach essentially preserves the GCM signal, but because of the stochastics involved, it provides a slightly better idea of the uncertainty of indices not explicitly accounted for in the process. The approach yields downscaled projections at a monthly time-step but not yet at a daily time-step. For this reason, statistically downscaled GCM data was not used in this project.

2.3.4.5 Dynamical downscaling

The CSIR approach applies the variable resolution Conformal-Cubic Atmospheric Model (CCAM) to downscale the coarse resolution GCM projections. This Regional Climate Model (RCM) was developed by the Commonwealth Scientific and Industrial Research Organisation, CSIRO (McGregor, 2005; McGregor and Dix, 2001; 2008). CCAM is coupled to a dynamic land-surface model called CABLE, i.e. CSIRO Atmosphere Biosphere Land Exchange model. The coupled model's ability to realistically simulate present-day southern African climate has been extensively demonstrated (e.g. Winsemius et al., 2014; Engelbrecht et al., 2015).

CCAM simulations were performed using supercomputers at the Centre for High-Performance Computing (CHPC) located at the Meraka Institute, CSIR. CCAM was forced with bias-corrected daily sea-surface temperatures (SSTs) and sea-ice concentrations from each of the six GCMs. Each GCM was forced with CO₂, sulphate and ozone levels consistent with the RCP4.5 and RCP8.5 scenarios. The monthly bias correction is computed by subtracting the Reynolds (1988) SSTs (1961-2000) from the GCM SSTs. This procedure ensures that the intra-annual variability and climate change signal of the GCM SSTs are preserved.

The CCAM model produced dynamically downscaled projections at a 50 km spatial resolution. A multiple-nudging strategy was followed to obtain projections at 8 km resolution (~0.08° degrees in latitude and longitude), where CCAM was run in stretched-grid mode over South Africa. The higher resolution simulations were nudged within the quasi-uniform global simulations through a digital filter using a 600 km length scale. The filter was applied at six-hourly intervals and from 900 hPa upwards.

2.3.4.6 Regional bias correction

The CSIR applied a simple bias correction procedure to the 50 km dynamically downscaled climate projections obtained using the CCAM model forced by all six GCMs (Winsemius et al., 2014; Engelbrecht and Engelbrecht, 2015). Observed (i.e. historical) monthly averaged temperature and rainfall totals for the period 1961-1990 were used as the reference. A monthly correction factor was calculated as the ratio of observed monthly rainfall for 1961-1990 to the GCM rainfall for the same period. The simulated daily rainfall values over the full period (1961-2100) were multiplied by this monthly factor to bias correct each GCM. The daily minimum and maximum temperatures were bias-corrected using a similar procedure, except the monthly correction factor was additive. This method preserves the inter-annual variability in the GCM data.

2.3.4.7 Future trends

Projections of changes in temperatures are relatively accurate owing to the GCM's ability to model physical processes responsible for heating (Archer et al., 2018). Unfortunately, their ability to estimate changes in rainfall and other climatic conditions is less certain, because of the large spatial scale (~200-300km) at which the GCMs are applied (Garland *et al.*, 2015). According to Archer et al. (2018), the six GCMs show a mean drying trend over South Africa by 2100 (see **APPENDIX B**). The southwestern Cape emerged as a consistent area of rainfall decreases across all six downscaled GCMs. This drying trend is associated with a poleward displacement of the westerlies and frontal systems under low mitigation (e.g. Christensen et al., 2007; Engelbrecht et al., 2009). Five of the GCMs agree on drier conditions along the eastern coast and interior by 2100 (Archer et al., 2018).

2.3.5 Extraction of CSIR climate projections

This section explains the procedure for obtaining climate projections for each AZ in detail. For more detail, the reader is referred to Wolski et al. (2021).

2.3.5.1 Data format

Climate projections for six GCMs and two RCPs in NetCDF format were obtained from the CSIR. It was noted that climate values for both RCPs are identical for the period 1961-2004, as emissions do not diverge during this period. Each NetCDF file contained one month (up to 31 values) of daily data (6 variables) for each 0.5° grid point centroid (latitude and longitude) across the country as follows:

- *time* (day of the month),
- *latitude* (of the grid point's centroid),
- *longitude* (of the grid point's centroid),
- *rnd24* (precipitation in mm),
- *tmaxscr* (maximum screen temperature in °K),
- *tminscr* (minimum screen temperature in °K),
- *rhmaxscr* (maximum screen relative humidity in %),
- *rhminscr* (minimum screen relative humidity in %), and
- *u10* (wind speed at height 10 meters in m s⁻¹).

2.3.5.2 “Downscaling” to station level

The following approach was used to derive climate projections for each quaternary catchment using a Python script:

- The closest GCM grid point (or pixel) was selected for each of the 1240 driver rain gauges. The same grid point was assigned to more than one driver rain gauge in some cases. Hence, a total of 1207 GCM grid points were eventually selected.
- A daily time series of GCM data was then extracted from each NetCDF file to represent each driver rain gauge.
- Temperature values were adjusted to degrees Celsius, and the 10 m wind speed data were adjusted to a height of 2 m (u_2).
- For leap years, daily data did not exist for 29 February, and thus, climate variables were set to the average of values on the preceding (28 February) and following day (1 March).
- The extracted and adjusted data was saved to a separated Comma Separated Value (.CSV) file, as illustrated in **Figure 2.5**.

```
date,rnd24,tmaxscr,tminscr,rhmaxscr,rhminscr,u2
1961-01-01,0.0157187,27.3881,14.7181,72.5618,50.473,0.393950
1961-01-02,0.314198,28.5357,18.4709,70.2625,45.6859,19.952495
1961-01-03,0.769772,29.9881,17.7396,69.2279,39.3699,7.613547
1961-01-04,0.8169,30.8818,18.3084,65.0065,35.8751,475.443473
1961-01-05,2.19148,25.9408,17.5467,69.6831,57.4098,38.723450
1961-01-06,0.0314281,26.1592,17.4553,71.2673,54.8369,101.074524
1961-01-07,0.8169,25.8392,17.2877,72.4767,49.3578,91.0983489
1961-01-08,0.125685,24.3158,16.1807,73.5642,56.6487,90.704549
1961-01-09,1.32746,25.626,15.1904,73.4838,56.989,187.0533697
1961-01-10,26.0777,20.8474,17.8971,73.0239,66.6987,71.408539
```

Figure 2.5 Example of a portion of a .CSV file containing data extracted for a representative GCM grid point (Wolski et al., 2021)

2.3.6 Bias correction to station level

When compared to observed rain gauge data, rainfall from the extracted GCM climate files exhibited a substantially larger number of rain days, with many rain days having very small rainfall depths (i.e. < 0.1 mm). In addition, the GCM temperature values were lower than observed values for the period 1961-1999. These anomalies indicated the need to bias correct the GCM rainfall and temperature data. This section presents the development, evaluation, and application of the rainfall and temperature bias correction methodology. It includes lapse rate adjustments to account for altitudinal differences between the temperature station and each altitude zone.

2.3.6.1 Rainfall

Wolski et al. (2021) evaluated various rainfall bias corrections techniques, ranging from:

- simpler methods that aim to correct the mean and/or variance of the climate estimates, to
- more advanced methods (e.g. quantile mapping that applies corrections at all quantiles such that the full distribution of values is corrected to match a reference distribution).

Quantile mapping (QM) approaches ensure that the corrected distribution of a particular variable matches the distribution of the observed variable by applying statistical transformations classed as either i) distribution-derived, ii) parametric, or iii) non-parametric. Of these, the latter class is preferred, which develops empirical (not theoretical) Cumulative Density Functions (CDFs) and percentile values, where values in-between discrete percentiles are approximated using linear interpolation.

However, it can over-correct the magnitude of rainfall extremes compared to the uncorrected (i.e. GCM) data. To address this limitation, which relates to the assumption of stationarity, the Quantile Delta Mapping (QDM) method was selected. A 39-year moving window was used to calculate the CDF curve, based on the calibration period being 1961 to 1999. The QDM method was extensively tested and produced unrealistically high rainfall values in quantiles close to the 100th percentile. This problem was addressed by limiting the bias correction factors for quantiles above the 99th percentile to those for the 99th percentile of non-exceedance.

A Python script was developed to undertake the bias correction using the QDM method and a bias corrected time series of GCM rainfall values was created for each of the 1249 rain gauges in .CSV format (**Figure 2.6**). The three variables stored in each CSV file are as follows:

- *obs_rfl* (observed rainfall in mm),
- *rnd24* (original GCM rainfall in mm), and
- *rnd24_BC* (bias corrected GCM rainfall in mm).

Date	obs_rfl	rnd24	rnd24_BC
1961-01-01	0.0	0.0157187	0.0
1961-01-02	0.0	0.314198	0.0
1961-01-03	0.0	0.769772	0.0
1961-01-04	0.0	0.8169	0.0
1961-01-05	0.0	2.19148	0.000324

Figure 2.6 Example of a portion of a .CSV file containing observed rainfall, raw GCM rainfall and bias corrected GCM rainfall (Wolski et al., 2021)

An example of the QDM bias correction method is shown in **Figure 2.7**, where rainfall predicted by ACCESS1-0 GCM (RCP8.5) for the calibration period (1960-1999) was compared to observed rainfall from gauge 0002069 W. The effectiveness of the bias correction is demonstrated by the overall reduction in the number of small rainfall events (0-2 mm), with the majority of such events changed to zero rainfall. As described previously in **Section 2.3.3.2**, a unique set of 12 monthly adjustment factors derived for the driver rain gauge were applied to the bias-corrected GCM rainfall values to create a time series of catchment-specific daily rainfall values.

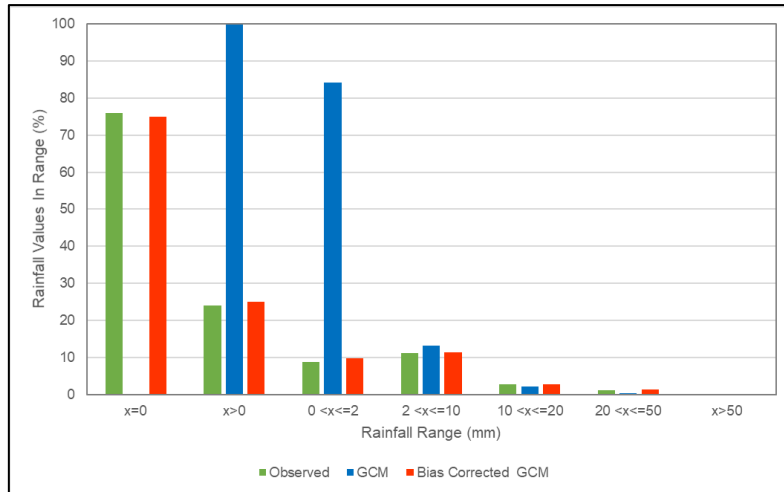


Figure 2.7 Comparison of daily rainfall distribution (raw and bias corrected) for the calibration period (1961-1999) obtained from ACCESS1-0 GCM (RCP8.5) compared to observed rainfall for rain gauge 0002069W (Wolski et al., 2021)

An analysis of the largest rainfall event predicted by each of the 6 GCMs for RCP8.5 is shown in **Table 2.8**. The bias correction method adjusted the largest rainfall totals for the baseline period (1961-1999) to 525 mm, which was measured on 28 September 1987 by gauge 0305308 W situated at Kwambonambi (Zululand coast in KwaZulu-Natal). For other rain gauges located mainly between Kwambonambi and Richards Bay, the September 1987 flood produced several record rainfall events ranging from 192 to 449 mm. This suggests that the 525 mm event is likely to be correct. Five GCMs unpredicted the largest rainfall event, with daily totals ranging from 357 to 493 mm. For GCM MPI, the largest event was decreased from 607 to 525 mm. The largest adjustment was made for GCM CCS in the present period (1961-1990), where the largest event was increased from 333 to 525 mm (192 mm adjustment).

Table 2.8 Largest daily rainfall value (uncorrected and corrected) obtained in each selected period for each GCM (RCP8.5)

GCM	Bias corrected (Y/N)	1961-1999	1961-1990	2015-2044	2070-2099
ACC	N	493	477	632	704
	Y	525	525	507	611
CCS	N	406	333	422	572
	Y	525	525	486	572
CNR	N	357	357	458	566
	Y	525	525	502	503
GFD	N	405	405	456	640
	Y	525	480	598	543
MPI	N	607	407	604	472
	Y	525	498	490	464
NOR	N	414	414	389	537
	Y	525	449	515	506

2.3.6.2 Temperature

For the temperature station assigned to each rain gauge, the observed maximum and minimum values were lapse-rate adjusted to account for the altitudinal difference between the two locations. Of the 1240 rain gauges that were assigned temperature stations, 156 were selected and compared to the GCM

temperature data from the nearest GCM grid point. The analysis showed that the GCM temperature data was biased and needed to be corrected.

The observed temperature data from 1961-1999 was then used to undertake a localised bias correction of the extracted GCM temperature time series. The Quantile Delta Mapping (QDM) method (described in the previous section) was again applied, but with an **additive** correction factor for temperature (as opposed to a **multiplicative** correction applied for rainfall). Thereafter, a lapse rate adjustment was performed to account for the altitude difference between the selected temperature station and the average altitude across each altitude zone.

The bias-corrected time series of GCM maximum and minimum temperature values for each temperature station was saved to a CSV file. Thus, a set of 1240 CSV files was created for each of the six GCM datasets and for both RCPs, which contained the following three variables:

- *date* (yyyy/mm/dd),
- *tmaxscr_BC* (bias-corrected GCM maximum temperature in °C), and
- *tminscr_BC* (bias-corrected GCM minimum temperature in °C).

An example of the QDM bias correction method is shown in **Figure 2.8**, where temperatures predicted by ACCESS1-0 GCM (RCP8.5) for the calibration period (1960-1999) were compared to observed temperatures rainfall from station 0002069 W. The first three ranges (on the left) demonstrate the correction applied to minimum temperature values. For this station, the GCM predicted much lower values than observed. Hence, the bias correction resulted in a substantial reduction in the number of days with minimum temperatures below ten °C and a corresponding increase in the number of days with values greater than 10°C.

The distribution of maximum temperatures predicted by the GCM was relatively similar to observations. The bias correction of maximum temperatures increased the number of days with values less than 20°C, and a decrease in the number of days in other temperature ranges. Overall, the bias correction improved the representation of daily maximum and minimum distributions over the calibration period.

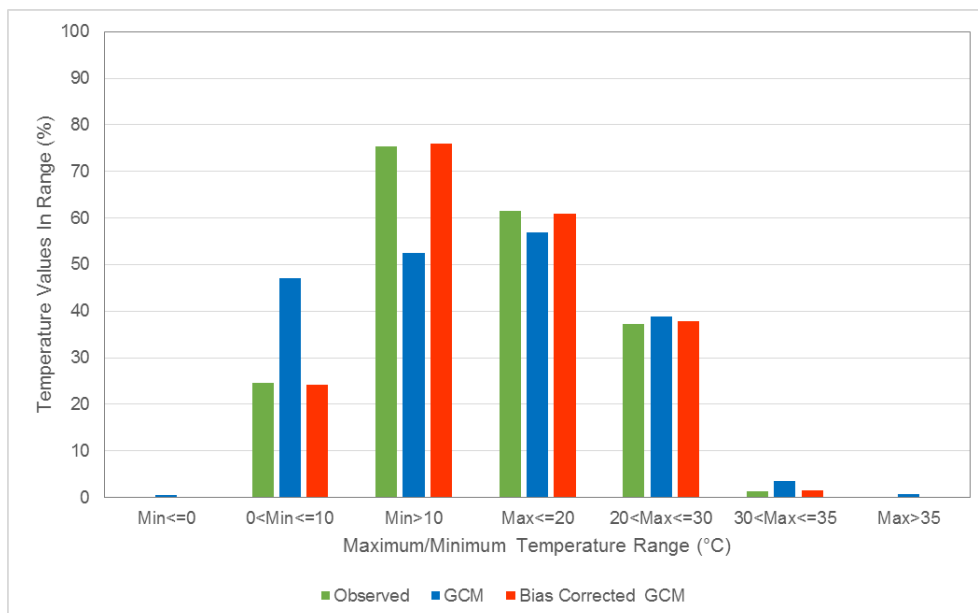


Figure 2.8 Comparison of daily temperature (maximum and minimum) distributions for the calibration period (1961-1999) obtained from ACCESS1-0 GCM (RCP8.5) compared to observed values for station 0002069W (Wolski et al., 2021)

To demonstrate the effectiveness of applying the QDM-based bias correction over the full GCM time series (1961-2099), annual mean temperatures were calculated from daily values. **Figure 2.9** shows the magnitude of the correction made to the annual means. For this temperature station, all GCMs underestimated temperatures across the historical calibration period and thus, the bias correction resulted in higher annual means. Furthermore, the bias is greater in the maximum temperatures than in the minimum temperatures.

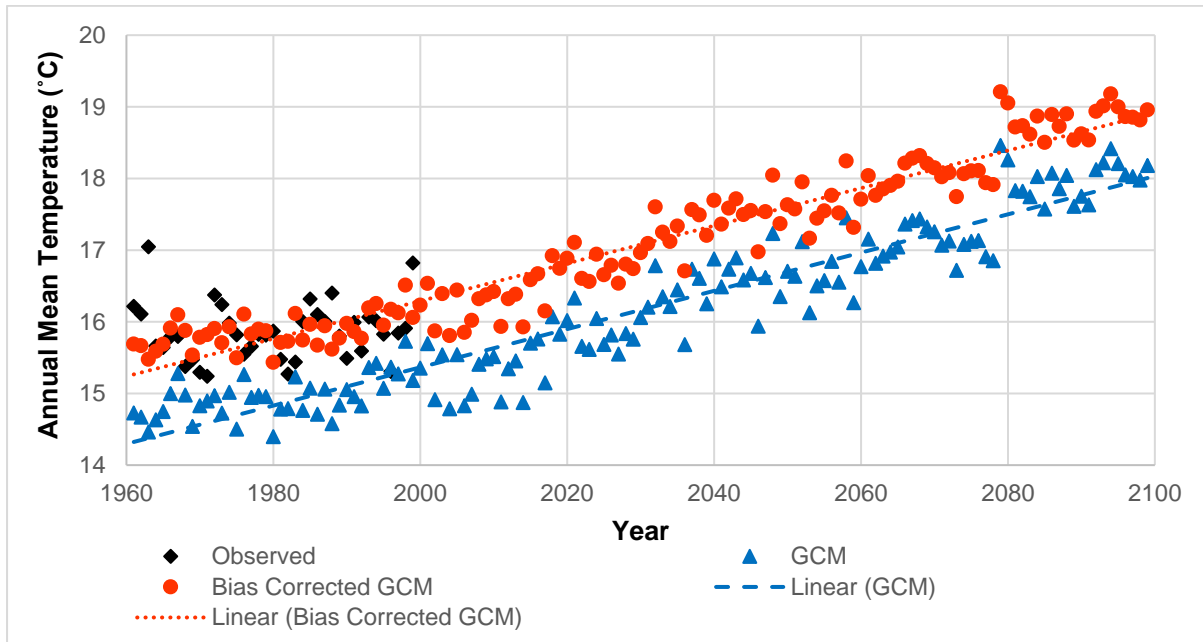


Figure 2.9 Comparison of annual mean temperatures (raw and bias corrected) for the calibration period (1961-1999) obtained from ACCESS1-0 GCM (RCP8.5) as compared to observed values for station 0002069W (after Wolski et al., 2021)

2.3.7 Generation of climate files

2.3.7.1 Lapse rate adjustment

A lapse rate adjustment was then applied to the bias-corrected temperature to account for the difference in mean altitude across the altitude zone and the GCM grid (or pixel). The purpose of this adjustment was to estimate more representative (i.e. catchment-specific) temperature values for each altitude zone.

2.3.7.2 Reference evapotranspiration

Daily solar radiation and relative humidity (maximum and minimum) values were then generated from the lapse-rate adjusted temperatures using the method described by Schulze et al. (2011). Due to the lack of wind speed data, a daily default value of 2 m s^{-1} was used, as suggested by Allen et al. (1998). Daily reference evapotranspiration values (ET_0) were then calculated using the FAO56 version of the Penman-Monteith equation (Allen et al., 1998).

2.3.7.3 Combining the climate data

The final step required generating climate files for ACRU and AquaCrop input. For each GCM, this involved reading the 1) bias-corrected rainfall, lapse-rate adjusted (and bias-corrected) temperatures and ET_0 data and combining the daily values to create an ACRU composite climate input file as defined by Smithers and Schulze (1995). The net result of all this work was the generation of 5838 climate input

files, i.e. one for each altitude zone. This was repeated for each of the 6 GCMs and both RCPs. Hence a total of 70056 files were created, each approximately 2.12 MB in size (145.4 GB in total).

According to Raes et al. (2017), AquaCrop requires a climate (.CLI) file, which contains the names of the daily rainfall (.PLU), air temperature (.TNX), reference evaporation (.ETo) and atmospheric CO₂ (.CO2) files. The format of the .PLU, .TNX and .ETo files are similar, with five header lines that provide station details, but more importantly, the start date of the climate record. A utility was developed in FORTRAN to convert the climate data from ACRU format to that required by AquaCrop, which required the creation of 280224 files (70056 x 4 files totalling 159.8 GB).

2.3.7.4 Summary

The above sections highlight the complexity of creating input climate files for simulation models using output from six GCMs for two RCPs, which was not a trivial exercise. The total number of files read and written (i.e. created) in this process is summarised in **Table 2.9**.

Table 2.9 Summary of number of files read and written in generating ACRU and AquaCrop climate input files

Data file type	Description	Files read	Files written
Observed rainfall data	1240 stations	1240	
Observed temperature data	1240 stations	1240	
NetCDF	2 RCPs x 6 GCMs x 139 years x 12 months	20016	
Extracted GCM data	2 RCPs x 6 GCMs x 1207 grid points (read twice: 1 x rainfall, 1 x temperature)	28968	14484
Bias corrected rainfall	2 RCPs x 6 GCMs x 1240 stations	14880	14880
Bias corrected temperature	2 RCPs x 6 GCMs x 1240 stations	14880	14880
ACRU composite file with: a) bias corrected rainfall b) lapse rate adjusted temperature	2 RCPs x 6 GCMs x 5838 altitude zones	29760	70056
ACRU composite file including: c) reference evapotranspiration	2 RCPs x 6 GCMs x 5838 altitude zones	70056	70056
AquaCrop .CLI, .PLU, .TNX and .ETo files	2 RCPs x 6 GCMs x 5838 altitude zones	70056	280224
Total		251096	464580
		715676	

2.3.8 Issues with RCP4.5

The GCM climate projections underwent two bias corrections applied at the following:

- 1) monthly level by the CSIR, by comparison to CRU historical data for each 0.5° pixel, and
- 2) daily level by UKZN, by comparison to historical data for each altitude zone.

The above two bias-corrected GCM datasets for both RCPs (4.5 and 8.5) were then evaluated by CSAG (UCT, Cape Town). The evaluation focused on annual rainfall totals and mean annual precipitation determined for climate stations located in each of the nine designated Water Management Areas (WMAs) of South Africa, as shown in **Figure 2.10**. Daily rainfall data from each climate station was aggregated to hydrological years, from which an unweighted average of annual totals was calculated for all stations falling within each WMA. To compare the different datasets, 30-year moving averages of WMA-averaged annual rainfall were calculated.

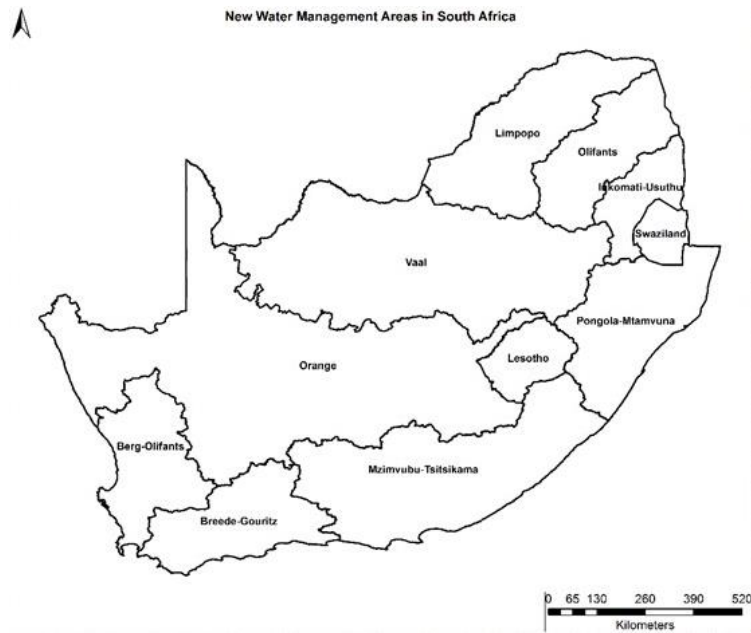


Figure 2.10 Designated Water Management Areas of South Africa

The dynamically downscaled climate projections produced by the CSIR's CCAM model was bias corrected against the historical CRU (gridded) database at the monthly level. This 6-member ensemble was evaluated by comparing annual rainfall totals against members of the CMIP5 ensemble, which were averaged across each WMA. As shown in **Figure 2.11** for RCP8.5, all six CCAM projections fall within the CMIP5 envelope containing 21 members.

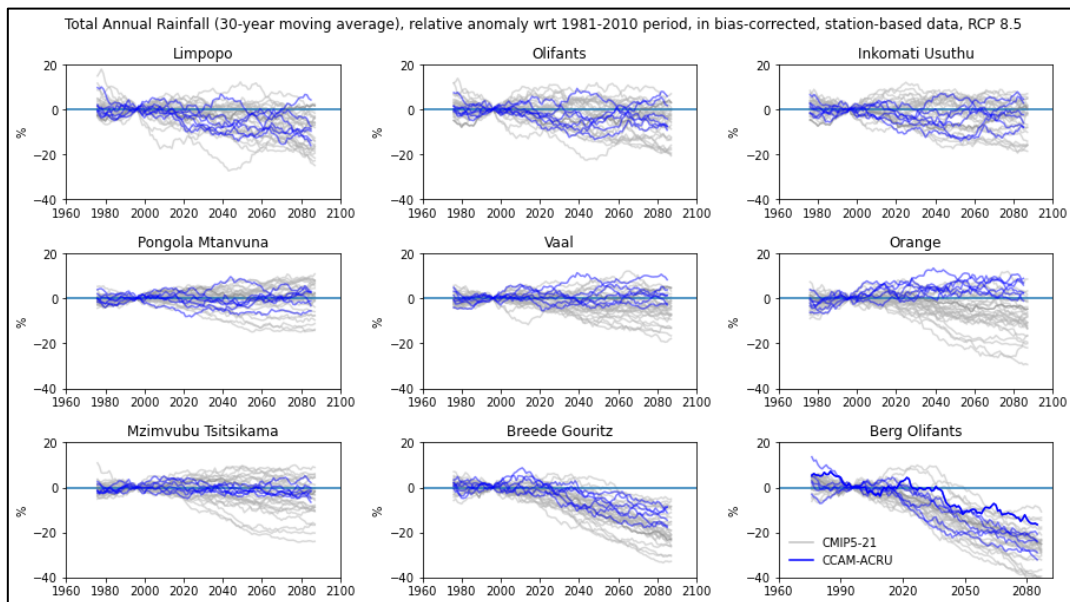


Figure 2.11 Comparison of annual rainfall totals derived for six CCAM-CRU datasets (RCP8.5) against the 21-member CMIP5 envelope and spatially averaged across each WMA (Wolski et al., 2021)

However, **Figure 2.12** for RCP4.5 clearly shows that the CCAM-CRU projections over the Limpopo, Olifants and Inkomati Usuthu WMAs extend beyond the range (or envelope) projected by CMIP5 (with 21 members). The climate projections follow a different "trajectory" into the future compared to the CMIP

ensemble, but only in certain WMAs (not all). In other words, the trend in the raw and bias corrected rainfall datasets diverged in some WMAs.

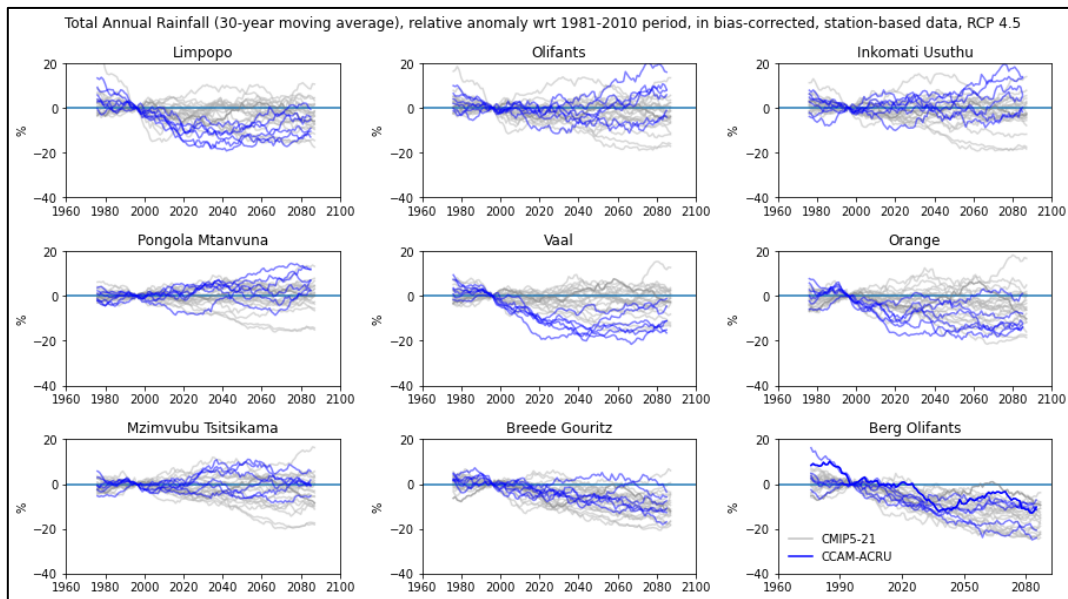


Figure 2.12 Comparison of annual rainfall totals derived for six CCAM-CRU datasets (RCP4.5) against the 21-member CMIP envelope and spatially averaged across each WMA

The problem becomes clearer at the daily level, as illustrated in **Figure 2.13**. Two daily rainfall indices were calculated for climate station 0512481 W (located in the Limpopo WMA), namely 1) mean daily rainfall on rain days with more than 1 mm, and 2) the number of rain days > 1 mm. There is a clear systematic difference between the pre-2005 (historical) and post-2005 (future) period (2005 is the year in which the climate projections start) for RCP4.5 (blue line), whereas RCP8.5 maintains continuity between these two periods (orange line).

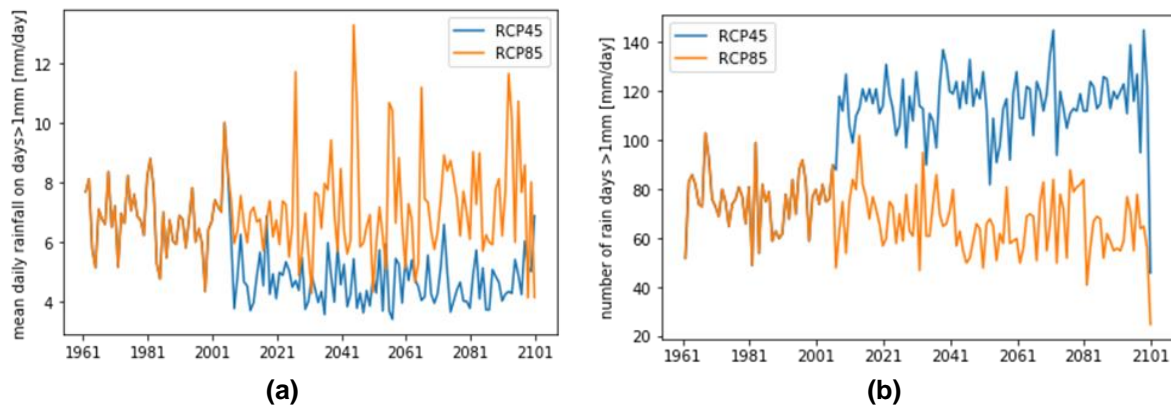


Figure 2.13 (a) Mean daily rainfall and (b) number of rain days calculated on days with rainfall above 1 mm for station 0512481 W using the CCS derived projections for RCP4.5 (blue) compared to RCP8.5 (orange)

In **APPENDIX C**, these two indices (mean daily rainfall mean rain days) were mapped for each of the six GCMs, as the ratio of the post-2005 to pre-2005 values. They clearly illustrate very strong future:past differences in RCP4.5, whereas RCP8.5 does not exhibit such differences. These figures show that the problem pertains to the entire country. The analysis at the WMA level only exposes the problem in some parts of the country.

The bias correction of rainfall and temperature undertaken by UKZN was applied to both the RCP4.5 and 8.5 datasets. However, the problem resides with RCP4.5 only, meaning the UKZN bias correction is not the issue. This was confirmed by calculating the ratio of total annual rainfall calculated from the UKZN bias-corrected dataset to those for the CSIR bias-corrected dataset. As shown in **Figure 2.14**, the same pre- and post-2005 problems are evident.

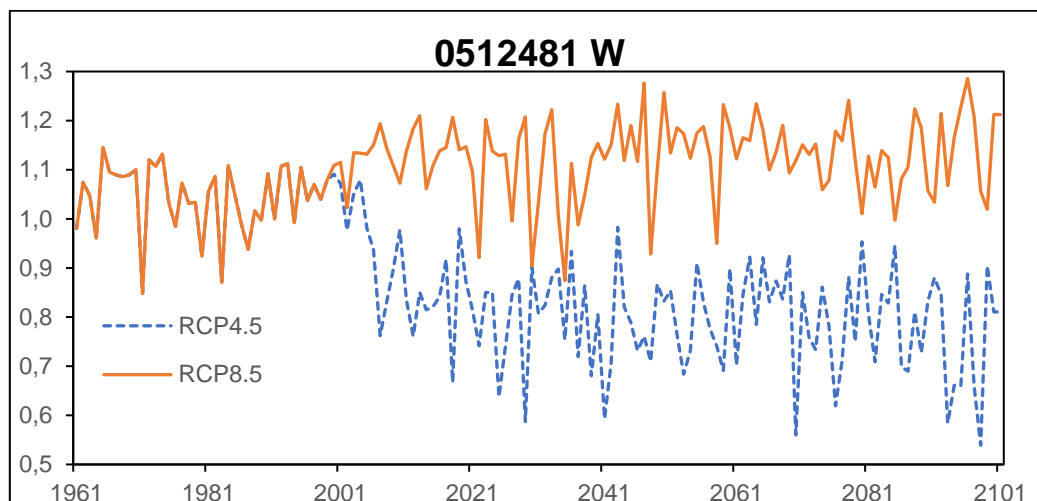


Figure 2.14 The ratio of UKZN- to CSIR-bias corrected total annual rainfalls for a selected location (0512481W) and GCM (CCS)

Wolski et al. (2021) also showed that a) more severe patterns of changes in rainfall were noted for RCP4.5 than RCP8.5, and b) RCP4.5 rainfall maps show a wetting trend over KwaZulu-Natal, Mpumalanga and parts of Limpopo that is completely absent in the RCP8.5 maps. In addition, rainfall maps produced by Schütte et al. (2021b) for RCP4.5 are inconsistent with those produced in other studies (e.g. Engelbrecht, 2019; Engelbrecht et al., 2020). Wolski et al. (2021) concluded that the RCP4.5 dataset supplied by the CSIR to WRC Project No. K5/2833 was not the same as that presented in previous publications where the data were originally developed and described. The CSIR attempted to locate the correct RCP4.5 dataset to accompany the RCP8.5 dataset supplied to WRC Project No. K5/2833. However, this dataset could unfortunately not be located. It is believed that the correct RCP4.5 dataset may have been accidentally deleted to urgently increase storage space on the CSIR data server. For more information, the reader is referred to Wolski et al. (2021).

In addition, the CSIR were unable to re-run the CCAM model for RCP4.5 due to a lack of time and resources needed for this computationally expensive task, as the CSIR were at the time, busy downscaling CMIP6 GCMs. The use of CORDEX climate scenarios for RCP4.5 was also not possible as they would not be comparable to the CSIR's RCP8.5 projections. Due to time constraints in this project, it was also not possible to re-run AquaCrop using CORDEX projections for both RCP8.5 and 4.5. Hence, for this project, climate projections representing RCP8.5 were only used to assess the impact of climate change on crop response.

2.4 Crop parameter files

As noted in **Section 1.3**, 13 drought tolerant and nutrient-dense underutilised crops have been targeted and prioritised for future research, development and innovation (Modi and Mabhaudhi, 2016). Calibrated and validated crop parameter files for South African growing conditions exist for amaranth, bambara groundnut, sorghum, sweet potato, and taro. It is important to note that these crop parameters were developed as part of other WRC-funded research projects and, in some cases, have been published in peer-reviewed journals (**Table 2.10**). It is worth noting that the AquaCrop model has been calibrated and validated for other underutilised crops such as:

- cassava (Wellens et al., 2022),
- cowpea (Kanda et al., 2021),
- groundnut (Chibarabada et al., 2020),
- pearl millet (Modi and Mabhaudhi, 2013),
- potato (Razzaghi et al., 2017),
- quinoa (Geerts et al., 2009), and
- sweet potato (Beletse et al., 2011; 2013).

Table 2.10 Source of existing crop parameter files for underutilised indigenous crops

Crop	Landrace/ cultivar	WRC Project	Source
Amaranth	<i>Amaranthus cruentus</i>	K5/1771 (Modi and Mabhaudhi, 2013)	Bellow and Walker (2017)
Bambara groundnut	Jozini red landrace	K5/1771 (Modi and Mabhaudhi, 2013)	Mabhaudhi et al. (2014b)
Sorghum	PAN8906	K5/2491 Kunz et al. (2020)	Kunz et al. (2020)
Taro	Dumbe dumbe (eddoe type landrace)	K5/1771 (Modi and Mabhaudhi, 2013)	Mabhaudhi et al. (2014a)

For certain underutilised crops (e.g. bambara groundnut and sorghum), AquaCrop has been calibrated and validated elsewhere (i.e. international studies). However, “fine-tuning” of crop parameters was undertaken to match local conditions, thus ensuring that realistic yield estimates are obtained.

2.4.1 Amaranth

Bellow and Walker (2017) calibrated AquaCrop for amaranth (*Amaranthus cruentus*) using greenhouse, lysimeter and field experiments carried out at Free State University (Bloemfontein). Irrigated field experiments were conducted during the 2008/09 and 2009/10 seasons, while pot experiments were carried out in 2010/11 season. These datasets were collected as part of WRC Project No. K5/1771 (Modi and Mabhaudhi, 2013). The pot and field data sets were used for parameterisation, calibration and validation of the model. The model was adequately calibrated for biomass and cumulative evapotranspiration (ET) under irrigation and rainfed conditions. Canopy cover was moderately simulated (RMSE = 20.8%; ME = 0.11; $R^2 = 0.577$; $d = 0.75$; MAPE = 43.4%). During validation, the model was also able to adequately predict biomass (RMSE = 1.96 t ha⁻¹; ME = 0.89; $R^2 = 0.92$; $d = 0.91$; MAPE = 24.1%) and ET (RMSE = 76.5 mm; ME = 0.76; $R^2 = 0.91$; $d = 0.91$; MAPE = 37.61%). The prediction of soil water content by the model was moderate (RMSE = 50.62 mm; ME = 0.19; $R^2 = 0.30$; $d = 0.67$; MAPE = 40.09) but needs improvement. Bellow and Walker (2017) recommended that datasets from other agro-ecological regions be used to improve calibration and validation for this crop.

Nyathi et al. (2018) also calibrated (2013/14 season) and validated (2014/15 season) for amaranth using data collected in Pretoria over two consecutive seasons. The experiments were conducted to assess the effect of two water levels (well-watered and water-stressed) on nutritional water productivity and calibrate and validate AquaCrop for repeatedly harvested leaves of amaranth. Data was collected as part of WRC Project No. K5/2171 (Nyathi et al., 2016). Total dry leaf mass was obtained from four-leaf harvests during each season. For the calibration, statistical indicators suggested that AquaCrop was able to simulate canopy cover with acceptable accuracy for well-watered (RMSE = 0.06%; RSR= 0.04; $R^2 = 0.99$) and water-stressed (RMSE = 1.24%; RSR= 0.05; $R^2 = 0.98$) treatments. In addition,

there was a strong agreement between measured and simulated soil water content for both treatments ($1.43 \leq \text{RMSE} \leq 1.48 \text{ mm m}^{-1}$; $0.07 \leq \text{RSR} \leq 0.10$; $0.87 \leq R^2 \leq 0.93$). These statistics suggest that AquaCrop was calibrated satisfactorily.

For the validation, AquaCrop simulated canopy cover better for the well-watered treatment (RMSE = 1.26%; RSR= 0.12; $R^2 = 0.98$), compared to the water-stressed treatment (RMSE = 1.65%; RSR= 0.79; $R^2 = 0.64$). However, soil water content was adequately simulated for both treatments ($1.44 \leq \text{RMSE} \leq 1.56 \text{ mm m}^{-1}$; $0.06 \leq \text{RSR} \leq 0.10$; $0.80 \leq R^2 \leq 0.88$). For both calibration and validation, the model was able to simulate dry edible biomass well ($0.02 \leq \text{RMSE} \leq 0.05 \text{ t ha}^{-1}$; $0.09 \leq \text{RSR} \leq 0.79$; $0.64 \leq R^2 \leq 0.98$). Again, validation of the well-watered treatment produced better results than the water-stressed treatment. Nyathi et al. (2018) concluded that the model is limited in parameters for leafy vegetable crops. A crop module should be included in AquaCrop to account for sequential harvests in a single season.

In this study, the crop parameters developed by Bellow and Walker (2017) were used. However, there were large differences in certain parameter values, such as the upper temperature limit (30 vs 40°C) and maximum rooting depth (1.75 vs 0.80 m) between the two studies, i.e. Bellow and Walker (2017) vs Nyathi et al. (2018). The latter study obtained a much better fit between observed vs simulated canopy cover ($0.06 \leq \text{RMSE} \leq 1.24\%$) compared to the previous study (RMSE = 20.8%).

2.4.2 Bambara groundnut

2.4.2.1 International

Karunaratne et al. (2011) calibrated and validated AquaCrop for irrigated and water deficient bambara groundnut. Crop measurements of canopy cover, biomass and pod yield obtained from glasshouse experiments (2006 and 2007 at University of Nottingham, UK) and field experiments (2007/08 in Botswana) were used to calibrate the model. Model validation was undertaken using independent datasets from glasshouse (2002 and 2008) and field experiments (2002/03 in Swaziland) for different landraces. Although AquaCrop simulations for four different bambara groundnut landraces showed good agreement with observed data, some landraces showed significant under-estimation. Since landraces that originate from various locations exhibit diverse adaptations to agro-ecological zones, it is difficult to develop one set of parameters to adequately represent all underutilised landraces.

2.4.2.2 Local

Since AquaCrop was previously calibrated for bambara groundnut by Karunaratne et al. (2011), a “fine-tuning” of their crop parameters was conducted for South African (i.e. local) conditions. This work was undertaken as part of WRC Project No. K5/1771 (Modi and Mabhaudhi, 2013), with results published by Mabhaudhi et al. (2014b). For calibration purposes, controlled (pot), field and rain shelter experiments were conducted in 2010/11 at Ukulinga (University of KwaZulu-Natal, Pietermaritzburg), Hatfield (University of Pretoria, Pretoria) and the rainshelter facility owned by the Agricultural Research Council (ARC) in Roodeplaatt. Validation was undertaken using Ukulinga and the ARC data in 2011/12.

The calibration results showed a reasonably good fit for canopy cover and biomass with R^2 of 0.94 and 0.96, respectively. Therefore, the model was able to predict canopy cover and biomass reasonably well. Although the model over-estimated final biomass by 14% and yield by about 9% compared to observations, this was regarded as acceptable. The validation results also showed a good fit between simulated and observed canopy cover for the irrigated ($R^2 = 0.86$; $d = 0.96$) and rainfed ($R^2 = 0.95$; $d = 0.98$) field trials. Therefore, the model showed a very good simulation for rainfed production. Using data from the rainshelter experiments, model validation showed a relatively good fit between observed and

simulated canopy cover under varying water regimes (R^2 of 0.95, 0.90 and 0.81 for 100, 60 and 30% ETa, respectively). In all three cases, the model was shown to under-estimate canopy cover in the early and later parts of the season.

The model predicted final biomass and yield very well for bambara groundnut grown under irrigated and rainfed field conditions, strengthening the model's suitability for simulating yield response to water availability. However, the model over-estimated both biomass and yield in the rainshelter irrigation treatments, which may be due to the rainshelter's microclimate being affected by periodic closing and opening of the shelter during rainfall events. Mabhaudhi et al. (2014b) concluded that model performance under rainfed conditions makes it particularly suited for extrapolation to marginal agricultural production areas in South Africa and the region.

The crop parameter file for bambara groundnut was applied for assessing climate change impacts for the whole of South Africa (Mabhaudhi et al., 2016b). This study was done as part of the Climate Change Adaptation Handbook for South Africa (Schulze, 2016). Hence, the parameter values were not improved further as it has been calibrated, validated and successfully applied for South Africa.

2.4.3 Sorghum

2.4.3.1 International

Araya et al. (2016) conducted a study in Southwest Kansas to determine optimum limited-irrigation strategies for grain sorghum (unknown cultivar). Experimental datasets for grain sorghum were used to calibrate and validate AquaCrop. Calibration was done using growth and yield data measured in 2005 for the full and two deficit irrigation treatments. The inclusion of deficit irrigation treatments proved useful in estimating water stress factors. Crop phenological development was determined from field experiments. Canopy cover was estimated from LAI measurements for optimal growing conditions using the Beer-Lambert equation and an extinction coefficient (k) of 0.416. Since biomass data were not collected, WP^* was calibrated using stomatal conductance and canopy senescence and adjusted to 30 g m^{-2} to improve model predictions. The reference harvest index was set to 0.46, the most common value obtained under optimal growing conditions in 2005. In total, 11 crop parameters were adjusted by Araya et al. (2016).

Experimental data from the full and deficit irrigation treatments measured during the 2007 and 2010 growing seasons were used to validate the model. The goodness-of-fit statistics for model validation showed that soil water content was adequately simulated ($0.71 \leq R^2 \leq 0.98$; $0.66 \leq d \leq 0.94$), together with biomass ($0.44 \leq R^2 \leq 0.80$; $0.79 \leq d \leq 0.93$), yield ($0.26 \leq R^2 \leq 0.85$; $0.60 \leq d \leq 0.77$) and crop evapotranspiration ($0.91 \leq R^2 \leq 0.94$; $0.61 \leq d \leq 0.96$). Araya et al. (2016) concluded that the goodness-of-fit values for both calibration and evaluation datasets indicated that AquaCrop could be used to simulate biomass and yield and evapotranspiration of grain sorghum and soil water content.

2.4.3.2 Local

Hadebe et al. (2017) mentioned that local sorghum genotypes differ significantly in growth and development characteristics from the default sorghum in AquaCrop, and thus, specific crop parameters should be calibrated. Hence, using research funded by WRC Project No. K5/2274 (Modi and Mabhaudhi, 2017), they performed a partial calibration of AquaCrop for three grain sorghum genotypes using data collected during the 2012/13 season at Ukulinga. However, low yields were obtained due to low and erratic rainfall experienced over the late season, which caused relatively high water stress. Hadebe et al. (2017) validated their calibration using observations from field experiments conducted in the 2014/15 season. Once canopy senescence was triggered, AquaCrop simulated a rapid canopy decline, whereas, in reality, sorghum's canopy decline is deemed moderate. This resulted in a slight over-

estimation ($\leq 7.8\%$) of time to physiological maturity by the model. However, Hadebe et al. (2017) reported that AquaCrop significantly over-estimated crop yield of all three genotypes. For the late (January) planting, biomass and yield were significantly over-estimated by the model. For these reasons, the parameters' values obtained by Hadebe et al. (2017) were not used in this study.

As part of WRC Project No. K5/2491, Kunz et al. (2020) performed a partial calibration of AquaCrop for grain sorghum by utilising 11 sorghum parameters published by Araya et al. (2016), together with measured parameter values defining phenological growth stages for cultivar PAN8906. The authors then simulated final biomass and yield, which was then compared to observations obtained from a rainfed trial at Swayimane (KwaZulu-Natal) in the 2017/18 season. The model over-estimated the final biomass and yield of PAN8906 by 36.8% and 32.0%, respectively. Kunz et al. (2020) then used crop parameters developed by Hadebe et al. (2017) and showed that the model over-estimated the final biomass and yield by 280.2% and 295.4%, respectively. They concluded that AquaCrop produced improved simulations of final biomass and grain yield using parameters suggested by Araya et al. (2016) compared to those provided by Hadebe et al. (2017). For these reasons, crop parameters developed by Kunz et al. (2020) were utilised in this study.

2.4.4 Taro

As part of WRC Project No. K5/1771 (Modi and Mabhaudhi, 2013), Mabhaudhi et al. (2014a) calibrated and validated AquaCrop for taro. Taro was calibrated using measurements from optimum conditions at Ukulinga (irrigated) and ARC's rainshelter at Roodeplaas (100% ETa). Rainfed trials at Ukulinga and Hatfield were also used to fine-tune the calibrations. Validation was undertaken using data for rainfed taro obtained at Umbumbulu in 2007/08 and taro data from Ukulinga and the ARC in 2011/12.

AquaCrop simulated canopy cover under irrigated conditions reasonably well ($R^2 = 0.79$; $d = 0.92$) between predicted and observed canopy cover for taro under irrigated conditions. Simulated biomass and yield were respectively, 6 and 7% greater than observations. The results indicated the model could successfully predict the growth and yield of the taro landrace. The validation results showed the model could simulate canopy cover under irrigated conditions very well ($R^2 = 0.84$) but was not as accurate under rainfed conditions at Ukulinga in 2011/12. AquaCrop was unable to simulate the sharp decline in taro's canopy cover in response to water stress. However, an independent dataset obtained from Mare and Modi (2009) gave a very good fit for both biomass ($R^2 = 0.99$; $d = 0.99$) and yield ($R^2 = 0.98$; $d = 0.99$). Using data from Ukulinga and Roodeplaas, the model was shown to simulate both final biomass ($R^2 = 0.90$; $d = 0.88$) and yield ($R^2 = 0.96$; $d = 0.99$) relatively well. The low RMSE values also indicated very good model performance under rainfed conditions, which further strengthens the model's applicability in simulating rainfed or water-limited production

The crop parameter file for taro was applied for assessing climate change impacts for the whole of South Africa (Mabhaudhi et al., 2016a). The latter study was done as part of the Climate Change Adaptation Handbook for South Africa (Schulze, 2016). Hence, the parameters were not improved further as it has been calibrated, validated and successfully applied for South Africa.

2.5 Minimising computational expense

2.5.1 Background

This study required a relatively large number of model simulations to be performed, which is time-consuming without access to a high-performance computing system. According to Jones (2018), model performance can be dramatically improved on most computers by:

- running the model on a desktop PC as opposed to a laptop computer,
- dividing the simulation run into smaller tasks and spreading the smaller tasks across each processing core on the computer,
- instructing the model to read inputs from and write outputs to a small virtual disk drive defined in the computer's random-access memory (called a RAM drive),
- post-processing model output whilst it is temporarily stored on the RAM drive, and
- executing large runs in "batch" mode using scripts designed for Windows- or Linux-based PCs.

For WRC Project K5/1874, Kunz et al. (2015b) developed a methodology designed to improve the performance of model simulations, which incorporated some of the suggestions listed above. For WRC Project K5/2491, Kunz et al. (2020) made further improvements, reducing the time required to perform large model runs. A detailed explanation was provided by Kunz et al. (2020) to allow researchers working on other WRC-funded projects to implement and benefit from similar speed improvements. A summary of the methodology followed in this study is provided next.

2.5.2 Desktop PC vs laptop

It is well understood that laptops are typically slower than desktop PCs. This is mainly due to cooling issues that result from the need to keep laptops as thin and light as possible (i.e. portable). Hence, CPU's built into laptops have a reduced number of cores (and threads) compared to desktop PCs.

Model runs were conducted on a high-end computer running the MS Windows operating system for this study. This PC has a Core i9 CPU with ten cores (20 threads) capable of handling AVX-512 instruction sets. This CPU can process twice the number of data elements than an Intel AVX2 CPU and four times that of an SSE-based CPU. The PC also has 32 GB of RAM, which is adequate for working with a RAM drive.

2.5.3 Derivation of smaller tasks

Since the high-end PC has 20 threads, two were set aside for use by the operating system, while the remaining threads ran AquaCrop as 18 simultaneous simulations. This meant that each CPU thread ran approximately 324 (i.e. 5838/18) altitude zones.

2.5.4 Grouping of tasks

National runs of AquaCrop on the high-end PC undertaken by Kunz et al. (2020) showed that each of the 18 individual tasks was completed at different times, ranging from 482 to 633 minutes. Further investigation revealed that this range was mainly related to the season length (crop cycle). Model runs for cooler zones at higher altitudes (e.g. zones 1297 to 1620) took 1.31 times longer than runs for warmer zones at lower altitudes (e.g. zones 1 to 324). Therefore, it was important to limit the crop cycle to a maximum of 12 months, particularly in altitude zones where insufficient growing degree-days exist for the crop to reach physiological maturity.

2.5.5 Load balancing

Although all 18 tasks were started concurrently, the slowest task finished 152 minutes after the fastest task. The time that each of the 5838 output files was written to the RAM drive was analysed to determine which altitude zones could be grouped together, so that all 18 tasks would complete in similar times. Hence, Task 5 was assigned 267 altitude zones, which takes a similar time to run as the 381 zones in Task 1 (**Table 2.11**).

Table 2.11 Load balancing of 5838 altitude zones, allowing 18 concurrent runs of AquaCrop to finish at the same time

Task number	Altitude zone number		Number of runs
	Start	End	
1	1	381	381
2	382	715	334
3	716	1057	342
4	1058	1383	326
5	1384	1650	267
6	1651	1980	330
7	1981	2304	324
8	2305	2634	330
9	2635	2935	301
10	2936	3248	313
11	3249	3567	319
12	3568	3889	322
13	3890	4209	320
14	4210	4513	304
15	4514	4840	327
16	4841	5171	331
17	5172	5507	336
18	5508	5838	331

2.5.6 Ram drive size

For each altitude zone, AquaCrop requires input files containing climate data, soils data, crop parameters, and a project file that instructs the model when to start and end each seasonal simulation. AquaCrop outputs a file of monthly seasonal data, from which statistics are generated. Hence, a national run involving all 5838 altitude zones requires a total of 8 and 21 GB for the historical and future simulations, respectively (**Table 2.12**). Therefore, the decision was made to copy all input files (climate, soils, project) into memory (RAM) to speed up the model runs.

Table 2.12 File size of input and output files required to run AquaCrop for the historical (baseline) and future climates

Input/ Output	File type	File size (KB)	
		Historical (1950-1999)	Future (1961-2099)
Input	Climate	968	2748
	Soils	4	4
	Project	57	161
Output	Seasonal output	220	620
	Statistics	132	132
Sub-total (KB)		1381	3665
Total (GB)		7.69	20.40

2.5.7 Automation procedure

Kunz et al. (2020) reported that considerable effort was spent on automating the procedure whereby AquaCrop runs non-stop for all 18 tasks concurrently (i.e. parallel). The automation procedure was first

developed in 2015 using a UNIX emulator (called UWIN) running on MS Windows 7. In 2019, the automation procedure was modified to run on a different Unix emulator (called WSL) compatible with MS Windows 10. Approximately 8600 lines of code (in Unix and Fortran) was developed to automate the national model runs for AquaCrop. In addition, over 1400 lines of code were written to convert the climate input files from ACRU format to that required by AquaCrop (Kunz et al., 2020).

2.5.8 Model run time

Kunz et al. (2015a) reported that sequential runs of AquaCrop at the national scale for sorghum took 61.8 hours to complete for grain sorghum. The improvements made by Kunz et al. (2020), where the model is run simultaneously on a RAM drive, has reduced the run time to approximately 12 hours. This represents a significant reduction in computational expense.

2.6 Mapping of results

To re-cap, the AquaCrop model was run:

- to determine seasonal yield, water use efficiency and season length (i.e. crop cycle),
- for four underutilised indigenous crops, viz. amaranth, bambara groundnut, grain sorghum and taro (amadumbe);
- for all 5838 altitude zones, regardless of whether the zone is deemed suitable for crop production; and
- using input climate projections for six CMIP5 GCMs that were dynamically downscaled with the CSIR's regional climate model (CCAM), then bias-corrected against observed data from 1961-1999.

Despite the considerable effort in reducing computational expense by improving model performance (as described previously in **Section 2.5**), it was still not possible to run AquaCrop across all 5838 altitude zones with 139 years of climate input data for six GCMs. Therefore, the decision was made to run the model for the following three 30-year periods: 1961-1990 (present; PR), 2015-2044 (near future; NF) and 2070-2099 (distant future; DF). These three periods were also selected for WRC Project K5/2833 (Schütte et al., 2021a).

2.6.1 Change maps

Yields were simulated for three 30-year periods, viz. present (PR; 1961-1990), near future (NF; 2015-2044) and distant future (DF; 2070-2099). As discussed in **Section 3.1**, the present period is deemed to accurately represent the historical period due to bias correction of GCM climate projections. For each period, the average dry yield (t ha^{-1}) and coefficient of variation (CV in %) of inter-seasonal yields were determined, as well as other useful statistics (e.g. standard deviation, range, etc.). To reduce the number of maps that can be shown, the mean seasonal yield from each GCM was also averaged. This implies that equal weighting was given to each GCM.

Maps highlighting the change in average yield from 1) present to near future, 2) near future to distant future, and 3) present to distant future period were generated for each NUS. The yield (Y) change from PR to NF (for example) can either be expressed as a:

- percentage change ($100 \cdot (Y_{NF} - Y_{PR}) / Y_{PR}$), or
- ratio (Y_{NF} / Y_{PR}).

For altitude zones where averaged crop yields for the present (Y_{PR}) or near future (Y_{NF}) period are zero, the change cannot mathematically be determined. Such areas appear white on the maps and are labelled as “Undefined”.

2.6.2 Confidence maps

At present, it is not possible to verify the GCM climate projections. This can only be done in the future, when looking back at the past. However, the climate projections from each GCM can be compared for similarities and differences, by calculating and analysing the ratio of climate variables for different periods. For example, the ratio of mean annual precipitation for the near future to the present period was calculated for each GCM, from which other statistics were derived (e.g. average, standard deviation and coefficient of variation) as shown in **Table 2.13**.

Table 2.13 Average (ave), standard deviation (std. dev.) and coefficient of variation (CV) calculated from ratios of near future to present mean annual precipitation (MAP) from six GCMs for altitude zone 1, i.e. quinary catchment A10A1 (Schütte et al., 2021b)

GCM	MAP (mm)		MAP ratio (Near future to present)			
	Present (1961-1990)	Near future (2015-2044)	Ratio	Ave	Std. Dev.	CV (%)
ACC	601	577	0.96	0.98	0.07	7.37
CCS	595	548	0.92			
CNR	575	579	1.00			
GFD	576	641	1.11			
MPI	562	563	1.00			
NOR	592	526	0.89			

A low coefficient of variation (CV in %) implies that the individual GCMs give similar ratios, while a higher CV implies a large discrepancy among the ratios. In this project, classes of CV values were used to provide a simple confidence index (CI), as shown in **Table 2.14**. Whilst the categories are somewhat subjective; they indicate the relative confidence in the climate projections in terms of the agreement between the six GCMs. A similar approach has been used in other studies (e.g. Schütte et al., 2021a).

Table 2.14 Confidence index derived from the coefficient of variation (Schütte et al., 2021b)

Coefficient of variation (CV in %)	Confidence Index (CI)
< 5	Very high
5-10	High
10-20	Medium-high
20-30	Medium
30-40	Medium-low
40-50	Low
> 50	Very low

Schütte et al. (2021b) reported that CI values for MAP ratios of the near future to the present period range from medium-high (arid west) to very high (east), i.e. CV < 20%. The latter is particularly so along the eastern seaboard of the country and the coastal (and adjacent inland) regions of the Eastern Cape. For the distant future relative to the present period, the confidence indices are lower, especially near the southern borders of Namibia (Northern Cape) and Zimbabwe (Limpopo). In essence, there is a reduction in areas with very high confidence and an increase in areas of medium or medium-high

confidence. In contrast, the CI for temperature (and reference evapotranspiration) is very high (CV < 5%) across the entire country for both the near and distant future, relative to the present period.

3 RESULTS AND DISCUSSION

To better understand the impacts of climate change on agricultural response, it is important to first consider the projected changes in rainfall and temperature expected over the country and highlight the importance of bias correcting GCM projections.

3.1 Bias correction

As noted in the methodology, the Quantile Delta Mapping method was used to bias correct dynamically downscaled climate projections from six GCMs against observed (i.e. historical) data from 1961 to 1999. A comparison of observed vs bias corrected mean annual precipitation (averaged from six GCMs) for the present period (1961-1990) shows a strong correlation with an R^2 value of 0.993 (**Figure 3.1**). Similarly, respectively, R^2 values of 0.935 (**Figure 3.2**) and 0.956 (**Figure 3.3**) were obtained for maximum, and minimum temperatures bias correction. Surprisingly, the correlation was stronger for bias correction of rainfall using a multiplicative correction factor when compared to bias correction of temperature involving an additive factor.

These results highlight the success of the bias correction method and show that the present period can be used to represent historical conditions. Without bias correction, GCM projections for the present climate do not adequately represent historical conditions. This necessitated a different approach in representing climate change-related impacts in past assessment studies, where a common approach was to show a map of historical conditions, together with a change map as ratios of near future to present. For example, historical crop yields would need to be multiplied by this ratio to obtain estimates of future yields.

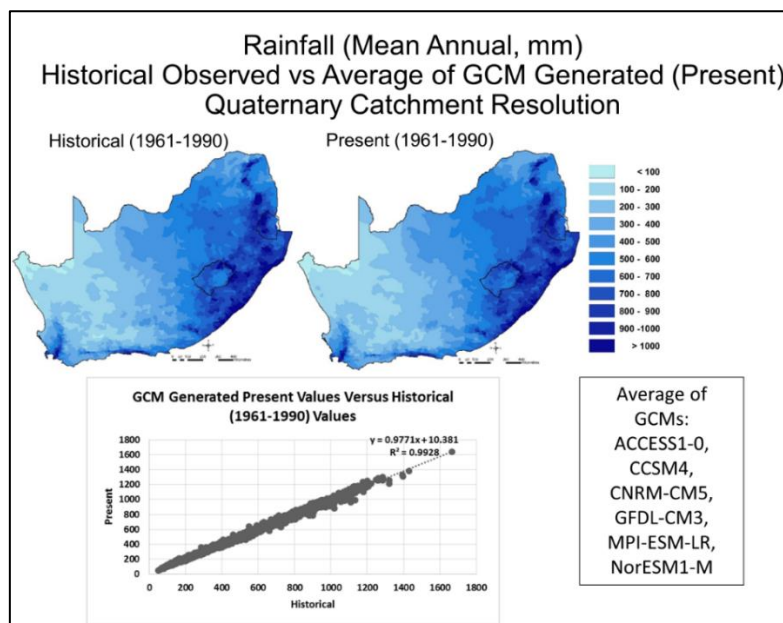


Figure 3.1 A comparison of mean annual precipitation derived from historical (i.e. observed) data (left) and that averaged from six dynamically downscaled and bias corrected GCMs (right) for the present period 1961-1990, together with a correlation between the two datasets (bottom) (Schütte et al., 2021b)

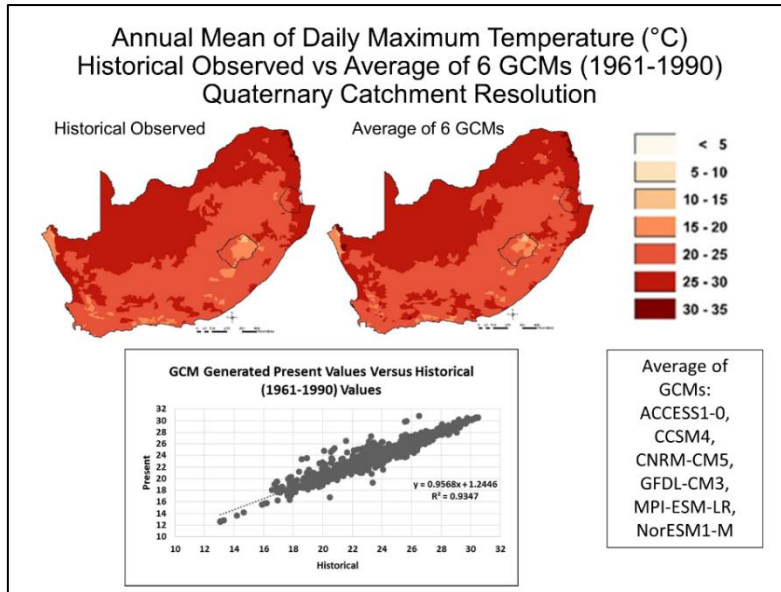


Figure 3.2 A comparison of annual means of daily maximum temperature derived from historical (i.e. observed) data (left) and that averaged from six dynamically downscaled and bias corrected GCMs (right) for the present period 1961-1990, together with a correlation between the two datasets (bottom) (Schütte et al., 2021b)

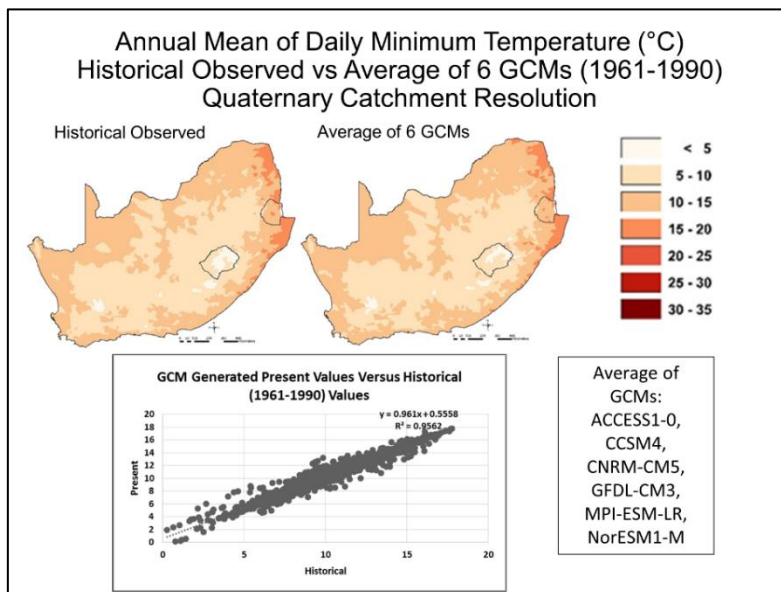


Figure 3.3 A comparison of annual means of daily minimum temperature derived from historical (i.e. observed) data (left) and that averaged from six dynamically downscaled and bias corrected GCMs (right) for the present period 1961-1990, together with a correlation (Schütte et al., 2021b)

3.2 Climate change projections

3.2.1 Rainfall

For each GCM, maps were developed that show relative changes (expressed in %) in projected mean annual precipitation (MAP) from present to near future ($100 \cdot \text{MAP}_{\text{NF}} / \text{MAP}_{\text{PR}}$) and present to distant future ($100 \cdot \text{MAP}_{\text{DF}} / \text{MAP}_{\text{PR}}$). These maps (not shown here) show similarities with reduced rainfall (i.e. drier

conditions) along the 1) west coast of South Africa, 2) northern regions of Limpopo, and 3) north-eastern areas of the Limpopo and Mpumalanga provinces. The projected drier conditions were more pronounced in the distant future (i.e. > 20% reduction in MAP). They increased in spatial extent to include most of the northern parts of the country along the border with Namibia and Botswana. However, increased rainfall (10-20%) is projected in the central reaches of South Africa, particularly to the west and north of Lesotho, especially for the GFD GCM. In the distant future, two GCMs (ACC and CCS) project increases in MAP in the north-eastern parts of Limpopo and Mpumalanga, whereas the remaining four GCMs project decreases.

To reduce the number of maps that can be shown, the average change in MAP was determined and expressed in both absolute (in mm) and relative (in %) terms, as shown in **Figure 3.4**. It shows a reduction in rainfall in the western and northern parts of the country, especially towards the distant future. Along the east coast, the changes are mixed. In the central interior (west and north of Lesotho), more rainfall is projected in the near future and even more in the distant future.

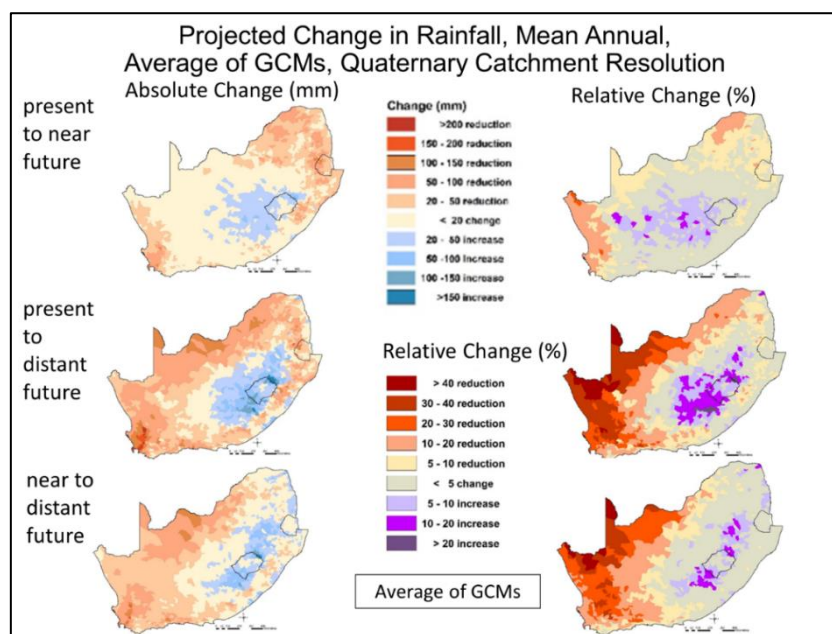


Figure 3.4 Averaged change in projected mean annual precipitation in absolute (mm on left) and relative (%) on right) terms from present to near future (top row), present to distant future (middle row) and near to distant future (bottom row) (Schütte et al., 2021b)

3.2.2 Temperature

There is a high degree of certainty that temperature will increase with climate change. The annual means of daily maximum and minimum temperatures represent broad indices of the environmental status of a location. GCM-based projections of maximum and minimum daily temperature in the near future (relative to the present climate) show increases of 1-2°C for most southern Africa. However, slightly higher increases of 2-3°C are projected for the country's northern parts near the Botswana border, more so for maximum than minimum temperatures (**Figure 3.5**). From the present to the distant future, projected changes range between 3°C at the coast to more than 6°C in the north-west for daily maximum temperatures, whilst minimum temperatures are also projected to increase by between 3°C at the coast and to up to 6°C in the north-west (**Figure 3.5**). Most of the warming is expected to occur from the near to distant future.

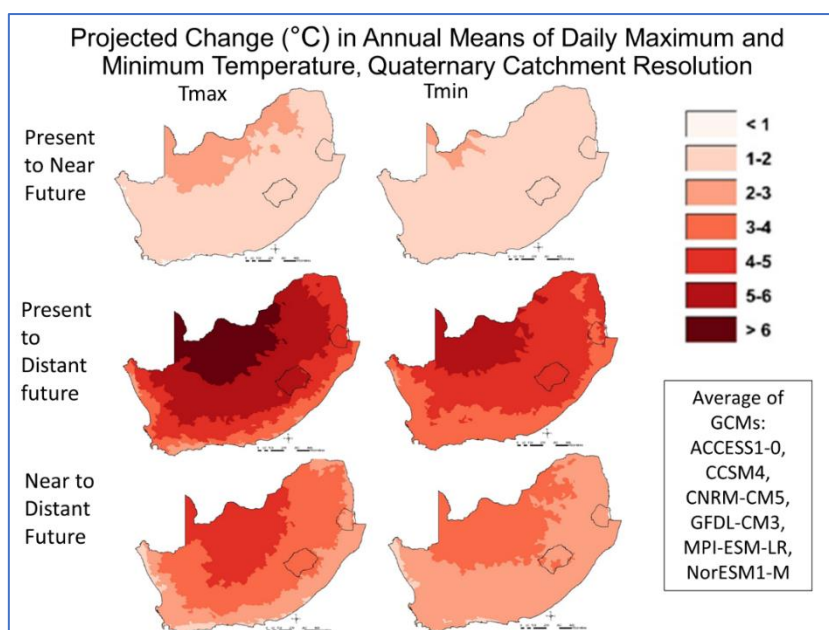


Figure 3.5 Averaged change in projected annual means of daily maximum (left) and minimum (right) temperatures (°C) from present to near future (top row), present to distant future (middle row) and near to distant future (bottom row) (Schütte et al., 2021b)

3.3 Climate change and crop yield

As noted in **Section 2.6.1**, maps were produced that express change from one time period to another as percentages and ratios. The percentage change maps are presented next in **Section 3.3.1** to **Section 3.3.3**, whilst the ratio maps are given in **APPENDIX D1**.

3.3.1 Present to near future

For each of the six GCMs, the mean seasonal yield was calculated for the present and near future periods. The six yield values were then averaged and used to calculate the relative change in each of the 5838 altitude zones. From **Figure 3.6a**, the model simulated non-zero yields in most altitude zones for amaranth (except for those in Lesotho), in contrast to the other three crops. This suggests that amaranth is more suited to a wider range of growing conditions than the other crops. However, the simulated yields may be very low (i.e. 0.01 to 0.10 dry t ha⁻¹) and thus, economically unviable.

In response to the projected warmer and drier climate conditions in the near future, amaranth yields are expected to decline by up to 10% across most of the Limpopo, Mpumalanga, Gauteng and North West provinces, including the northern regions of KwaZulu-Natal and Free State. In addition, yield declines of up to 30% may occur in certain parts of the Limpopo and North West provinces. For most KwaZulu-Natal and Eastern Cape, yield increases up to 10% were simulated, with larger improvements up to 30% in the western parts of the Free State and Eastern Cape provinces.

For bambara groundnut (**Figure 3.6b**), yield declines exceeding 50% are expected across most Limpopo and eastern Mpumalanga and the north-eastern parts of KwaZulu-Natal and North West provinces. However, the central and western parts of Mpumalanga and Free State can expect yields to more than double (> 100% change) and certain parts of KwaZulu-Natal and Eastern Cape. A review by Franke (2021) of 20 climate change studies over southern Africa cited the work of Mabhaudhi et al. (2018) that showed yields of bambara groundnut (including potato and sugarcane) are expected to increase. The bambara groundnut study was undertaken using AquaCrop for only one location in

KwaZulu-Natal with climate scenarios from five CMIP3 GCMs (A2 CO₂ trajectory). Hence, this work is superseded by that presented here.

Sorghum yields are expected to decline for most growing areas along the country's eastern seaboard, with the highest yield losses (> 50%) predicted for the Limpopo and eastern Mpumalanga provinces. Yield increases may occur in the central parts of the Eastern Cape and western regions of the Free State (**Figure 3.6c**). In contrast, taro yields should improve for most growing areas in Limpopo, North West and KwaZulu-Natal (except in the north-east and along the coast) provinces. However, taro is not suited to the central and western parts of Mpumalanga, central and southern regions of the Free State, south-western KZN and northern areas of the Eastern Cape province (**Figure 3.6d**). The review by Franke (2021) showed that changes in sorghum yield across southern Africa are highly variable and exhibit inconsistent patterns.

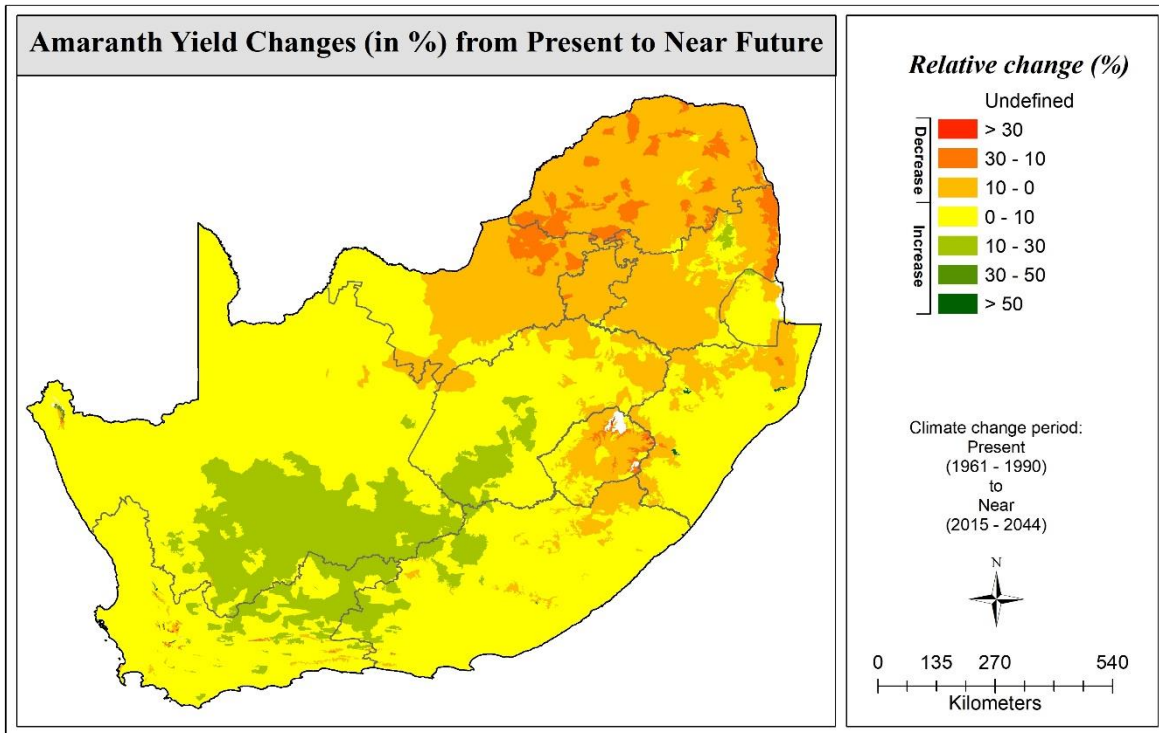
The results presented in this study for bambara groundnut, sorghum and taro supersede previous studies undertaken in 2016, which were derived using:

- AquaCrop version 4.0,
- an older version of the Altitude Zones Climate Database,
- climate scenarios from four CMIP3 GCMs that were statistically downscaled and not bias-corrected, and
- different 20-year climate periods, i.e. 1971-1990 (present) and 2046-2065 (intermediate future).

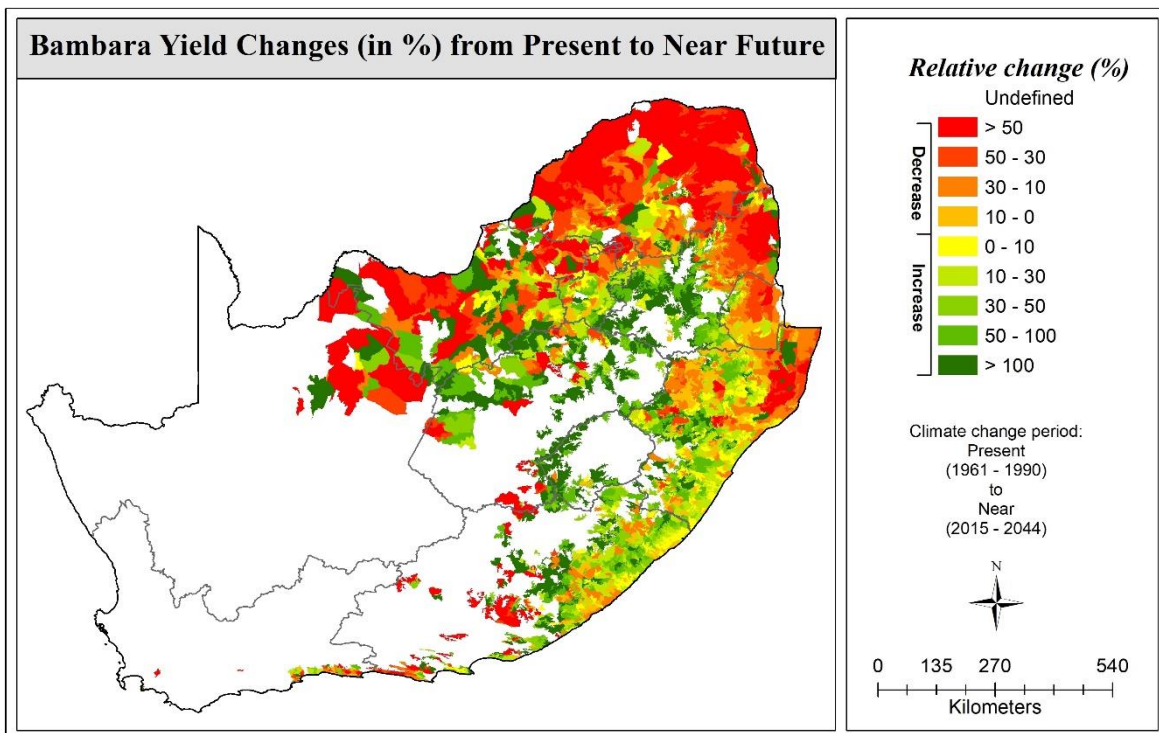
Kunz and Schulze (2016) reported increasing sorghum yields (ranging from 10 to over 100%) in the North West, Limpopo (southern and eastern), Gauteng, Mpumalanga (western), KZN (western) and Eastern Cape (northern and western) provinces. For the remaining areas along the eastern seaboard, no significant change in yield ($\pm 10\%$) was simulated. In contrast, this study predicts significant yield declines exceeding 50% for the North West, Limpopo and Gauteng provinces, and at least 30% lower yields in Mpumalanga, KZN and most of the Eastern Cape.

The results presented in this study for taro also supersede those developed by Mabhaudhi et al. (2016a), who showed more than a doubling of yield for production areas along the eastern seaboard of South Africa. However, in this study, lower yield increases of 50% or less were simulated for the same areas, and significant increases in areas deemed suitable for taro production, particularly in the Limpopo and North West provinces. Similarly, the climate change impact assessment by Mabhaudhi et al. (2016b) for bambara groundnut is also outdated, which showed yield increases of up to 10% for most of Limpopo and KZN, as well as higher yield increases in western Mpumalanga and eastern Free State. This is in contrast to the results of this study that show yield declines exceeding 30% for Limpopo and eastern Mpumalanga, yet increasing yields over 50% in western Mpumalanga and eastern Free State. There is also a significant reduction in areas deemed suitable for bambara groundnut production, particularly in the Mpumalanga and Free State provinces.

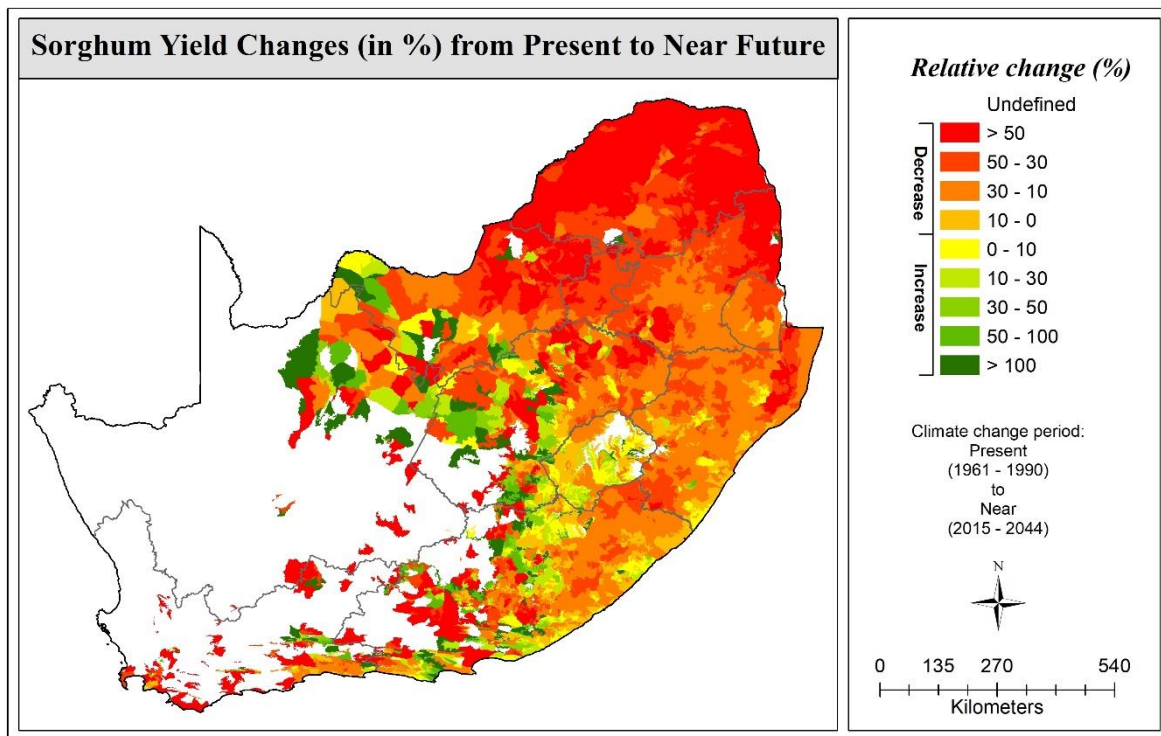
Besides the work undertaken in 2016, the authors are unaware of any other studies that assessed the impact of climate change on neglected and underutilised indigenous crops. Hence, this study represents the first assessment for amaranth and an updated assessment for bambara groundnut, sorghum and taro. Overall, yield declines in the Limpopo province are largely driven by drier conditions that may be expected in the near future relative to present conditions. Taro may benefit the most from projected changes in rainfall, temperature and reference evapotranspiration, followed by bambara groundnut, amaranth and sorghum. This implies that taro is more drought tolerant than sorghum.



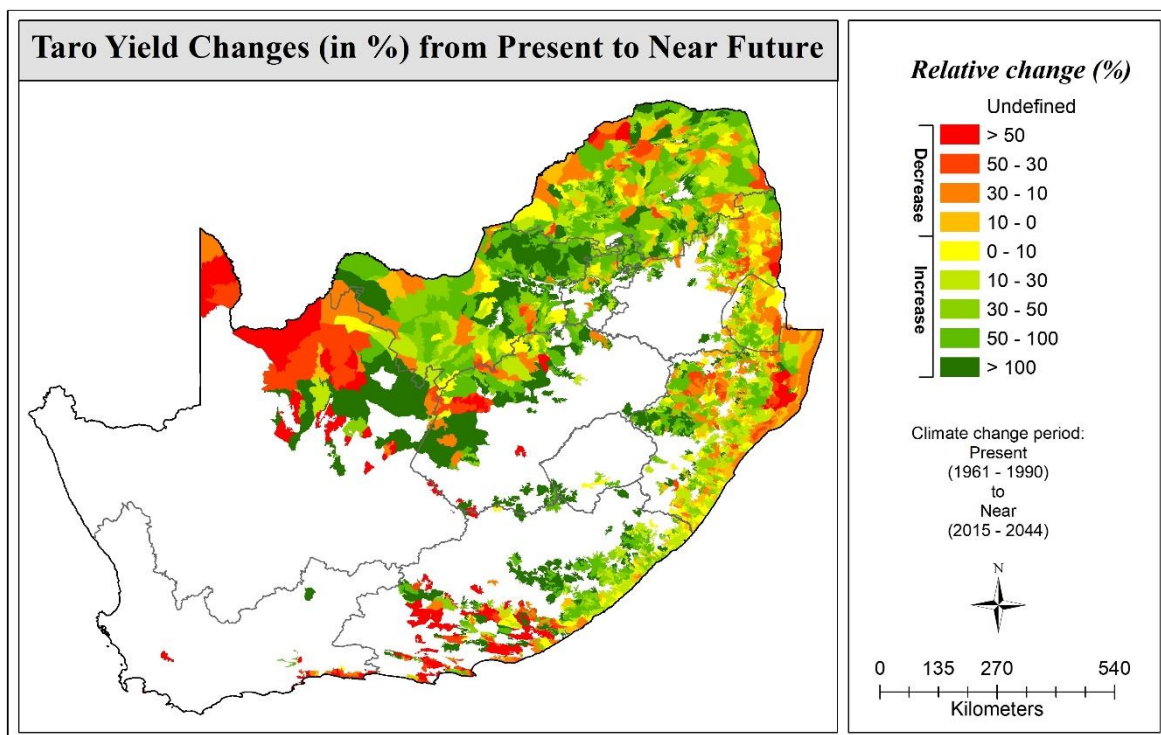
(a)



(b)



(c)



(d)

Figure 3.6 Change in mean dry yield (as %) from present to near future for (a) amaranth, (b) bambara groundnut, (c) sorghum and (d) taro

3.3.2 Near to distant future

From the near to the distant future, a reduction in rainfall is projected for most of the country, except for the central interior (north-east and south-west of Lesotho). Maximum temperatures may increase by 3-

5°C, compared to 2-4 °C for minimum temperatures. The drier and hotter climate is expected to negatively impact crop yield in general.

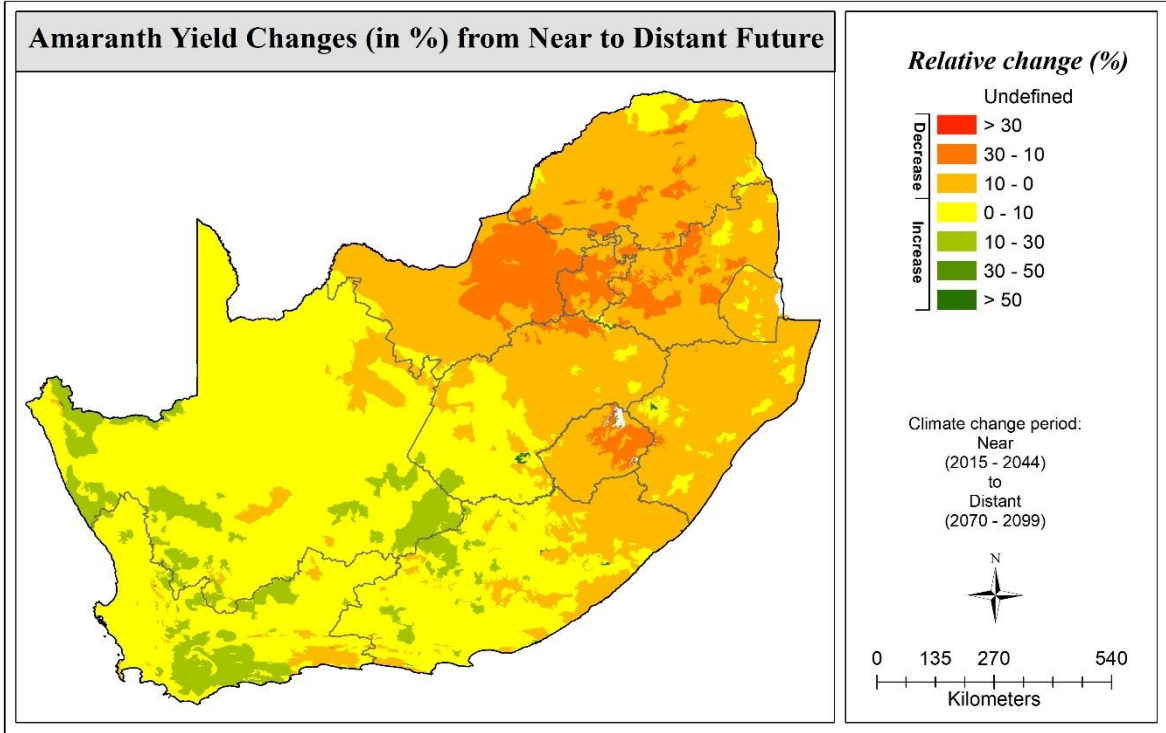
Compared to the present to near future scenario (**Figure 3.6a**), areas highlighted in yellow that show a 0-10% increase in yield have substantially reduced in spatial extent and indicate a yield decline by up to 10% (**Figure 3.7a**). This occurs mainly in eSwatini and the following provinces in South Africa: KZN (central and coastal), Free State (central), North West (western) and Eastern Cape (north-eastern). Similarly, areas showing a 10-30% decline in yield have expanded, especially those in the North West (eastern) and Mpumalanga provinces. There is a decline in areas where the yield is expected to increase by 10-30%, i.e. for altitude zones located in the Eastern Cape (western) and Free State (south-western).

For bambara groundnut (**Figure 3.7b**), there is a marked increase in areas deemed suitable for crop production, especially in Mpumalanga and Free State. Most of these “new” areas show a doubling of yield (> 100%) from the near to distant future (dark green). Furthermore, there is a large reduction in areas where the yield is expected to decline by 50% or more (red). Hence, this crop is expected to benefit from climate change.

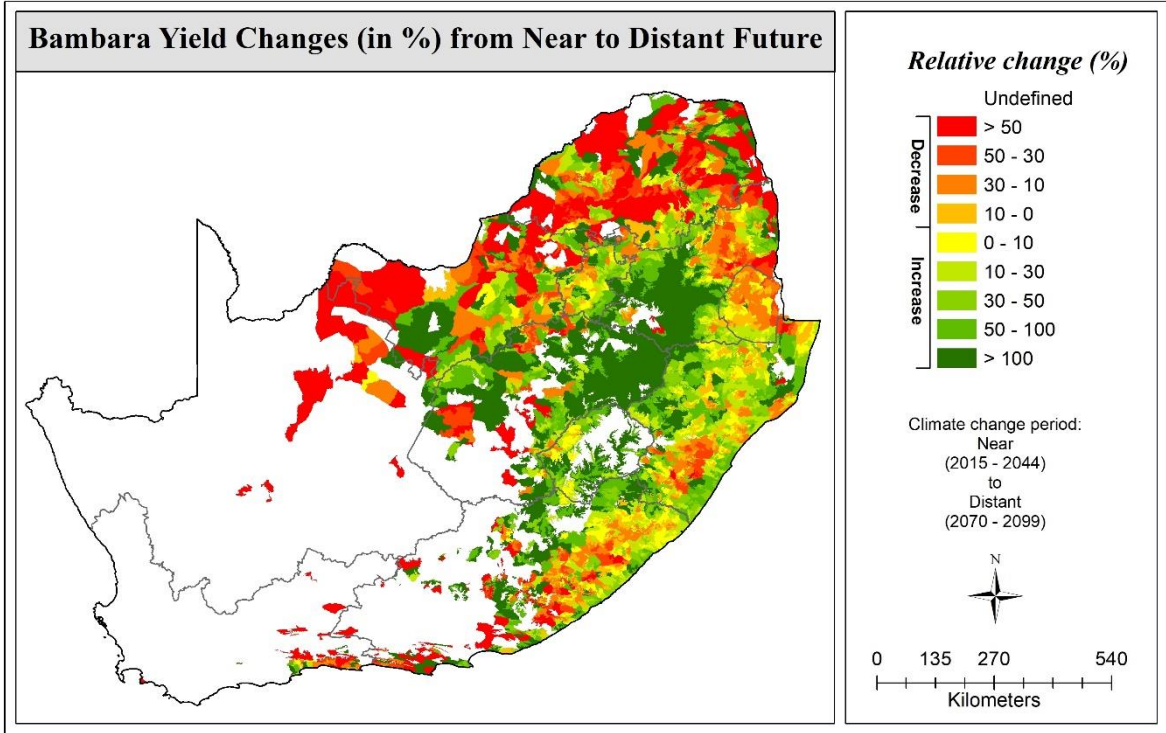
Comparing **Figure 3.7c** with **Figure 3.6c** for sorghum revealed that certain areas have changed from a yield decrease to a yield increase. Examples can be found in the north-eastern regions of Limpopo and Mpumalanga, northern and eastern regions of Free State and north-eastern KZN. Overall, areas with more than a 50% decrease in yield have reduced spatial extent, particularly in the North West, Limpopo and Mpumalanga provinces.

Similar to bambara groundnut, there is a marked increase in areas deemed suitable for taro production, especially in the Mpumalanga, Free State and Eastern Cape provinces (**Figure 3.7d**). Yields are expected to be more than double in these “new” areas in Mpumalanga and the Free State. However, in the western regions of the Eastern Cape and North West provinces, substantial reductions in yields were simulated, i.e. from increases to decreases in taro yield.

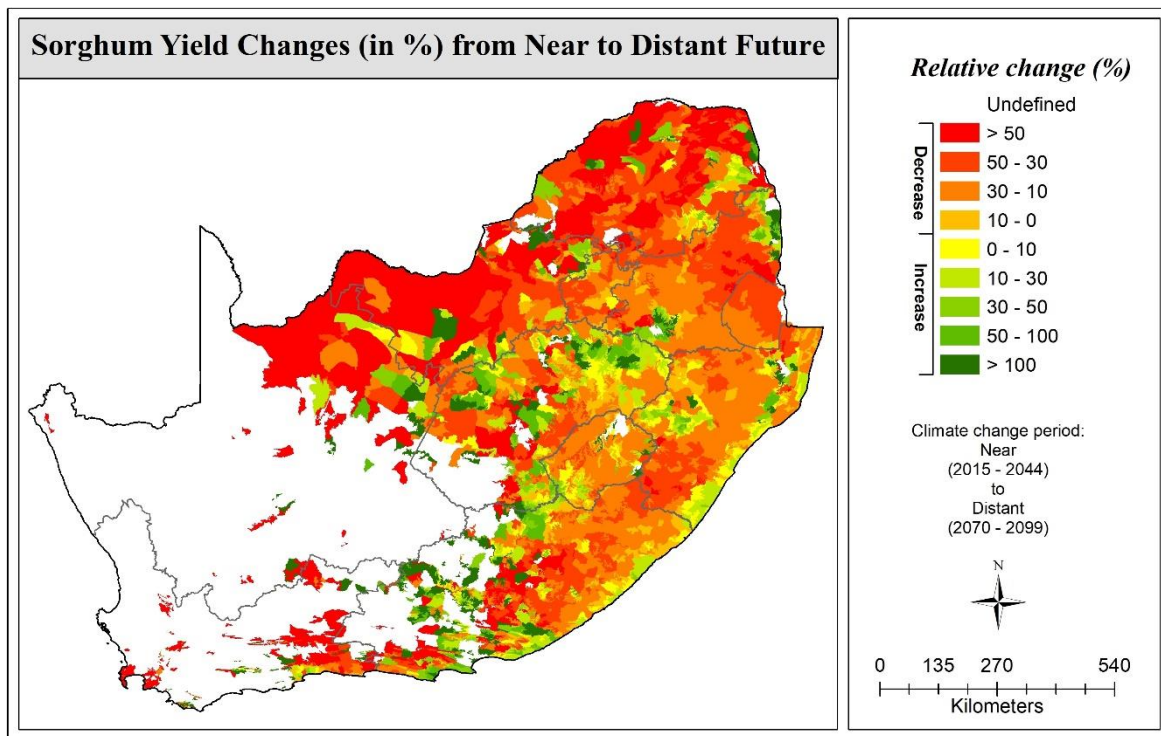
Overall, amaranth may not benefit from climate change, whereas sorghum production may respond positively to climate change. Both bambara groundnut and taro could benefit the most, with a large expansion in areas deemed suitable for crop production in the Mpumalanga and Free State provinces. These areas are likely too cold for crop production up to 2044, especially in the higher altitude zones. Of the four neglected and underutilised species, taro seems to benefit the most from climate change, particularly towards the distant future. However, it is important to note that confidence in yield changes into the distant future is much lower than those for the near future due to increasing uncertainty in climate projections towards the year 2100.



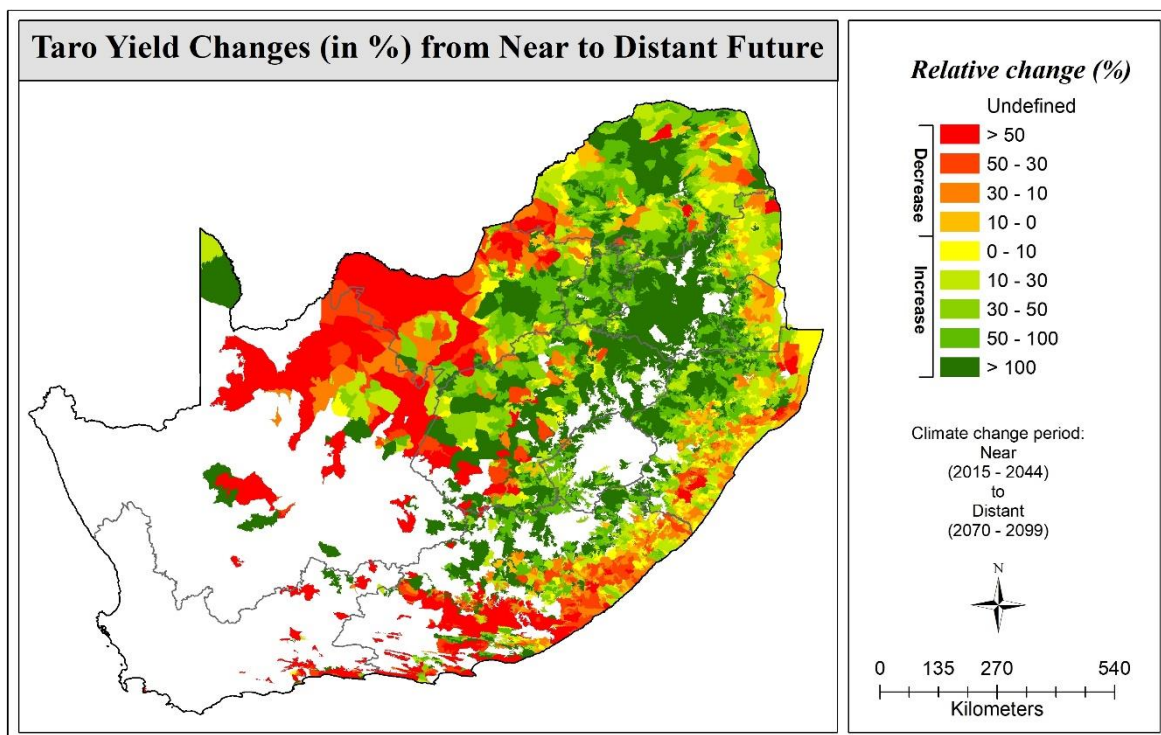
(a)



(b)



(c)



(d)

Figure 3.7 Change in mean dry yield (as %) from near to distant future for (a) amaranth, (b) bambara groundnut, (c) sorghum, and (d) taro

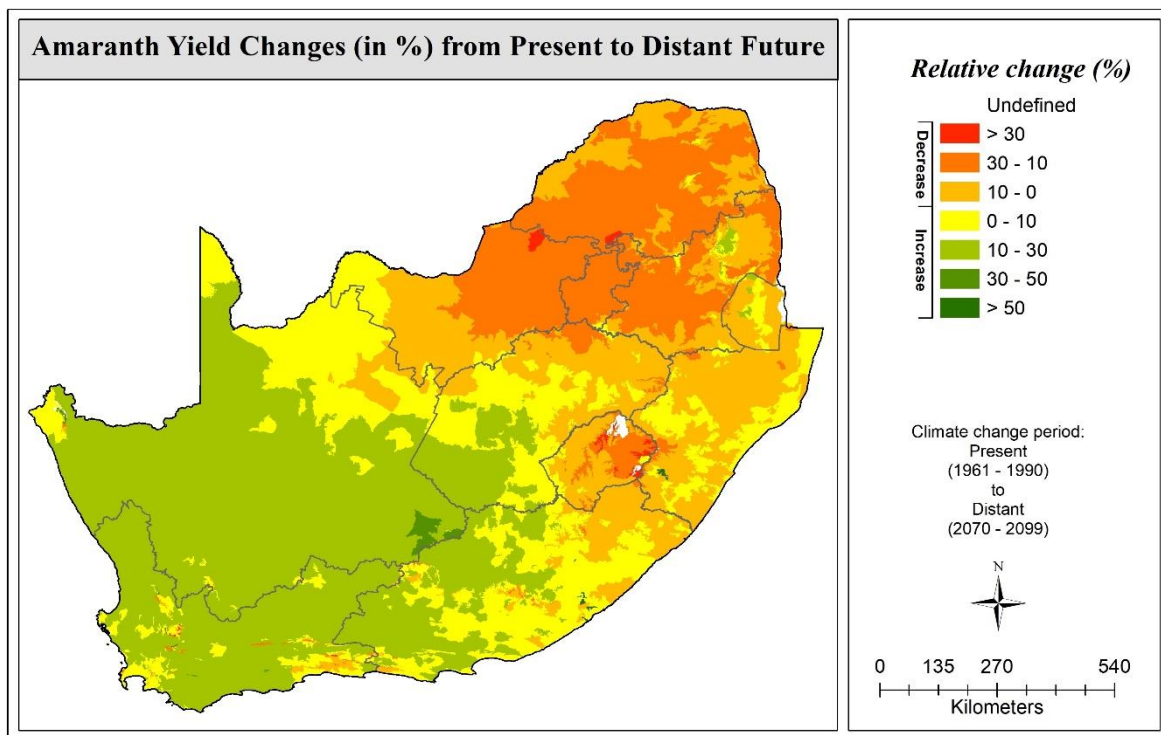
3.3.3 Present to distant future

The areas that can support rainfed crop production are mostly situated along the country's eastern seaboard. In addition, Gauteng and the central to eastern regions of the North West and Free State

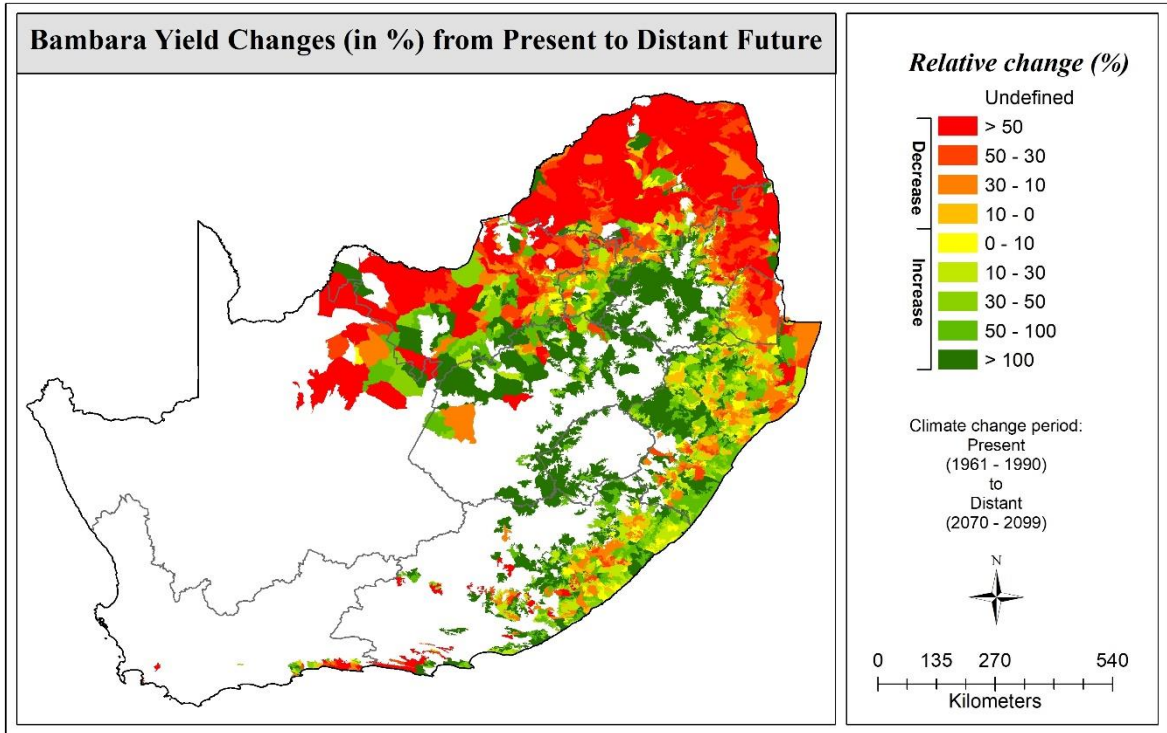
provinces can also support rainfed crop production. In other words, arable land located in the Limpopo, North West, Gauteng, Mpumalanga, KwaZulu-Natal and Eastern Cape provinces, where MAP exceeds 450 mm, are deemed suitable for rainfed crops. For most of these areas, simulations for the distant future compared to the present indicate the following trends:

- Amaranth yields could mostly decrease by up to 30%, especially in the northern provinces (Limpopo, North West, Gauteng and Mpumalanga), compared to a 0-10% yield increase in parts of the Free State, KZN and Eastern Cape (**Figure 3.8a**).
- Bambara groundnut yields may be more than halved (i.e. > 50% reduction) across most of the Limpopo, including eastern parts of the North West and Mpumalanga provinces, whereas yields may more than double (i.e. > 100% increase) in the Free State and western parts of Mpumalanga and KZN (**Figure 3.8b**).
- Sorghum yields may decline by at least 50% across the northern provinces of Limpopo, North West, Gauteng and Mpumalanga (central to western region), compared to yield increases up to 30% for parts of the Free State, western KZN and coastal areas of KZN and Eastern Cape (**Figure 3.8c**).
- Taro yields may more than double over large parts of the northern provinces and the western regions of the Free State and KZN, compared to yield declines being simulated for most other areas (especially in north-eastern KZN south-western parts of the Eastern Cape) (**Figure 3.8d**).

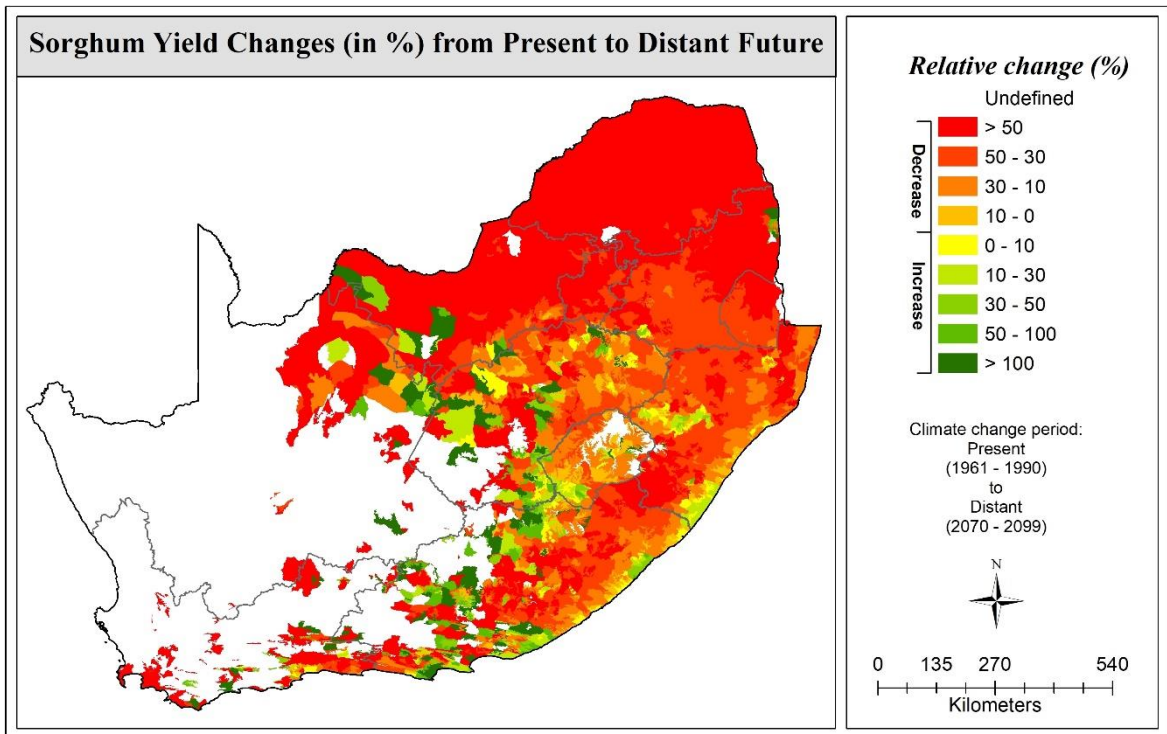
The present to distant future maps shown in **Figure 3.8** highlight the overall trends in yield changes that may result from climate change for areas that currently produce a non-zero averaged yield (i.e. $Y_{PR} > 0$ t ha⁻¹). In other words, these maps do not highlight the potential expansion (or contraction) in crop growing areas that may result from climate change, which is discussed further in **Section 3.4**. As noted earlier, it is important to remember that confidence in yield changes into the distant future is much lower than those for the near future, due to increasing uncertainty in climate projections towards the year 2100. The confidence in yield simulations is discussed further in **Section 3.3.4**.



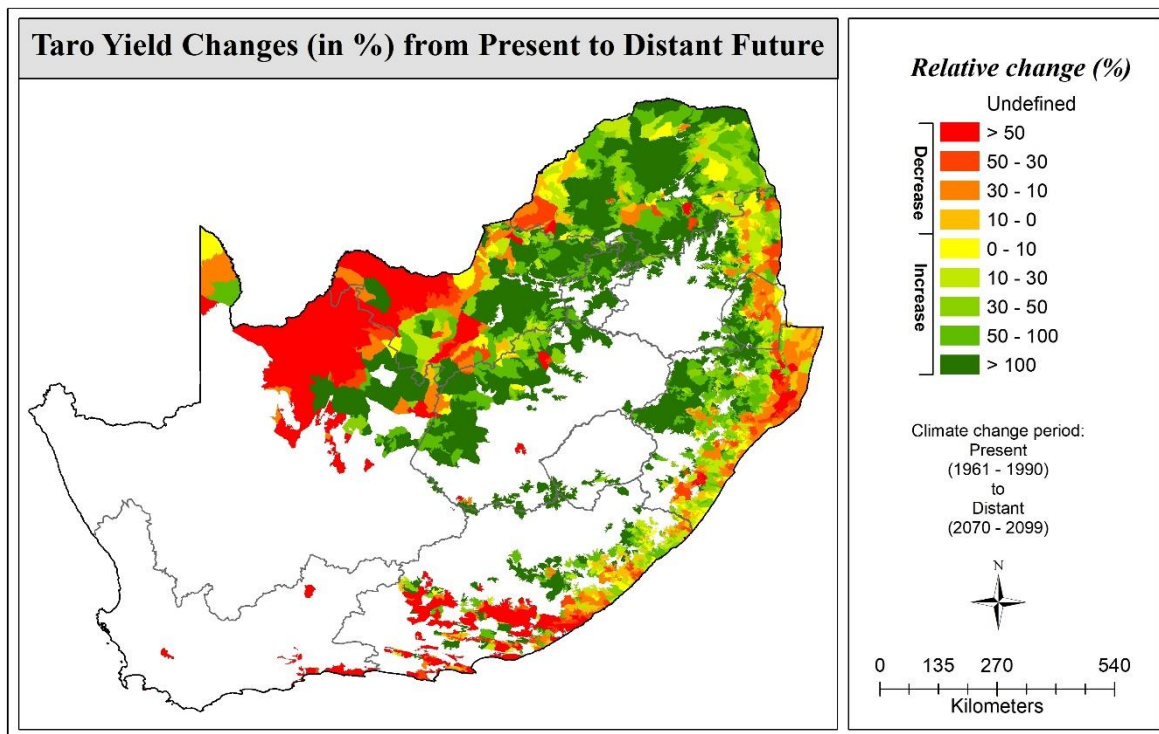
(a)



(b)



(c)



(d)

Figure 3.8 Change in mean dry yield (as %) from present to distant future for (a) amaranth, (b) bambara groundnut, (c) sorghum, and (d) taro

3.3.4 Confidence index

For each of the three climate periods (present, near future and distant future), the average and coefficient of variation were determined from the mean seasonal yields produced for all six GCMs. The GCM-averaged yields were then compared (as percentage changes and ratios) to produce the figures shown in **Section 3.3.1** to **Section 3.3.3**.

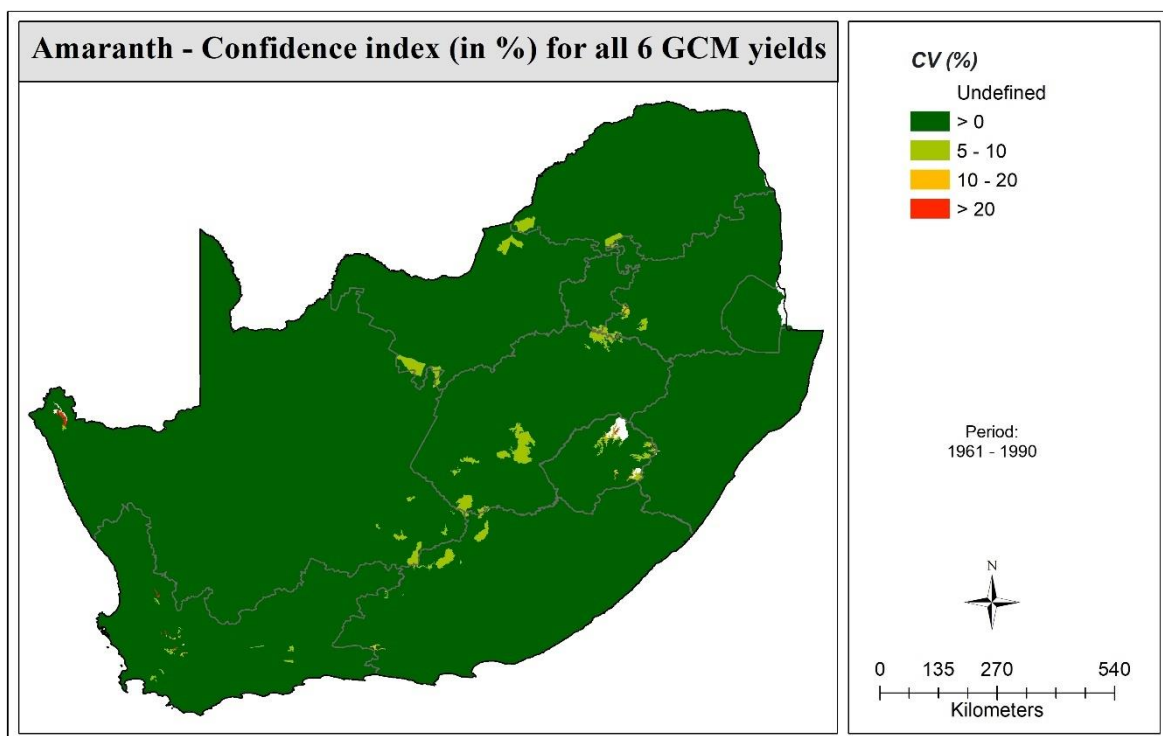
The coefficient of variation (CV) in yield represents the ratio of the standard deviation to the mean yield and is typically expressed as a percentage. In other words, the CV indicates the variability in the yield estimates. The higher the CV, the greater the level of dispersion around the mean, i.e. more variation in the yield values. Therefore, a low CV implies the yields are similar. For each crop, the variation in yield map for the near future was compared to that for the present period to determine if future yields are becoming more variable, which is expected.

As shown in **Figure 3.9**, the variability (or dispersion) between the six GCM-based yields is very low ($CV < 5\%$) for amaranth in the present period, which increases slightly ($5 < CV < 10\%$) in the central interior (i.e. central to western region of the Free State and Eastern Cape provinces) and in eastern Limpopo.

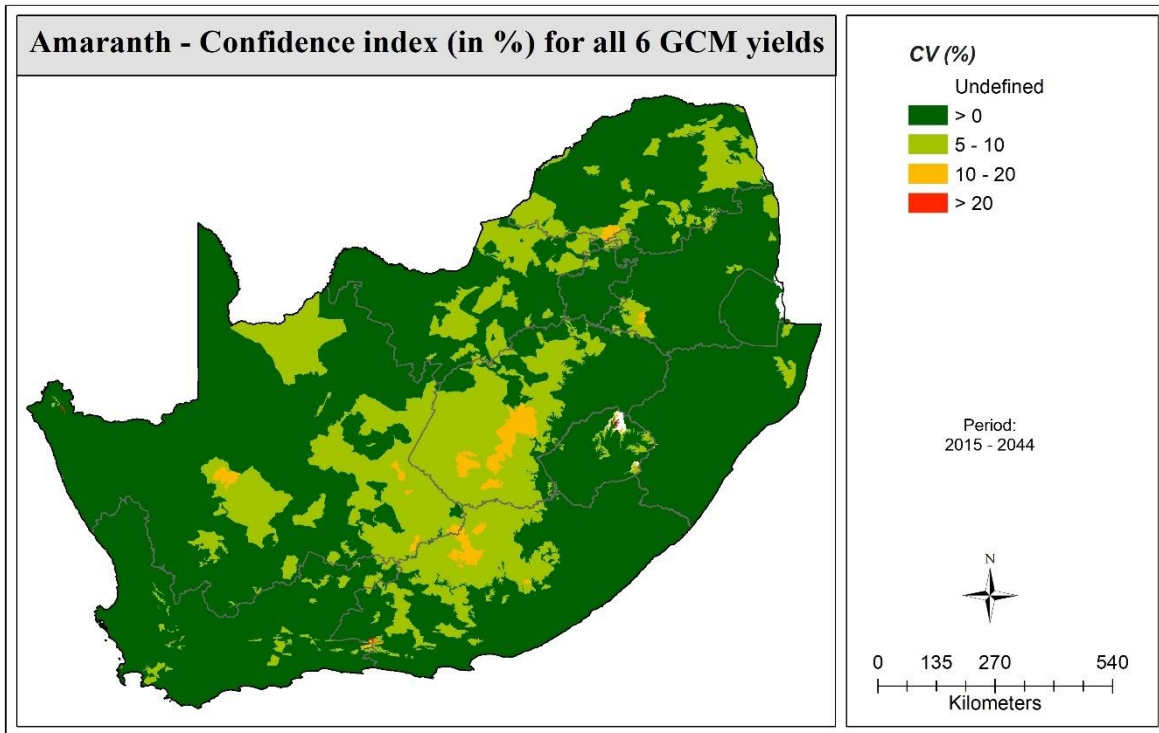
For bambara groundnut (**Figure 3.10**), the CV for present conditions is generally medium-low to medium ($10 < CV < 30\%$) along the eastern seaboard, in areas where commercial forestry is currently produced. In the near future, variability becomes very high ($CV > 50\%$), indicating much less agreement between the six yield values, especially in the Limpopo province and western Mpumalanga, as well as north-eastern parts of KZN and Eastern Cape. The yield variability remains very high in the North West and Free State provinces.

Sorghum's yield variation (**Figure 3.11**) in the present future is generally medium-low ($CV < 20\%$) across Mpumalanga, KZN and Eastern Cape provinces. The CV of yield in these areas increases slightly to 30% in the near future. However, yields become far more variable across most of the Limpopo province, with CVs increasing to over 50%. The variation in taro yield (**Figure 3.12**) increases from below 30% (present) to above 30% (future), especially in the Limpopo, Mpumalanga and KZN provinces.

From the above, yield variability is generally higher in the Limpopo province than in other provinces, which is expected to increase (i.e. worsen) in the near future, especially for taro, sorghum and bambara groundnut. This is likely in response to increased variability in rainfall across Limpopo from the present to the near future. The CV of distant future yields are shown in **Figure 12.1 (APPENDIX E1)** for each crop, which highlights even greater yield variability when compared to the near future maps. This indicates that rainfall variability increases into the distant future, along with increasing uncertainty and decreasing confidence in rainfall projections towards the year 2100. Hence, the distant future maps should not be used for decision-making purposes.

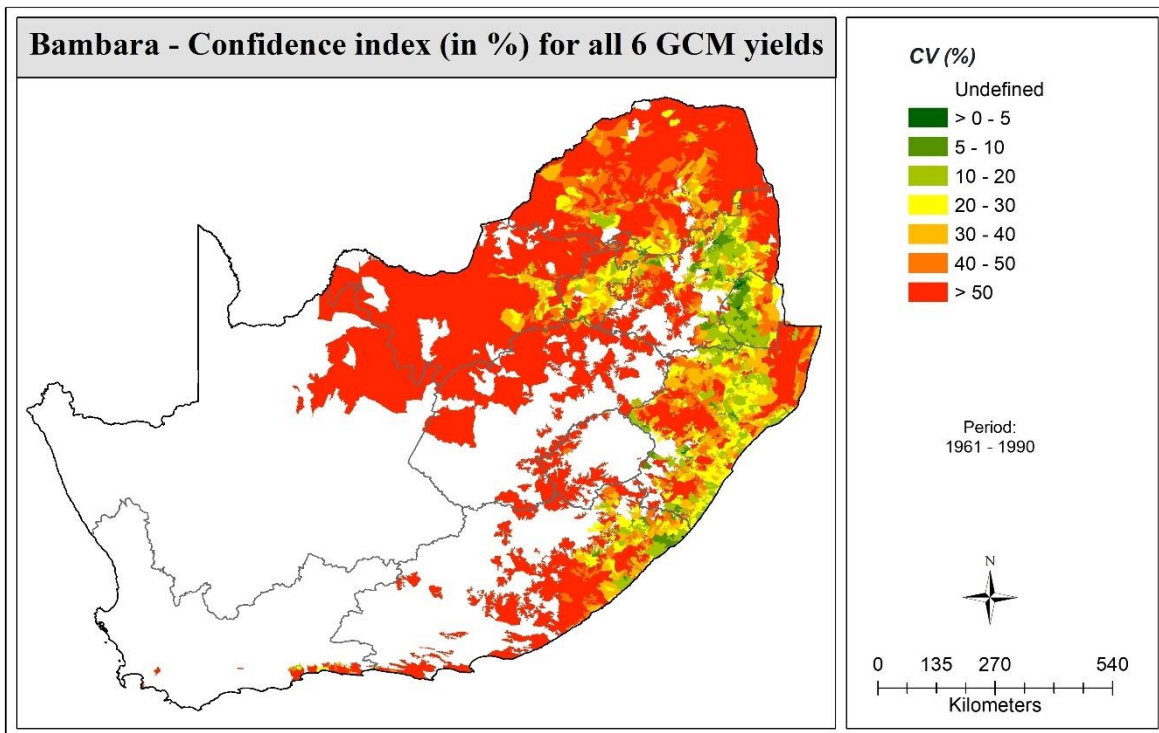


(a)

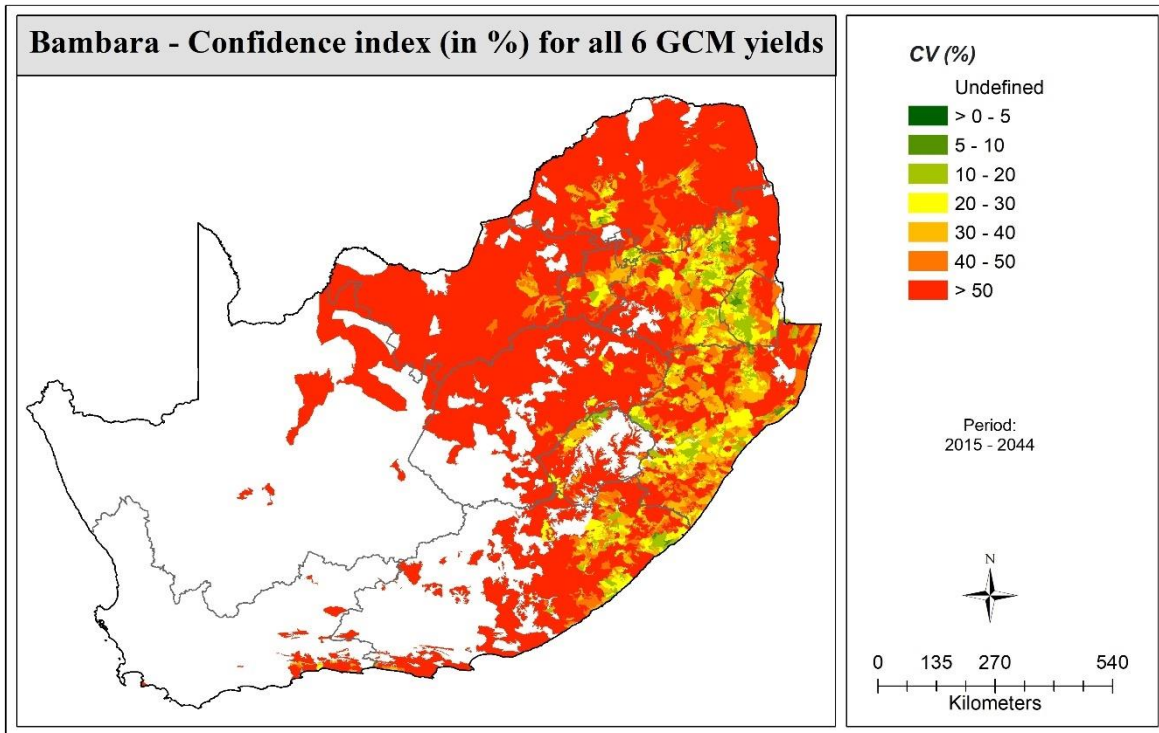


(b)

Figure 3.9 Coefficient of variation (CV in %) in mean yield for amaranth obtained from the six GCMs for the (a) present and (b) near future periods

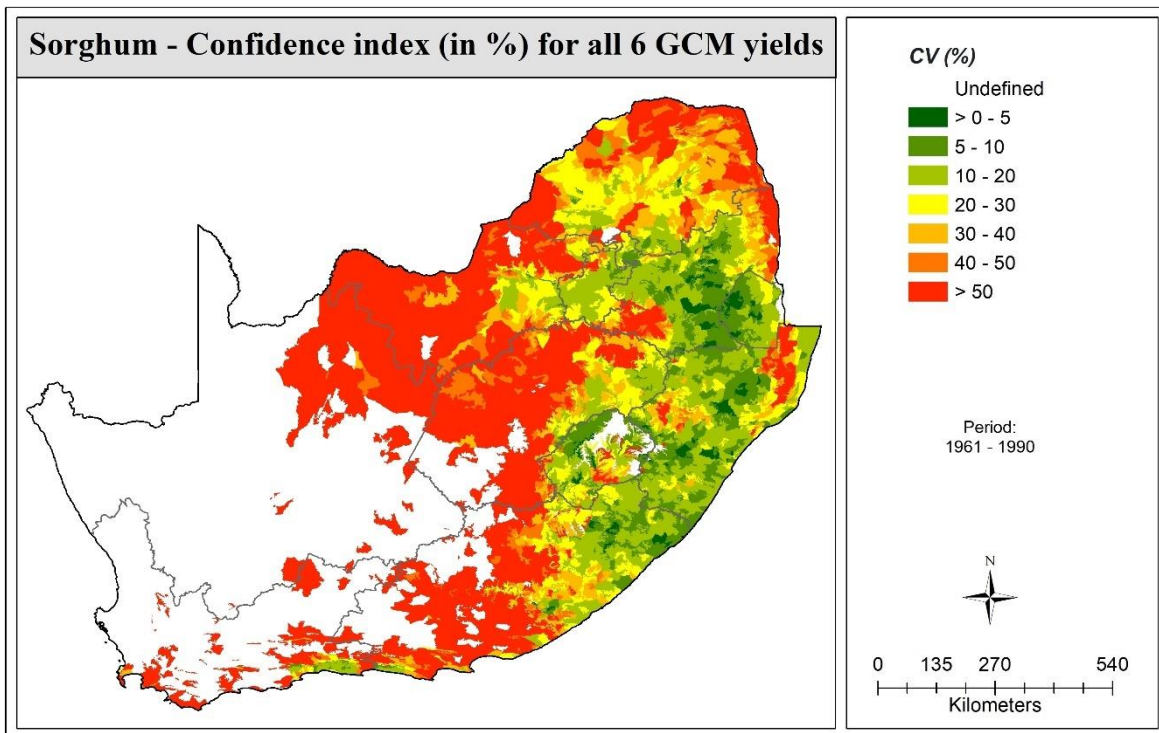


(a)

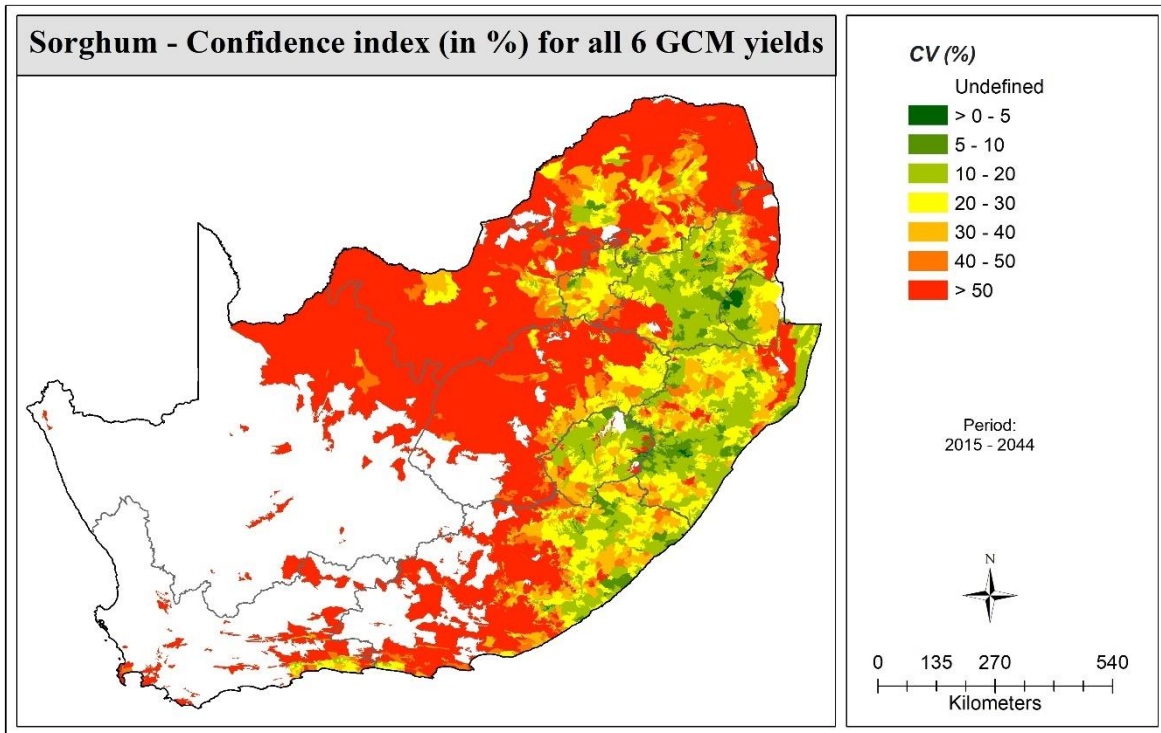


(b)

Figure 3.10 Coefficient of variation (CV in %) in mean yield for bambara groundnut obtained from the six GCMs for the (a) present and (b) near future periods

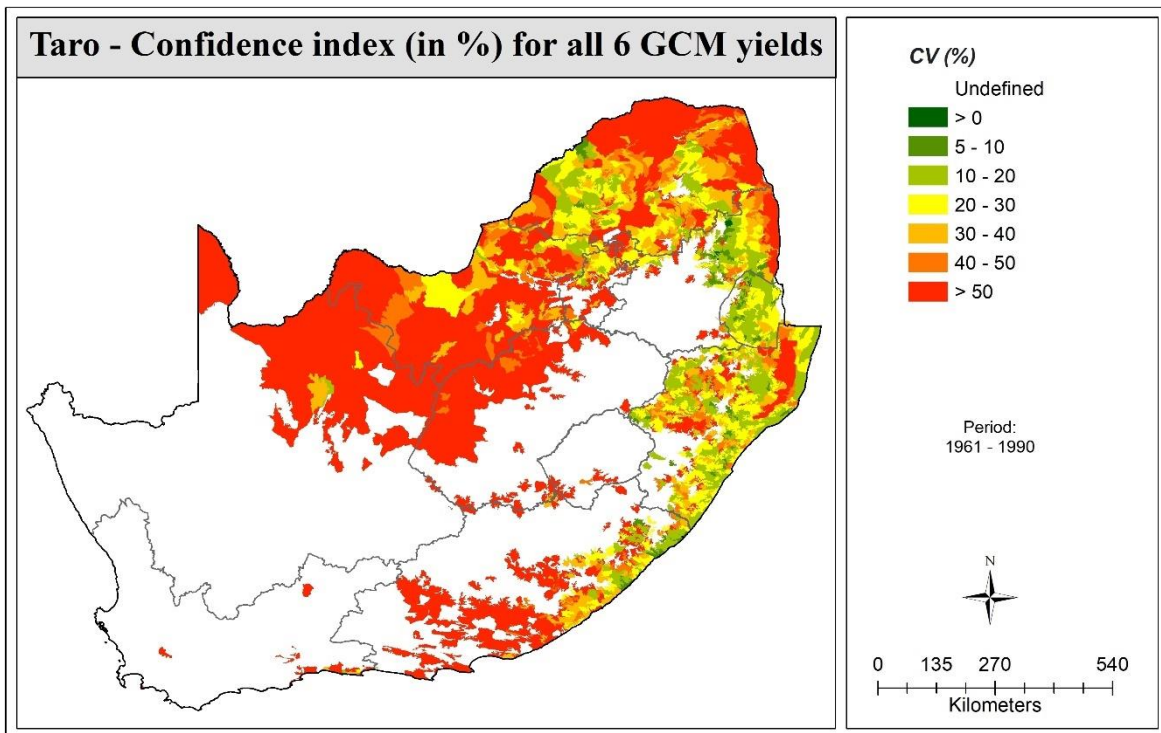


(a)

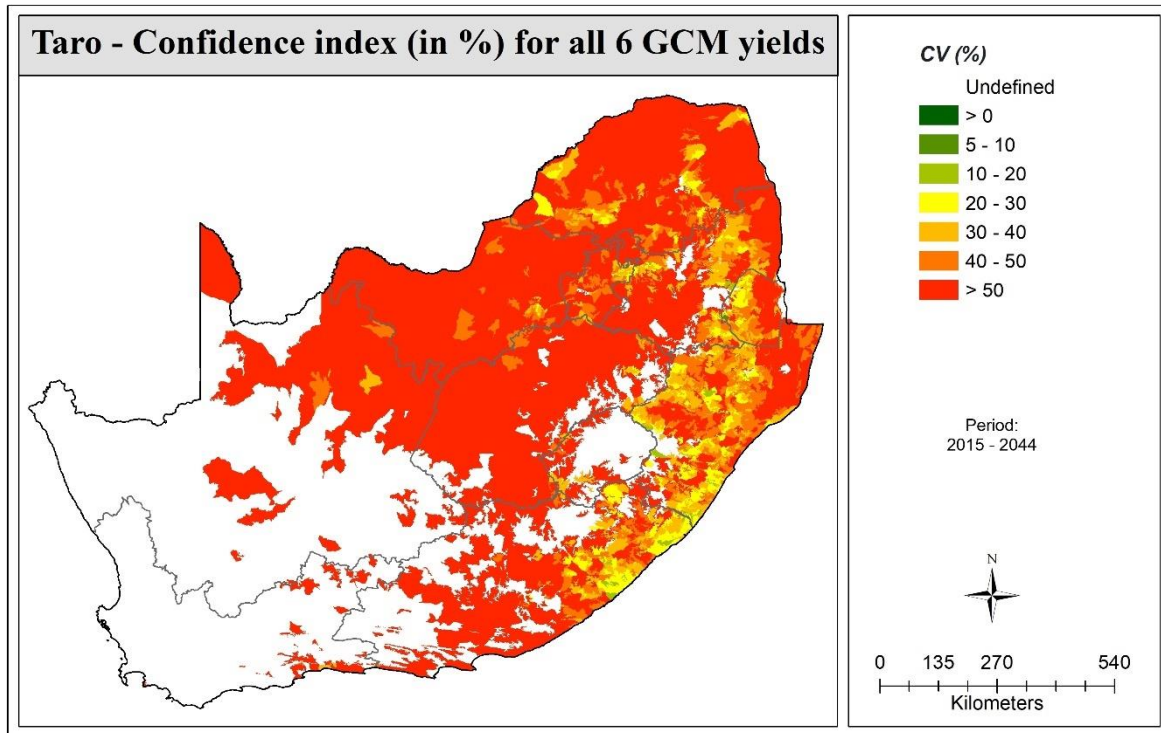


(b)

Figure 3.11 Coefficient of variation (CV in %) in mean yield for sorghum obtained from the six GCMs for the (a) present and (b) near future periods



(a)



(b)

Figure 3.12 Coefficient of variation (CV in %) in mean yield for taro obtained from the six GCMs for the (a) present and (b) near future periods

3.4 Expansion of cropping areas

The present to distant future maps shown in this report highlight overall trends that may result from climate change in areas that currently produce a non-zero averaged yield. In other words, these maps do not highlight the potential expansion in crop growing areas that may result from climate change. This is another reason why the present to distant maps should not be used for decision-making purposes.

In AquaCrop, a zero seasonal yield in the present climate period (1961-1990) indicates total crop failure. This usually occurs when the seedling dies shortly after emergence, due to climate conditions considered too dry (water stress) and/or too cold (temperature stress) to support initial plant growth. If zero crop yields are simulated for most of the 29 seasons spanning 1961/62 to 1989/90, the averaged seasonal yield will be very low (but not zero). If an averaged seasonal yield of 0 t ha⁻¹ was produced for all six GCMs, then the mean yield would also be zero, and the altitude zone is not deemed suitable for crop growth at present. However, as the climate warms and/or becomes wetter towards the near future (up to 2044), the altitude zone may be deemed suitable for crop growth, and yields would increase.

Hence, a comparison of the CV maps of yield presented in **Section 3.3.4** for present and near future conditions can show the likely expansion in crop growing areas, except for amaranth as the model simulated averaged non-zero yields for all altitude zones in South Africa. For bambara groundnut, the expansion in growing areas (where the model simulated non-zero yields) occurs mainly in western Mpumalanga, along the Free State border with Lesotho and KZN, and in the Eastern Cape (northern regions). Certain altitude zones remain unsuitable for crop growth into the future (e.g. western parts of Mpumalanga and in the Eastern Cape, just south of the Lesotho border), whilst other zones become unsuitable when growing conditions are too hot and/or too dry (i.e. expansion of areas in white). However, their occurrence is minimal compared to the expansion of new growing areas.

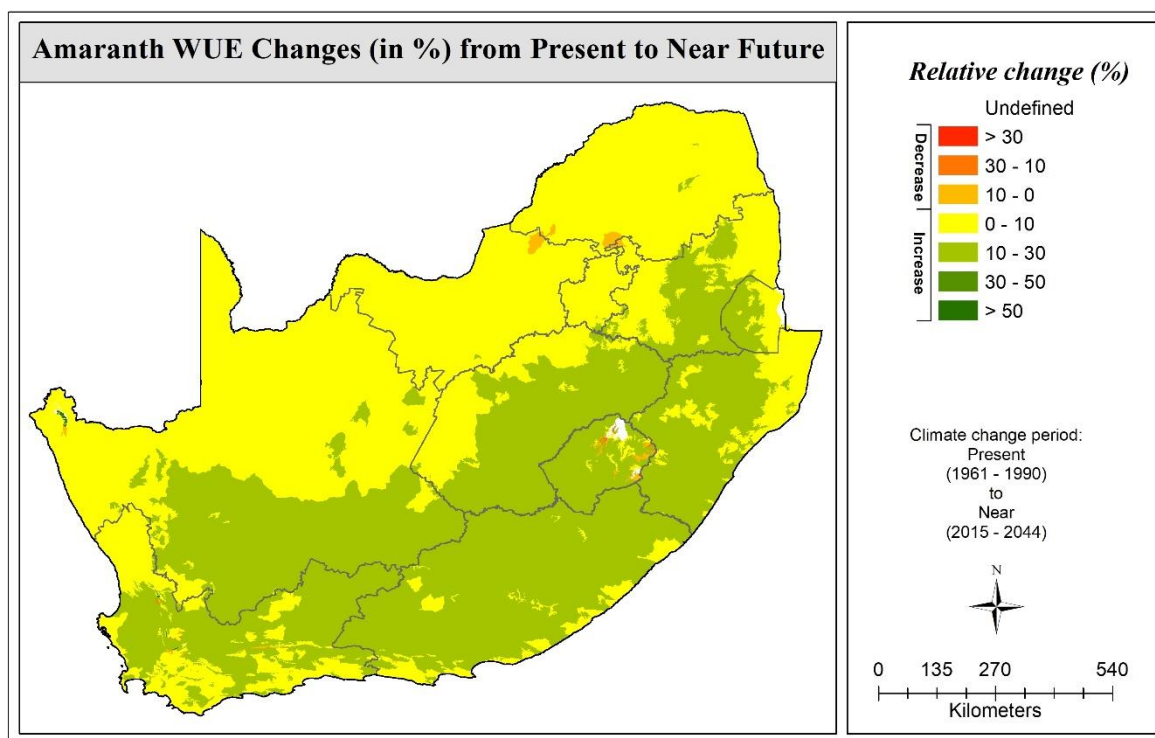
For sorghum, the model simulated no noticeable expansion in suitable growing areas from present to near future, except in the higher altitude zones in Lesotho. As shown in **Figure 3.12**, taro appears to benefit the most from warmer climate conditions projected in the near future, with a large expansion in areas deemed suitable for growth in the central interior (i.e. Free State, Mpumalanga and Eastern Cape).

3.5 Climate change and WUE

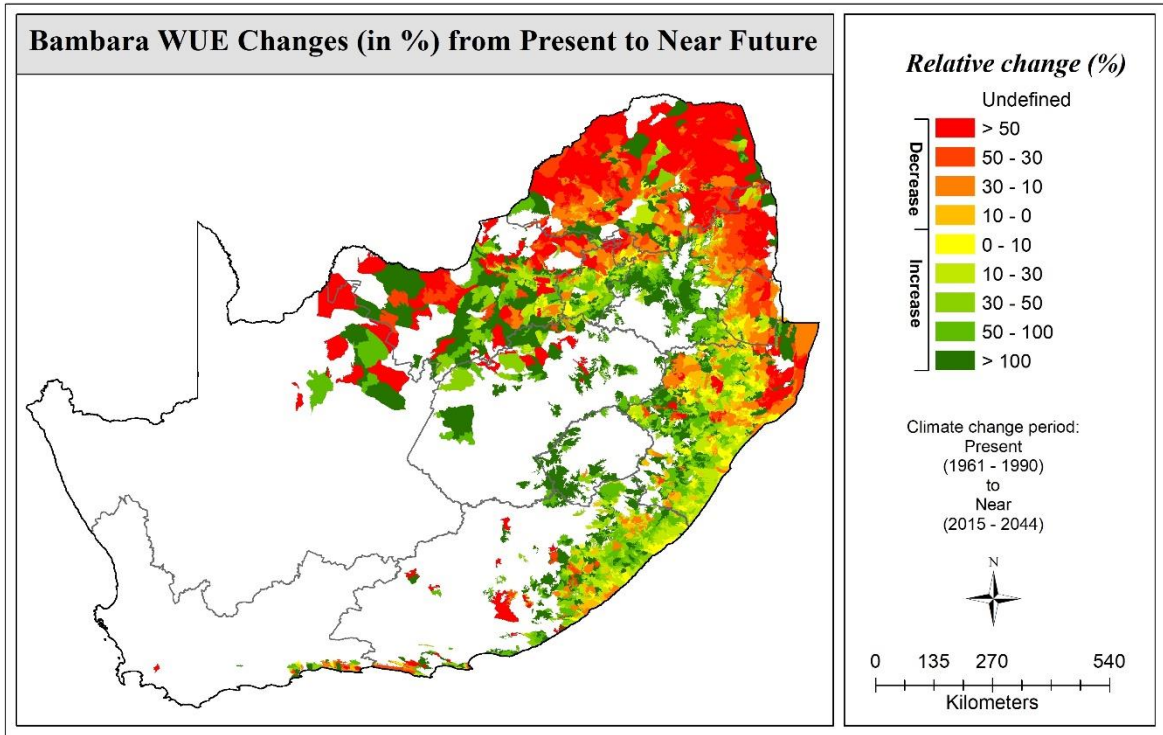
For each GCM, water use efficiency (WUE) obtained for all 30 seasons were averaged to determine the mean seasonal value. Thereafter, the six values for each GCM were also averaged (i.e. each GCM assigned equal weighting) to reduce the number of maps shown. This exercise was repeated for each of the three time periods (i.e. present, near future and distant future). Maps highlighting the change in average WUE from 1) present to near future, 2) near future to distant future, and 3) present to distant future period were generated for each NUS. The percentage change maps are presented next in **Section 3.5.1** to **Section 3.5.3**, and the ratio maps are given in **APPENDIX D2**. The change cannot mathematically be determined for AZs where the averaged WUE for the present period is zero. Such areas appear white on the maps and are labelled as “Undefined”. It is worth noting that the spatial extent of the WUE maps is almost identical to the yield maps.

3.5.1 Present to near future

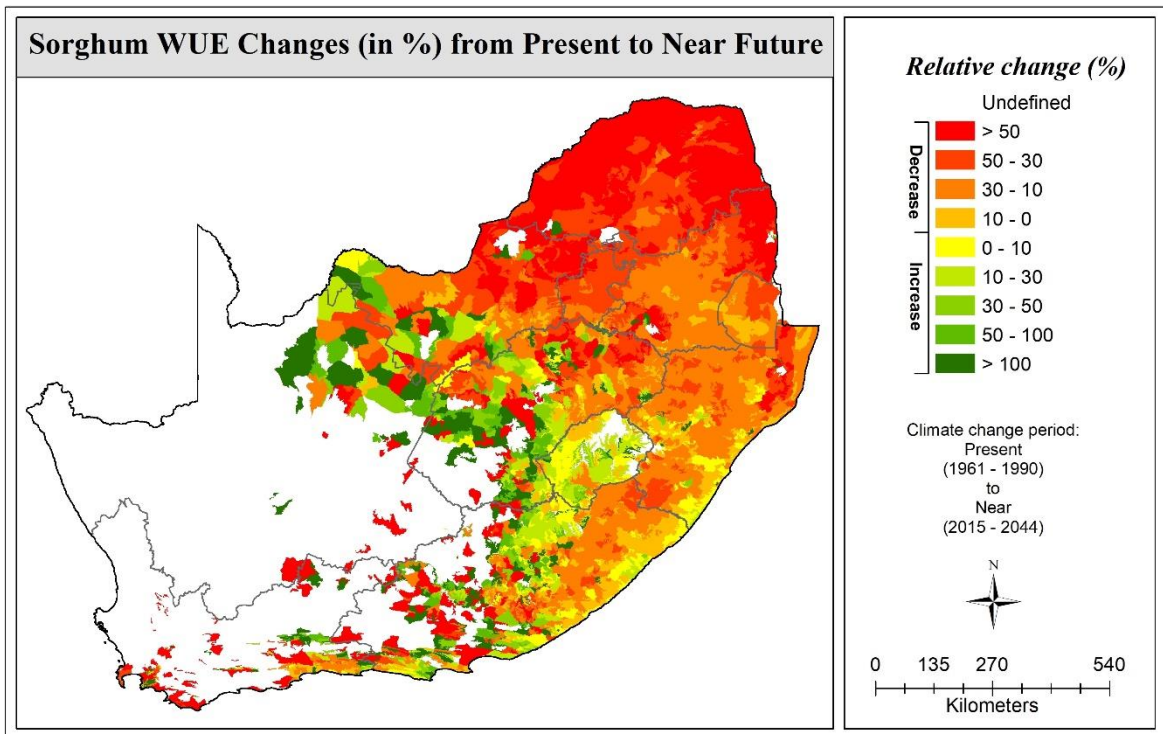
From **Figure 3.13**Figure 3.6a, the model simulated non-zero WUEs in most altitude zones for amaranth (except for those in Lesotho), in contrast to the other three crops. This suggests that amaranth is more suited to a wider range of growing conditions than the other crops. Amaranth’s WUE is expected to increase in the near future (relative to the present climate) by 10-30% for areas deemed suitable for crop production. For the other three crops (**Figure 3.13b-d**), changes in WUE mimicked the expected changes in yield as discussed in **Section 3.3.1**.



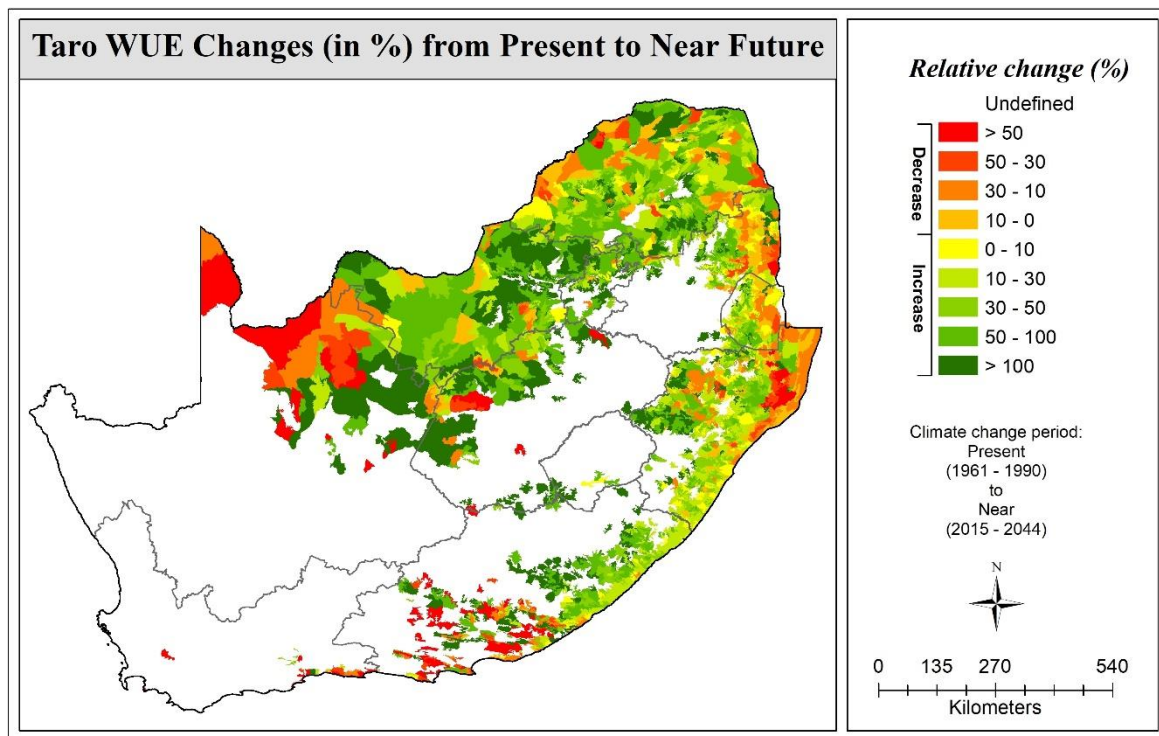
(a)



(b)



(c)



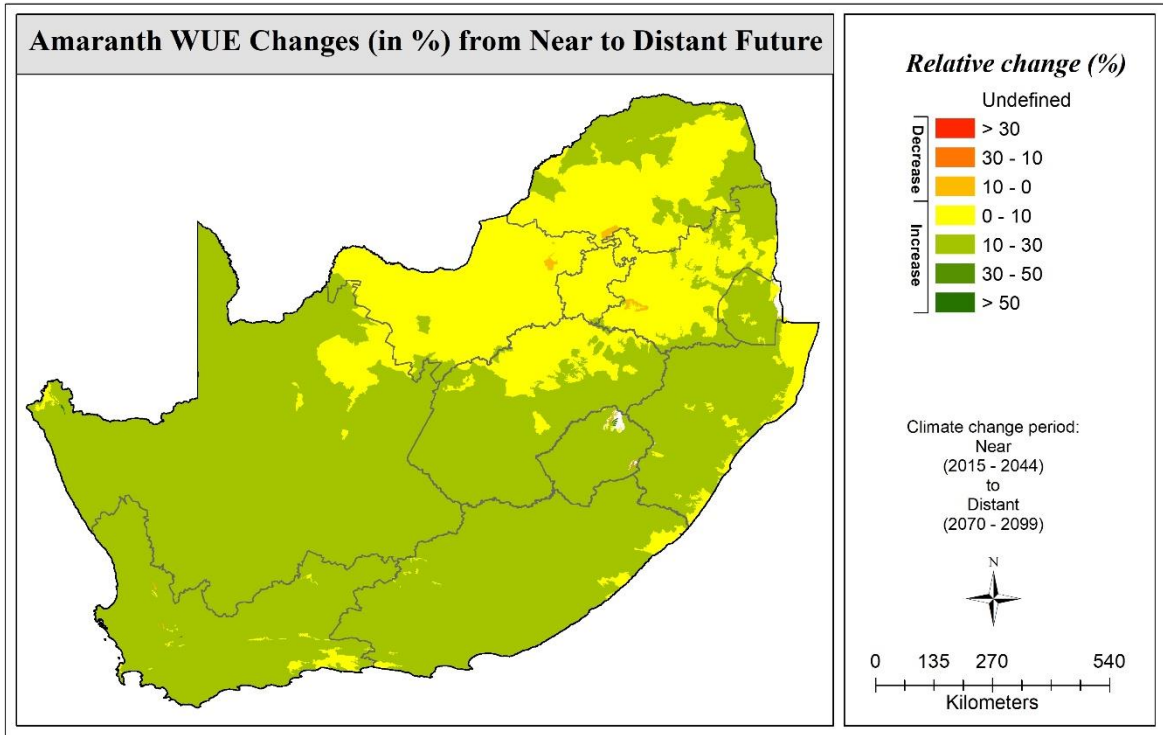
(d)

Figure 3.13 Change in mean water use efficiency (WUE; as %) from present to near future for (a) amaranth, (b) bambara groundnut, (c) sorghum and (d) taro

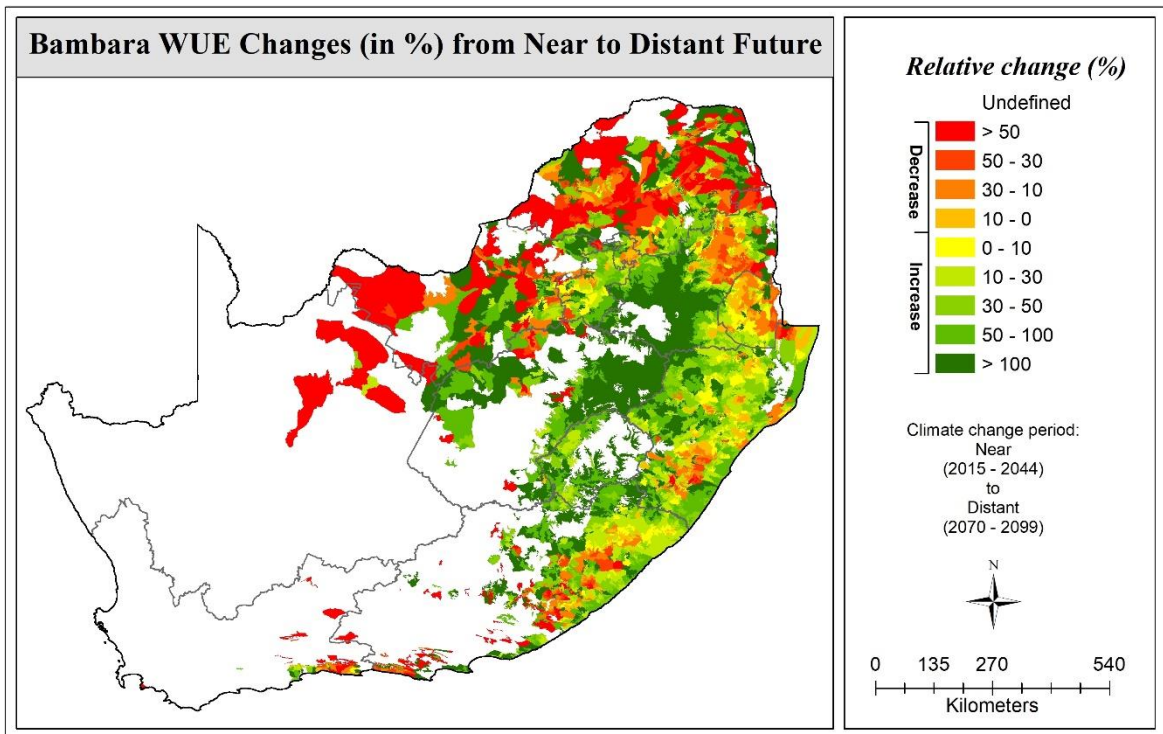
As noted in **Section 1.1**, higher CO₂ levels can induce stomatal closure (i.e. decrease stomatal conductance), resulting in lower transpiration, decreasing crop water use, increasing crop water use efficiency, and improving soil water content. This increased efficiency in converting water into dry matter has been shown to raise above ground and, in some cases, below-ground plant biomass.

3.5.2 Near to distant future

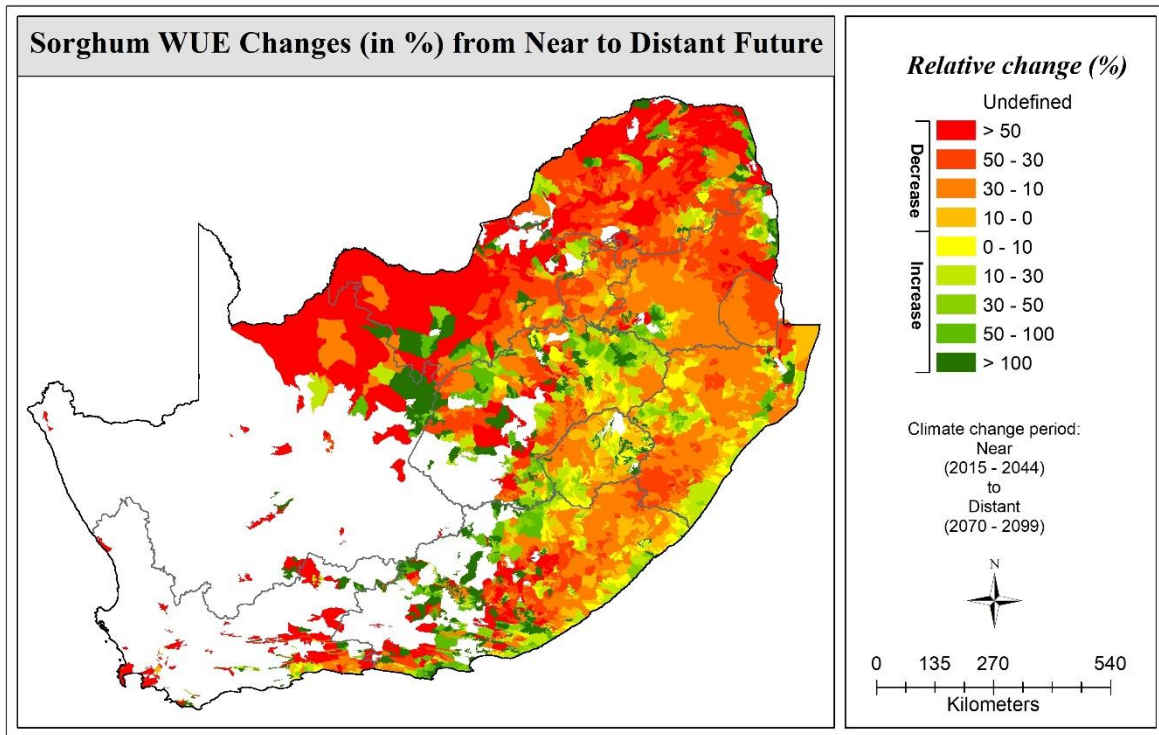
From the near to the distant future, amaranth WUE is expected to increase by 10-30% for most areas, except for the North West and Mpumalanga provinces, as well as northern parts of the Free State and central and southern parts of Limpopo, where the increase is below 10% (**Figure 3.14a**). For the other three crops (**Figure 3.14b-d**), changes in WUE mimicked the expected changes in yield as discussed in **Section 3.3.2**, i.e. both increases and decreases for bambara groundnut, mostly decreases for sorghum and mainly increases for taro.



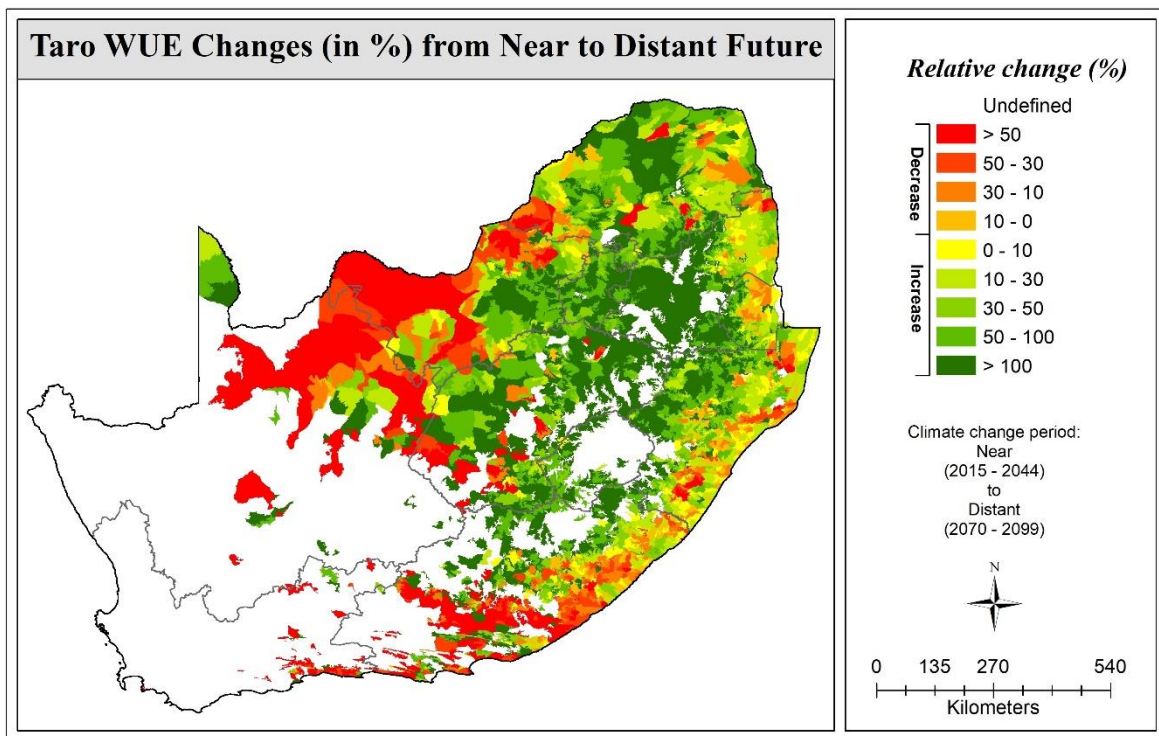
(a)



(b)



(c)



(d)

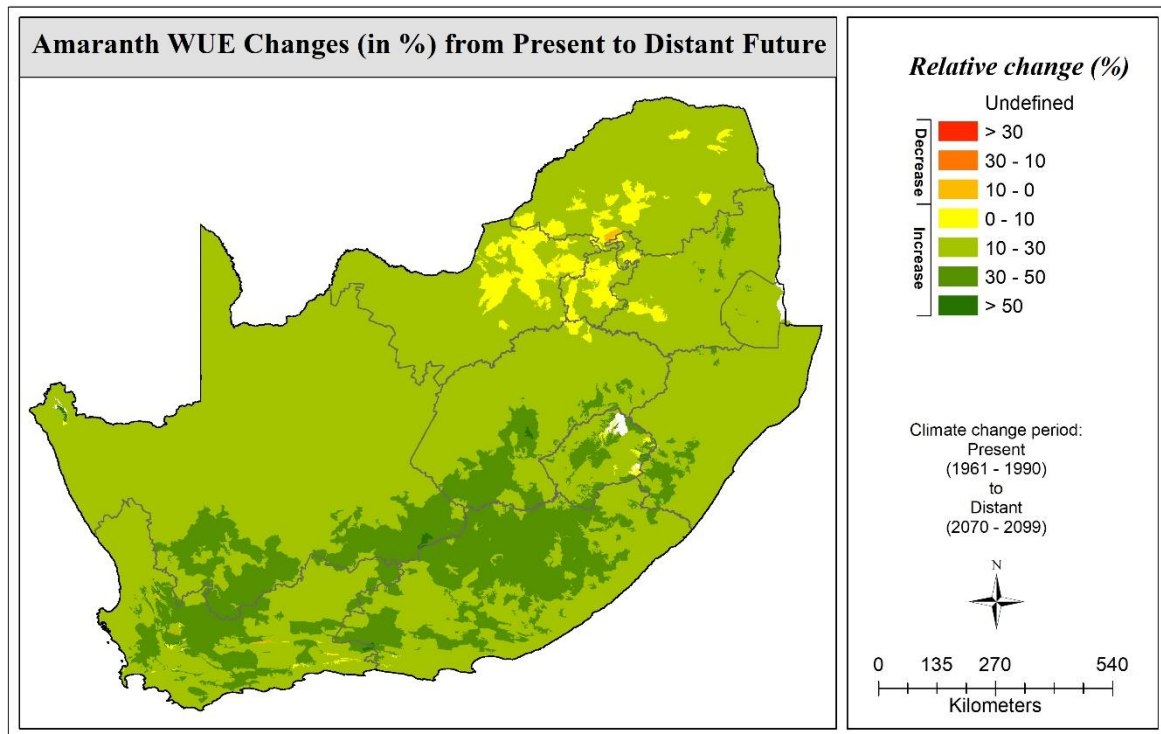
Figure 3.14 Change in mean water use efficiency (WUE; as %) from near to distant future for (a) amaranth, (b) bambara groundnut, (c) sorghum, and (d) taro

3.5.3 Present to distant future

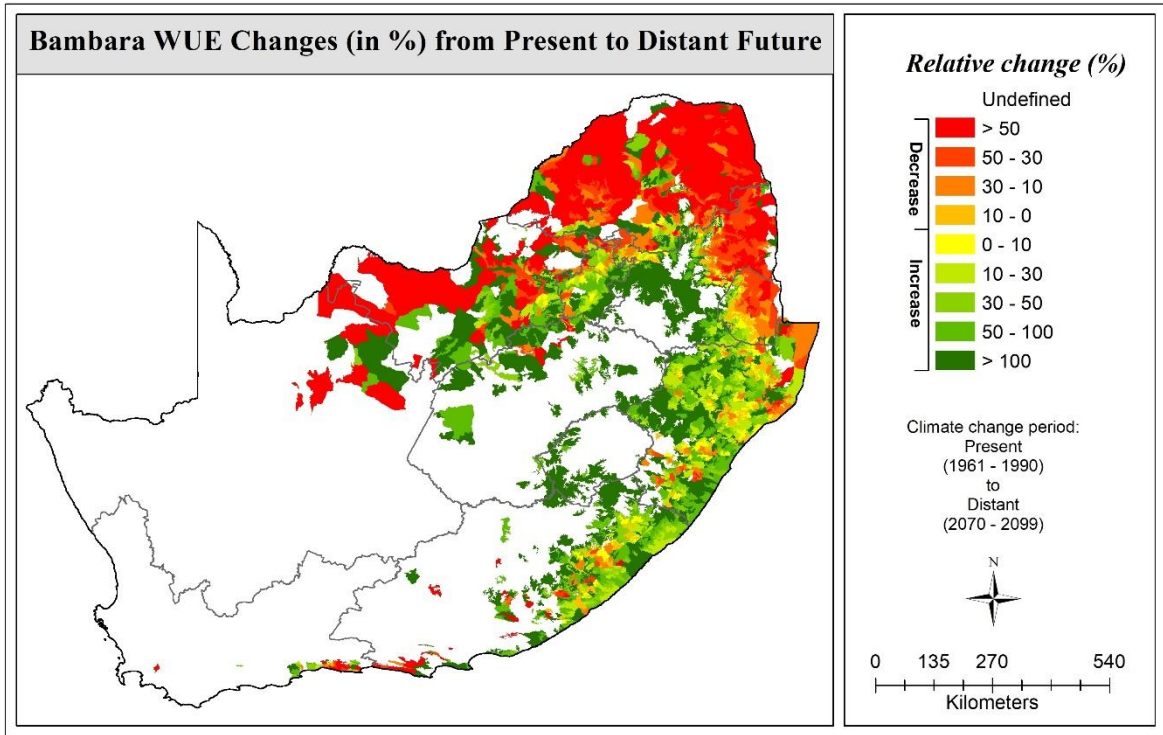
Simulations for the distant future compared to the present are shown in **Figure 3.15**. As noted in **Section 3.3.3**, the four maps do not highlight the potential expansion (or contraction) in crop growing

areas that may result from climate change, which is discussed further in **Section 3.4**. Despite this, the following trends were noted:

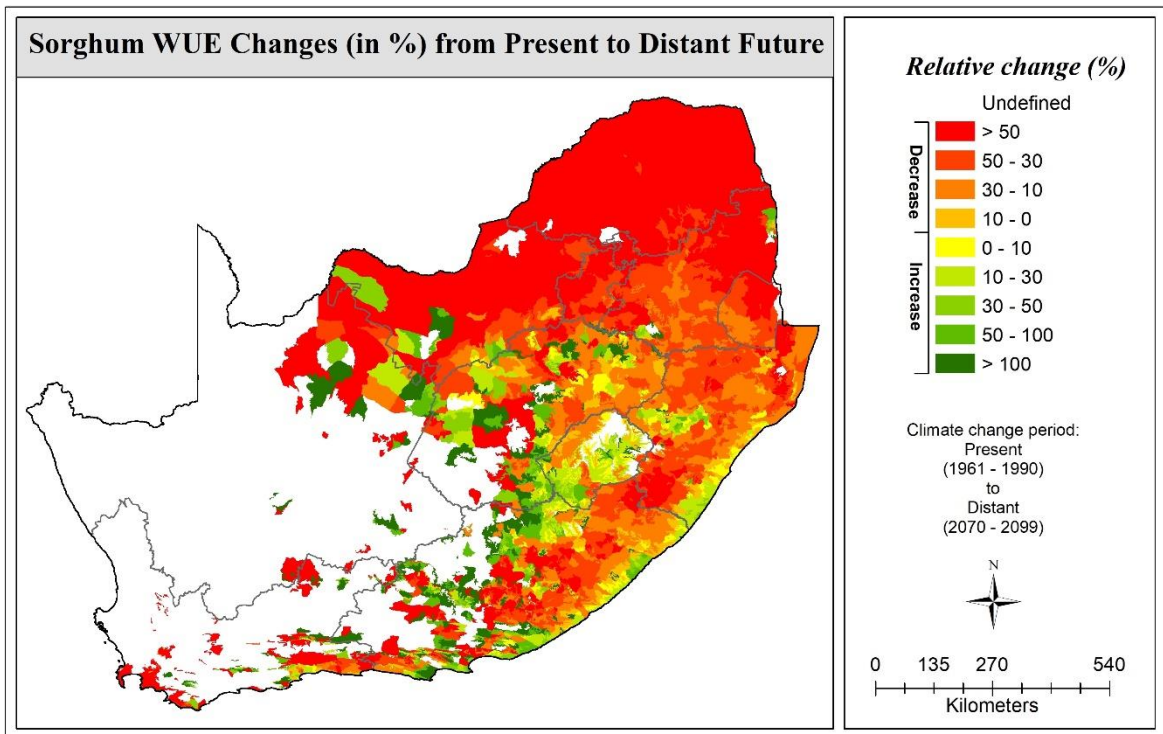
- Amaranth WUE could mostly increase by 10-30%, compared to a 0-10% yield increase in parts of the Limpopo, North West and Gauteng provinces. However, increases in WUE from 30-50% may be expected in the south-western parts of KwaZulu-Natal and Free State and large parts of the Eastern and Western Cape provinces.
- For the other three crops, changes in WUE mimicked the expected changes in yield as discussed in **Section 3.3.3**, i.e. both increases and decreases for bambara groundnut, mostly decreases for sorghum and mainly increases for taro.



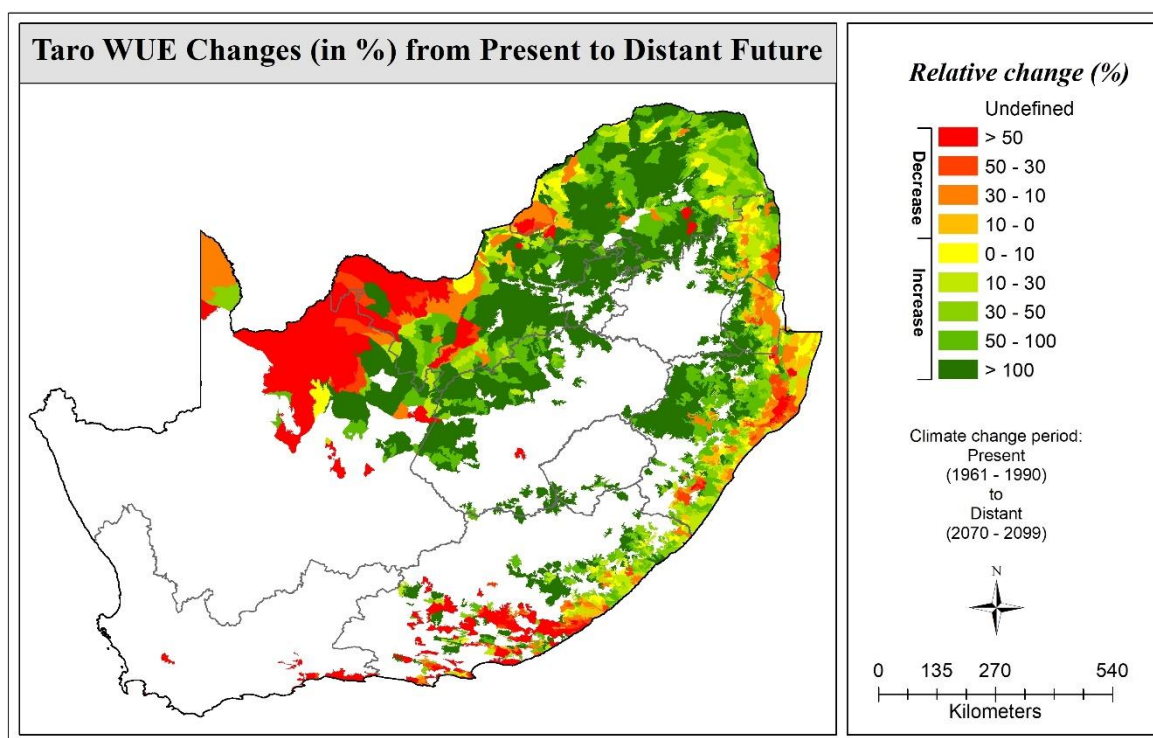
(a)



(b)



(c)



(d)

Figure 3.15 Change in mean water use efficiency (WUE; as %) from present to distant future for (a) amaranth, (b) bambara groundnut, (c) sorghum, and (d) taro

Mabhaudhi et al. (2018) evaluated the impact of climate change on bambara groundnut using AquaCrop driven with climate scenarios from 5 CMIP3 GCMs (A2 CO₂ trajectory). When compared to the past (1961-1990) period, the results given in **Table 3.1** were obtained for the present (1995-2025), mid (2030-2060) and late century (2065-2095) periods. Rainfall decreased by 4.6, 12.3 and 19.1% for the present, mid and late century periods. Despite decreasing rainfall, the CO₂ fertilisation effect may result in increased biomass (13.2-42.1%) and yield (12.5-37.5%), decreased crop water use (1.8-8.4%) and improved WUE (14.5-50.2%).

Table 3.1 Percentage change in biomass (B), yield (Y), water use (ET) and water use efficiency (WUE) for bambara groundnut, relative to the past (1961-1990) period (after Mabhaudhi et al., 2018)

Period	B (t ha ⁻¹)	Y (t ha ⁻¹)	ET (mm)	WUE (kg m ⁻³)	Change relative to past (%)			
					B	Y	ET	WUE
Past	7.6	1.6	785	0.20				
Present	8.6	1.8	771	0.23	13.2	12.5	-1.8	14.5
Mid century	9.8	2.0	752	0.27	28.9	25.0	-4.2	30.4
Late century	10.8	2.2	718	0.31	42.1	37.5	-8.4	50.2

Kimball (2016) reviewed FACE studies that assessed the impact of elevated CO₂ (eCO₂) on biomass production, crop yield and evapotranspiration (ET). The photosynthetic rate, biomass accumulation and yield of C3 crops (e.g. wheat, legumes and potato) should increase due to eCO₂, irrespective of water availability. For example, C3 crop yields increased by 15-30% for eCO₂ levels of 550 ppm (Van der Kooi et al., 2016). The ET of C3 crops was reduced by 10% on average (maximum of 18%) when soil water was nonlimiting (**Figure 3.16**). Mwamlima et al. (2021) reported that low soil moisture (25% of crop water requirement or CWR) significantly reduced the photosynthetic rate and stomatal conductance of soybean cultivars (C3 plant) by 86.45% and 36.64%, respectively, compared to CWR

of 100%. Photosynthetically active radiation and sub-stomatal CO₂ concentration also declined ($P < 0.05$) due to limited soil moisture availability, resulting in reduced ($P < 0.05$) soybean shoot growth and yield. Lower yields and reduced evapotranspiration (due to stomatal closure) will decrease WUE.

On the other hand, C4 crops (e.g. sorghum) exhibit a more efficient photosynthetic mechanism than C3 crops and, thus, will typically respond to eCO₂ under water-limited conditions (not when water is nonlimiting) (Kimball 2016). Hence, C4 crops are expected to produce more biomass under eCO₂ by using the limited available water more efficiently. For example, the yield response of sorghum to eCO₂ was negligible when water was nonlimiting, but increased to 30% when water was limiting (Figure 3.16 Kimball, 2016).

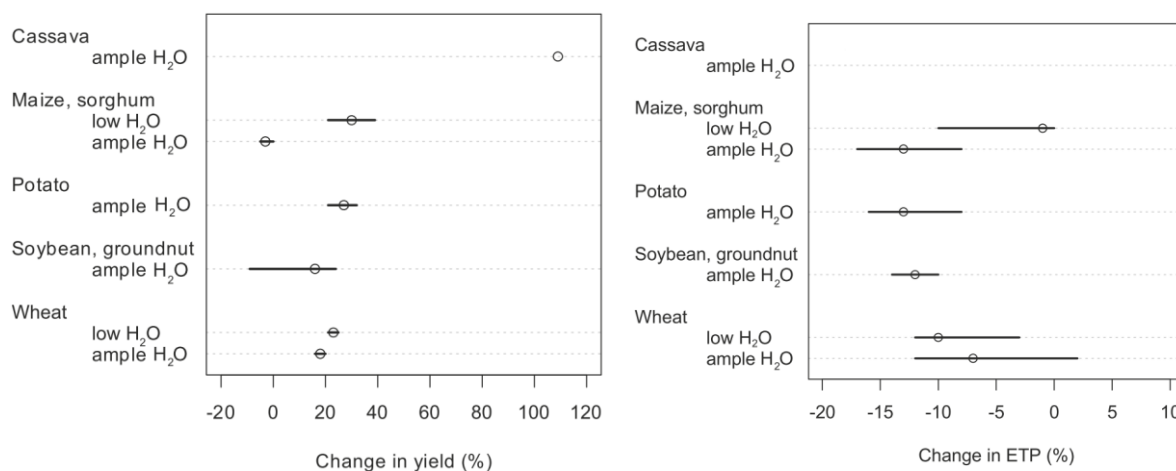
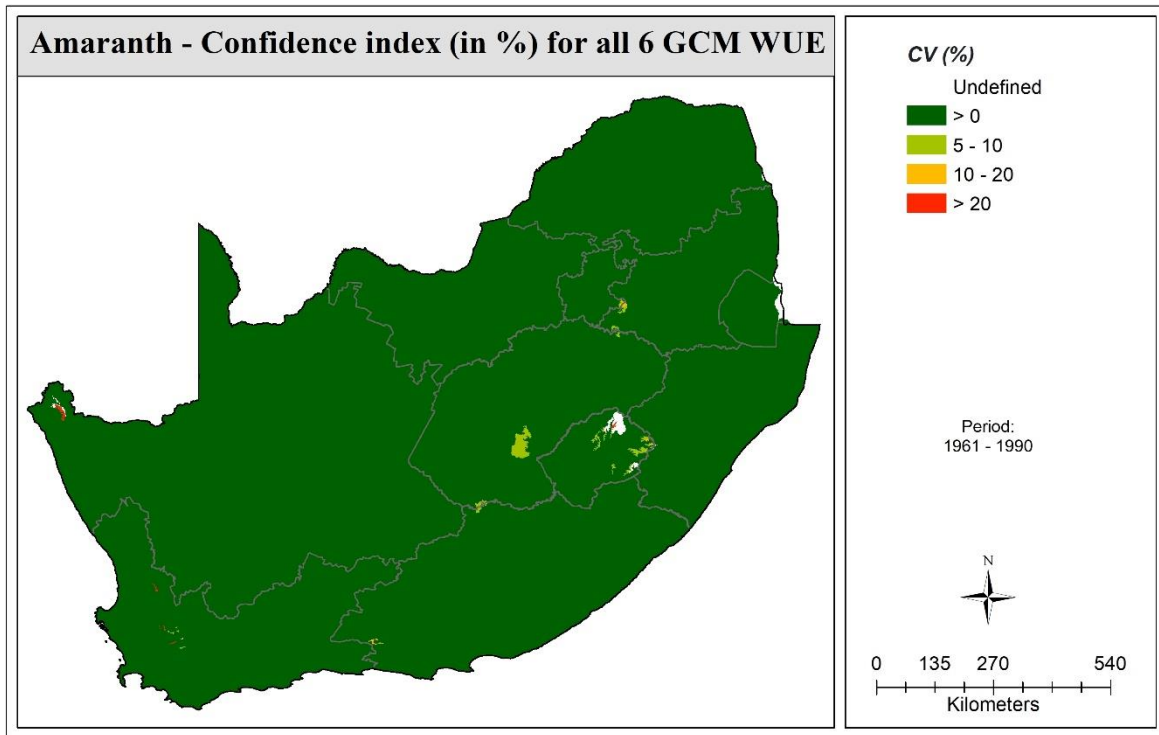


Figure 3.16 Responses (o average; – range) of (a) crop yield and (b) evapotranspiration (ETP) to elevated CO₂ (550 ppm) for optimal (ample water) and water stressed (low water) conditions (after Kimball, 2016)

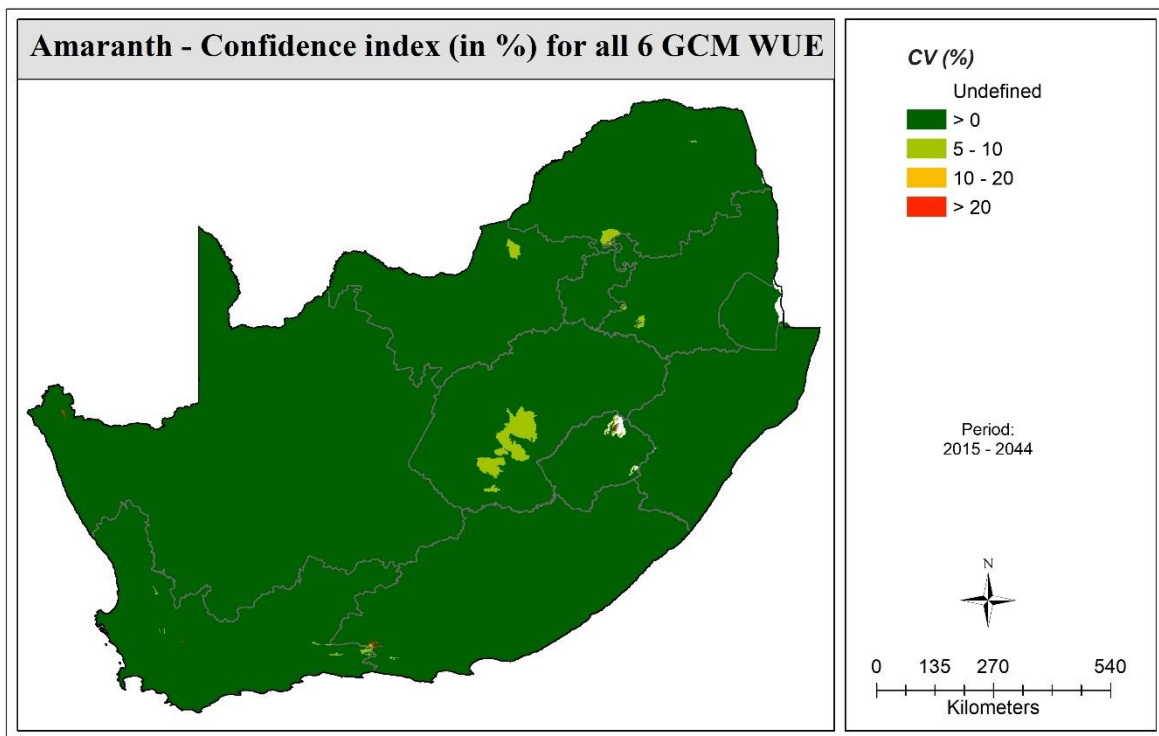
3.5.4 Confidence index

As shown in Figure 3.17, the variability (or dispersion) between the six GCM-based WUEs is mostly very low ($CV < 5\%$) for amaranth in both the present and near future periods. Thus, all six GCMs predict similar changes in Amaranth's WUE, and thus, confidence is deemed high. For the near future period, the CV of WUE was lower than that for yield (cf. Figure 3.9 in Section 3.3.4). For the other three crops (Figure 3.18 to Figure 3.20), the CV of WUE is lower (i.e. higher confidence) in areas where crop production is more likely, compared to areas where cultivation is unlikely due to low and more variable yields. In addition, the CV of WUE is mostly similar for both the present and near future periods, but is higher in the near future (as expected), especially for sorghum

The CV of amaranth's WUE in the distant future is shown in Figure 13.1a (APPENDIX E2), highlighting greater variability in parts of the North West, Free State and Mpumalanga provinces. For the other three crops (Figure 13.1b-d in APPENDIX E2), confidence is much lower (i.e. higher CVs of WUE), and hence, the distant future maps should not be used for decision-making purposes.

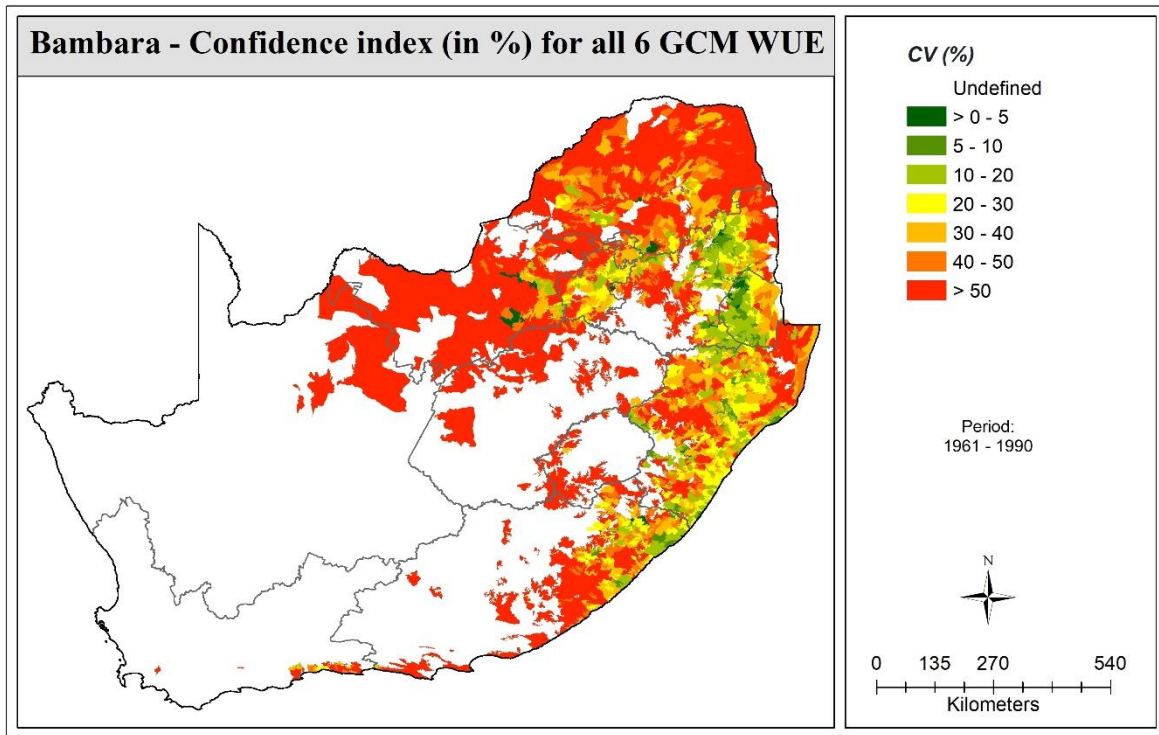


(a)

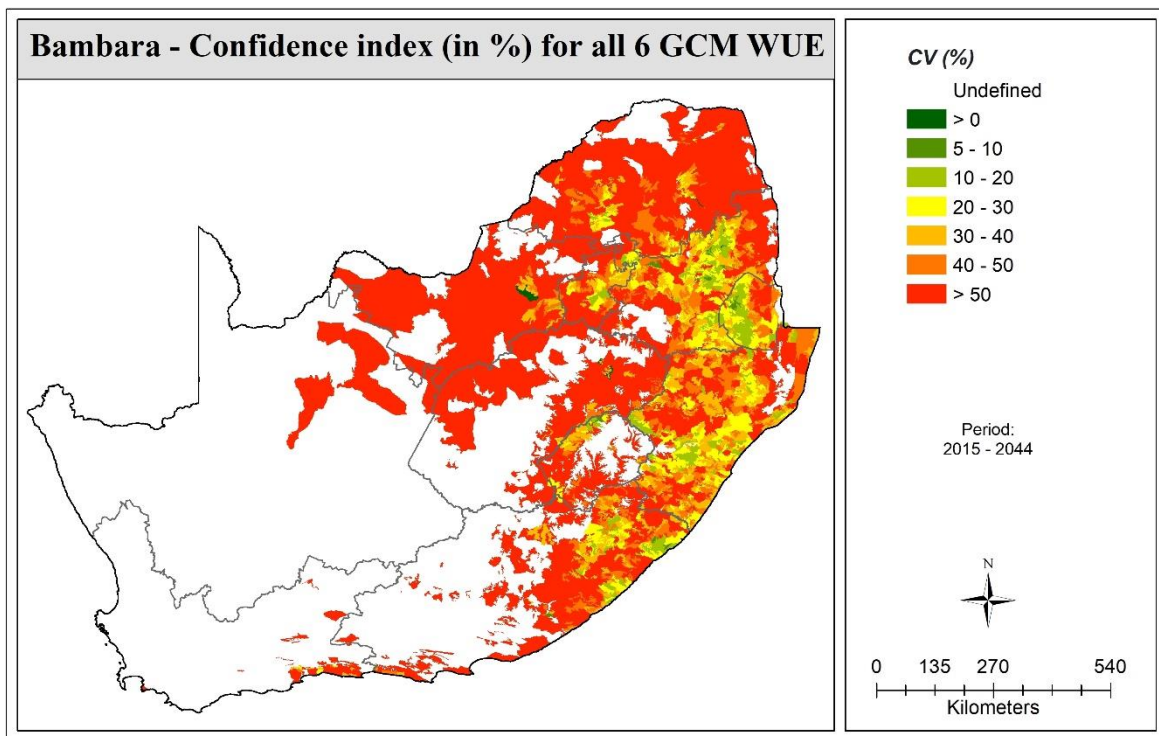


(b)

Figure 3.17 Coefficient of variation (CV in %) in mean water use efficiency for amaranth obtained from the six GCMs for the (a) present and (b) near future periods

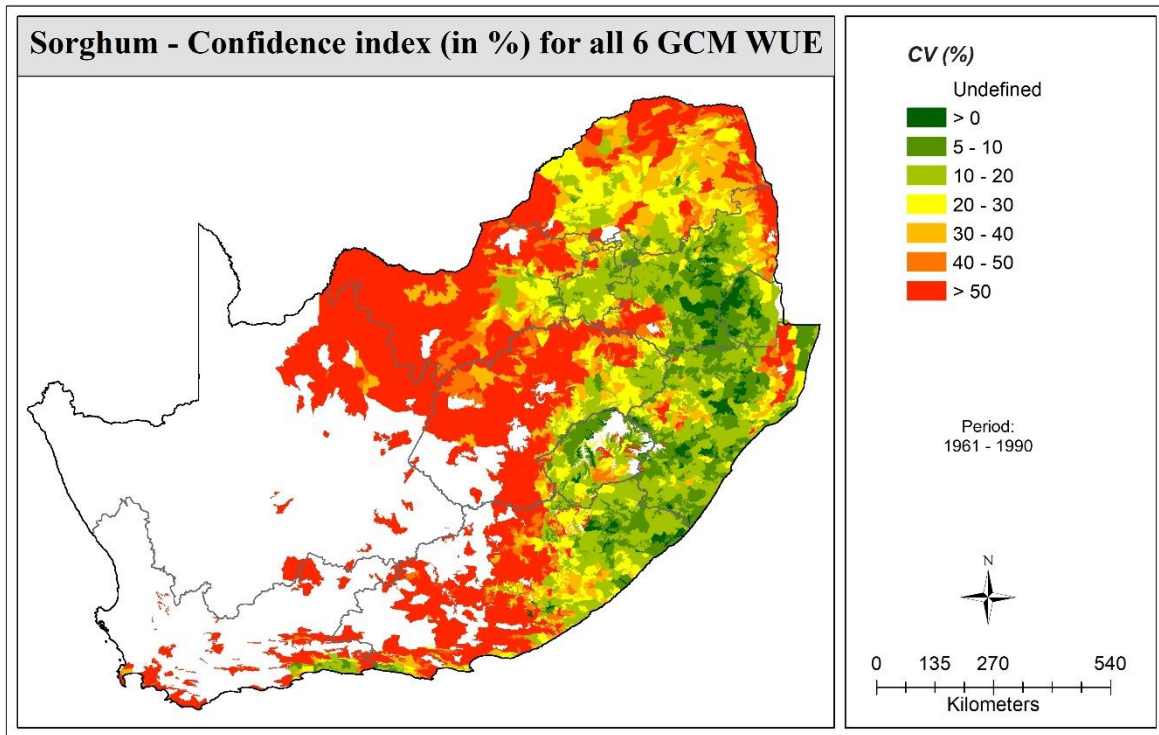


(a)

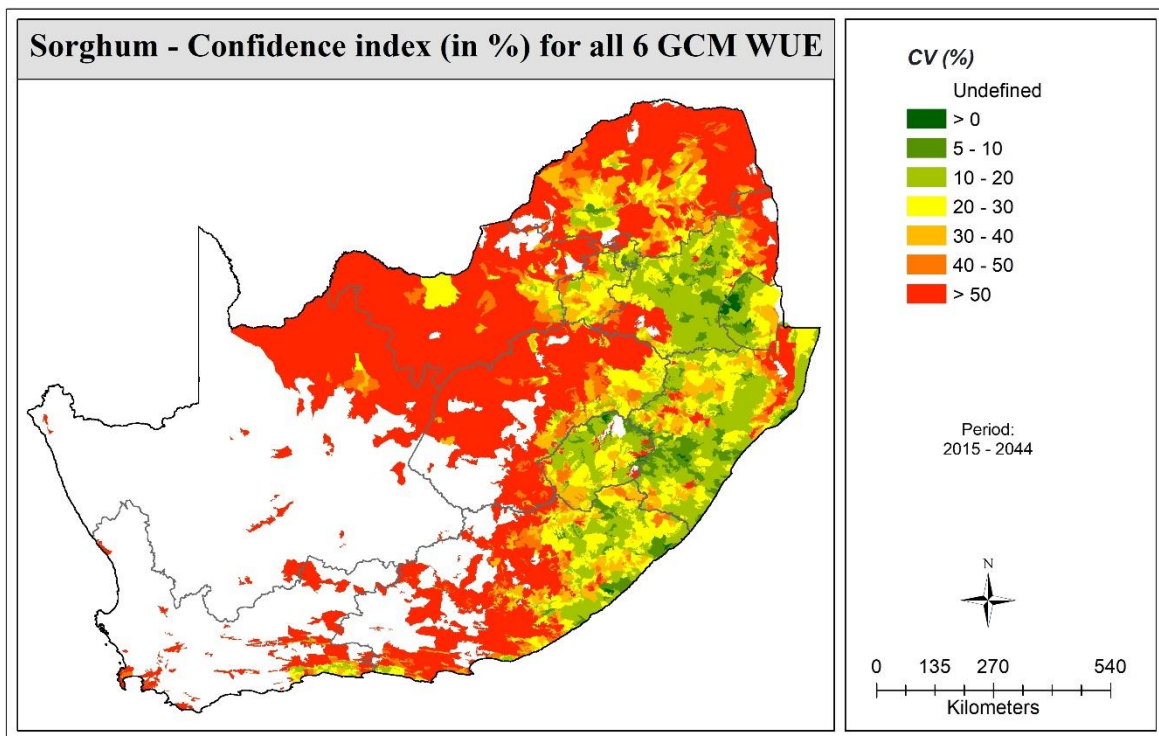


(b)

Figure 3.18 Coefficient of variation (CV in %) in mean water use efficiency for bambara groundnut obtained from the six GCMs for the (a) present and (b) near future periods

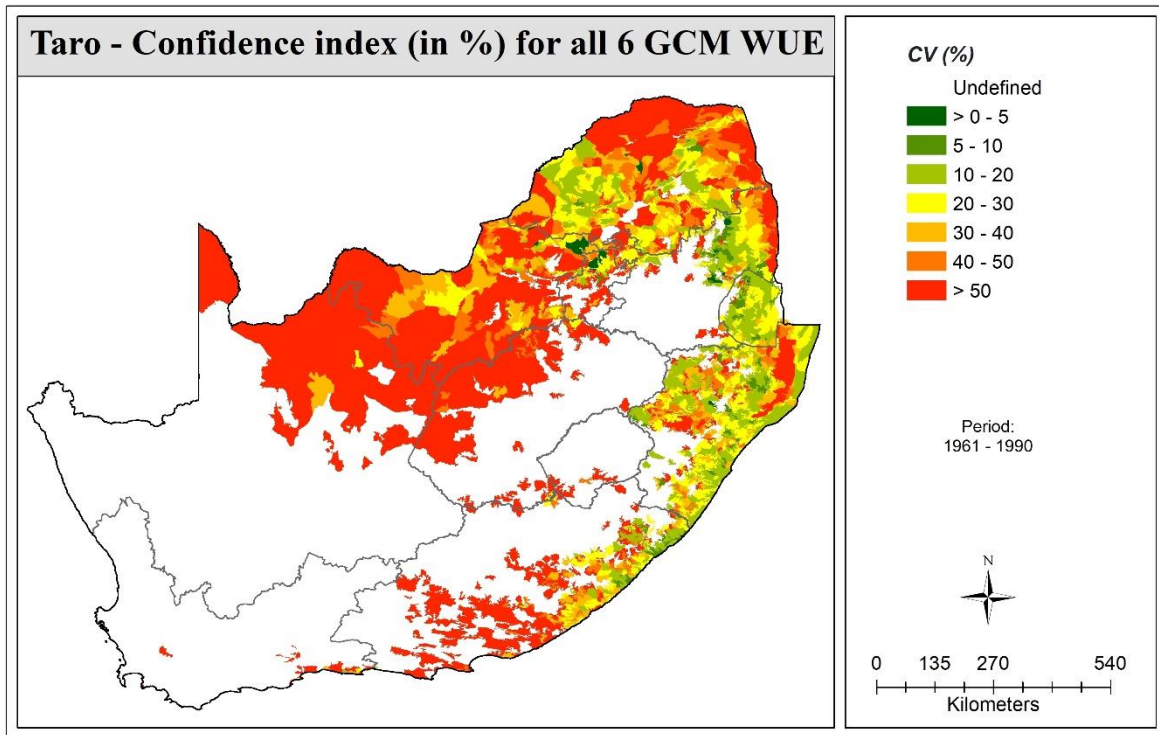


(a)

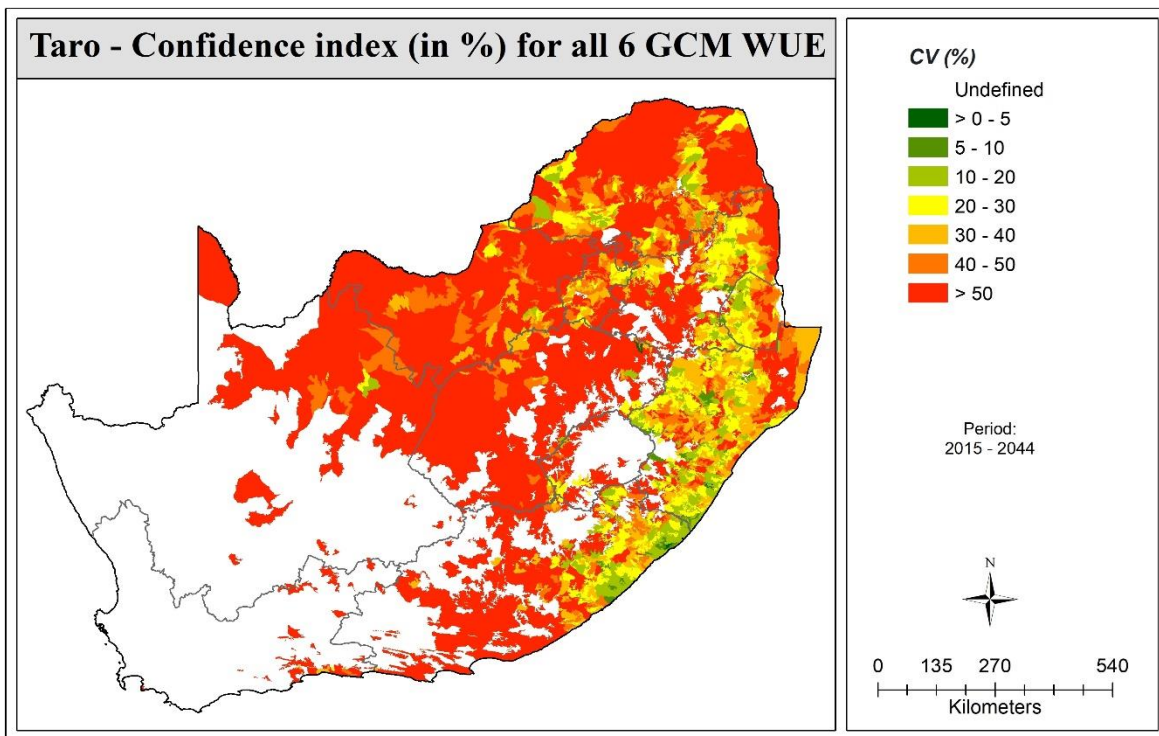


(b)

Figure 3.19 Coefficient of variation (CV in %) in mean water use efficiency for sorghum obtained from the six GCMs for the (a) present and (b) near future periods



(a)



(b)

Figure 3.20 Coefficient of variation (CV in %) in mean water use efficiency for taro obtained from the six GCMs for the (a) present and (b) near future periods

3.6 Climate change and season length

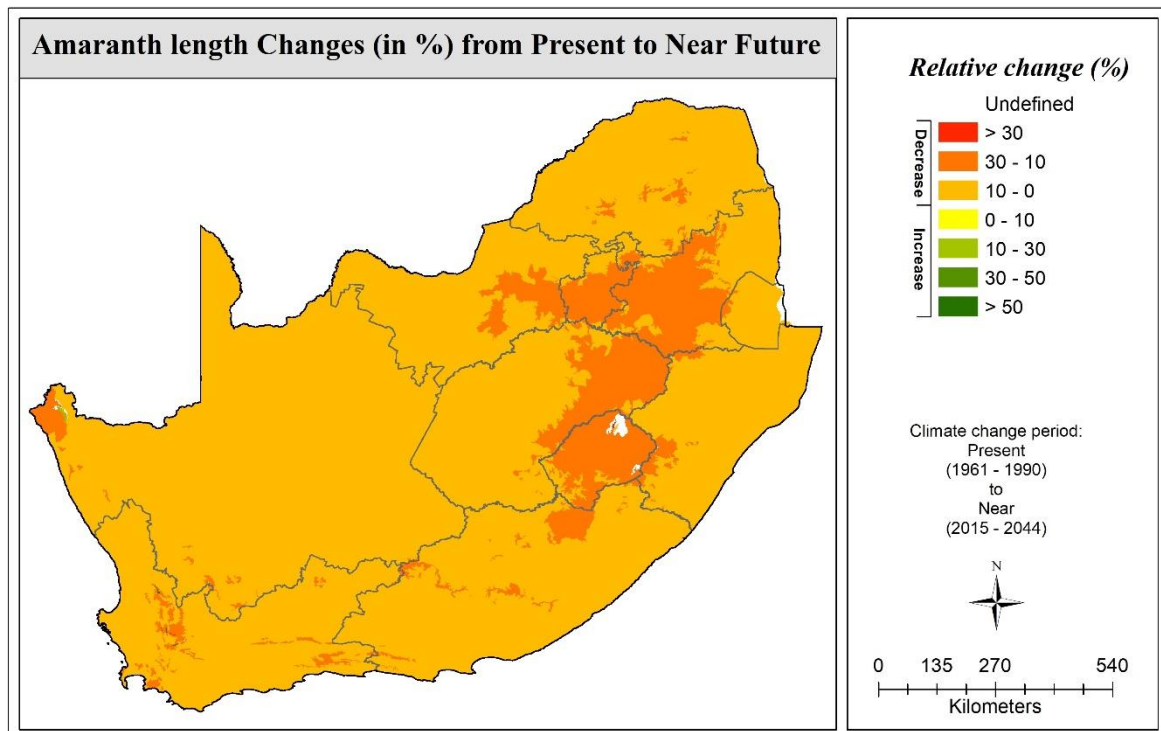
For each GCM, season lengths (i.e. crop cycle) simulated by AquaCrop for all 30 seasons were averaged to determine the mean seasonal value. Thereafter, the six values for each GCM were also

averaged (i.e. each GCM assigned equal weighting) to reduce the number of maps shown. This exercise was repeated for each of the three time periods (i.e. present, near future and distant future). Maps highlighting the change in average season from 1) present to near future, 2) near future to distant future, and 3) present to distant future period were generated for each NUS. The percentage change maps are presented next in **Section 3.6.1** to **Section 3.6.3**, and the ratio maps are given in **APPENDIX D3**. The change cannot mathematically be determined for AZs where the averaged WUE for the present period is zero. Such areas appear white on the maps and are labelled as “Undefined”. It is worth noting that the spatial extent of the WUE maps is almost identical to the yield maps.

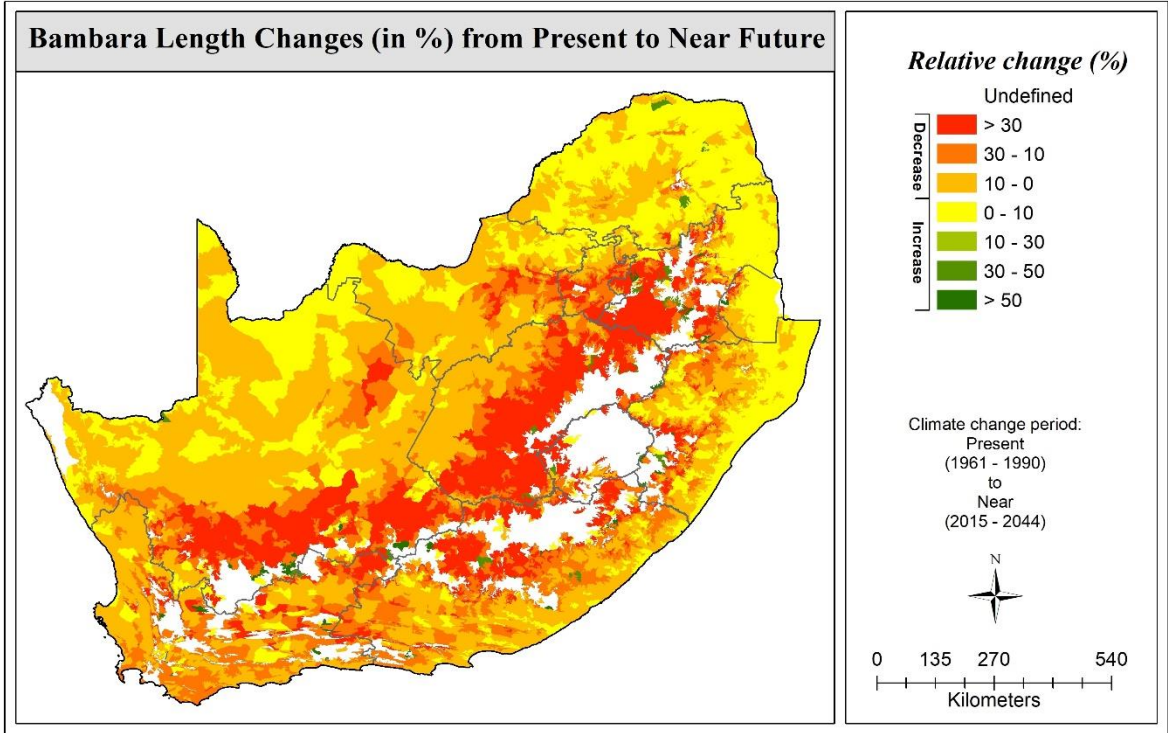
3.6.1 Present to near future

For the near future (relative to the present period), amaranth’s season length is expected to reduce by up to 10% for most crop production areas in the Limpopo, North West and KwaZulu-Natal provinces. However, in western and central Mpumalanga and the eastern Free State, the crop cycle may be reduced by up to 30% (**Figure 3.21a**). For bambara groundnut, a reduction in season length of up to 20% is expected in most areas. However, the reduction exceeds 30% in the interior regions of the country, e.g. western Mpumalanga and central Free State (**Figure 3.21b**). Sorghum’s season length may decrease by up to 30% (**Figure 3.21c**), whereas for taro, decreases are mainly 30% or less, except in the western parts of Limpopo, where they range from 30-50% (**Figure 3.21d**).

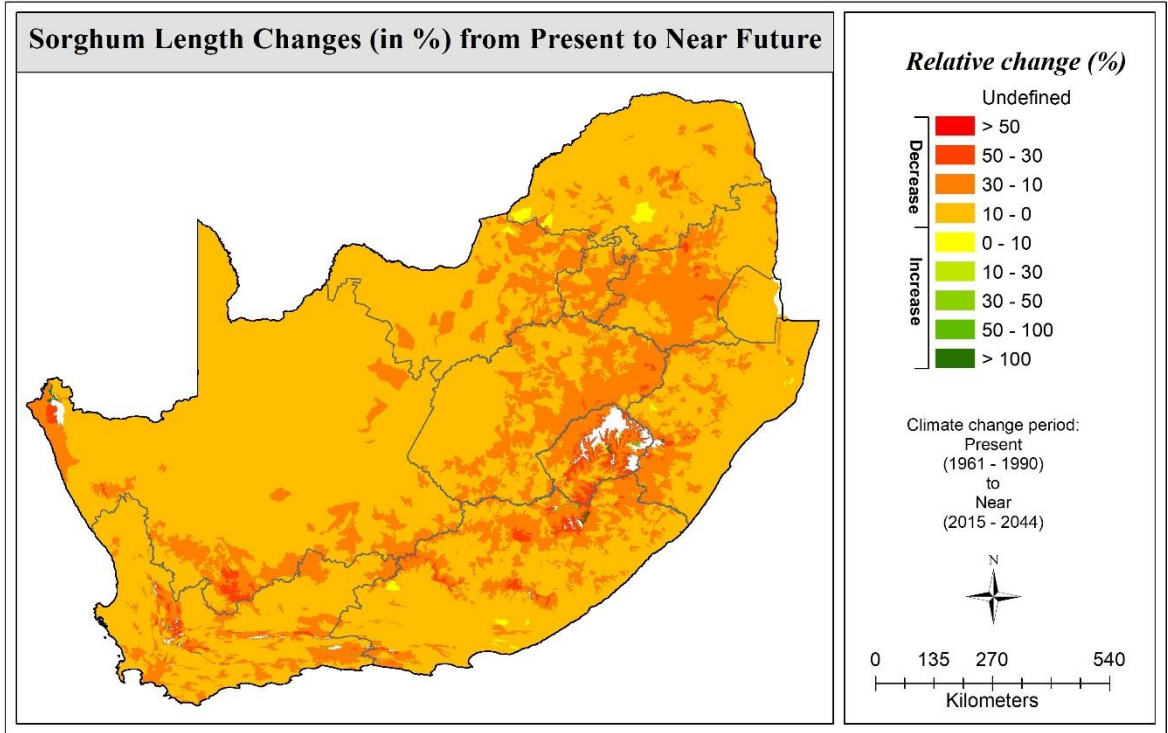
These findings are expected since a warmer future climate will accelerate the accumulation of heat units (i.e. growing degree-days). Thus, each crop phenological growth state will be reached sooner, resulting in a shorter time to reach physiological maturity. Adaptation strategies include shifting to earlier planting dates and growing early maturing cultivars with shorter season lengths and a high harvest index.



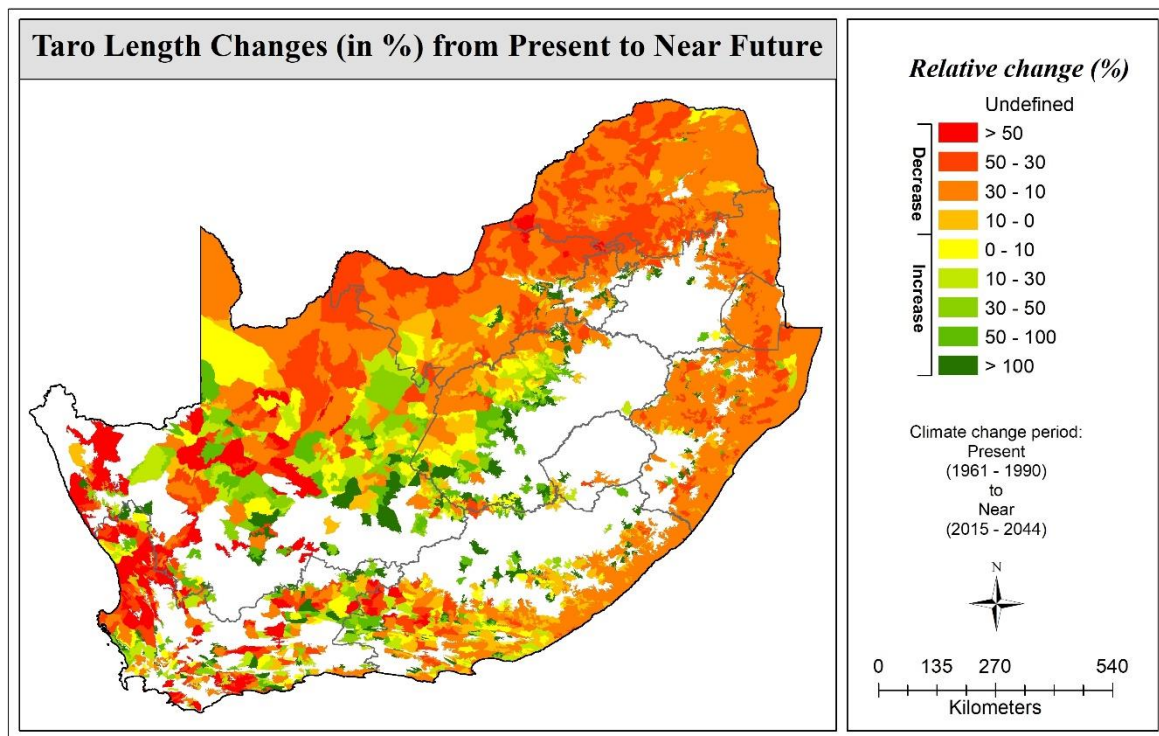
(a)



(b)



(c)

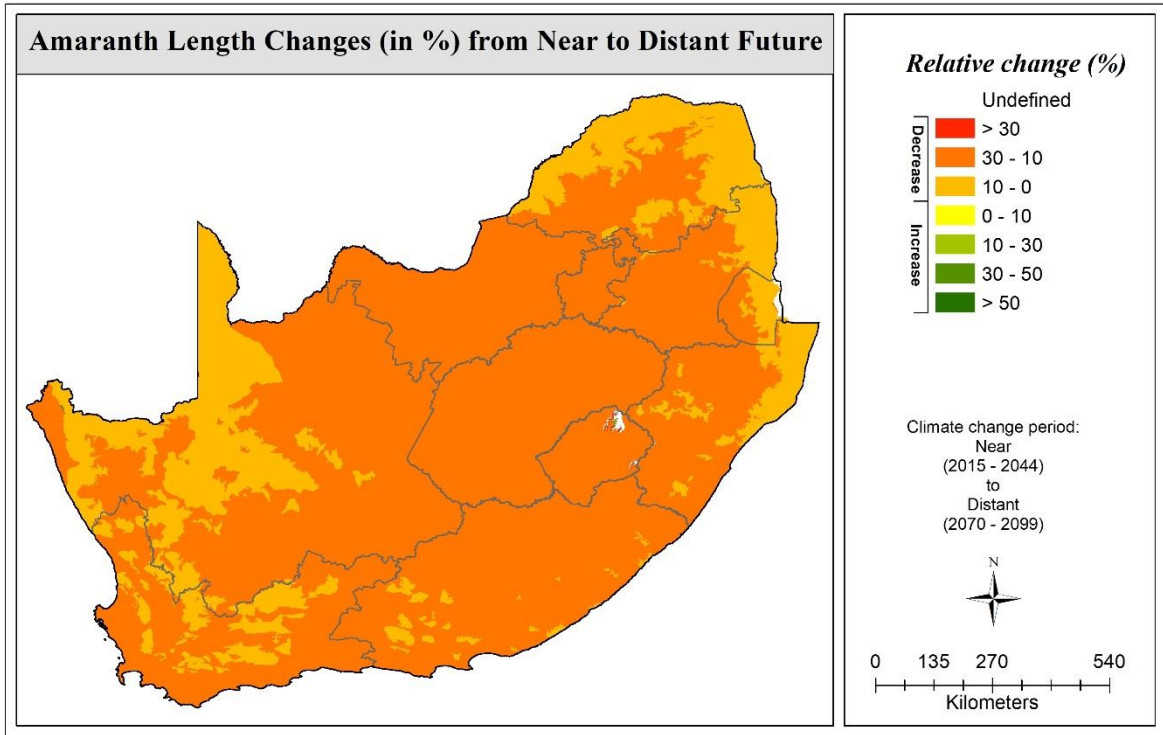


(d)

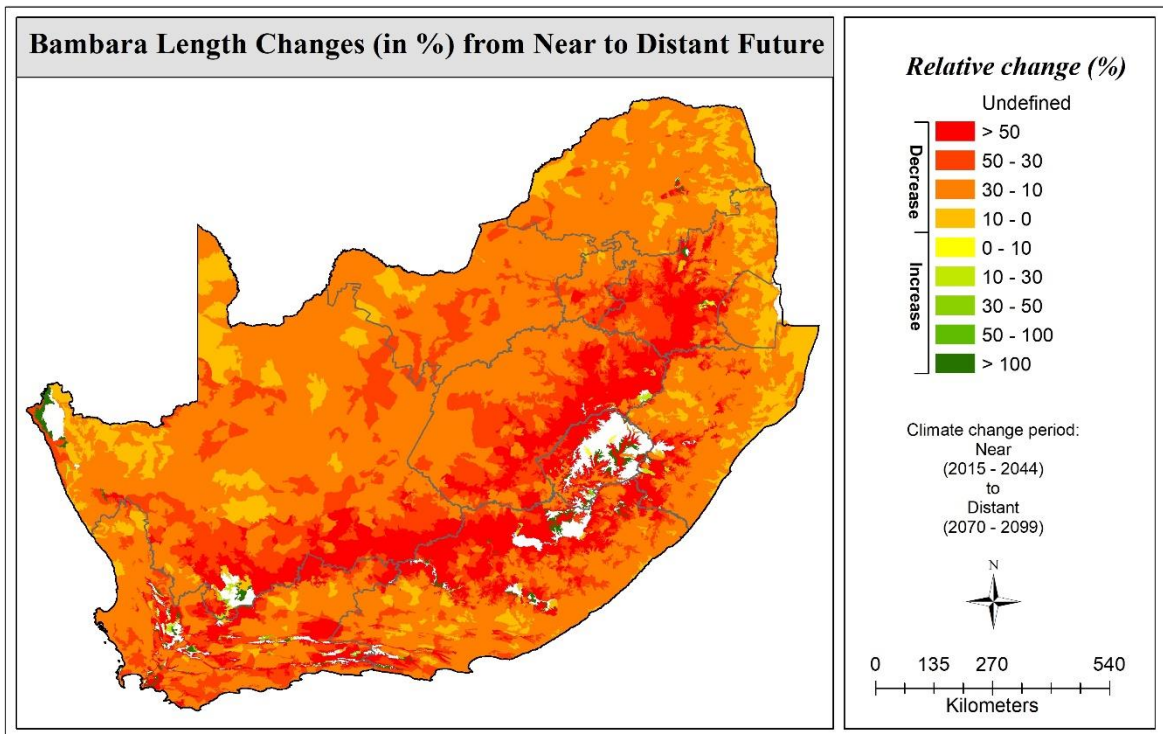
Figure 3.21 Change in mean season length (as %) from present to near future for (a) amaranth, (b) bambara groundnut, (c) sorghum and (d) taro

3.6.2 Near to distant future

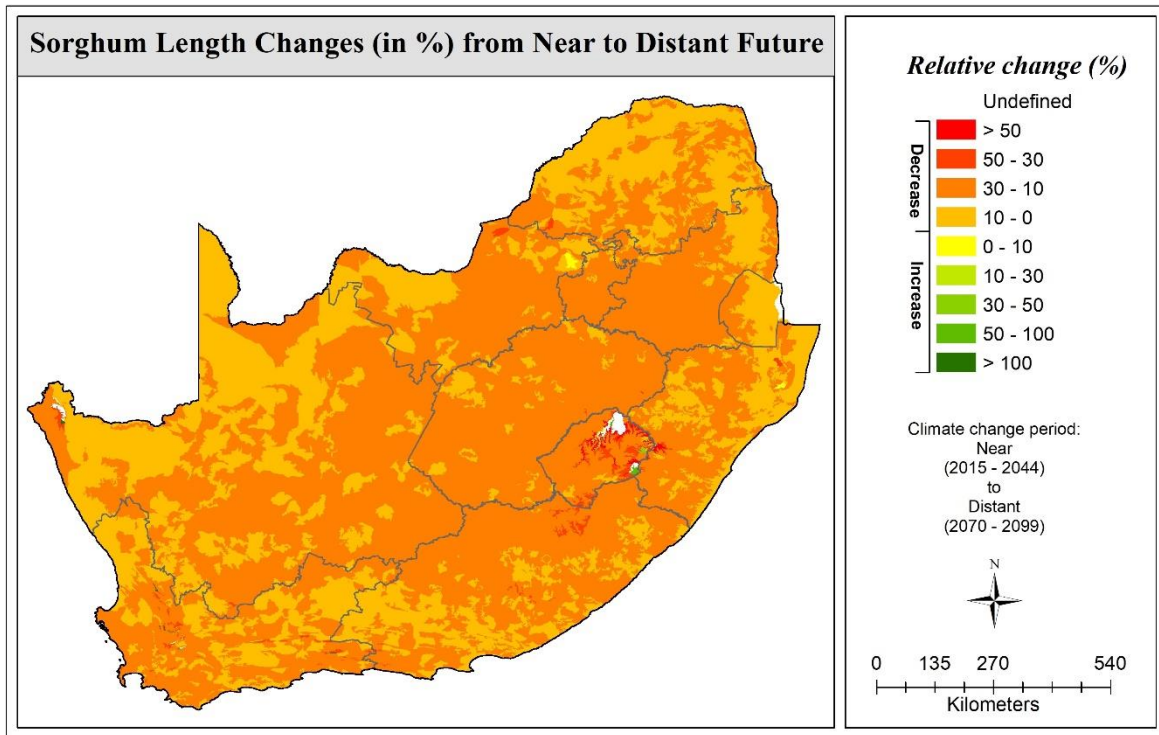
From the near (2015-2044) to the distant future (2070-2099), season lengths are expected to reduce further to continued warming. For example, Amaranth's season length decreases by 10-30% for most crop production areas, except for north eastern KZN, eastern Mpumalanga, and the eastern and northern parts of Limpopo (**Figure 3.22a**). In other words, the 10-30% reduction region expands outwards from the interior towards the borders of neighbouring countries, as is the case for bambara groundnut (**Figure 3.22b**) and sorghum (**Figure 3.22c**). For taro, there is a substantial reduction in areas deemed too cold to currently grow the crop, particularly in western and central Mpumalanga, eastern and southern Free state and south western KZN (**Figure 3.22d**). This indicates that taro may benefit from climate change due to expanding potential crop growing areas.



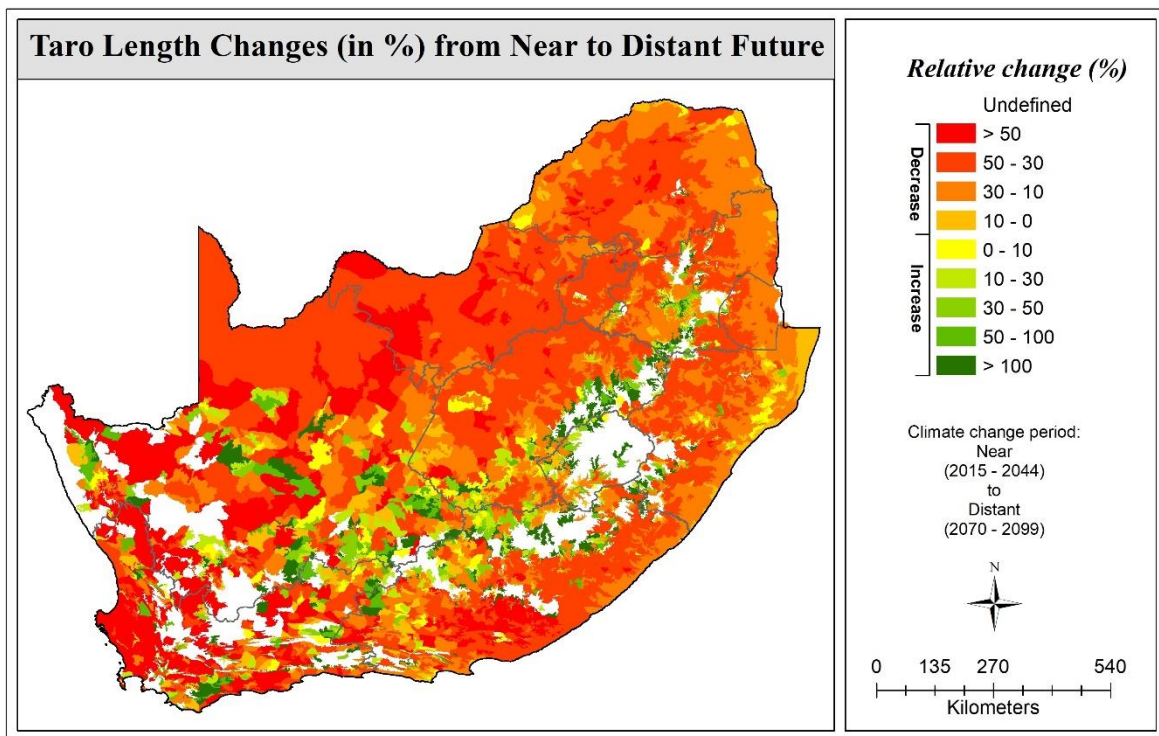
(a)



(b)



(c)



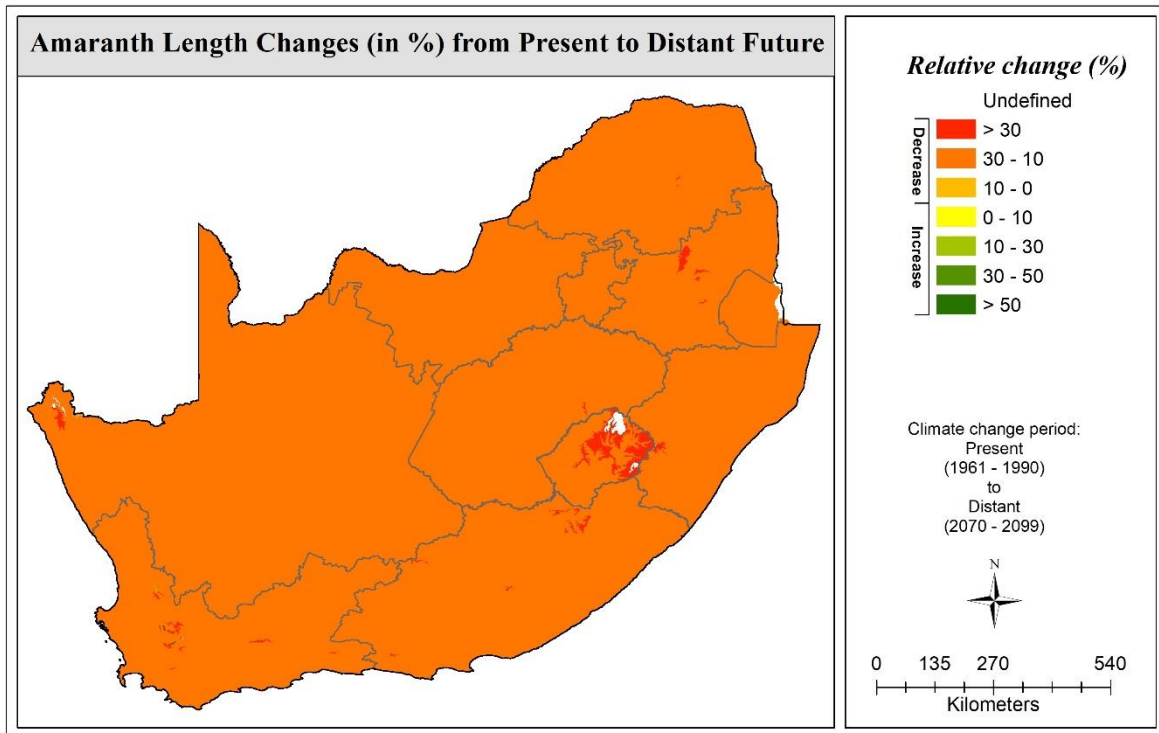
(d)

Figure 3.22 Change in mean season length (as %) from near to distant future for (a) amaranth, (b) bambara groundnut, (c) sorghum, and (d) taro

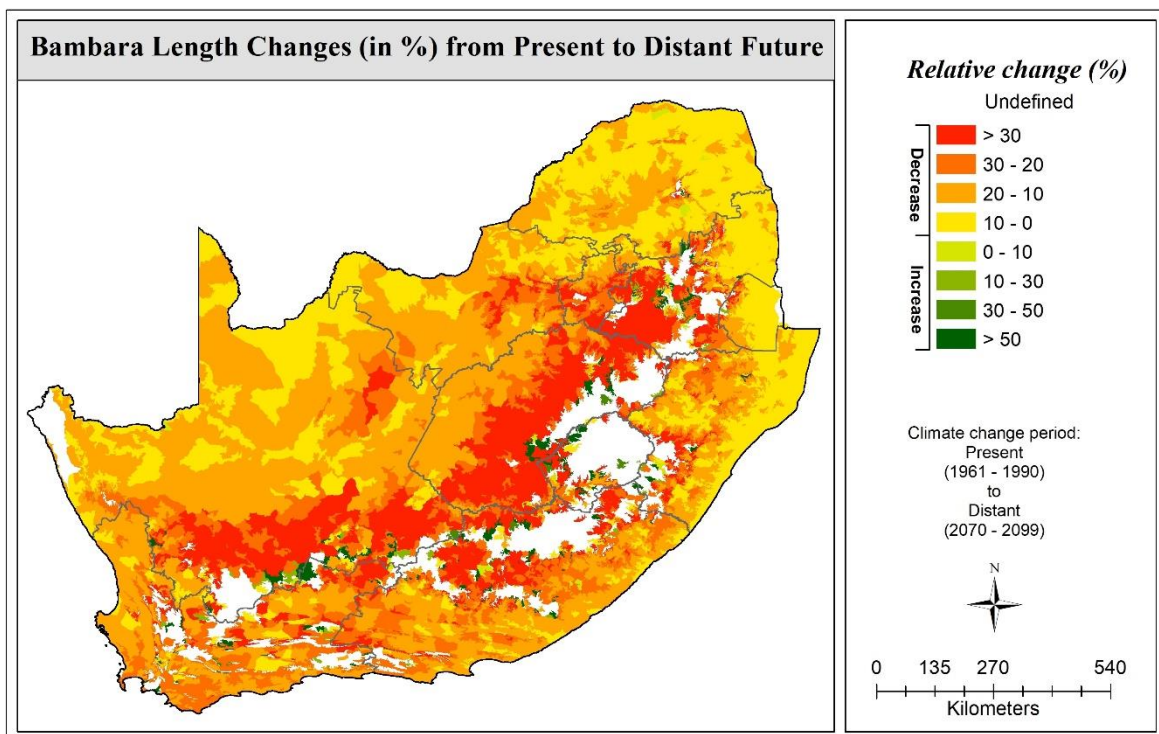
3.6.3 Present to distant future

The present to future distant maps shown in **Figure 3.23** highlight the large reduction in crop season length that can be expected due to the projected warming climate. For example, a 10-30% decrease in

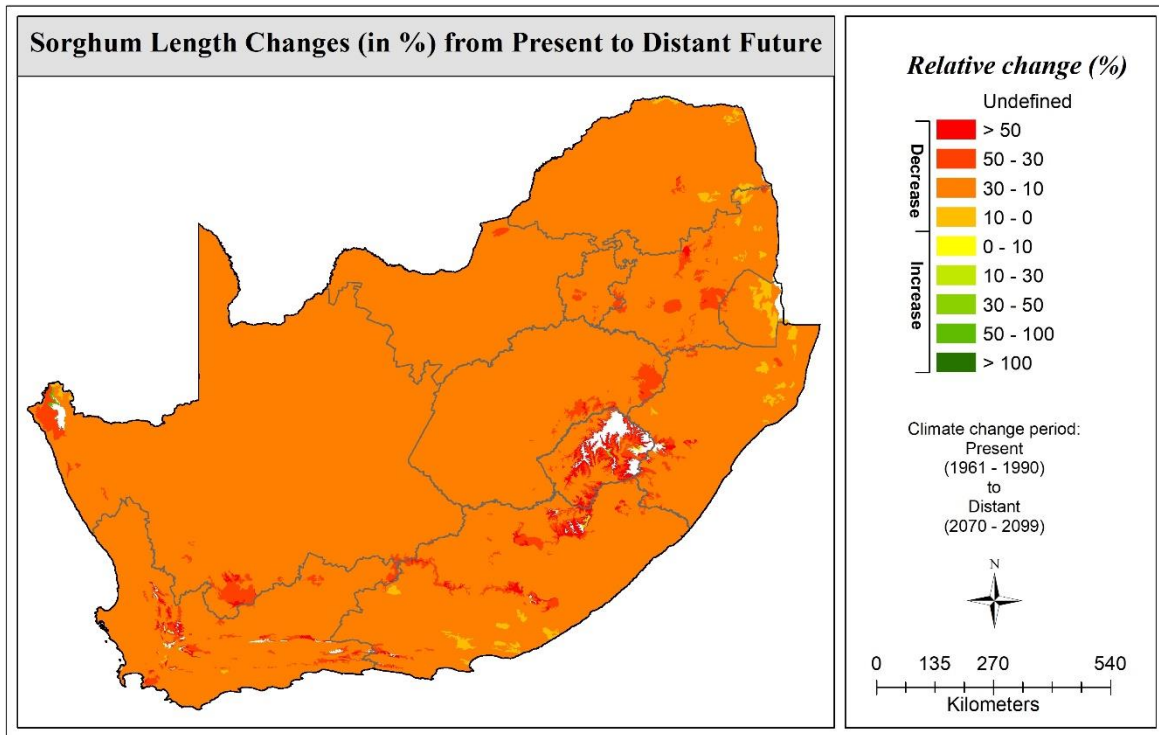
the crop cycle may be expected for amaranth and sorghum. For taro, the reduction changes from 10-30% (present to near future) to 30-50% (present to distant future).



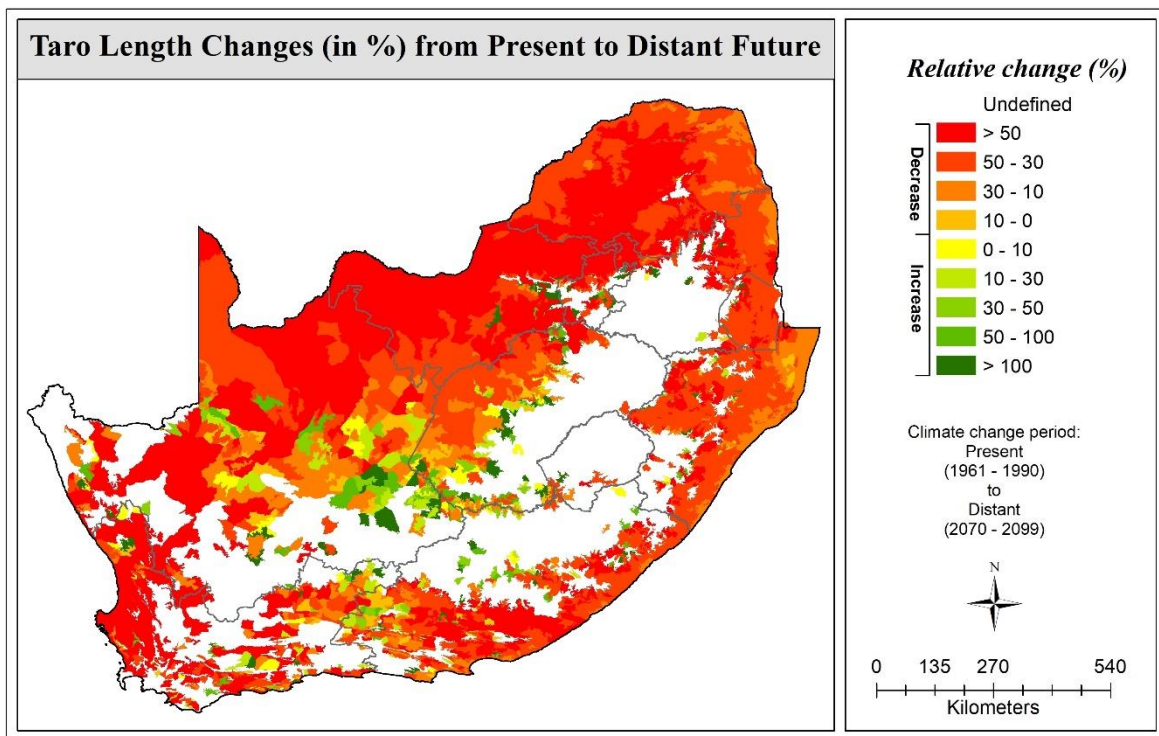
(a)



(b)



(c)



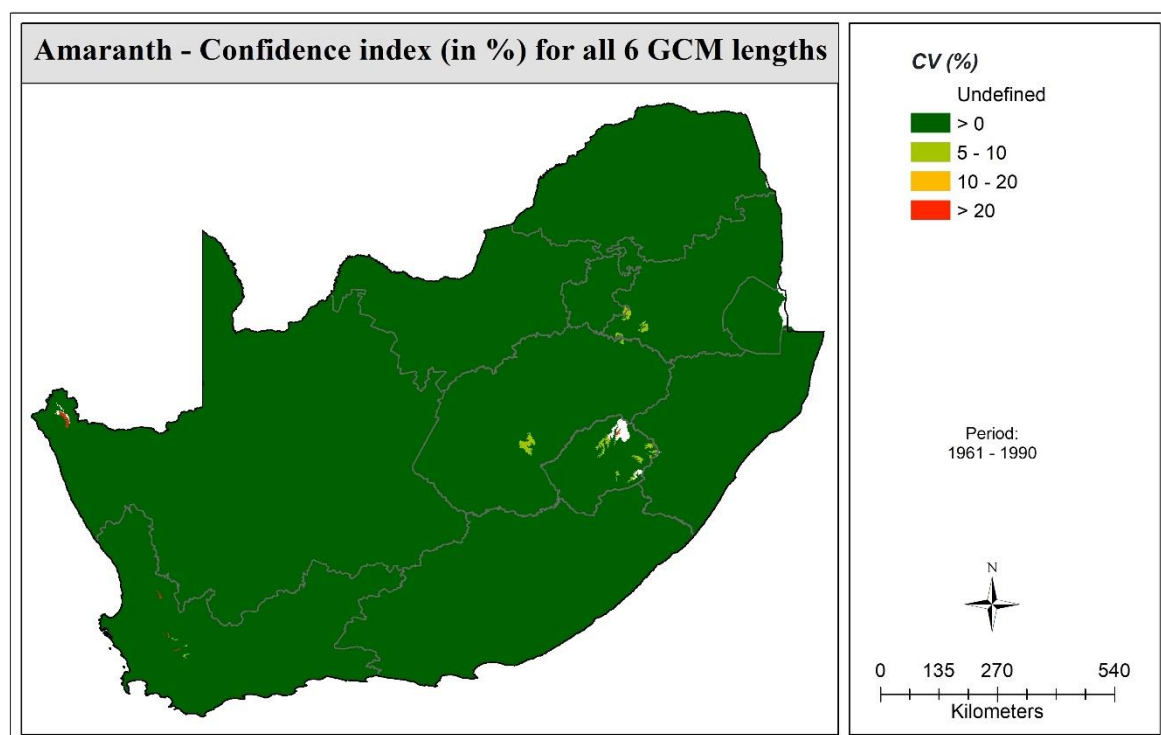
(d)

Figure 3.23 Change in mean season length (as %) from present to distant future for (a) amaranth, (b) bambara groundnut, (c) sorghum, and (d) taro

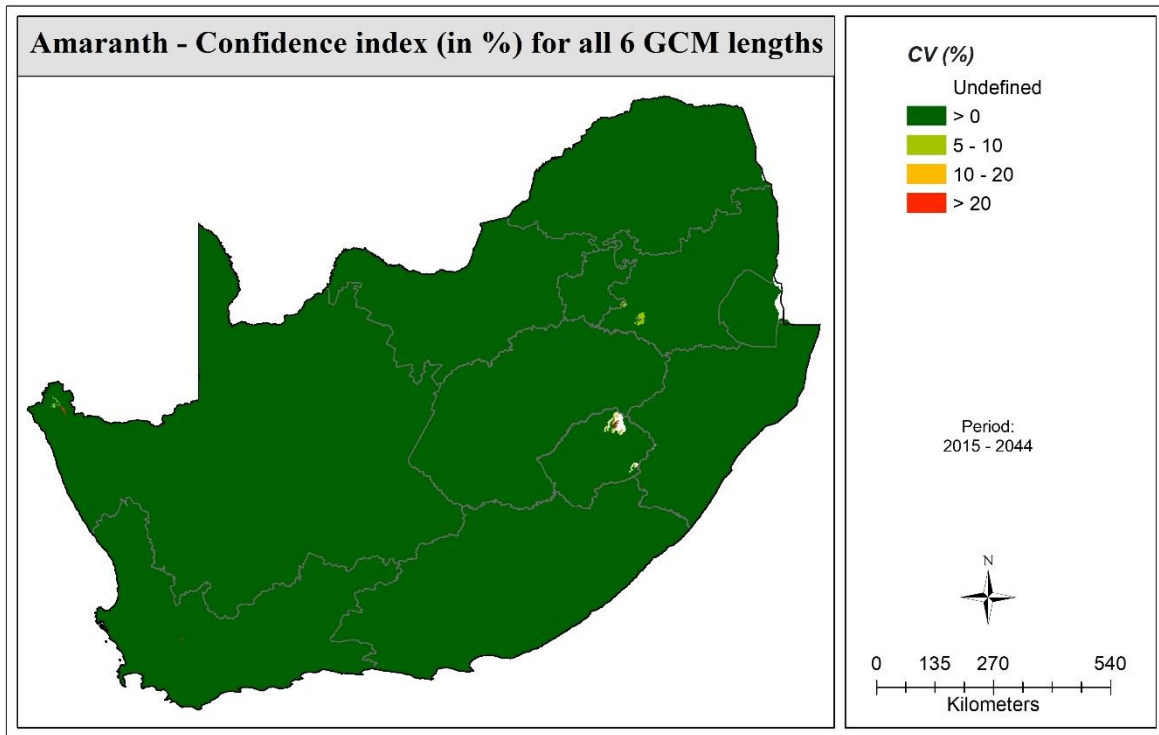
3.6.4 Confidence index

The variability (or dispersion) between the six GCM-based season length estimates is mostly very low (CV < 5%) for amaranth (**Figure 3.24**), bambara groundnut (**Figure 3.25**) and sorghum (**Figure 3.26**) in both the present and near future periods. Thus, all six GCMs predict very similar changes in season length; thus, confidence is deemed high. However, the CV of season length for taro is higher (i.e. lower confidence) for taro (**Figure 3.27**) and ranges from 5-20% for most areas deemed suitable for rainfed crop production.

The CV of taro's season length in the distant future is shown in **Figure 14.1d (APPENDIX E3)**, highlighting greater variability (20-40%) in the northern parts of the Limpopo province. For the other three crops (**Figure 14.1a-c in APPENDIX E3**), confidence is much higher (i.e. lower CVs) when compared to taro. In general, confidence is higher (i.e. lower CV) for season length than WUE and yield, especially for bambara groundnut, sorghum and taro.

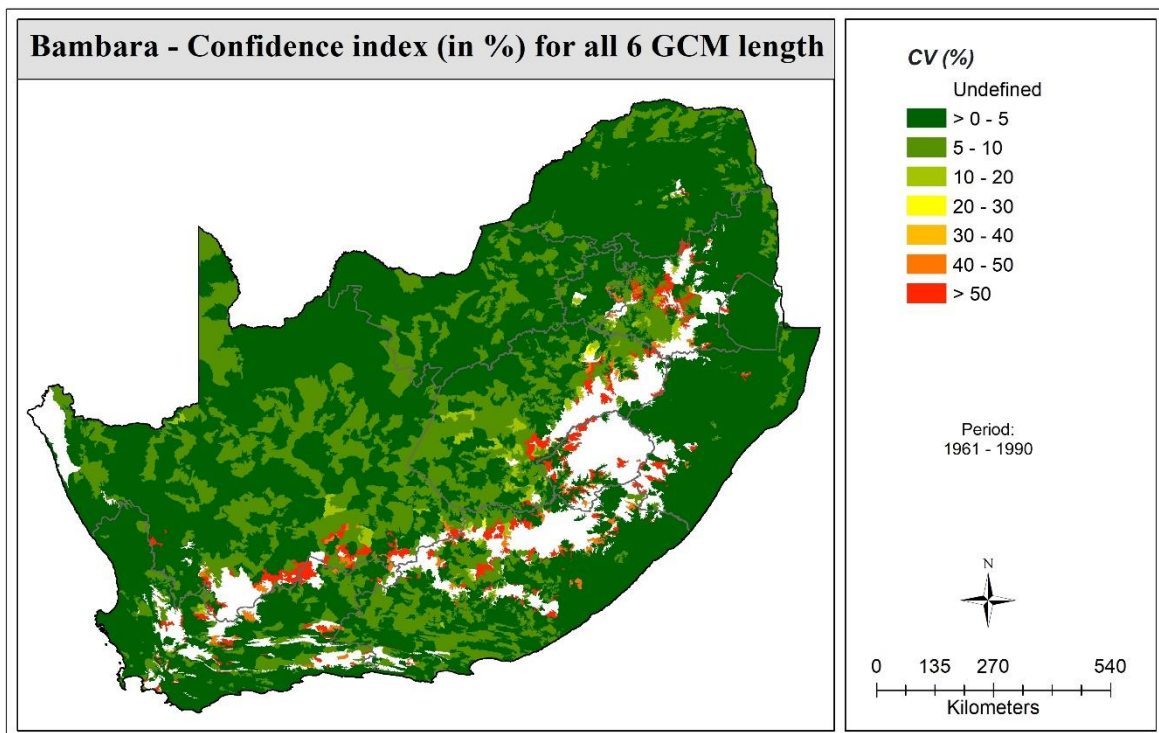


(a)

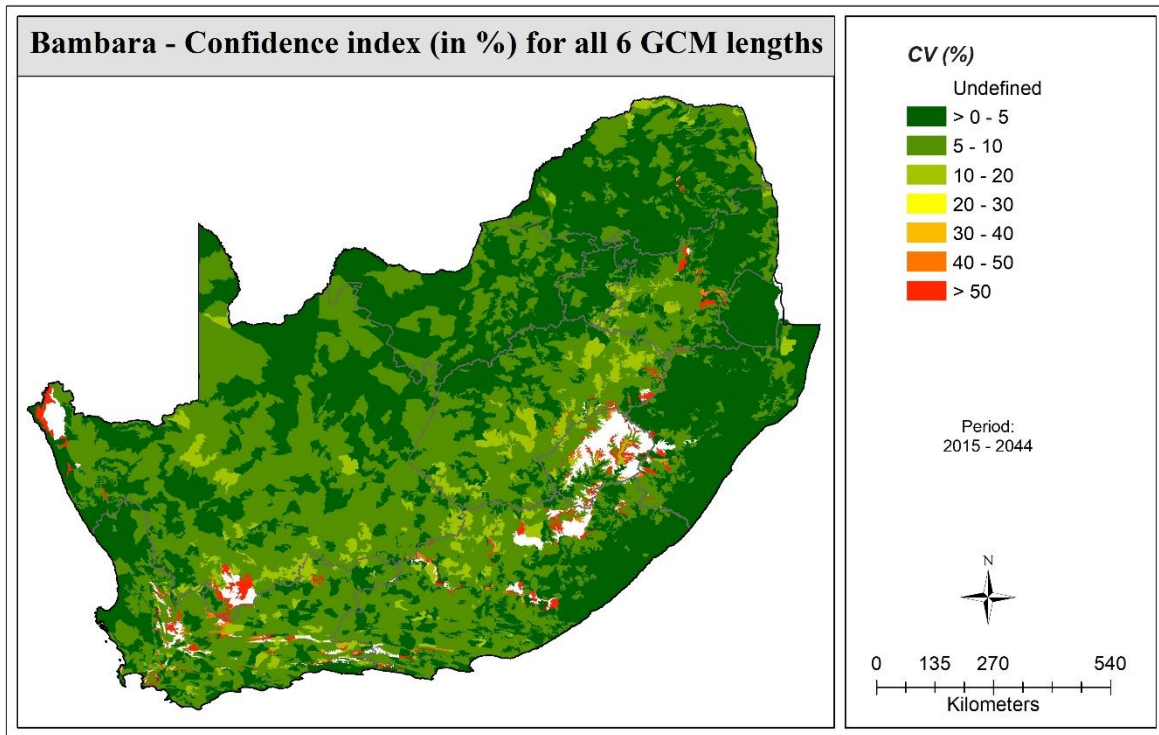


(b)

Figure 3.24 Coefficient of variation (CV in %) in mean season length for amaranth obtained from the six GCMs for the (a) present and (b) near future periods

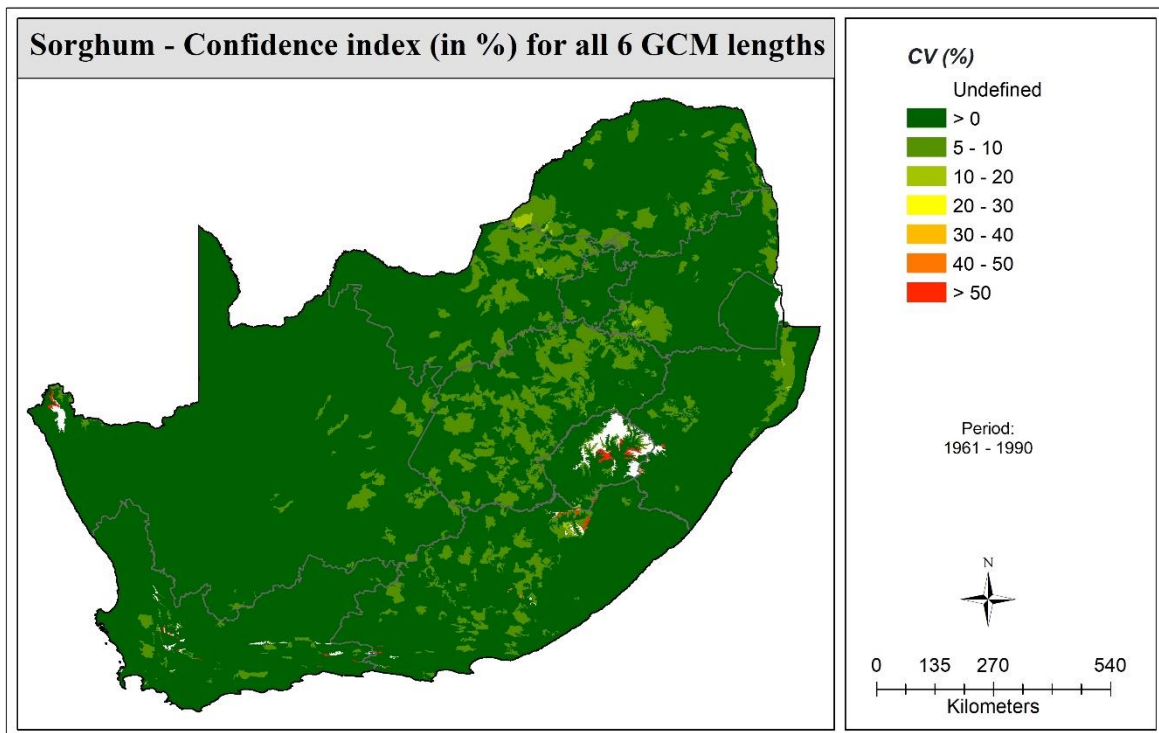


(a)

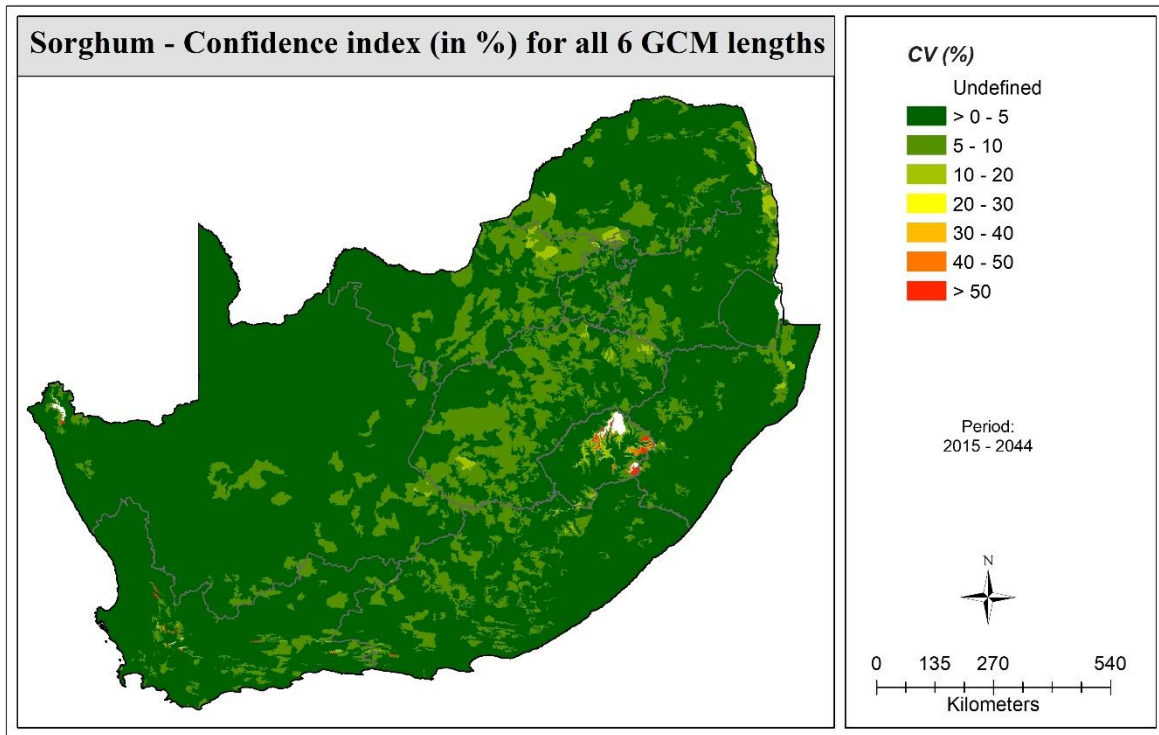


(b)

Figure 3.25 Coefficient of variation (CV in %) in mean season length for bambara groundnut obtained from the six GCMs for the (a) present and (b) near future periods

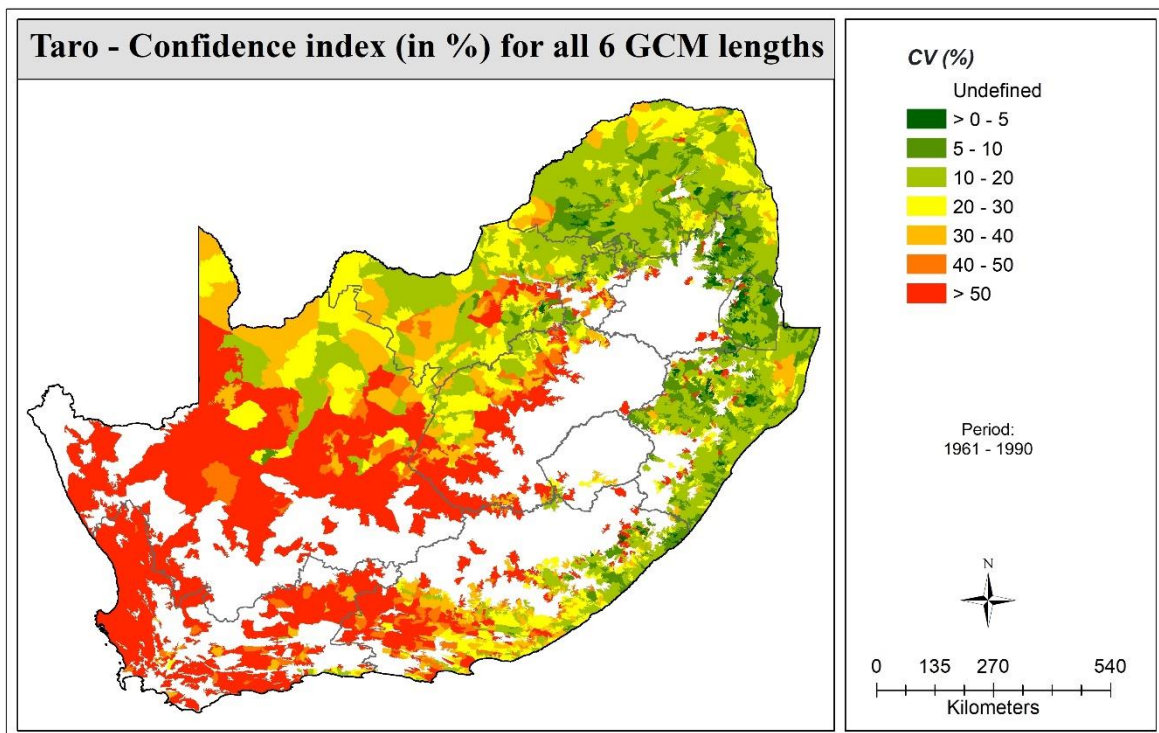


(a)

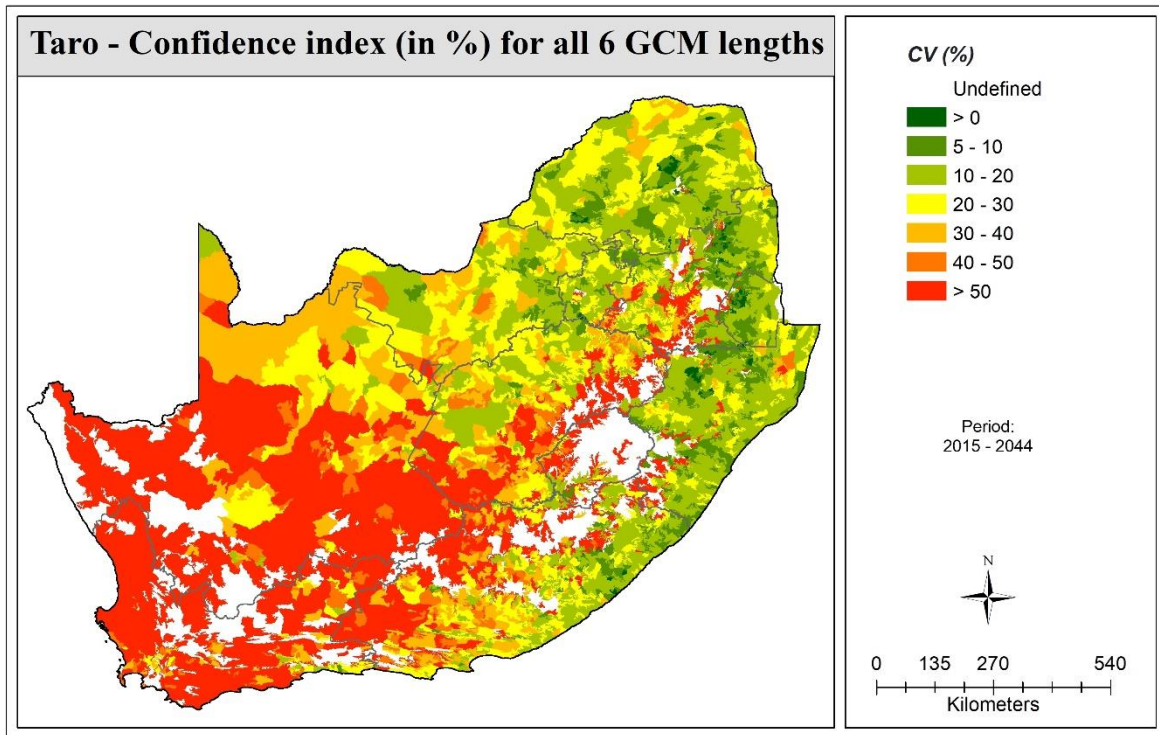


(b)

Figure 3.26 Coefficient of variation (CV in %) in mean season length for sorghum obtained from the six GCMs for the (a) present and (b) near future periods



(a)



(b)

Figure 3.27 Coefficient of variation (CV in %) in mean season length for taro obtained from the six GCMs for the (a) present and (b) near future periods

4 SUMMARY, CONCLUSIONS AND RECOMMENDATIONS

4.1 Summary of approach

The AquaCrop model developed by the FAO was used to assess the potential impacts of climate change on crop response in South Africa. More specifically, the model was run for:

- a) four neglected and underutilised crops
 - i. amaranth
 - ii. bambara groundnut
 - iii. grain sorghum and
 - iv. taro (amadumbe)

- b) four time periods
 - i. historical (1950-1999: 49 seasons)
 - ii. present (1961-1990: 29 seasons)
 - iii. near future (2015-2044: 29 seasons)
 - iv. distant future (2070-2099: 29 seasons)

- c) six GCMs that were dynamically downscaled (using the CSIR's CCAM model) and bias-corrected against historical (i.e. observed) climate data
 - i. ACC Australian Community Climate and Earth System Simulator
 - ii. CCS Community Climate System Model
 - iii. CNR National Centre for Meteorological Research Coupled GCM v5
 - iv. GFD Geophysical Fluid Dynamics Laboratory Coupled Model
 - v. MPI Max Planck Institute Coupled Earth System Model
 - vi. NOR Norwegian Earth System Model

- d) two representation concentration pathways (RCPs)
 - i. 4.5
 - ii. 8.5

In order to automate the national model runs, approximately 10000 lines of code (written in UNIX and Fortran) have been developed. Despite this high level of automation, the crop model was not run for 138 consecutive seasons from 1961/62 to 2098/99 using projected climate data, simply because AquaCrop runs very slowly with large input climate datasets. Hence, the model was run for specific periods to reduce computational expense. Furthermore, the model was not run for RCP4.5 because anomalies were discovered in the climate projections. A single planting date and plant density were selected for each crop to further minimise computational expense.

4.2 Summary of main findings

From the climate change results and discussion presented in **Chapter 3**, it is important to highlight the following:

- This study is based on climate projections from six dynamically downscaled GCMs driven by the RCP8.5 (low mitigation) scenario.
- The RCP4.5 (high mitigation) scenario was not used in this study due to inconsistencies in climate projections compared to the RCP8.5 datasets.
- Currently, it is not possible to verify GCM climate projections except to assess the GCM's ability to model present climate conditions.

- Bias correction of GCM projections is necessary to improve the confidence for near future climate scenarios.
- Bias correction allows the present period to represent historical conditions.
- There is greater confidence (lower uncertainty) associated with temperature projections than future rainfall scenarios.
- Rainfall variability and extreme events may increase into the distant future, along with increasing uncertainty and decreasing confidence in rainfall projections towards the year 2100. Hence, the present to distant future maps should not be used for decision-making purposes.
- More rainfall is projected for the central interior (west and north of Lesotho) in the near future, whereas all other areas (particularly the Western Cape) may experience decreased rainfall.
- Relative to the present climate, the maximum and minimum daily temperature in the near future will likely increase by 1-2°C for most southern Africa.
- Changes in maximum temperature are predicted to be greater than those for minimum temperature.
- For amaranth, yields in most areas north of the Free State and KZN borders are expected to decline by up to 30% in the near future, whilst a 10% yield increase may occur for most other areas.
- Yield declines exceeding 50% for bambara groundnut may be expected across the majority of Limpopo and eastern Mpumalanga and the north-eastern parts of KwaZulu-Natal and North West provinces.
- Sorghum yields are expected to decline for most growing areas along the country's eastern seaboard, with the highest yield losses (> 50%) predicted for the Limpopo and eastern Mpumalanga provinces.
- In contrast, taro yields should improve for most areas in Limpopo, North West and KwaZulu-Natal (except in the north-east and along the coast) provinces.
- The Limpopo province appears to be least favourable for crop production in the near future, except for taro production.
- For bambara groundnut, the expansion in growing areas occurs mainly in western Mpumalanga, southern Free State and in the Eastern Cape (northern regions).
- No noticeable expansion in suitable growing areas for sorghum was simulated by the model from present to near future.
- Taro exhibits a large expansion in areas deemed suitable for growth in the central interior.
- Expansion of crop production from present to near future is most likely to occur in the Mpumalanga province.
- The CO₂ fertilisation effect may offset the negative impacts of climate change on crop production in southern Africa.
- Relative to the present climate, amaranth's WUE is expected to increase in both the near future and distant future.
- For the other three crops, changes in WUE mimicked the expected changes in yield, i.e. both increases and decreases for bambara groundnut, mostly decreases for sorghum and mainly increases for taro.
- A warmer future climate will result in accelerated accumulation of heat units (i.e. growing degree-days), thus shortening the time to reach physiological maturity (i.e. shorter growing season).
- Adaptation strategies include shifting to earlier planting dates and growing early maturing cultivars with shorter season lengths and a high harvest index.
- Crop season length is expected to shorten from the present to the near future, except in some altitude zones for bambara groundnut and taro.
- Towards the distant future, taro may experience the largest reduction (> 30%) in season length across most areas, compared to a 10-30% reduction for the other three crops.

- The variability in simulations between the six GCMs is lowest (i.e. highest confidence) for season length, since it is mostly affected by temperature.
- Since crop yield is mostly affected by rainfall and temperature, variability in simulations between the six GCMs is highest (i.e. lowest confidence).

Crop simulation models will remain a primary tool for assessing potential impacts of climate change on crop yield, water use and water productivity. The main outcomes listed above vary spatially and for each crop, thus highlighting the importance of simulating individual crop response to increased temperature and CO₂ levels and changes in rainfall that varies spatially in both magnitude and direction. Elevated atmospheric CO₂ levels should positively impact photosynthesis and WUE, which override the negative effects of increased temperature (i.e. heat) stress, thus resulting in higher future crop yields.

However, water stress is the major limitation in rainfed farming systems. Decreased rainfall in the future will result in higher water stress and reduced transpiration cooling, which can negate the positive effects of elevated CO₂ and therefore, yields are likely to decline. For smallholder farmers producing crops in water-stressed environments with low nutrient availability, crop benefits from elevated CO₂ are considerably reduced or even eliminated. Such farmers will be disadvantaged by higher temperatures, irregular rainfall and more extremes into the future. The maps presented in this report should help assess the likely impact of climate change on farming communities in South Africa.

4.3 Limitations of study

4.3.1 Distant future projections

It is important to note that confidence in crop yield changes into the distant future is much lower than those for the near future, due to increasing uncertainty in climate projections towards the year 2100. Hence, trends identified from the present to near future maps should be used for decision-making and policy development. The near future to distant future (or present to distant future) maps should only be used as a rough guide in assessing the direction of possible change towards the end of the 21st century.

4.3.2 Rejection of RCP4.5 scenarios

As noted in **Section 2.3.8**, issues were found with the RCP4.5 projections developed by the CSIR using their CCAM regional climate model (RCM). Hence, these projections were not used to assess the impact of climate change on crop response. Although RCP8.5 represents the “business as usual” scenario, it is important to note that the results obtained in this study do not span all possible future outcomes.

4.3.3 CMIP5 six-member GCM ensemble

Dynamical downscaling is performed with RCMs that require output from GCMs to set (i.e. force) atmospheric boundary conditions. For this study, the CSIR’s CCAM model was driven using output from six CMIP5 GCMs deemed to best replicate (i.e. mimic) climate conditions experienced over southern Africa, particularly the ability to model the El Niño-Southern Oscillation (ENSO) phenomenon. It is understandable that a subset of only six GCMs cannot fully represent the entire CMIP5 ensemble of over 70 GCMs. From **Section 2.3.8**, it is clear that the downscaled projections for RCP8.5 do not span the whole CMIP5 ensemble, particularly for the Orange and Vaal WMAs, where CCAM rainfall projections represent the wetter end of the envelope. Therefore, CCAM projections for the Orange and Vaal WMAs represent a more optimistic view of the full range of possibilities that could be expected in these two regions.

4.3.4 CMIP5 vs CMIP6 GCM projections

As this study was nearing completion, climate projections from CMIP6 GCMs became available. It is important to note that the CMIP6 ensemble of GCMs project slightly drier conditions in the central part of the country (especially for a 4°C rise in global temperature; cf. **Figure 15.1** in **APPENDIX F**), which none of the CMIP5 GCMs used in this study show. In other words, they do not capture the entire range of possibilities represented by the CMIP6 GCM ensembles. However, the six selected GCMs do fall within the uncertainty range of the latest CMIP6 ensemble, and thus, results from this study are compatible with the CMIP6 envelope of possible projections.

For the Western Cape region (**Figure 4.1**), rainfall projections for the CCAM 6-member ensemble for RCP8.5 show a much drier distant future, which agrees with projections from both the larger CMIP5 and CMIP6 35-member ensembles, as well as the CORDEX projections. Therefore, results presented in this study must be interpreted on the understanding that no GCM provides “perfect” future climate scenarios. The modelling results represent six possible futures, and again, they are unlikely to span all possible futures.

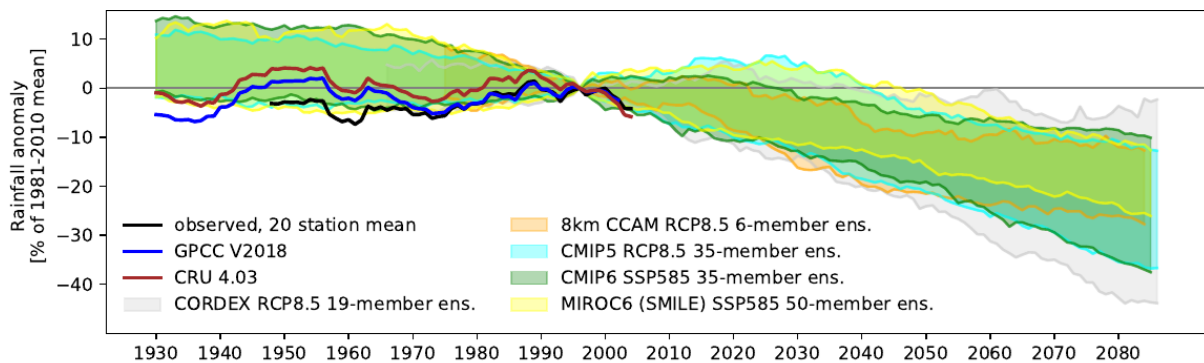


Figure 4.1 Rainfall signal for past, present and future conditions obtained from different generations of GCMs (CMIP5 vs CMIP6) for the Western Cape province

4.3.5 CO₂ fertilisation effect

From the review by Franke (2021) of 20 climate changes studies across southern Africa, 70% modelled the CO₂ fertilisation effect on crop growth. The CO₂ fertilisation effect is likely to increase crop yield, reduce water use and thus, higher water use efficiency, especially for C3 crops. The results presented in this study show substantial increases in crop yield in certain regions. Hence, the negative impacts of climate change on crop production in southern Africa may be offset by the CO₂ fertilisation effect.

Of particular concern is the f_{SINK} crop parameter used in AquaCrop. Certain FACE experiments (e.g. Manderscheid et al., 2010) showed that root and tuber crops such as sugarbeet failed to optimally respond to elevated CO₂ levels. For this reason, f_{SINK} values were not altered, and the default value of 50% was used for all crops in this study. However, Vanuytrecht et al. (2011) recommended that future research is necessary to better understand crop responsiveness to elevated CO₂ to provide updated crop f_{SINK} values and reduce uncertainty in modelling future agricultural production. Franke (2021) also recommended that FACE experiments should be a priority to improve the understanding of how climate change will impact crop performance in southern Africa.

4.3.6 Biotic and abiotic stresses

In this study, soil fertility was assumed nonlimiting to growth, and the impact of weed growth was not considered. AquaCrop cannot account for the effects of pests and diseases (cf. **Section 2.1**). However, pest and disease incidence is expected to increase due to the warmer climate conditions predicted for

the future, which will likely reduce crop yields. Furthermore, weed growth may be stimulated more by elevated CO₂ than crop growth (Valero et al., 2013), leading to increased competition for light, water and nutrients.

Besides water stress, nutrient stress can also become the overriding factor determining crop growth, and thus, crops are less likely to respond to elevated CO₂. For example, nitrogen deficiency reduces radiation use efficiency, resulting in lower growth stimulation under elevated CO₂ (Dier et al., 2018). Nitrogen deficiency can also lessen the improvements in WUE under elevated CO₂ (Manderscheid et al., 2018).

4.4 Recommendations and future research

Much effort was spent producing simulated output that is considered reliable and error-free. Furthermore, the approach developed and implemented in this study is by no means considered “exhaustive”. Therefore, it is strongly recommended that this study is repeated in the near future and that the following recommendations are taken into consideration:

- Kunz et al. (2020) showed that planting date had a greater impact on simulated yield than plant density. In this study, only one planting date was considered to reduce computational expense. In the future, at least two planting dates (in November and December) are recommended, as suggested by Kunz et al. (2020).
- Similarly, only one plant density was simulated, and thus, future studies should consider two densities that represent both commercial and smallholder farming environments.
- Climate projections for the RCP4.5 mitigation scenario should be modelled in future studies and results compared to those derived from the RCP8.5 scenario.
- Ideally, this study should be repeated using representative GCMs from the CMIP6 ensemble, which represent the latest climate projections currently available. If possible, more than six GCMs should be included to better understand the range of possible future outcomes.
- All climate change impact assessments should be conducted with and without the CO₂ fertilisation effect to also show a wider range of possible future outcomes.
- As noted in **Section 4.3.5**, further research is required to quantify fSINK values for crops better. Future studies should consider f_{SINK} values of 60-80% for root and tuber crops and 0-20% for cereal crops, as suggested by Vanuytrecht et al. (2011). This suggests that root and tuber crops (e.g. taro) may benefit more from the CO₂ fertilisation effect than cereal crops (e.g. sorghum).
- Allen et al. (2020) noted that due to fluctuating CO₂ levels in FACE experiments, plant response is reduced when compared to constant CO₂ levels. Therefore, future studies should consider applying a correction factor of about 1.5 needs to FACE results.

The above-mentioned recommendations will certainly increase computational expense, and thus, additional effort is required to further improve the performance of the AquaCrop model. AquaCrop was coded using the Delphi programming language by the FAO. Recently, the model was re-coded in open-source languages such as R (Rodriguez and Ober, 2019), MATLAB/Octave (Foster et al., 2017) and Python (Kelly and Foster, 2021). However, it is recommended that the open-source version of AquaCrop is re-coded in the FORTRAN programming language to further improve model performance. This will facilitate the development of a multi-threaded version that takes full advantage of all CPU cores on a PC and, thus, should run considerably faster.

Since 2009, the WRC and former DAFF have funded numerous research projects where AquaCrop was run to simulate crop water use and yield using the historical climate and soils databases developed for all 5838 altitude zones (e.g. Kunz et al., 2015a; Mabhaudhi et al., 2016a; Mabhaudhi et al., 2016b; Kunz et al., 2020; this project). However, different versions of the climate database were used in these studies, which means the results are not comparable. Thus, the results presented in this study

supersede those obtained by Mabhaudhi et al. (20116a; 2016b) for taro and bambara groundnut. It is highly recommended that the latest versions of the altitude zone climate and soils databases (described in the next two paragraphs) are used to run AquaCrop for up to eight underutilised crops that AquaCrop has been calibrated for (i.e. amaranth, bambara groundnut, cowpea, grain sorghum, groundnut, pearl millet, sweet potato and taro). This will result in developing a single database of crop, yield, water use and water productivity data that can then be used to increase agricultural diversification in South Africa. As noted in **Section 2.4.1**, amaranth should be remodelled using the crop parameters values developed by Nyathi et al. (2018), which may provide better results than those obtained using parameter values developed by Bellow and Walker (2017).

In April 2020, the WRC funded a project to update the altitude zone climate database. This involves extending the daily record beyond 1999 to 2019 (i.e. an additional 20 years). This will facilitate improved assessments of hydrological and agricultural responses to climate variability, since the additional 20-year record accounts for anthropogenically induced changes in extreme climatological events that have occurred from 2000 onwards. As discussed earlier, it will provide an additional 19 seasons of crop simulations, highlighting the importance of the necessary speed improvements to AquaCrop.

As part of ongoing efforts by the CWRR, the altitude zone soils database was updated in 2021. Soil water retention parameters were determined for five terrain units (crest, scarp, mid slope, foot slope and valley bottom) for both the A- and B-horizons using available information on soil type and clay content (Schütte and Schulze, 2019). The terrain units located within the 5838 altitude zones were then determined. This significantly improved the spatial accuracy of the soils data assigned to each altitude zone.

The size and scale of the maps presented in **Sections 3.3 to 3.6** of this report limit their usefulness and applicability. Therefore, it is recommended that the output data files described in **Section 6.1.2** be made readily available to end-users. These data files could be disseminated using the Water Research Observatory (WRO), which is designed to house data related to agricultural water use (Van der Laan et al., 2021). A web-based application could be developed that simplifies the extraction of required data, thus making the data files more accessible and easier to use. Once downloaded from the WRO, end users (e.g. agricultural extension officers) could generate additional maps not presented in this study that better suit their specific needs. For example, maps identifying altitude zones with high water or temperature stress may prove useful in developing guidelines to improve crop yield.

5 REFERENCES

Ainsworth EA, Leakey ADB, Ort DR and Long SP (2008) FACE-ing the facts: inconsistencies and interdependence among field, chamber and modeling studies of elevated [CO₂] impacts on crop yield and food supply. *New Phytologist* **179** 5-9.

Allen RG, Pereira LS, Raes D and Smith M (1998) *Crop evapotranspiration – Guidelines for computing crop water requirements*. FAO Irrigation and Drainage Paper 56. Food and Agricultural Organisation (FAO), Rome, Italy.

Allen LH, Kimball BA, Bunce JA, Yoshimoto M, Harazono Y, Baker JT, Boote KJ and White JW (2020) Fluctuations of CO₂ in Free-Air CO₂ Enrichment (FACE) depress plant photosynthesis, growth, and yield. *Agricultural Forest Meteorology* **284** 107899.

Araya A, Kisekka I and Holman J (2016) Evaluating deficit irrigation management strategies for grain sorghum using AquaCrop. *Irrigation Science* **34** (6) 465-481.

Archer E, Engelbrecht F, Hänsler A, Landman W, Tadross M and Helmschrot J (2018) Seasonal prediction and regional climate projections for southern Africa. In: *Climate change and adaptive land management in southern Africa – assessments, changes, challenges and solutions*, Revermann R, Krewenka KM, Schmiedel U, Olwoch JM, Helmschrot J and Jürgens N, Biodiversity and Ecology **6** 14-21. Klaus Hess Publishers, Göttingen and Windhoek.

Beletse YG, Laurie R, du Plooy CP, Laurie SM, Van den Berg A (2013) Simulating the yield response of orange fleshed sweet potato 'Isondlo' to water stress using the FAO AquaCrop model. *ISHS Acta Horticulturae* **1007** 935-941.

Beletse YG, Laurie R, Du Plooy CP, Van den Berg A, Laurie S (2011) *Calibration and validation of AquaCrop model for orange fleshed sweet potatoes*. In: Capacity Development for Farm Management Strategies to Improve Crop Water Productivity using AquaCrop: Lessons Learned, Ardakanian R, Walter T. UNW-DPC Publication Series, Knowledge No. 7, Bonn, Germany.

Bello ZA and Walker S (2017) Agricultural and Forest meteorology evaluating AquaCrop model for simulating production of amaranthus (*Amaranthus cruentus*) a leafy vegetable, under irrigation and rainfed conditions. *Agricultural Forest Meteorology* **247** 300-310.

Challinor AJ, Osborne T, Shaffrey L, Weller H, Morse A, Wheeler T and Vidale P (2009) Methods and resources for climate impacts research. *Bulletin of the American Meteorological Society* **90** (6) 836-848.

Chibarabada TP, Modi AT and Mabhaudhi T (2020) Calibration and evaluation of AquaCrop for groundnut (*Arachis hypogaea*) under water deficit conditions. *Agricultural and Forest Meteorology* **281** 1-8.

Department of Agriculture, Forestry and Fisheries (DAFF) (2010a) Amaranthus production guideline. Pretoria, South Africa. Available online:

<https://www.nda.agric.za/docs/brochures/amaranthus.pdf>
(accessed on 06 July 2020).

Department of Agriculture, Forestry and Fisheries (DAFF) (2010b) Amadumbe. Pretoria, South Africa. Available online:

https://www.nda.agric.za/docs/Brochures/Amadumbe_1.pdf
(accessed on 06 July 2020).

Department of Agriculture, Forestry and Fisheries (DAFF) (2011) Production guidelines for bambara groundnut. Pretoria, South Africa. Available online: <https://www.nda.agric.za/docs/Brochures/ProdguideBambara.pdf> (accessed on 06 July 2020).

Department Of Agriculture, Forestry and Fisheries (DAFF) (2014) *National Policy on Food and Nutrition Security*. Pretoria, South Africa. Available online: <https://www.gov.za/documents/national-policy-food-and-nutrition-security-south-africa> (accessed on 26 July 2021).

Dier M, Sickora J, Erbs M, Weigel H-J, Zörb C and Manderscheid R (2018) Decreased wheat grain yield stimulation by free air CO₂ enrichment under N deficiency is strongly related to decreased radiation use efficiency enhancement. *European Journal of Agronomy* **101** 38-48.

Directorate Plant Production/Agriculture Research Council (DPP/ARC) (2006) Sorghum production. Pretoria, South Africa. Available online: <https://www.arc.agric.za/arc-gci/Fact%20Sheets%20Library/Sorghum%20Production.pdf> (accessed on 26 July 2020).

Engelbrecht F (2019). *Green Book – Detailed projections of future climate change over South Africa*. Workstream 2: Research report, CSIR, Pretoria, South Africa.

Engelbrecht CJ and Engelbrecht FA (2016) Shifts in Köppen-Geiger climate zones over southern Africa in relation to key global temperature goals. *Theoretical and Applied Climatology* **123** 247-261.

Engelbrecht FA, Adegoke J, Bopape MM, Naidoo M, Garland R, Thatcher M, McGregor J, Katzfey J, Werner M, Ichoku C and Gatebe C (2015) Projections of rapidly rising surface temperatures over Africa under low mitigation. *Environmental Research Letters* **10**.

Engelbrecht F, Dedekind Z, Muthige M, Malherbe J, Beraki A, Engelbrecht C, Ngwana I, Lumsden T, Landman W, Maisha R, Mpheshea L, Van der Merwe J and Eatwell K (2020) *Predictability of hydroclimatic variability over eastern South Africa under climate change*. Report No. 2457/1/19, Water Research Commission (WRC), Pretoria, South Africa.

Food and Agricultural Organisation (FAO) (2017) *AquaCrop update and new features – Version 6.0*. FAO, Rome, Italy.

Franke AC (2021) Assessing the impact of climate change on crop production in southern Africa: a review. *South African Journal of Plant and Soil* 01-12.

Foster T, Brozović N, Butler AP, Neale CMU, Raes D, Steduto P, Fereres E and Hsiao TC (2017) AquaCrop-OS: An open source version of FAO's crop water productivity model. *Agricultural Water Management* **181** 18-22.

Garland R, Matoane M, Engelbrecht FA, Bopape M, Landman W, Naidoo M, Van der Merwe J and Wright C (2015) *Regional projections of extreme apparent temperature days in Africa and the related potential risk to human health*. *International Journal of Environmental Research and Public Health* **12** 12577-12604.

Geerts S, Raes D, Garcia M, Miranda R, Cusicanqui JA, Taboada C, Mendoza J, Huanca R, Mamani A, Condori O, Mamani J, Morales B, Osco V and Steduto P (2009) Simulating yield response to water of quinoa (*Chenopodium quinoa* Willd) with FAO-AquaCrop. *Agronomy Journal* **101** (3) 499-508.

Hadebe ST, Modi AT and Mabhaudhi T (2017) Calibration and testing of AquaCrop for selected sorghum genotypes. *Water SA* **43** (2) 209-221.

Harle KJ, Howden SM, Hunt LP and Dunlop M (2007) The potential impact of climate change on the Australian wool industry by 2030. *Agricultural Systems* **93** 61-89.

Hewitson B and Tadross M (2011) Developing regional climate projections. In: *Methodological approaches to assessing eco-hydrological responses to climate change in South Africa*, Schulze R, Hewitson B, Barichiev K, Tadross M, Kunz R, Horan M and Lumsden T. WRC Report No. 1562/1/10, Chapter 1, 1-17. Water Research Commission (WRC), Pretoria, South Africa.

Intergovernmental Panel on Climate Change (IPCC) (2014) *Climate Change 2014: Synthesis Report. Contribution of Working Groups I, II and III to the Fifth Assessment Report of the Intergovernmental Panel on Climate Change*. IPCC, Geneva, Switzerland, 151 pp.

Jones MR (2018) *Fast DSSAT simulations with low-performance computers*. South African Sugarcane Research Institute, Mt. Edgecombe, South Africa.

Kanda EK, Senzanje A and Mabhaudhi T (2021) Calibration and validation of the AquaCrop Model for full and deficit irrigated cowpea (*Vigna unguiculata* (L.) Walp). *Physics and Chemistry of the Earth* **124** (1) 102941.

Karunaratne S, Azam-Ali SN, Izzi G and Steduto P (2011) Calibration and validation of FAO-AquaCrop model for irrigated and water deficient bambara groundnut. *Experimental Agriculture* **47** (3) 509-527.

Kelly TD and Foster T (2021) AquaCrop-OSPy: Bridging the gap between research and practice in crop-water modelling. *Agricultural Water Management* **254** 106976.

Kephe PN, Ayisi KK and Petja BM (2021) Challenges and opportunities in crop simulation modelling under seasonal and projected climate change scenarios for crop production in South Africa. *Agriculture and Food Security* **10** (10). 24 pp.

Kimball BA (2016) Crop responses to elevated CO₂ and interactions with H₂O, N, and temperature. *Current Opinion in Plant Biology* **31** 36-43.

Kunz RP (2004) *Daily rainfall data extraction utility user manual version 1.4*. Institute for Commercial Forestry Research (ICFR), Pietermaritzburg, South Africa.

Kunz RP and Schulze RE (2016) Grain sorghum production in South Africa and climate change. In: *Handbook on adaptation to climate change for farmers, officials and others in the agriculture sector of South Africa*, Schulze RE. Section C: Crops in South Africa and climate change, Chapter C5.

Kunz RP, Davis NS, Thornton-Dibb SLC, Steyn JM, Du Toit ES and Jewitt GPW (2015a) *Assessment of biofuel feedstock production in South Africa: Atlas of water use and yield of biofuel crops in suitable growing areas (Volume 3)*. WRC Report No. TT 652/15. Water Research Commission (WRC), Pretoria, South Africa.

Kunz RP, Mengistu MG, Steyn JM, Doidge IA, Gush MB, Du Toit ES, Davis NS, Jewitt GPW and Everson CS (2015b) *Assessment of biofuel feedstock production in South Africa: Synthesis report on*

estimating water use efficiency of biofuel crops (Volume 1). WRC Report No. 1874/1/15. Water Research Commission (WRC), Pretoria, South Africa.

Kunz R, Masanganise J, Reddy K, Mabhaudhi T, Lembede L, Naiken V and Ferrer S (2020) *Water use and yield of soybean and grain sorghum for biofuel production*. WRC Report 2491/1/20, Water Research Commission (WRC), Pretoria, South Africa.

Leakey ADB, Ainsworth EA, Bernacchi CJ, Rogers A, Long SP and Ort DR (2009) Elevated CO₂ effects on plant carbon, nitrogen, and water relations: six important lessons from FACE. *Journal of Experimental Botany* **60** 2859-2876.

Lynch S (2004) *Development of a raster database of annual, monthly and daily rainfall for southern Africa*. WRC Report 1156/1/04. Water Research Commission (WRC), Pretoria, South Africa.

Mabhaudhi T, Chibarabada TP, Chimonyo VGP and Modi AT (2018) Modelling climate change impact: A case of Bambara groundnut (*Vigna subterranea*). *Physics and Chemistry of the Earth* **105** 25-31.

Mabhaudhi T, Chimonyo VGP and Modi AT (2017) Status of underutilised crops in South Africa: Opportunities for developing research capacity. *Sustainability* **9** 1569.

Mabhaudhi T, Kunz RP and Schulze RE (2016a) Taro (*Amadumbe*) in South Africa and climate change. In: *Handbook on adaptation to climate change for farmers, officials and others in the agriculture sector of South Africa*, Schulze RE. Section C: Crops in South Africa and climate change, Chapter C6.

Mabhaudhi, T, Kunz RP and Schulze RE (2016b) Bambara groundnut in South Africa and climate change. In: *Handbook on adaptation to climate change for farmers, officials and others in the agriculture sector of South Africa*, Schulze RE. Section C: Crops in South Africa and climate change, Chapter C7.

Mabhaudhi T, Modi AT and Beletse YG (2014a) Parameterisation and evaluation of the FAO-AquaCrop model for a South African taro (*Colocasia esculenta* L. Schott) landrace. *Agricultural and Forest Meteorology* **192/193** 132-139.

Mabhaudhi T, Modi AT and Beletse YG (2014b) Parameterization and testing of AquaCrop for a South African bambara groundnut landrace. *Agronomy Journal* **106 (1)** 243-251.

Manderscheid R, Pacholski A and Weigel H-J. 2010. Effect of free air carbon dioxide enrichment combined with two nitrogen levels on growth, yield and yield quality of sugar beet: evidence for a sink limitation of beet growth under elevated CO₂. *European Journal of Agronomy* **32** 228-239.

Mare R and Modi AT (2009) Influence of planting date and organic fertilisation on growth and yield of taro landraces. *African Crop Science Conference Proceedings* **9** 179-189.

McGregor JL (2005) *C-CAM geometric aspects and dynamical formulation*. CSIRO Atmospheric Research Technical Paper 70.

McGregor JL and Dix MR (2001) *The CSIRO conformal-cubic atmospheric GCM*. Proceedings IUTAM Symposium on Advances in Mathematical Modelling of Atmosphere and Ocean Dynamics, 197-202, Hodnett PF, Dordrecht, Kluwer.

McGregor JL and Dix MR (2008) *An updated description of the Conformal-Cubic Atmospheric Model High Resolution Simulation of the Atmosphere and Ocean*, 51-76, Hamilton K and Ohfuchi W, Berlin, Springer.

Modi AT and Mabhaudhi T (2013) *Water use and drought tolerance of selected traditional crops*. WRC Report No. 1771/1/13. Water Research Commission (WRC), Pretoria, South Africa.

Modi AT and Mabhaudhi T (2016) *Developing a research agenda for promoting underutilised, indigenous and traditional crops*. WRC Report No. KV 362/16. Water Research Commission (WRC), Pretoria, South Africa.

Modi AT and Mabhaudhi T (2017) *Determining water use of indigenous grain and legume food crops*. WRC Report No. TT 710/17. Water Research Commission (WRC), Pretoria, South Africa.

Moss RH, Edmonds JA, Hibbard KA, Manning MR, Rose SK, Van Vuuren DP, Carter TR, Emori S, Kainuma M, Kram T, Meehl GA, Mitchell JFB, Nakicenovic N, Riahi K, Smith SJ, Stouffer RJ, Thomson AM, Weyant JP and Wilbanks TJ (2010) The next generation of scenarios for climate change research and assessment. *Nature* **463** 747-756.

Mwamlima LH, Cheruiyot EK and Ouma JP (2021) Soil moisture modulates carbon dioxide assimilation in soybean (*Glycine max*). *Agricultural Research* **10** (3). 11 pp.

Nyathi MK, Annandale JG, Beletse YG, Beukes DJ, Du Plooy CP, Pretorius B and Van Halsema GE (2016) *Nutritional water productivity of traditional vegetable crops*. WRC Report No. 2171/1/16. Water Research Commission (WRC), Pretoria, South Africa.

Nyathi MK, Van Halsema GE, Annandale JG and Struik PC (2018) Calibration and validation of the AquaCrop model for repeatedly harvested leafy vegetables grown under different irrigation regimes. *Agricultural Water Management* **208** 107-119.

Pike A and Schulze RE (1995) AutoSoils Version 3: A Soils Decision Support System for South African soils. Department of Agricultural Engineering, University of Natal, Pietermaritzburg.

Raes D, Steduto P, Hsiao TC and Fereres E (2018) *Reference manual AquaCrop (Version 6.0-6.1)*. Land and Water Division, Food and Agriculture Organisation (FAO), Rome, Italy.

Razzaghi F, Zhou Z, Andersen MN and Plauborg F (2017) Simulation of potato yield in temperate condition by the AquaCrop model. *Agricultural Water Management* **191** 113-123.

Rodriguez AVC and Ober ES (2019) AquaCropR: Crop Growth Model for R. *Agronomy* **9** (7) 378.

Schulze RE (1995) *Hydrology and agrohydrology: a text to accompany the ACRU 3.00 agrohydrological modelling system*. Water Research Commission (WRC), Pretoria, South Africa.

Schulze RE (Ed) (2016) *Handbook on adaptation to climate change for farmers, officials and others in the agriculture sector of South Africa*. Report to the Department of Agriculture, Forestry and Fisheries (DAFF), Pretoria, South Africa.

Schulze RE and Horan MJC (2008) Soils: Hydrological Attributes. In: *South African Atlas of Climatology and Agrohydrology*, Schulze RE. WRC Report 1489/1/06, Section 4.2. Water Research Commission (WRC), Pretoria, South Africa.

Schulze R and Horan M (2011) Methods 1: Delineation of South Africa, Lesotho and Swaziland into quinary catchments. In: *Methodological approaches to assessing eco-hydrological responses to climate change in South Africa*, Schulze R, Hewitson B, Barichievsky K, Tadross M, Kunz R, Horan M and

Lumsden T. WRC Report No. 1562/1/10, Chapter 6, 55-62. Water Research Commission (WRC), Pretoria, South Africa.

Schulze, R, Horan, M, Kunz, R, Lumsden, T and Knoesen D (2011) Methods 2: Development of the Southern African quinary catchments database. In: *Methodological approaches to assessing eco-hydrological responses to climate change in South Africa*, Schulze R, Hewitson B, Barichiev K, Tadross M, Kunz R, Horan M and Lumsden T. WRC Report No. 1562/1/10, Chapter 7, 63-74. Water Research Commission (WRC), Pretoria, South Africa.

Schulze RE and Maharaj M (2004) *Development of a database of gridded daily temperatures for Southern Africa*. WRC Report 1156/2/04. Water Research Commission (WRC), Pretoria, South Africa.

Schütte S and Schulze RE (2019) Mapping SCS hydrological soil groups over South Africa at terrain unit resolution. Paper in development.

Schütte S, Schulze RE and Clark DJ (2021a) *A national assessment of potential climate change impacts on the hydrological yield of different hydro-climatic zones of South Africa*. Water Research Commission (WRC), Pretoria, South Africa.

Schütte S, Schulze RE, Clark DJ, Kunz RP and Jele Z (2021b) Projections of rainfall, temperature and potential evaporation. In: *A national assessment of potential climate change impacts on the hydrological yield of different hydro-climatic zones of South Africa*, Schütte S, Schulze RE and Clark DJ (Eds), Report No. 2833/1/xx, Chapter 4. Water Research Commission (WRC), Pretoria, South Africa.

SIRI (1987) *Land Type Series*. Memoirs on the Agricultural Natural Resources of South Africa. Soil and Irrigation Research Institute, Pretoria, South Africa.

Smithers JC and Schulze RE (1995) *ACRU agrohydrological modelling system: User manual Version 3.00*. WRC Report TT 70/95. Water Research Commission (WRC), Pretoria, South Africa.

Smithers JC and Schulze RE (2000) *Long duration design rainfall estimates for South Africa*. WRC Report No. 811/1/00. Water Research Commission (WRC), Pretoria, South Africa.

Steduto P, Hsiao TC, Fereres E and Raes D (2012) *Crop yield response to water*. FAO Irrigation and Drainage Paper No. 66. Food and Agricultural Organisation (FAO), Rome, Italy.

Steduto P, Hsiao TC, Raes D and Fereres E (2009) AquaCrop – The FAO crop model to simulate yield response to water: I. Concepts and underlying principles. *Agronomy Journal* **101 (3)** 426-437.

Sun JD, Yang LX, Wang YL and Ort DR (2009) FACE-ing the global change: opportunities for improvement in photosynthetic radiation use efficiency and crop yield. *Plant Science* **177** 511-522.

Tadross M, Davis C, Engelbrecht FA, Joubert A. and Archer van Garderen E (2011) Regional scenarios of future climate change over southern Africa. In: *Climate Risk and Vulnerability: A Handbook for Southern Africa*, C. Davis, CSIR, Pretoria, South Africa, 28 pp.

Toucher ML, Ramjeawon M, McNamara MA, Rouget M, Bulcock H, Kunz RP, Moonsamy J, Mengistu M, Naidoo T, Vather T and Aldworth TA (2019) *Resetting the baseline land cover against which streamflow reduction activities and the hydrological impacts of land use change are assessed*. WRC Report 2437/1/19. Water Research Commission (WRC), Pretoria, South Africa.

Valerio M, Tomecek M, Lovelli S and Ziska L (2013) Assessing the impact of increasing carbon dioxide and temperature on crop-weed interactions for tomato and a C₃ and C₄ weed species. *European Journal of Agronomy* **50** 60-65.

Van der Kooi CJ, Reich M, Low M, De Kok LJ and Tausz M (2016) Growth and yield stimulation under elevated CO₂ and drought: a meta-analysis on crops. *Environmental and Experimental Botany* **122** 150-157.

Van der Laan M, Maseko S, Schütte C, Viviers C, Thomson A, Mudaly L, Silberbauer M, LE Roux J, Weepener H, Clark D, Scott-Shaw B, Mabhaudhi T, Hoogenboom G and Raghavan S (2021) *Development and application of a big data platform to improve agricultural water resources management in South Africa*. Water Research Commission (WRC), Pretoria, South Africa. Deliverable Report No. 1 for Project No. 2019/2020-00088 titled: Report on identification of key existing datasets and the online platform to be used. 40 pp.

Vanuytrecht E and Thorburn PJ (2017) Responses to atmospheric CO₂ concentrations in crop simulation models: a review of current simple and semicomplex representations and options for model development. *Global Change Biology* **23** 1806-1820.

Vanuytrecht E, Raes D and Willems P (2011) Considering sink strength to model crop production under elevated atmospheric CO₂. *Agricultural and Forest Meteorology* **151** 1753-1762.

Vanuytrecht E, Raes D, Steduto P, Hsiao TC, Fereres E, Heng LK, García-Vila M and Moreno PM (2014) AquaCrop: FAO's crop water productivity and yield response model. *Environmental Modelling and Software* **62** 351-360.

Weepener HL, Van den Berg HM, Metz M and Hamandawana H (2011) *The development of a hydrologically improved Digital Elevation Model and derived products for South Africa based on the SRTM DEM*. WRC Report 1908/1/11. Water Research Commission (WRC), Pretoria, South Africa.

Wellens J, Raes D, Fereres E, Diels J, Coppys C, Adiele JG, Ezui KSG, Becerra L-A, Selvaraj MG, Dercon G and Heng LK (2022) Calibration and validation of the FAO AquaCrop water productivity model for cassava (*Manihot esculenta* Crantz). *Agricultural Water Management* **263** 107491.

Winsemius HC, Dutra E, Engelbrecht FA, Archer van Garderen E, Wetterhall F, Pappenberger F and Werner MGF (2014) The potential value of seasonal forecasts in a changing climate in southern Africa. *Hydrology and Earth System Sciences* **18** 1525-1538.

Wolski P, Lumsden T, Kunz RP, Clark DJ, Schütte S and Schulze RE (2021) Establishing climate scenario projections. In: *A national assessment of potential climate change impacts on the hydrological yield of different hydro-climatic zones of South Africa*, Schütte S, Schulze RE and Clark DJ (Eds), Report No. 2833/1/xx, Chapter 2. Water Research Commission (WRC), Pretoria, South Africa.

6 APPENDIX A: DATA STORAGE

6.1 Data storage

This research project has generated over 80 GB of compressed data in WinRAR format of input and output files pertaining to FAO's AquaCrop model. This represents a wealth of simulated crop data generated from national model runs performed for each of the 5838 altitude zones (or quinary catchments). All simulated datasets described below are stored and archived on a fileserver located in the ICS Server Room on the University of KwaZulu-Natal's main campus in Pietermaritzburg. The contact person is Richard Kunz (kunzr@ukzn.ac.za).

6.1.1 AquaCrop input files

The following AquaCrop input files were generated to meet this project's objectives.

- a) AquaCrop climate (.cli, .plu, .tnx and .eto files) files for each of the 5838 altitude zones based on
 - i. observed (historical) climate data from 1950-1999 (024 files: 478 MB). This dataset was originally developed by WRC Project No. K5/2491 (Kunz et al., 2020).
 - ii. projected climate data from 1961-2099 (144 files: 8070 MB) derived from six dynamically downscaled and bias-corrected GCMs for RCP8.5. These datasets were originally developed by WRC Project No. K5/2833 (Schütte et al., 2021).
- b) AquaCrop soils (.sol) files for each of the 5838 altitude zones (006 files: 2.2 MB), which were originally developed by WRC Project No. K5/2491 (Kunz et al., 2020).
- c) Four crop parameter files in AquaCrop growing degree-day format that were originally developed by various WRC-funded projects.
- d) Project (.prm) files for multiple model runs that instruct AquaCrop to run sequentially for the following time periods:
 - i. historical - 49 seasons from 1950/51 to 1998/99 (18 files: 9.6 MB)
 - ii. present - 29 seasons from 1961/62 to 1989/90 (278 files: 14.1 MB)
 - iii. near future - 29 seasons from 2015/16 to 2043/44 (278 files: 14.1 MB)
 - iv. distant future - 29 seasons from 2070/71 to 2098/99 (278 files: 14.1 MB)

6.1.2 AquaCrop output files

The following AquaCrop output files were generated for each of the four neglected and underutilised crops and for each of the 5838 altitude zones.

- a) Monthly and seasonal files from planting date to physiological maturity date for each time period:
 - i. 49 seasons (18 files: 75.2 MB)
 - ii. 29 seasons (278 files: 54.0 MB)
- b) Monthly and annual statistics for 24 AquaCrop output variables and three additional variables for each time period:
 - i. 49 seasons (18 files: 56.7 MB)
 - ii. 29 seasons (278 files: 62.0 MB)

AquaCrop output variables:

No.	Variable	Description	Unit
1	Rain	Rainfall	mm
2	ETo	Reference evaporation	mm
3	GD	Growing degree-days	°C day
4	CO ₂	Atmospheric CO ₂ concentration	ppm
5	Irri	Amount of water applied as irrigation	mm
6	Infilt	Amount of water infiltrated into the soil profile	mm
7	Runoff	Amount of water lost to surface runoff	mm
8	Drain	Amount of water drained out of the soil profile	mm
9	Upflow	Amount of water moved upward by capillary rise	mm
10	E	Amount of water evaporated from the soil surface	mm
11	E/Ex	Mean soil water evaporation relative to the maximum	%
12	Tr	Amount of water transpired from the crop surface	mm
13	Trw	Mean crop transpiration in weed infested field	mm
14	Tr/Trx	Mean crop transpiration relative to the maximum	%
15	Cycle	Length of crop cycle	days
16	WeedStr	Average relative cover of weeds	%
17	TempStr	Average temperature stress	%
18	ExpStr	Average leaf expansion stress	%
19	StoStr	Average stomatal stress	%
20	BioMass	Above-ground biomass produced	t ha ⁻¹
21	Brelative	Biomass relative to that for an unstressed crop	%
22	HI	Harvest index	%
23	Yield	Dry crop yield	t ha ⁻¹
24	WPet	Crop water productivity	kg m ⁻³

Additional output variables:

No.	Variable	Description	Unit
1	ETc	Total amount of water evapotranspired from the crop	mm
2	cfa	Number of seasons with crop yield = 0 t ha ⁻¹	integer
3	CAY	Monthly averaged crop coefficients	fraction

In total, 17 statistics were generated for each of the above-listed variables as follows:

mean
variance, standard deviation, coefficient of variation (CV), skewness, kurtosis
minimum, maximum, sum
number of observations
percentile values (10, 20, 33, 50, 67, 80, 90)

- c) GIS-ready files to assist with mapping (i.e. extracted values for all 5828 altitude zones) for the following
- i. time periods:
 - 49 seasons (1 file: 0.4 MB)
 - 29 seasons (1 file: 0.4 MB)
 - ii. GCMs:
 - ACC, CCS, CNR, GFD, MPI, NOR
 - iii. Output variables and statistics:
 - ETc mean, CV
 - Cycle mean, CV
 - TempStr mean, CV
 - ExpStr mean, CV
 - StoStr mean, CV
 - BioMass mean, CV

HI	mean, CV
Yield	mean, CV
WPet	mean, CV
cfa	sum

7 APPENDIX B: PROJECTED CHANGES IN CLIMATE FOR RCP8.5

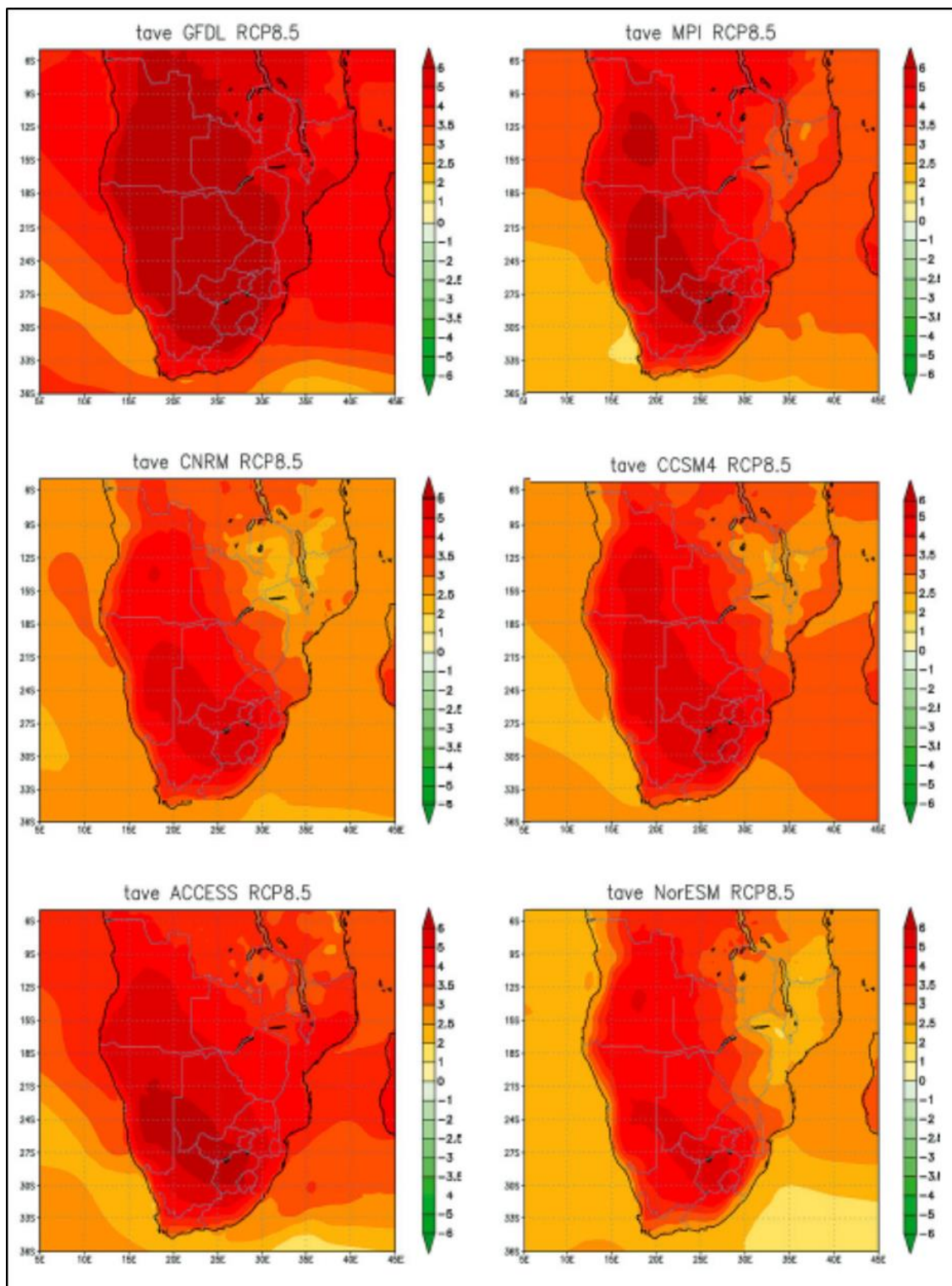


Figure 7.1 Projected changes in annual average temperatures (°C) over southern Africa for the time period 2080-2099 relative to 1971-2000 under RCP8.5, based on CCAM (50 km resolution) downscaling of six GCMs (Archer et al., 2018)

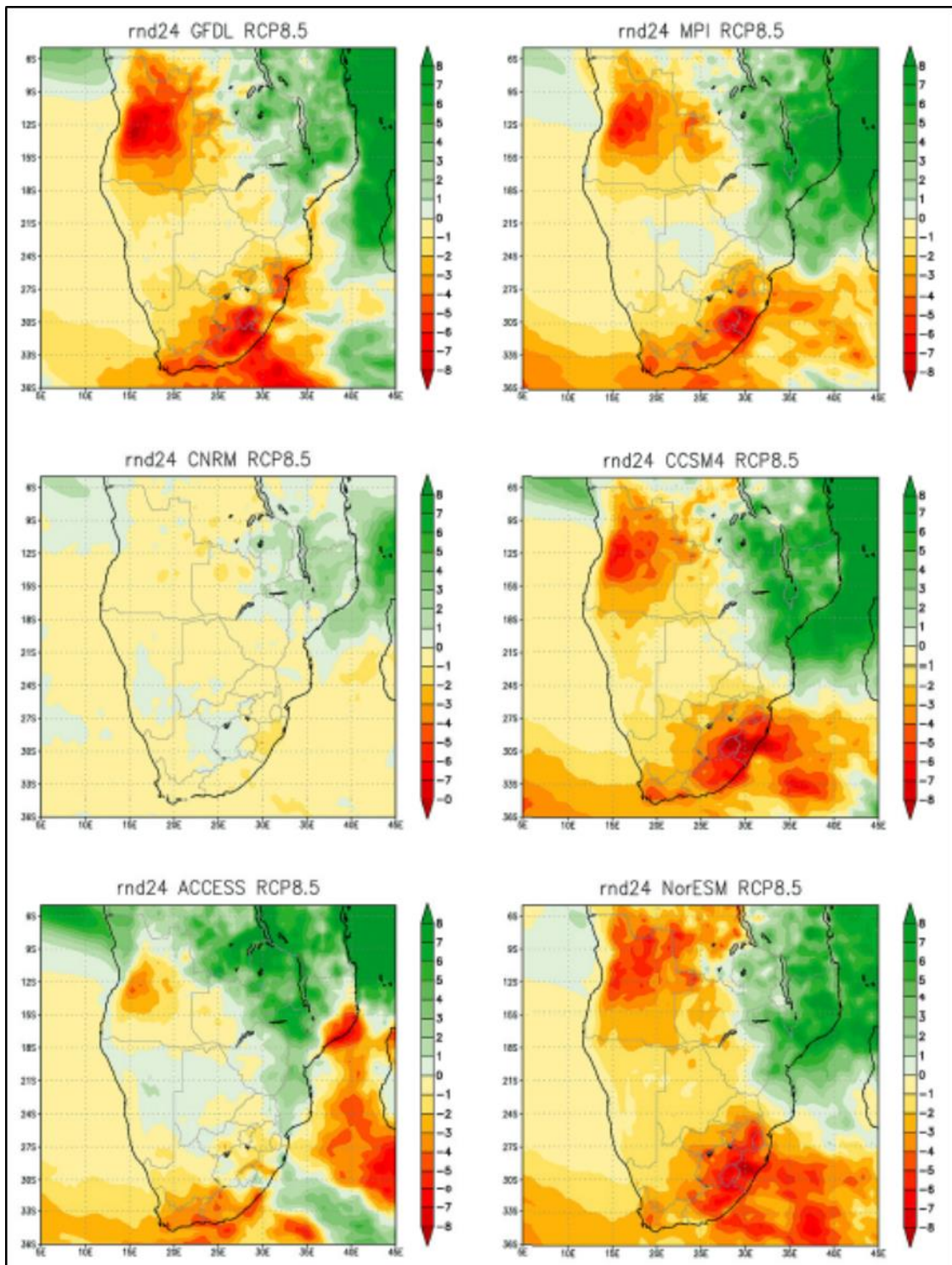


Figure 7.2 Projected changes in annual average rainfall ($10 \times \text{m m day}^{-1}$) over southern Africa for the time period 2080-2099 relative to 1971-2000 under RCP8.5, based on CCAM (50 km resolution) downscaling of six GCMs (Archer et al., 2018)

8 APPENDIX C: CHANGES IN RAINFALL FROM PRE- TO POST-2005

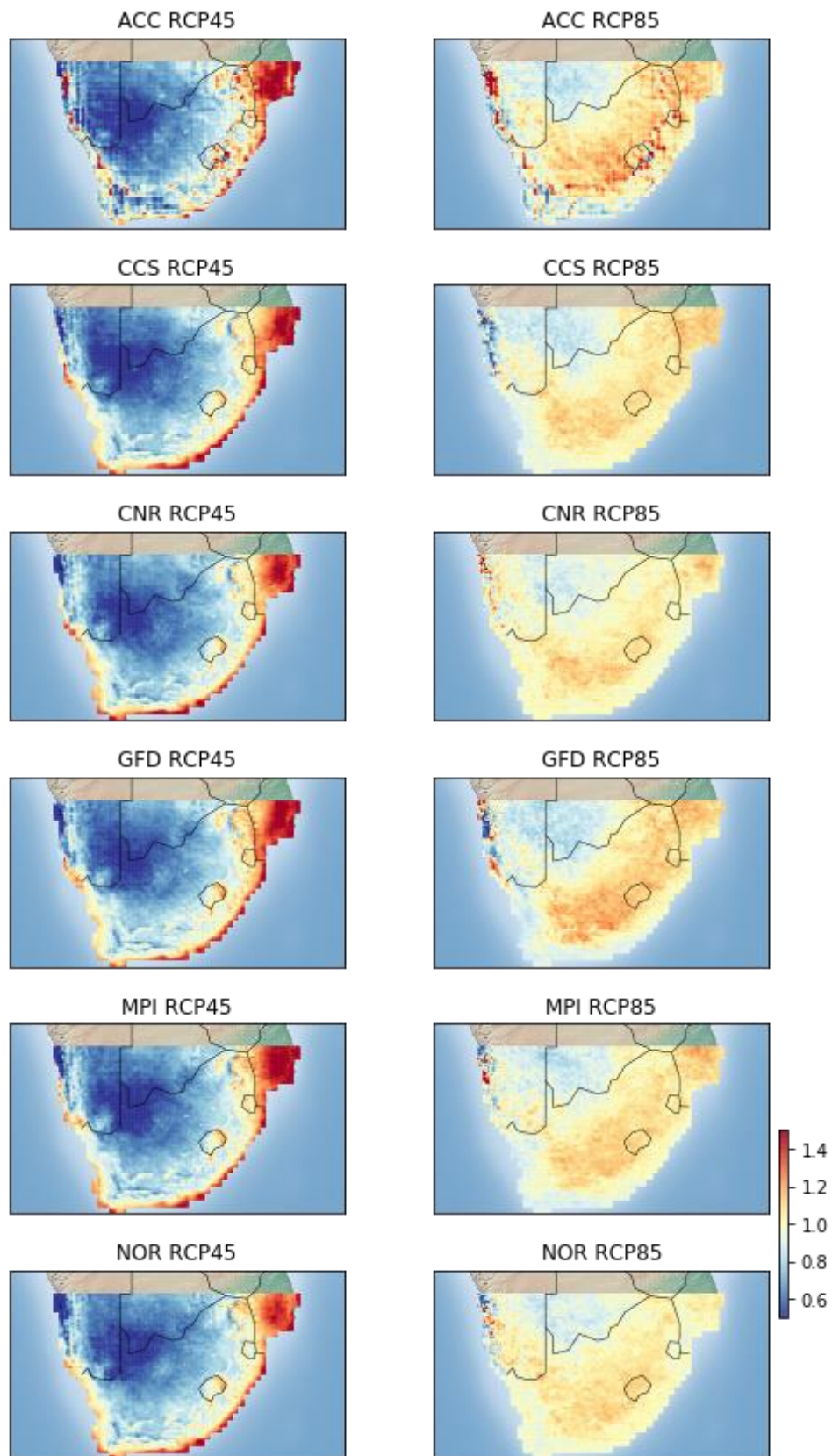


Figure 8.1 Ratio of mean daily rainfall per year in the post-2005 period (2005-2099) to the pre-2005 period (1961-2004)

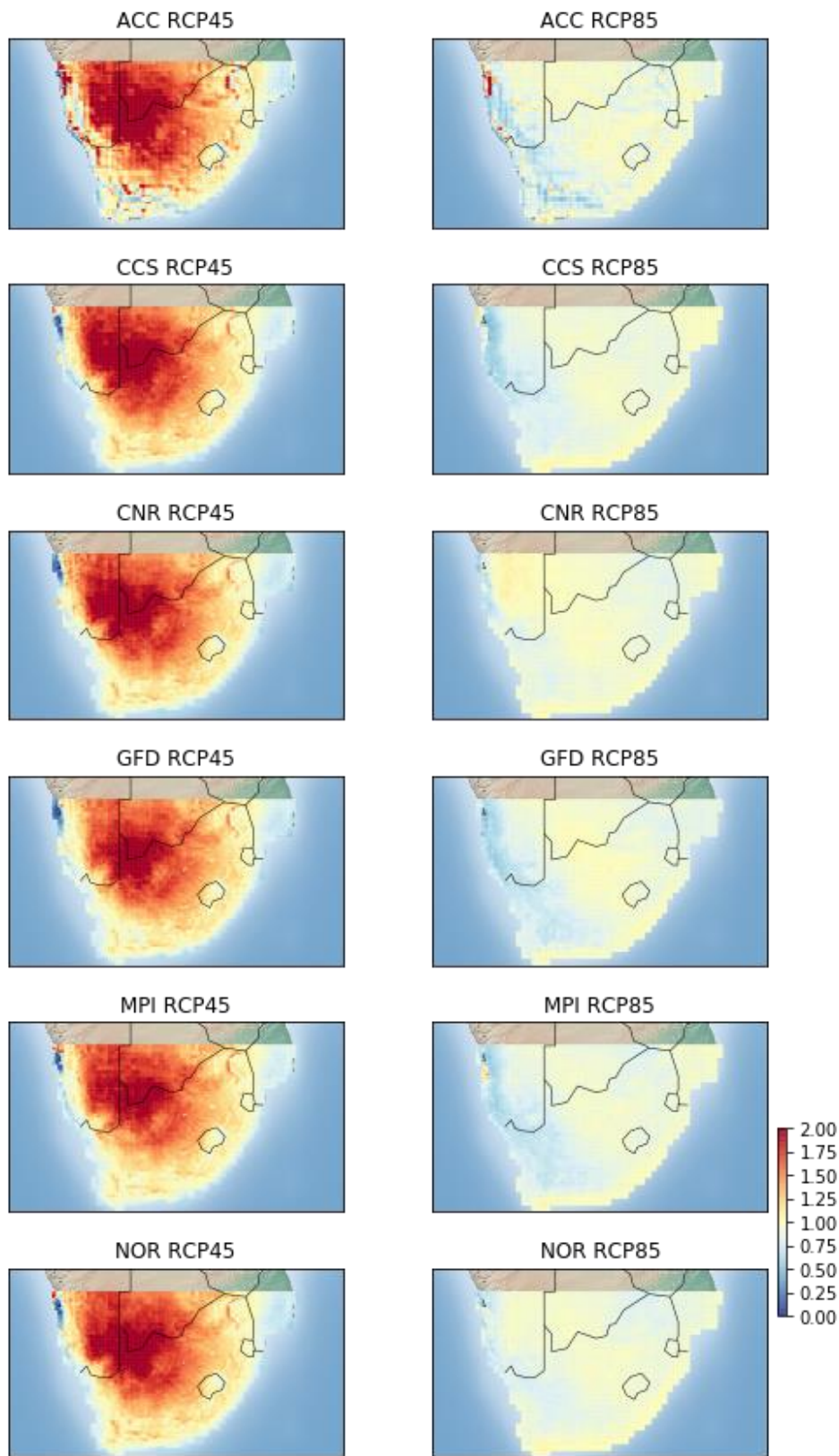
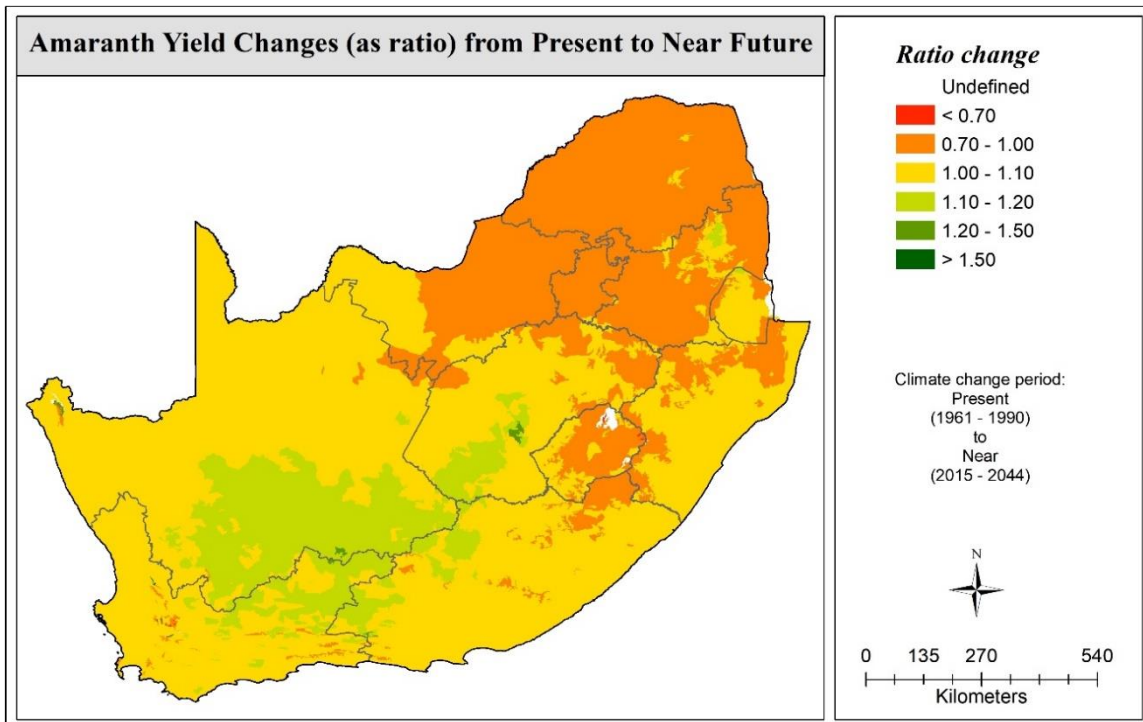
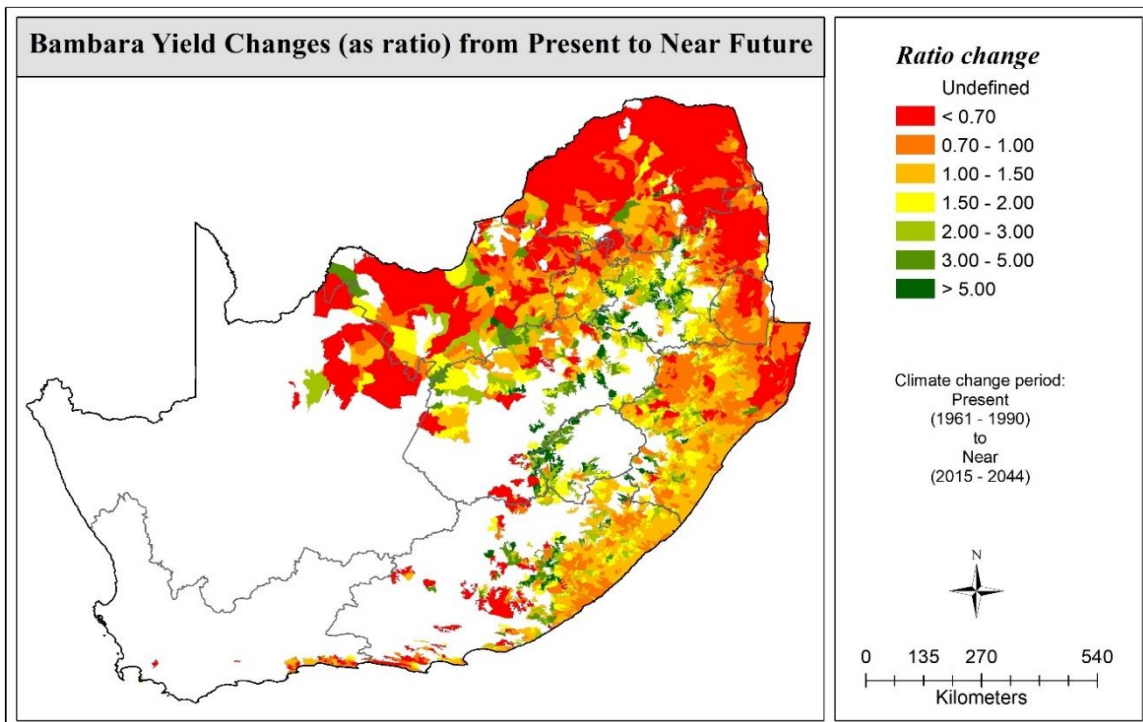


Figure 8.2 Ratio of mean rain days per year in the post-2005 period (2005-2099) to the pre-2005 period (1961-2004)

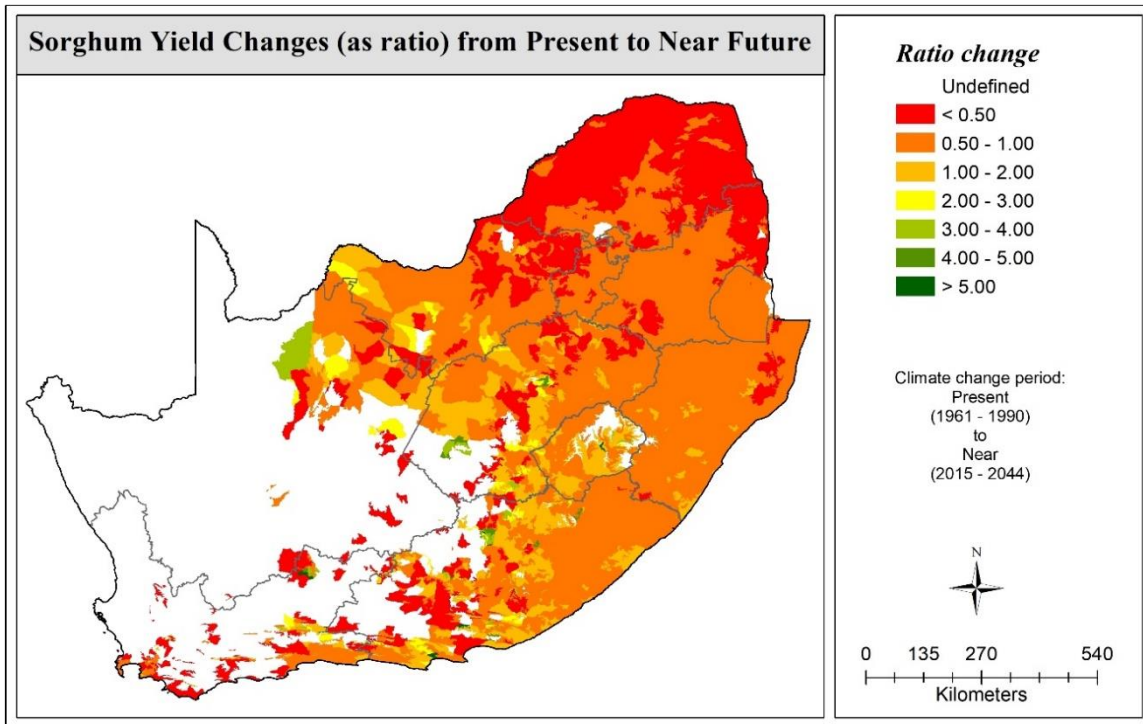
9 APPENDIX D1: MAPS OF CHANGE IN YIELD EXPRESSED AS A RATIO



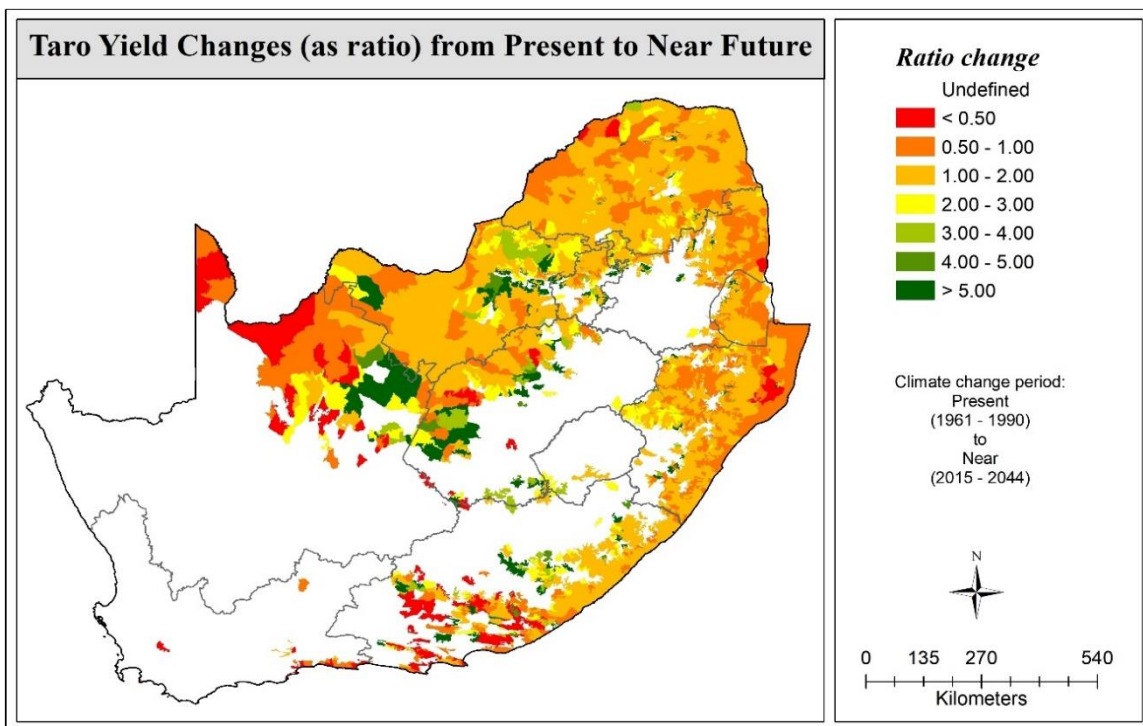
(a)



(b)

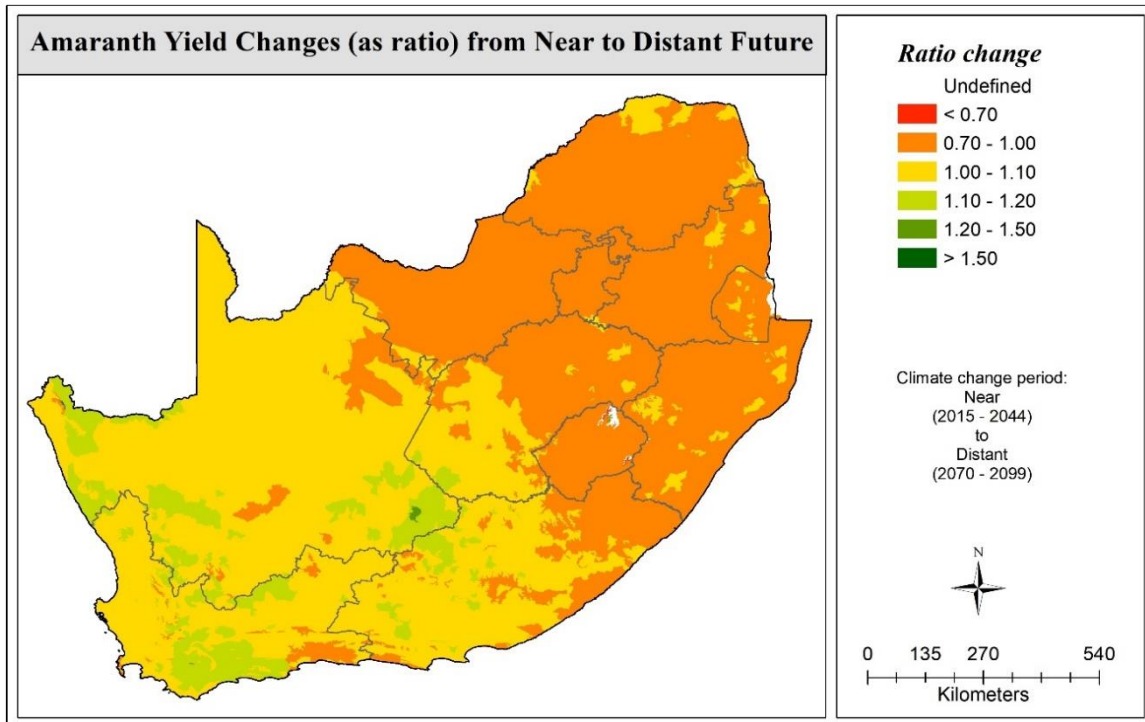


(c)

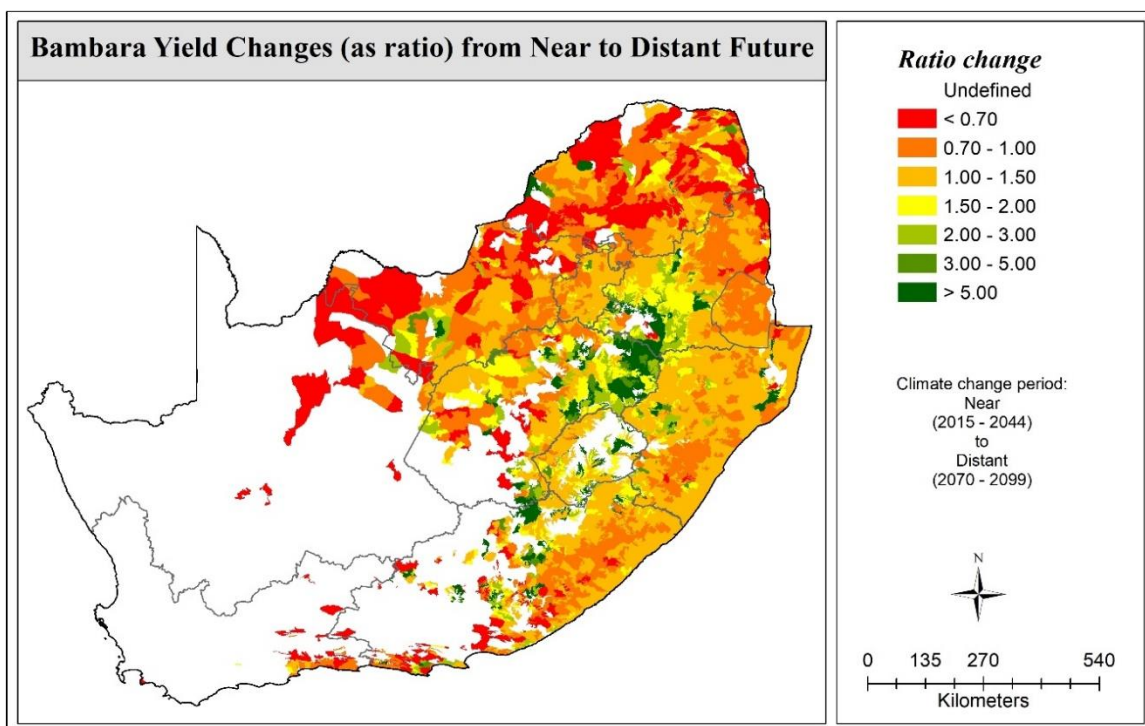


(d)

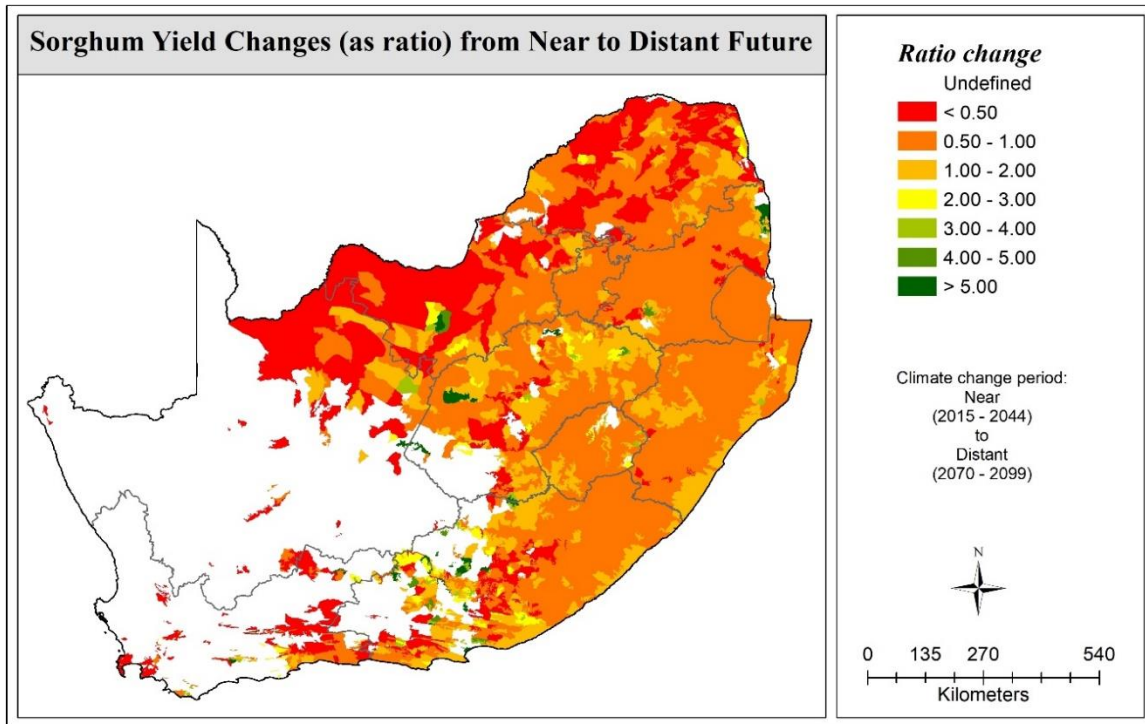
Figure 9.1 Change in mean dry yield (as ratio) from present to near future for (a) amaranth, (b) bambara groundnut, (c) sorghum, and (d) taro



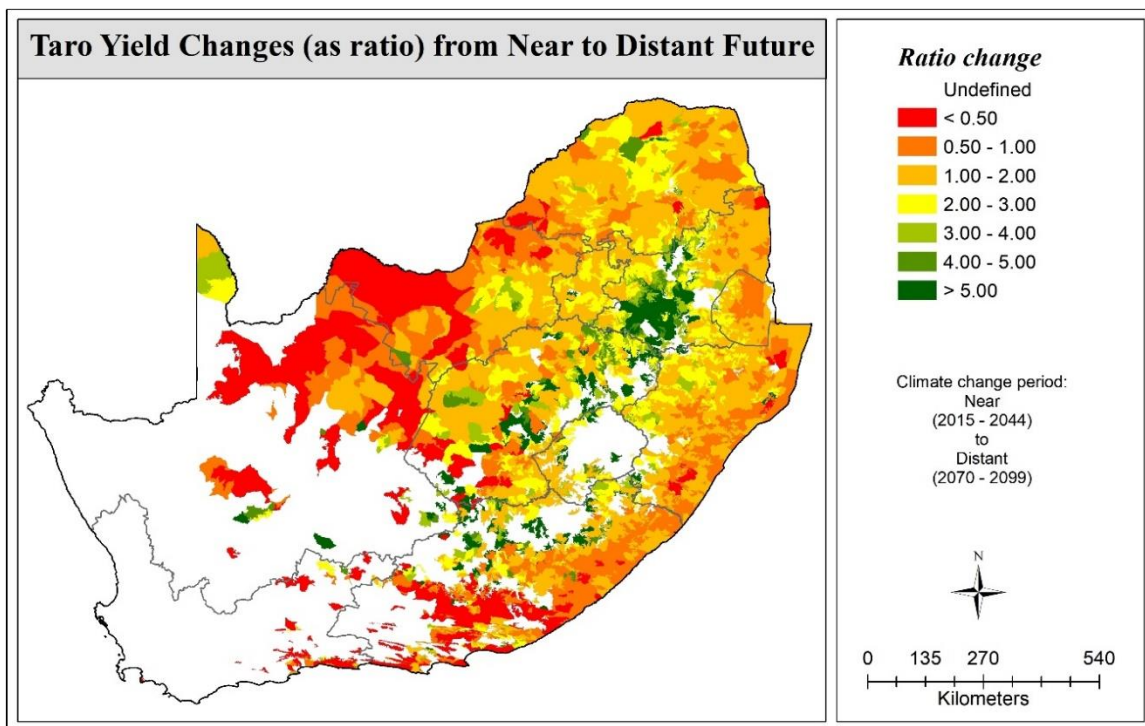
(a)



(b)

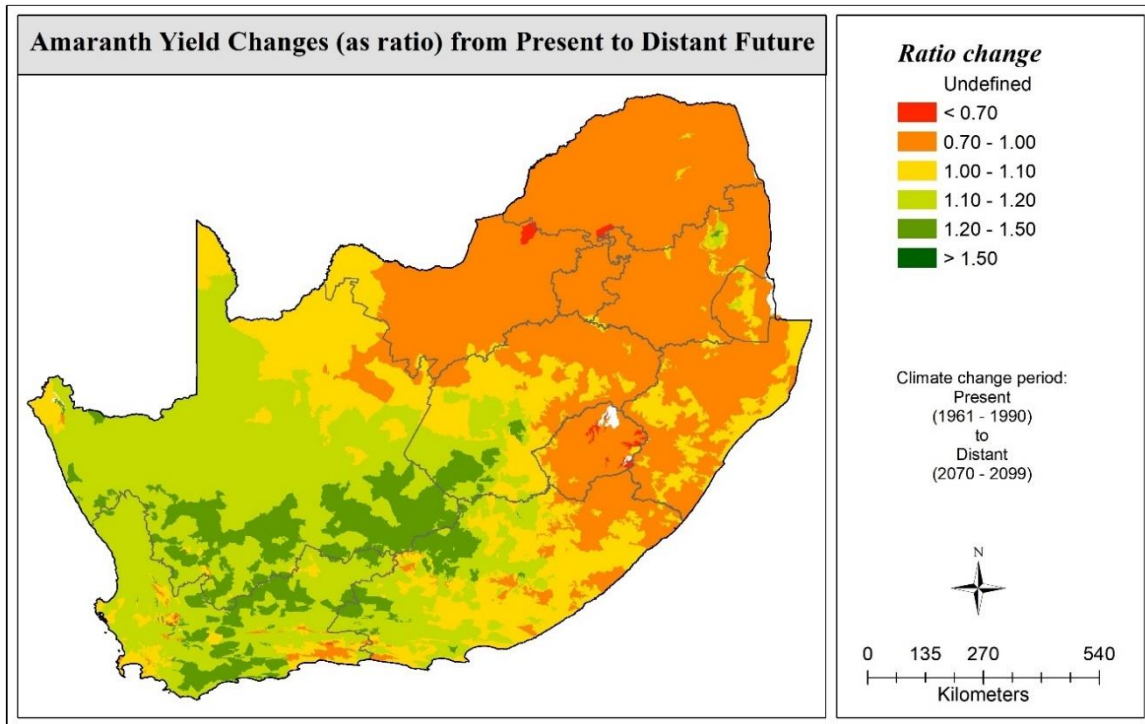


(c)

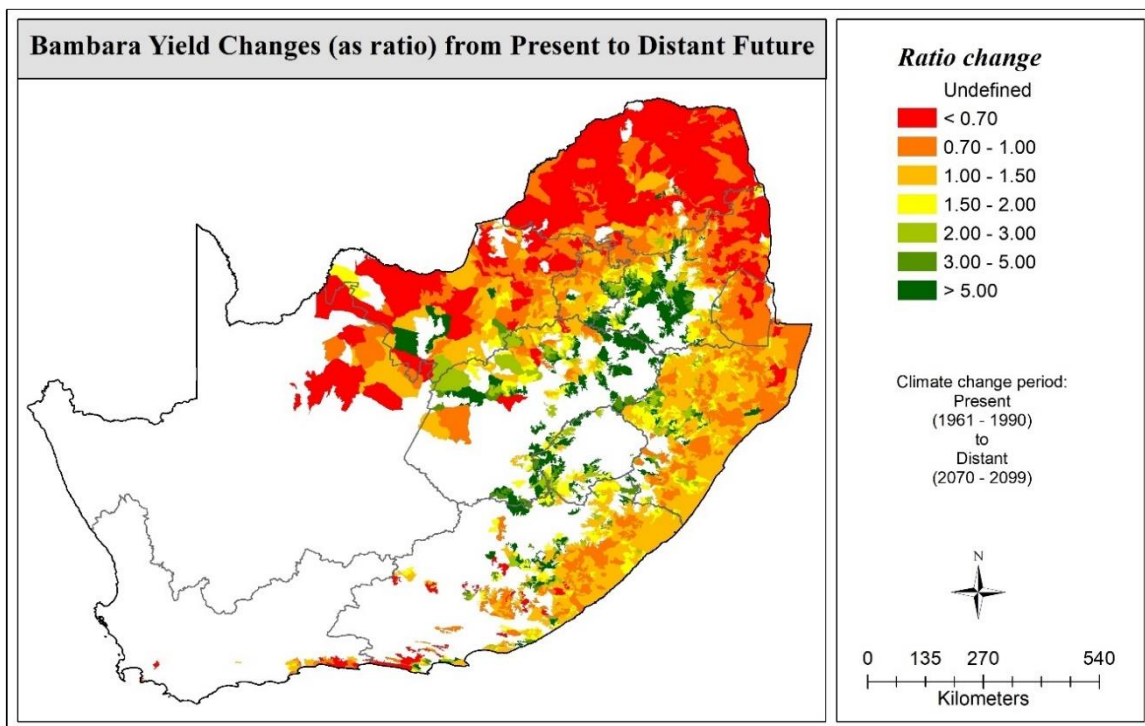


(d)

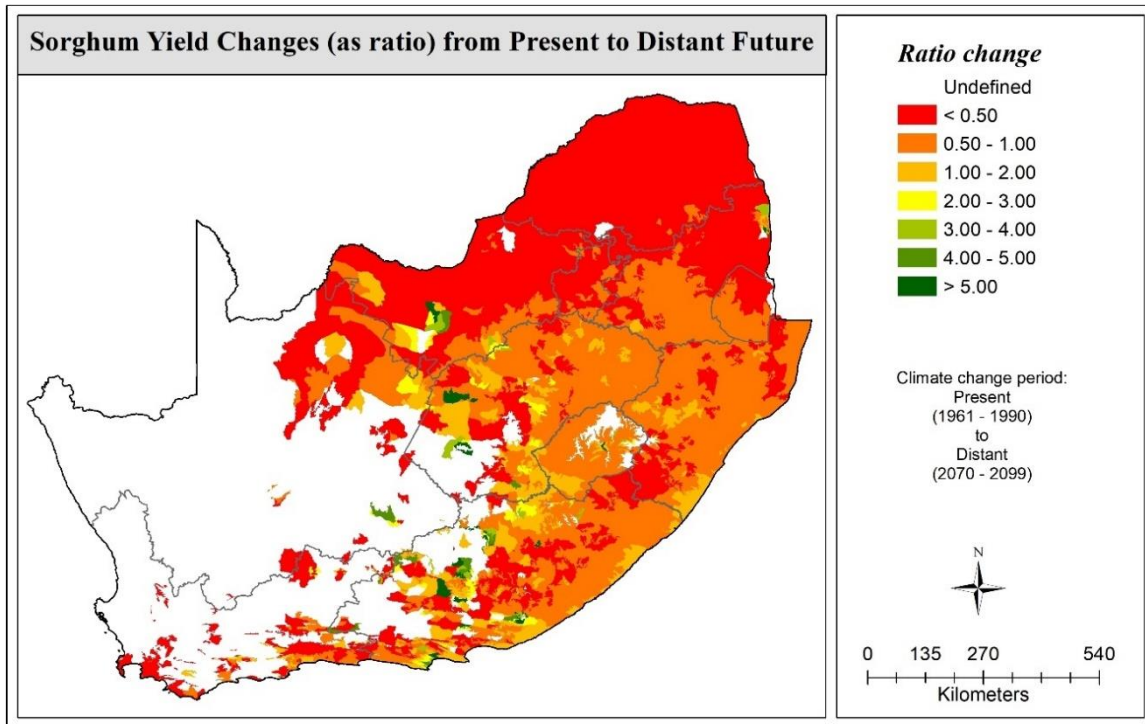
Figure 9.2 Change in mean dry yield (as ratio) from near to distant future for (a) amaranth, (b) bambara groundnut, (c) sorghum, and (d) taro



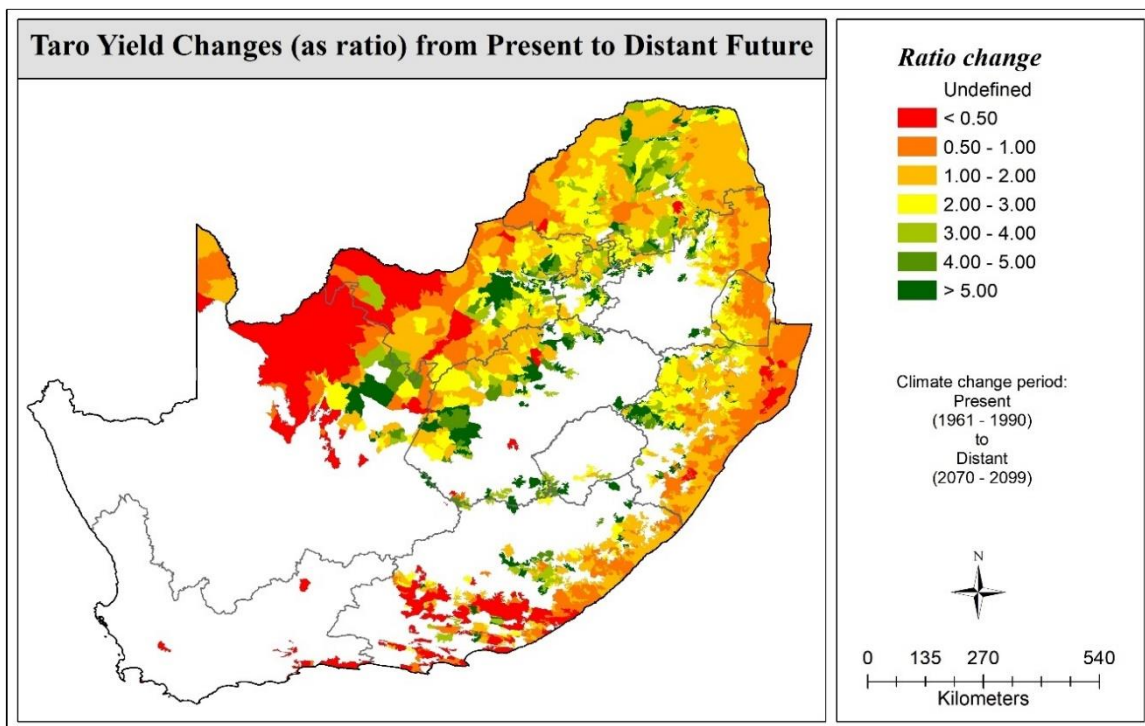
(a)



(b)



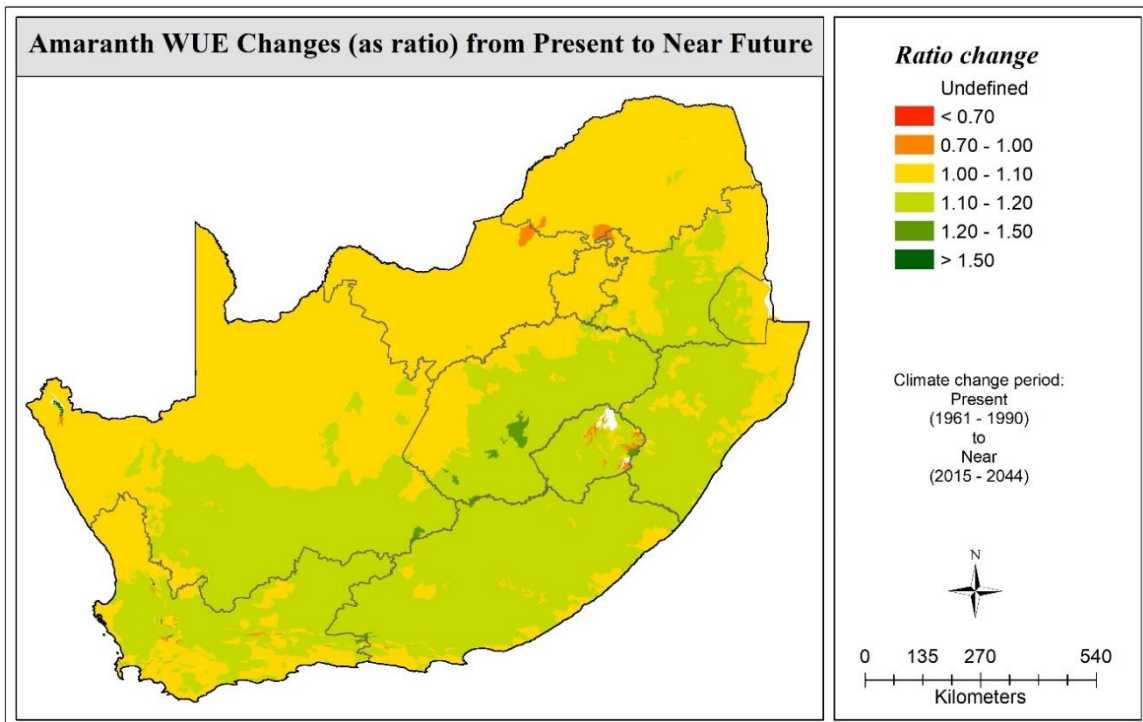
(c)



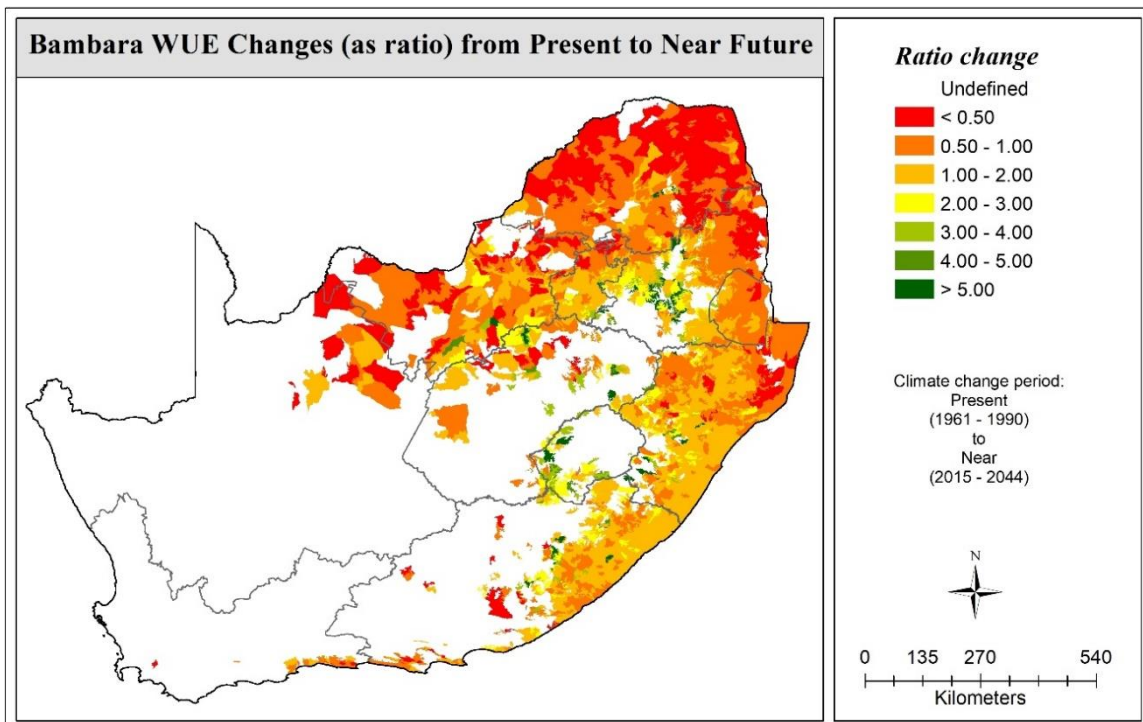
(d)

Figure 9.3 Change in mean dry yield (as ratio) from present to distant future for (a) amaranth, (b) bambara groundnut, (c) sorghum, and (d) taro

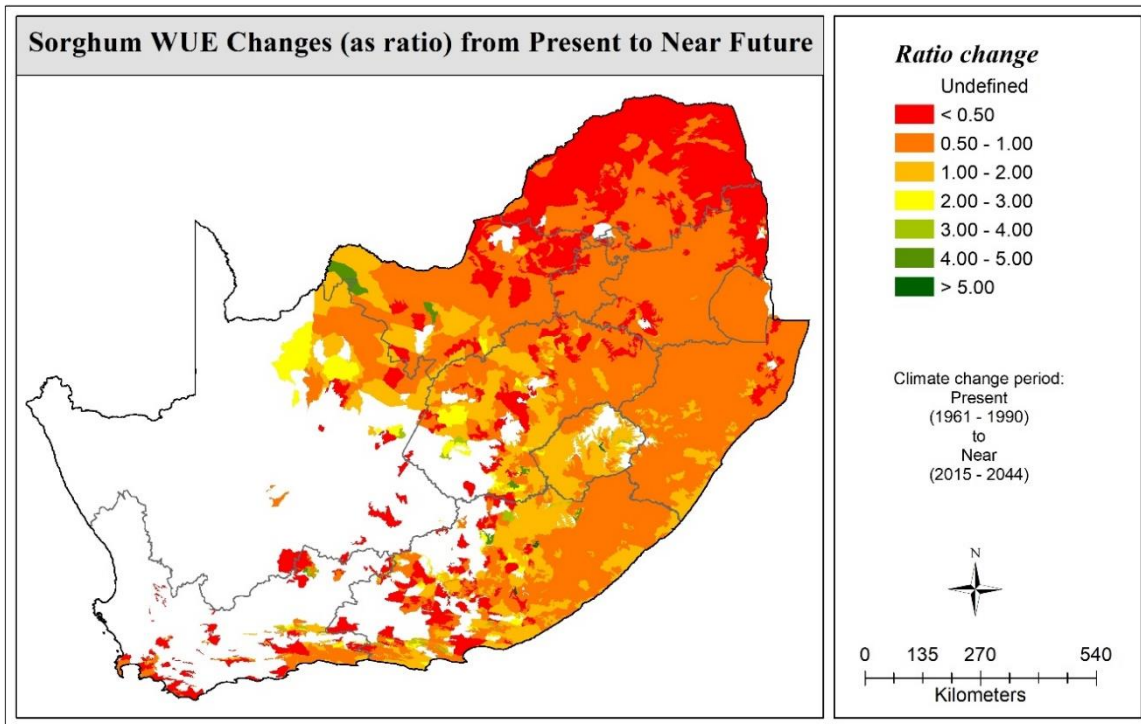
10 APPENDIX D2: MAPS OF CHANGE IN WUE EXPRESSED AS A RATIO



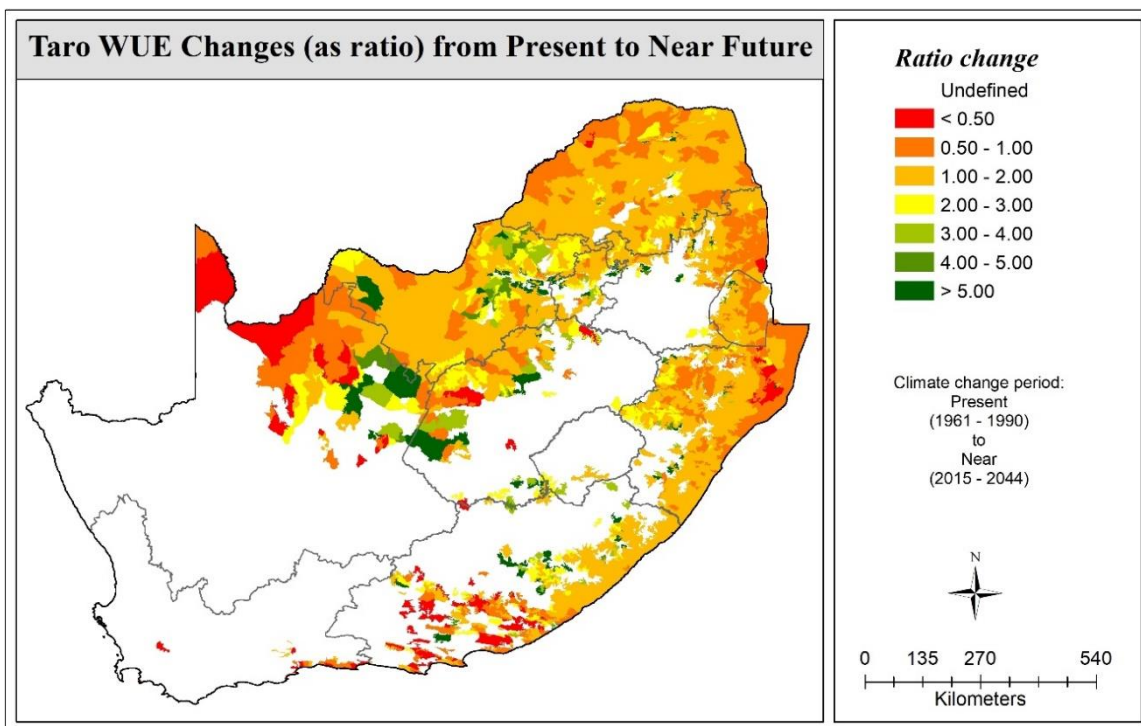
(a)



(b)

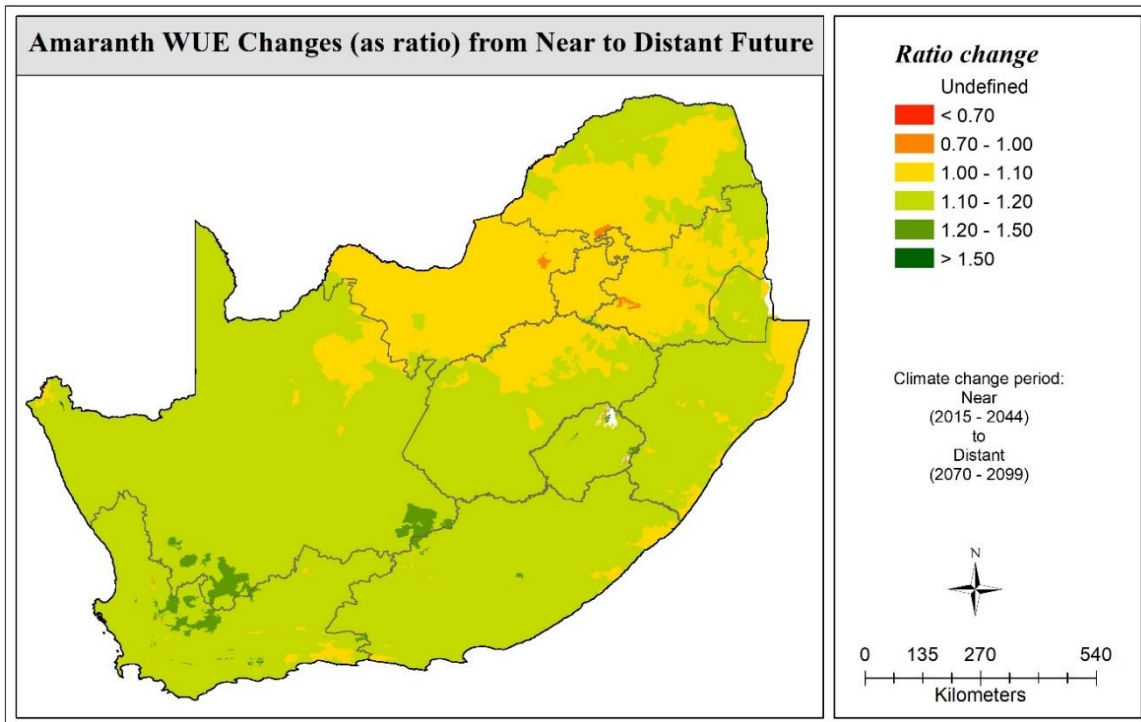


(c)

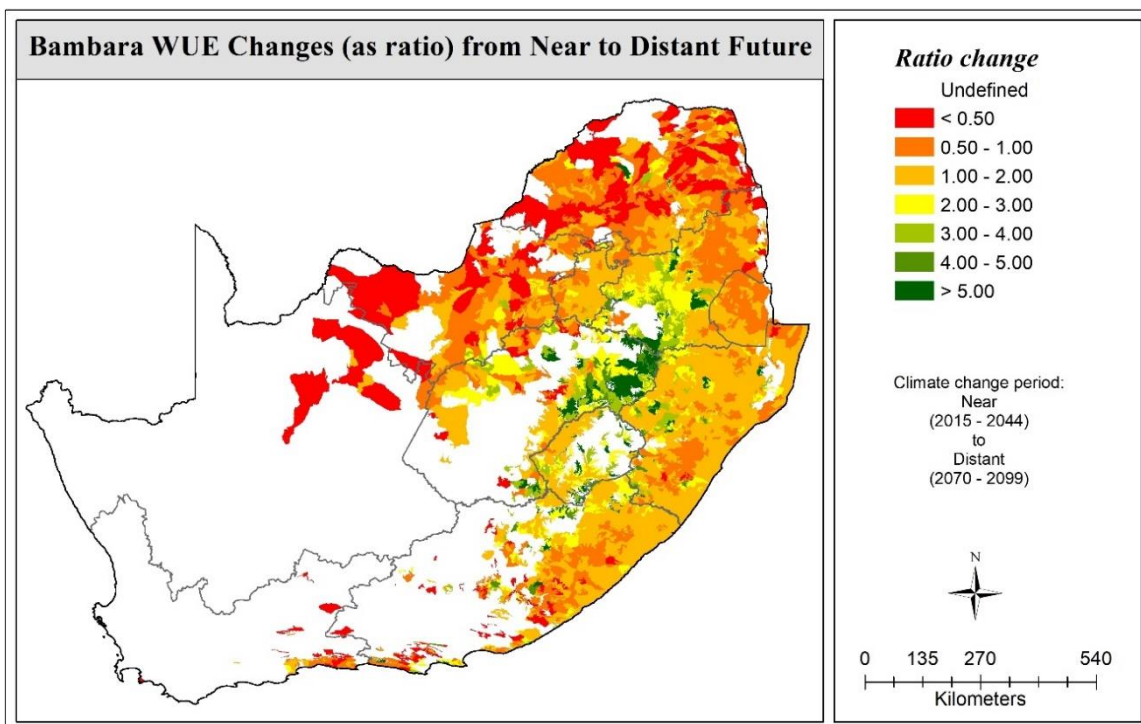


(d)

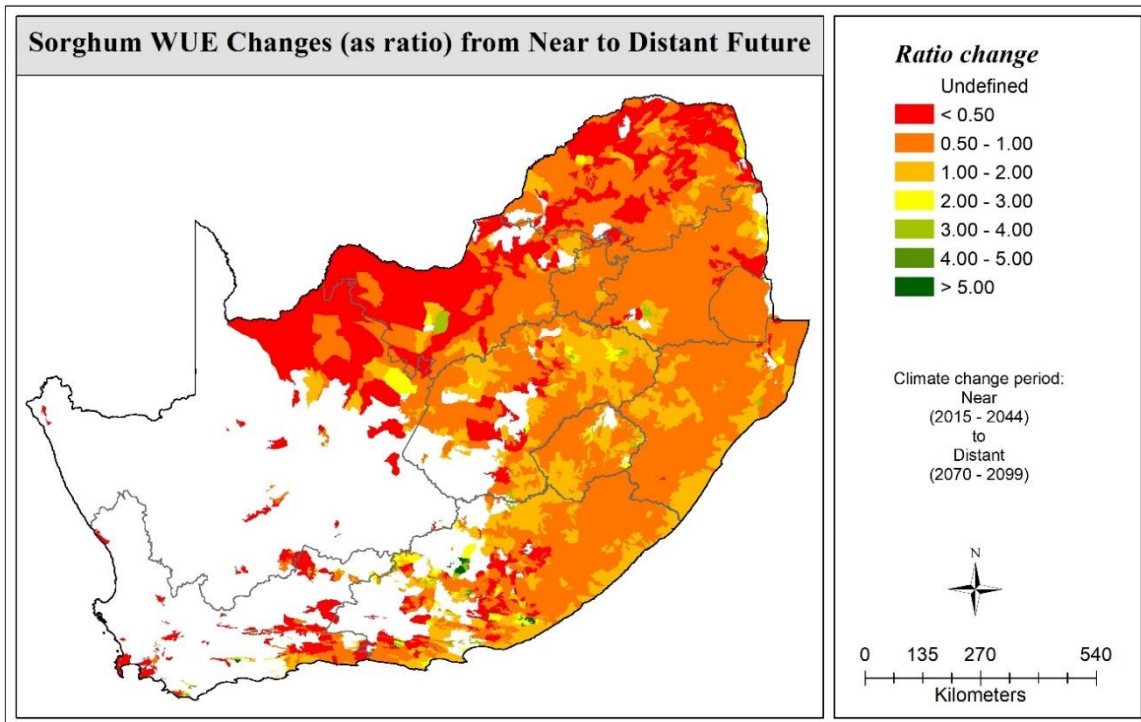
Figure 10.1 Change in mean water use efficiency (WUE; as ratio) from present to near future for (a) amaranth, (b) bambara groundnut, (c) sorghum, and (d) taro



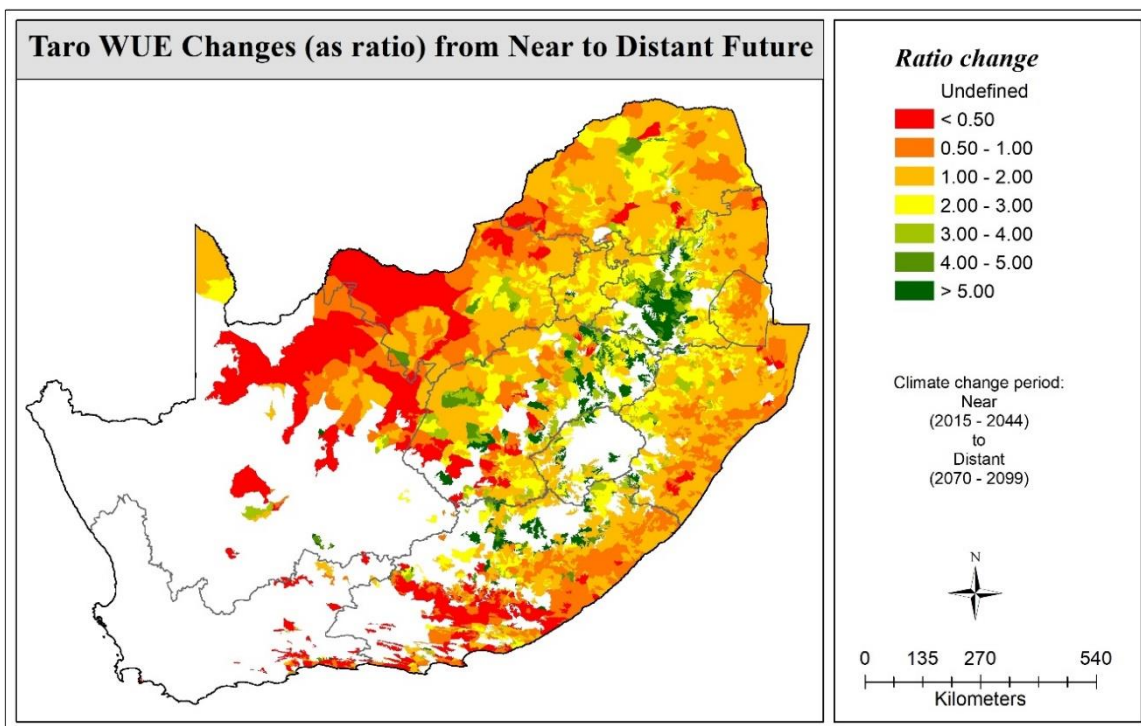
(a)



(b)

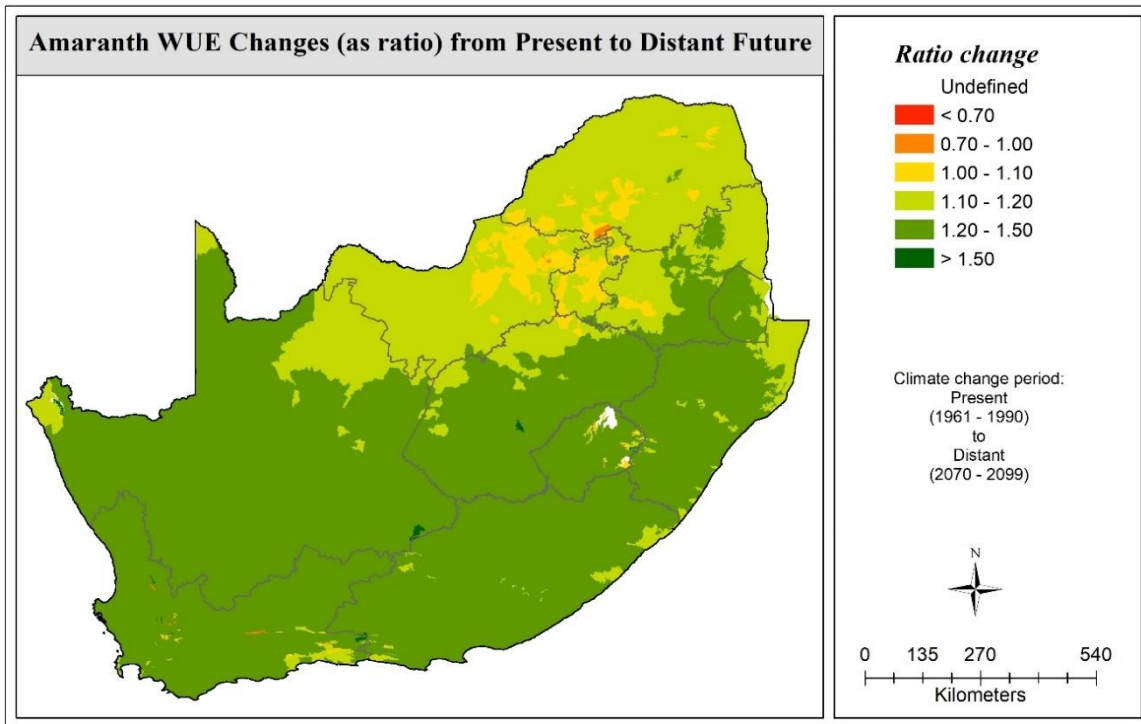


(c)

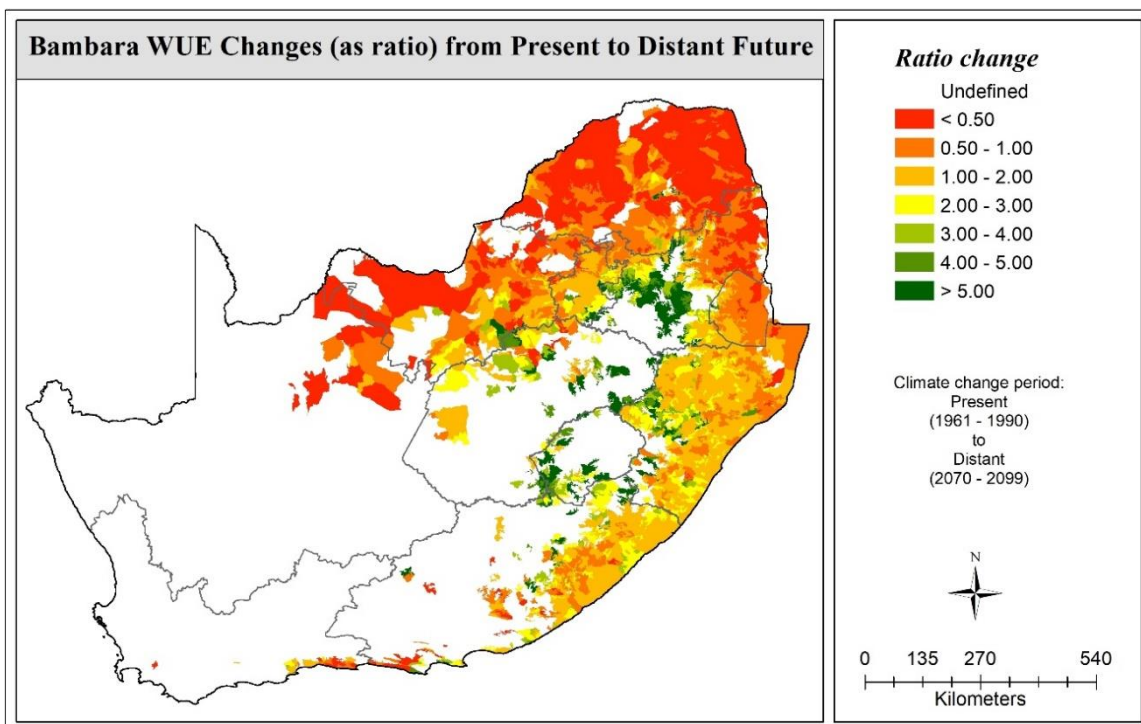


(d)

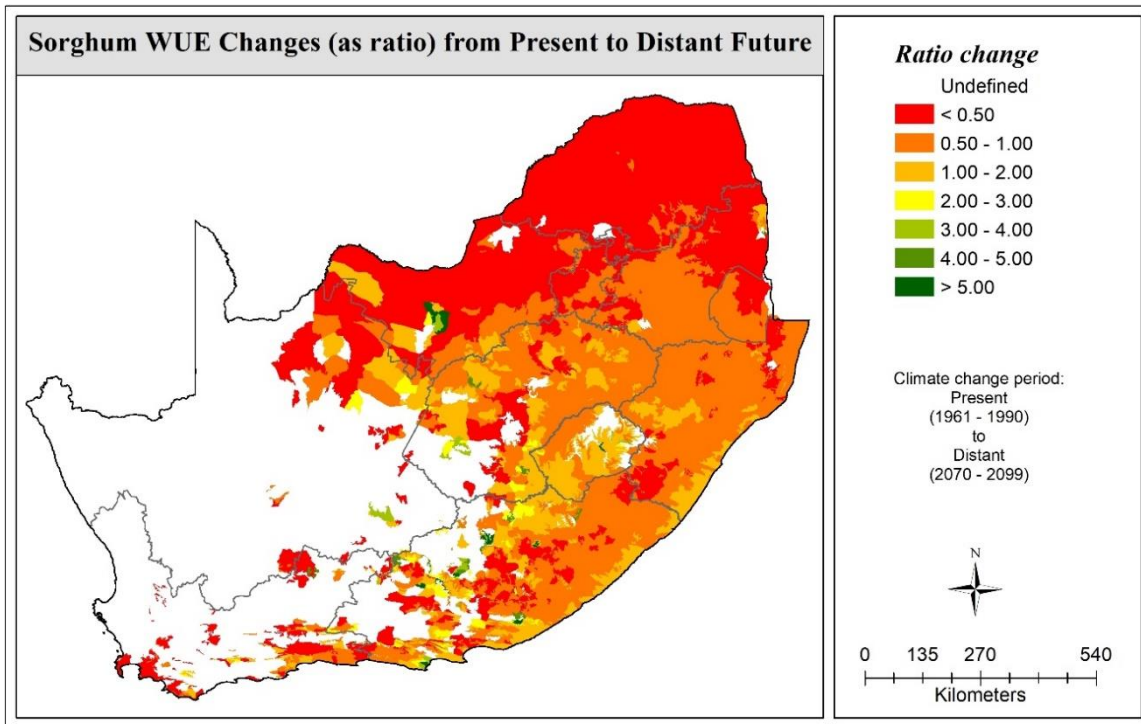
Figure 10.2 Change in mean water use efficiency (WUE; as ratio) from near to distant future for (a) amaranth, (b) bambara groundnut, (c) sorghum, and (d) taro



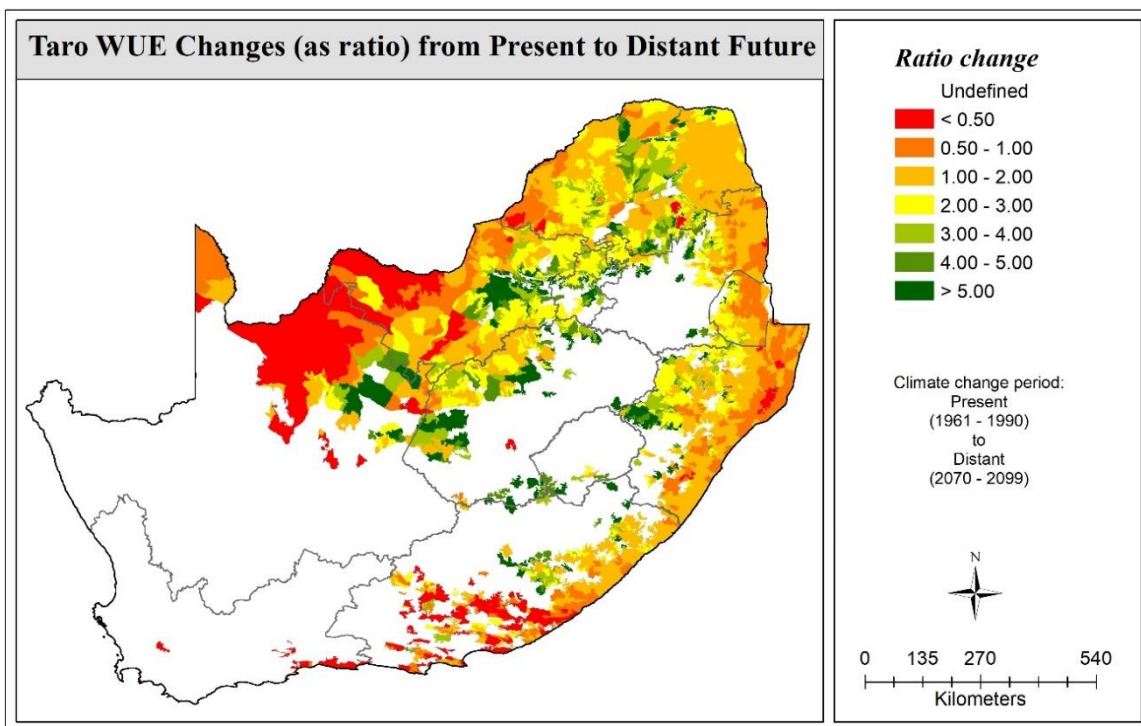
(a)



(b)



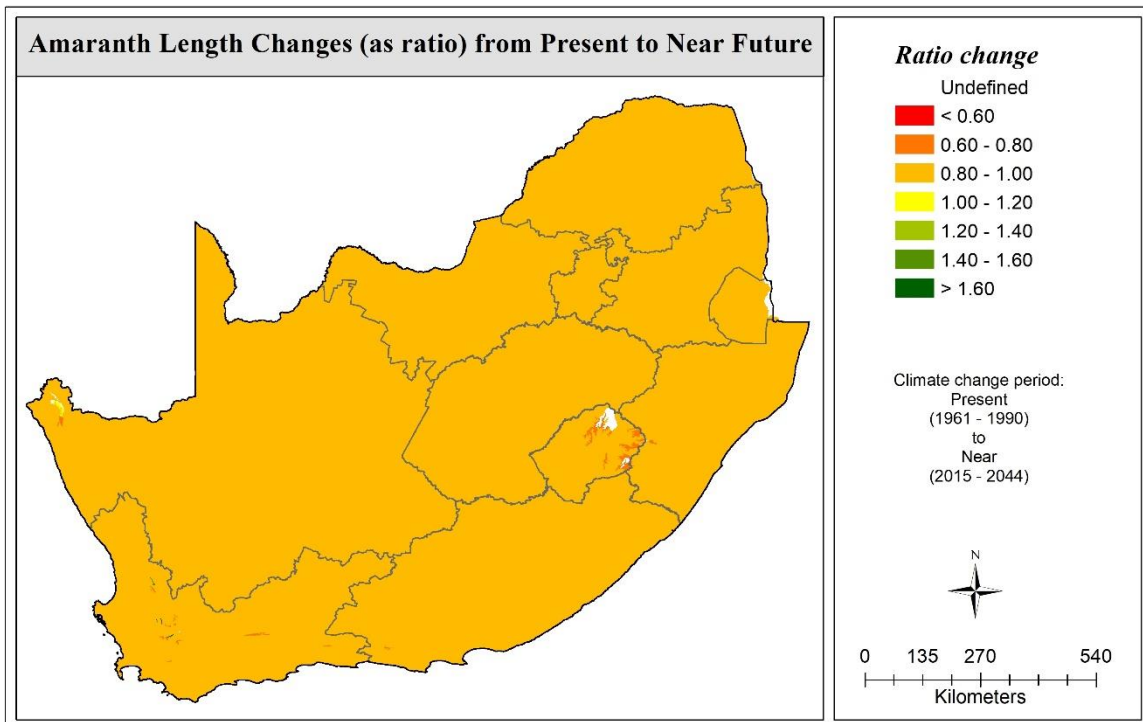
(c)



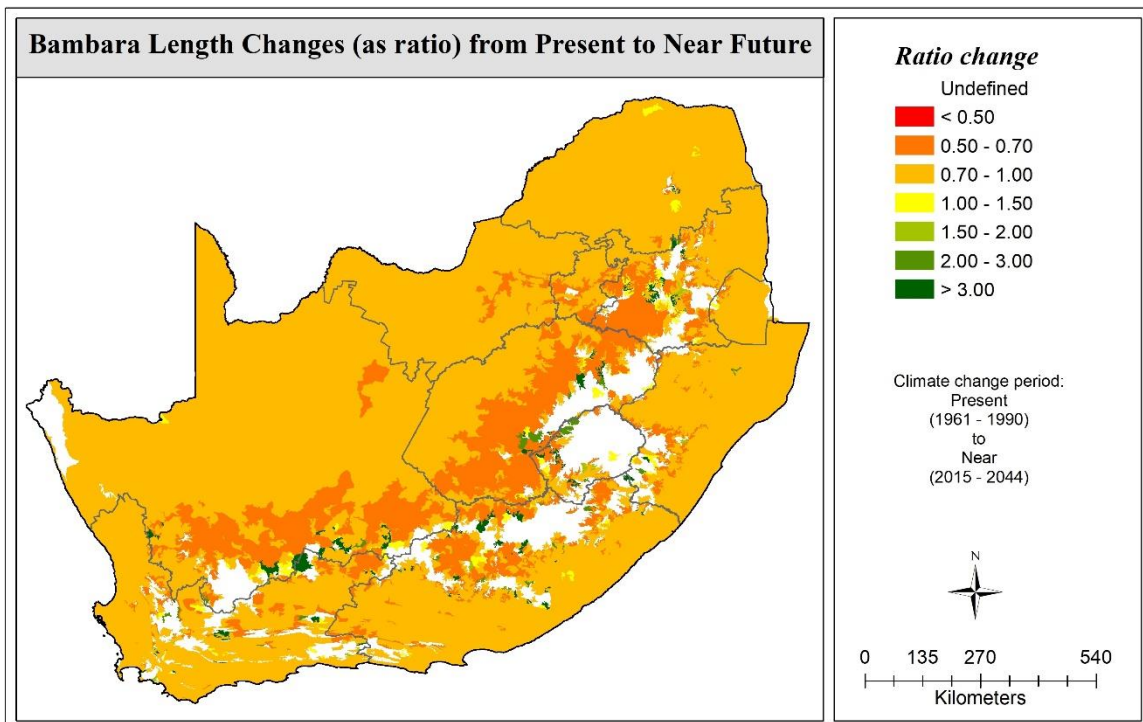
(d)

Figure 10.3 Change in mean water use efficiency (WUE; as ratio) from present to distant future for (a) amaranth, (b) bambara groundnut, (c) sorghum, and (d) taro

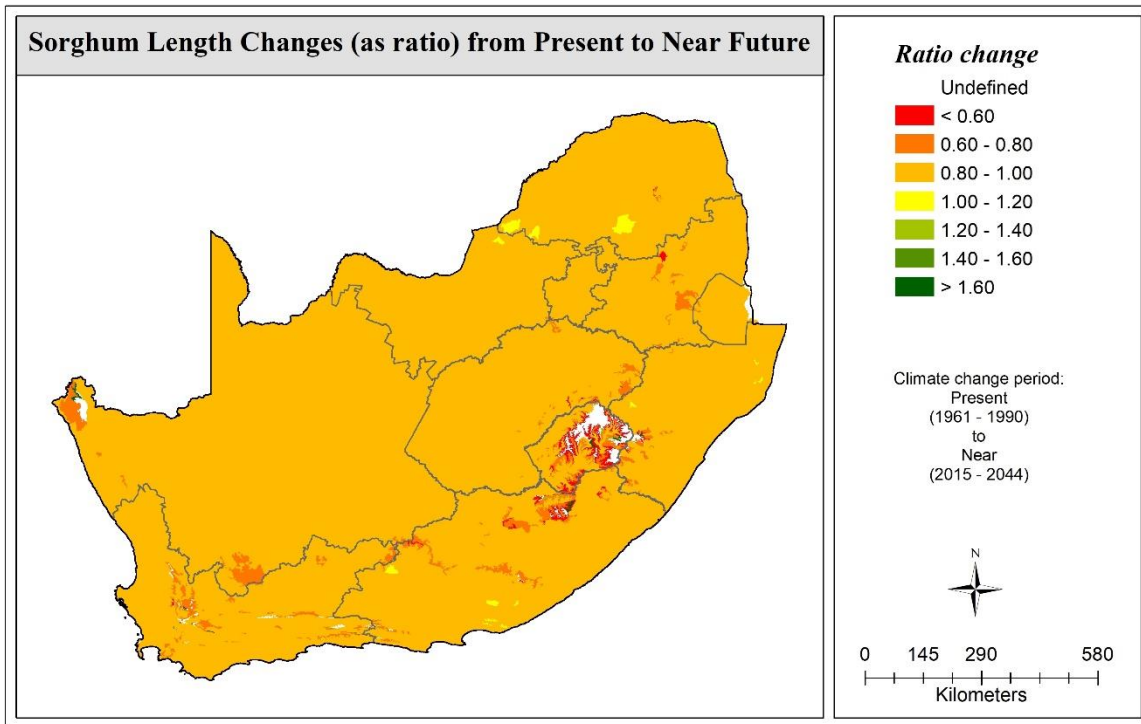
11 APPENDIX D3: MAPS OF CHANGE IN SEASON LENGTH EXPRESSED AS A RATIO



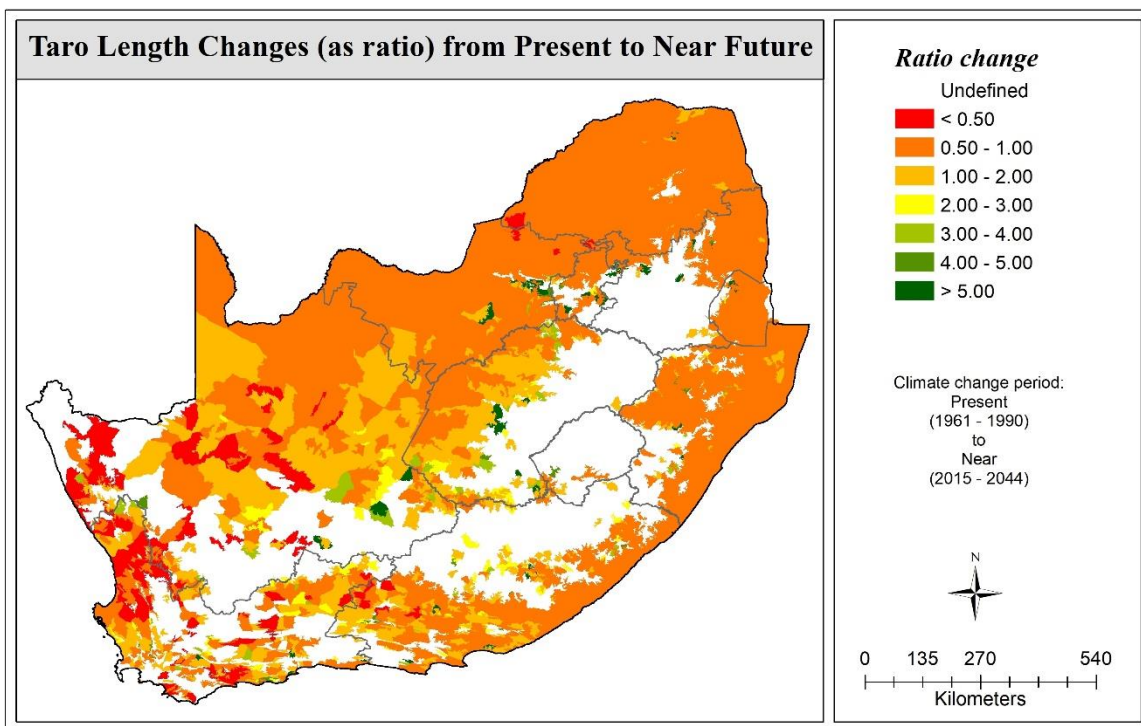
(a)



(b)

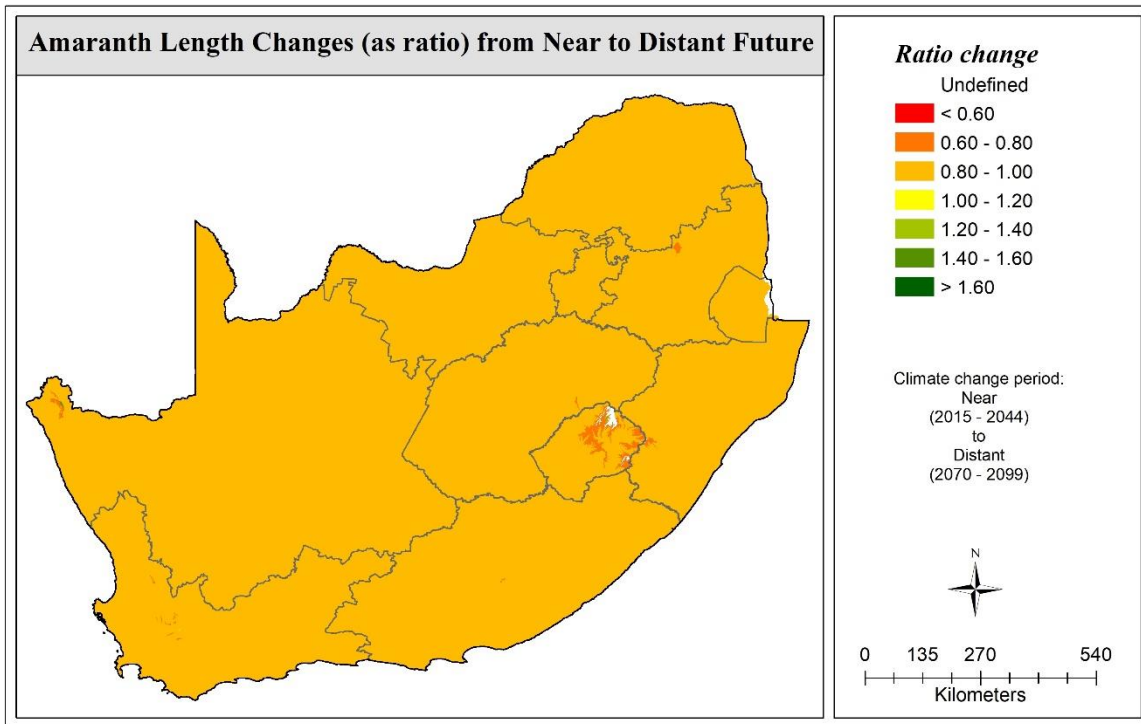


(c)

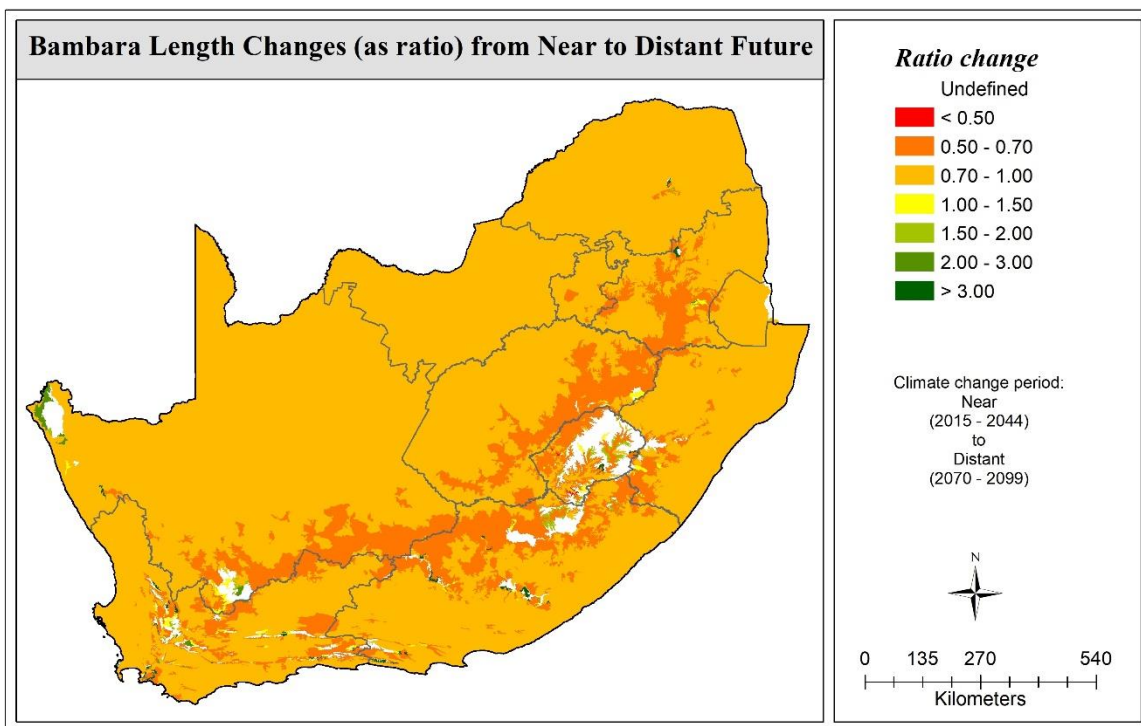


(d)

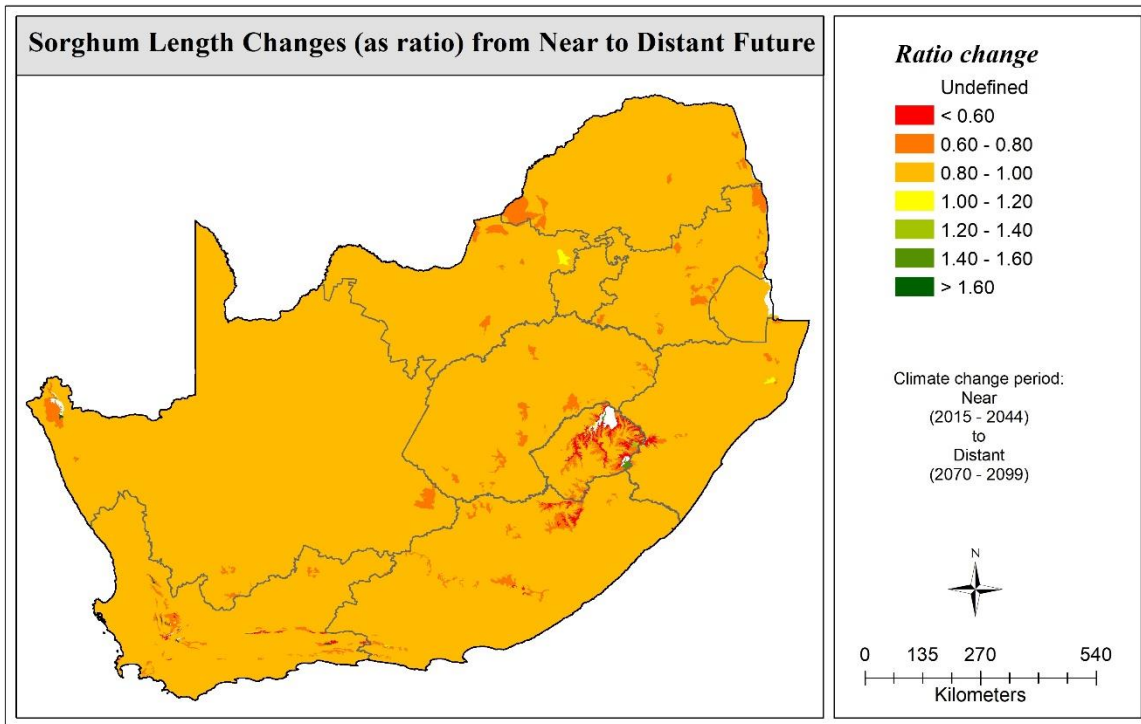
Figure 11.1 Change in mean season length (as ratio) from present to near future for (a) amaranth, (b) bambara groundnut, (c) sorghum, and (d) taro



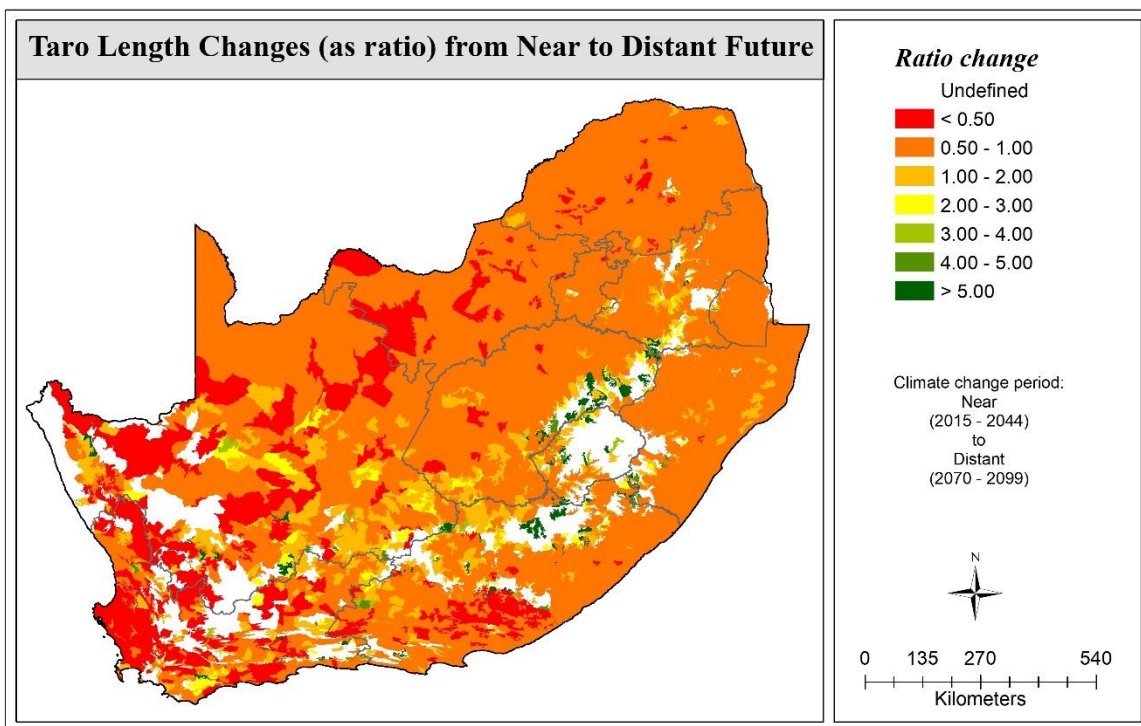
(a)



(b)

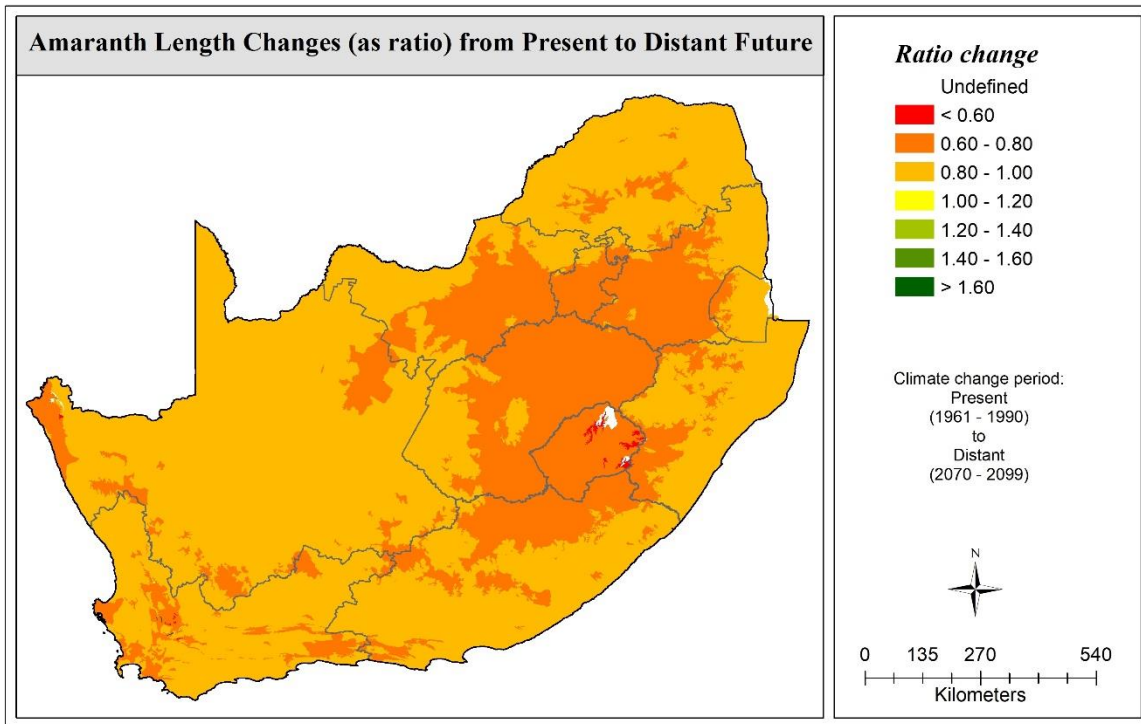


(c)

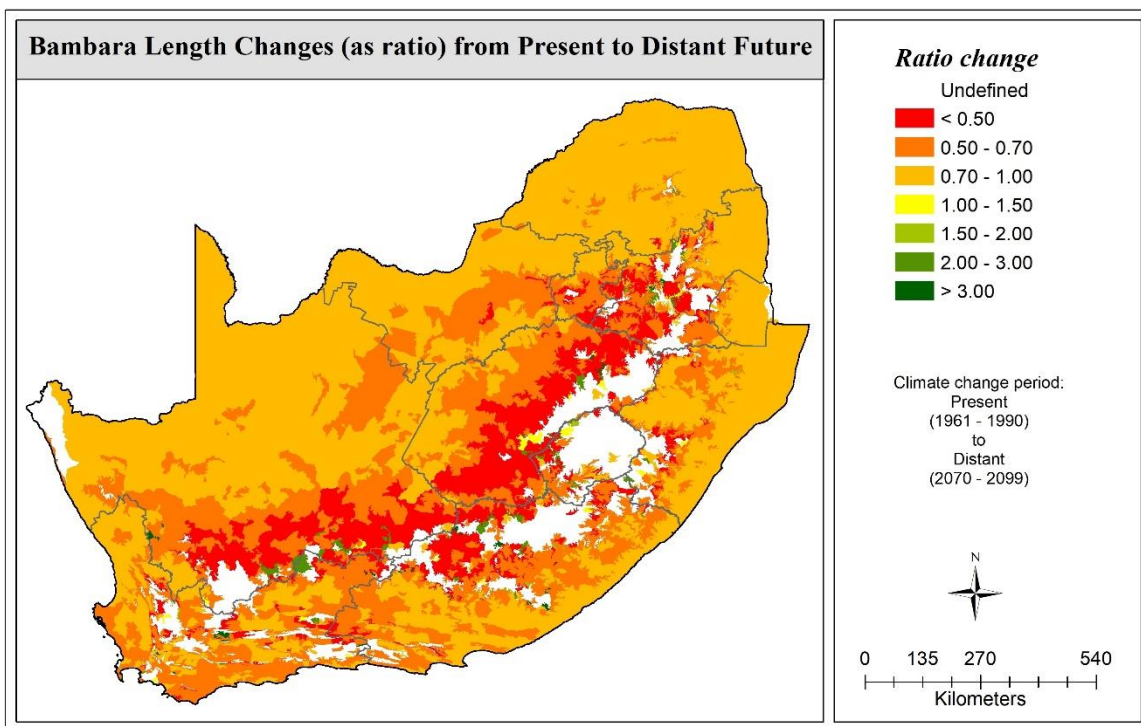


(d)

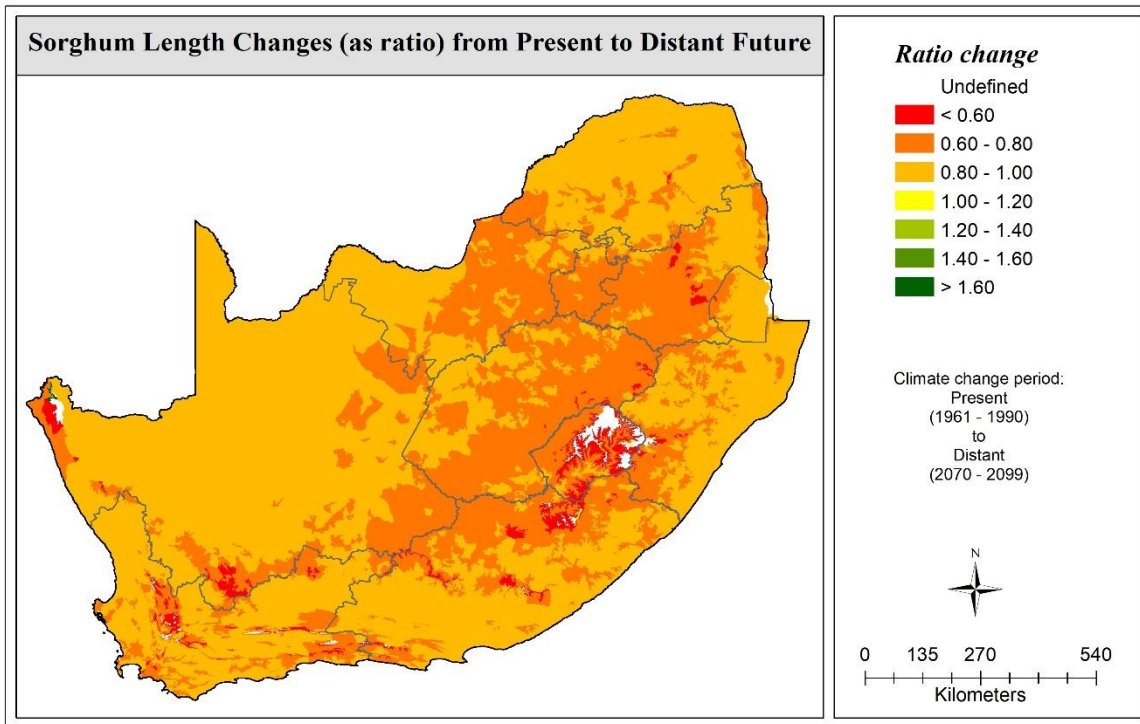
Figure 11.2 Change in mean season length (as ratio) from near to distant future for (a) amaranth, (b) bambara groundnut, (c) sorghum, and (d) taro



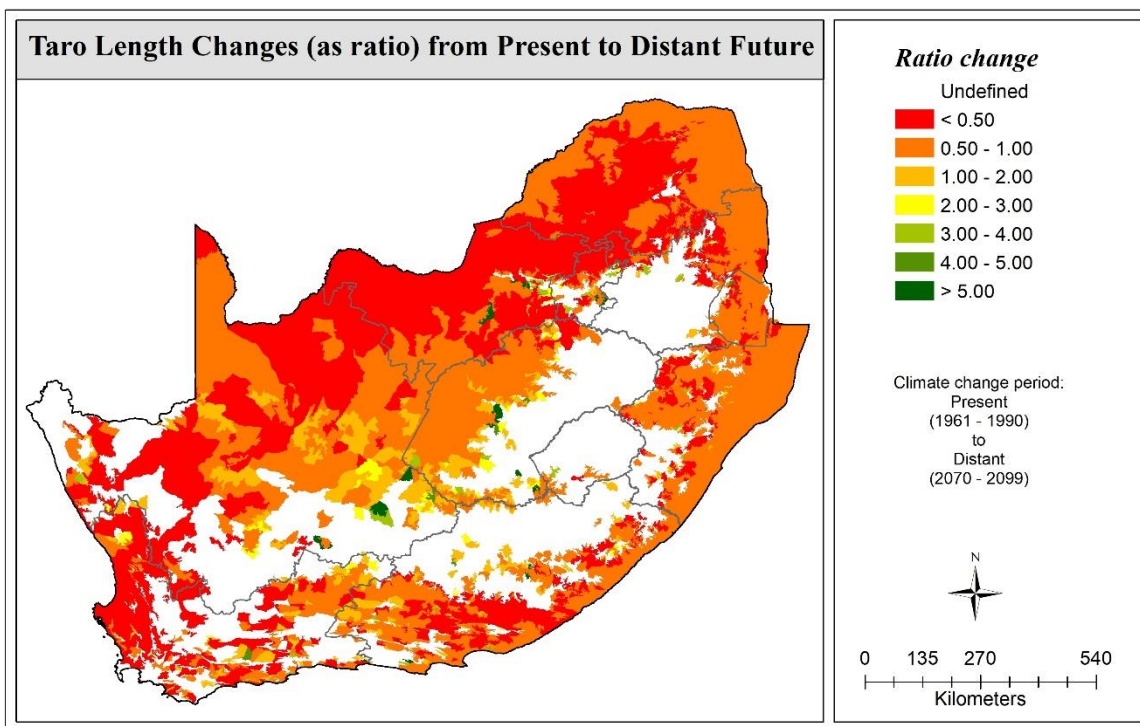
(a)



(b)



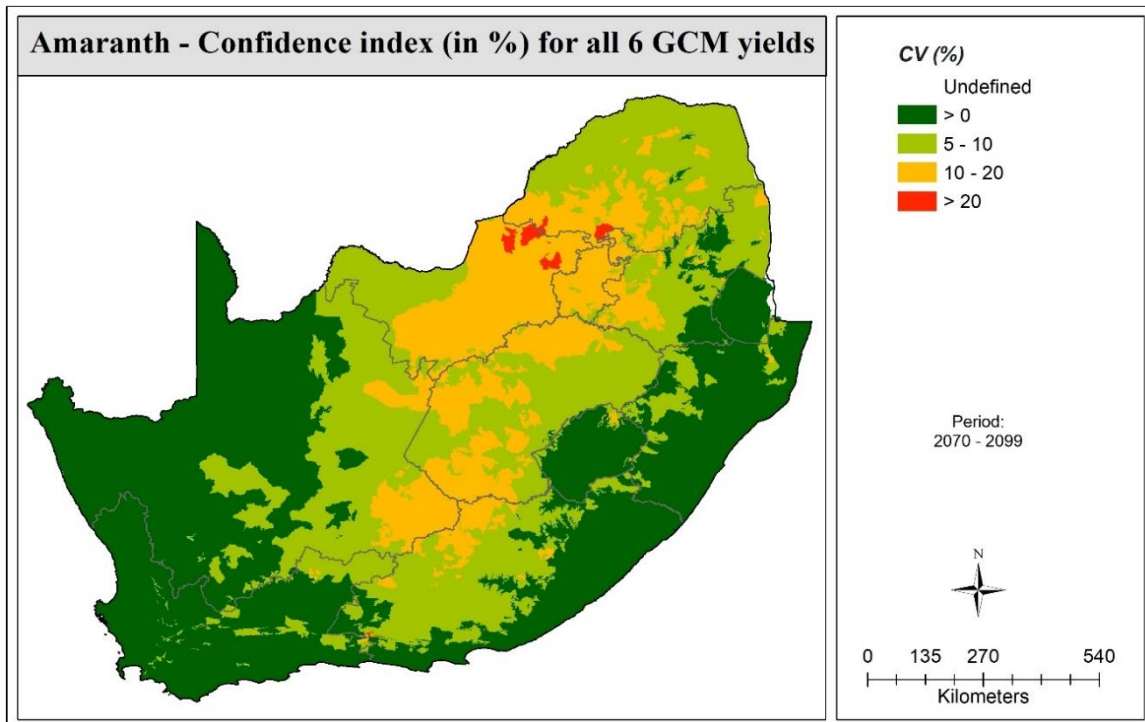
(c)



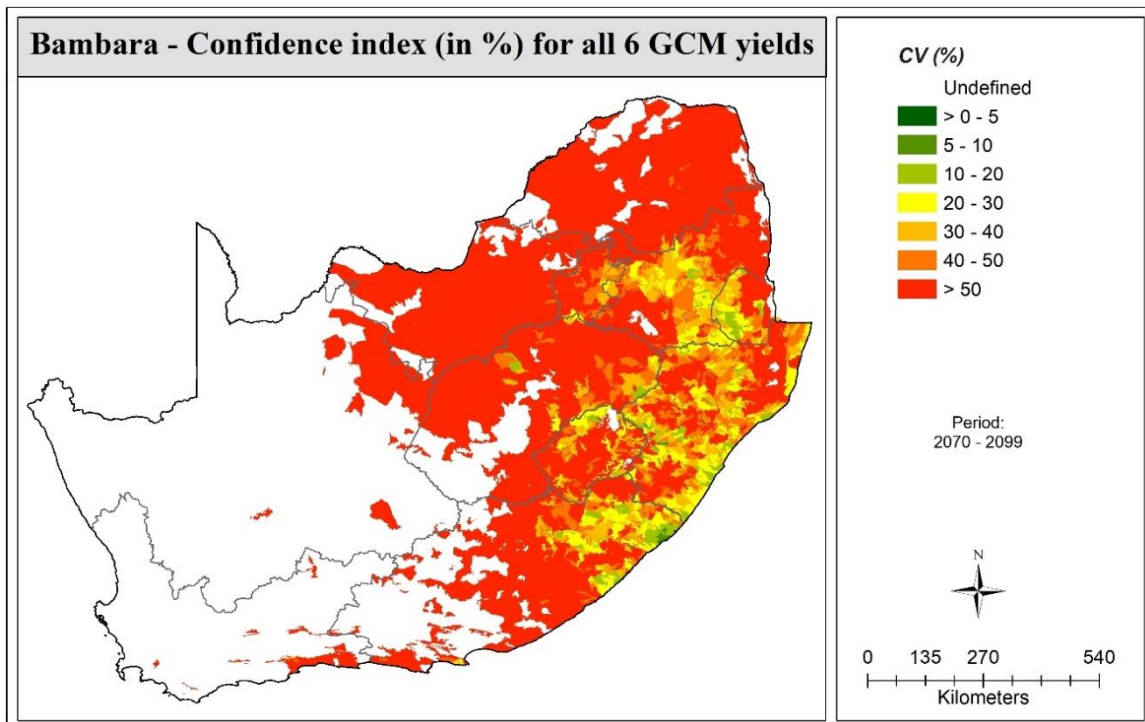
(d)

Figure 11.3 Change in mean season length (as ratio) from present to distant future for (a) amaranth, (b) bambara groundnut, (c) sorghum, and (d) taro

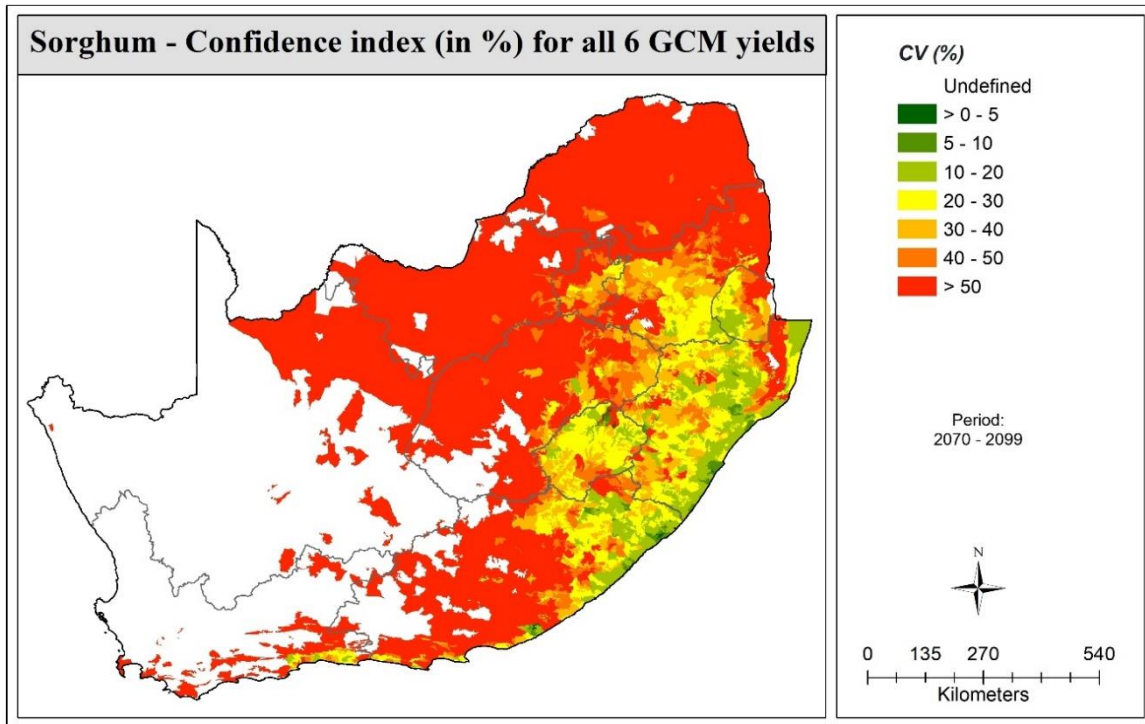
12 APPENDIX E1: VARIATION IN DISTANT FUTURE YIELD BETWEEN THE GCMS



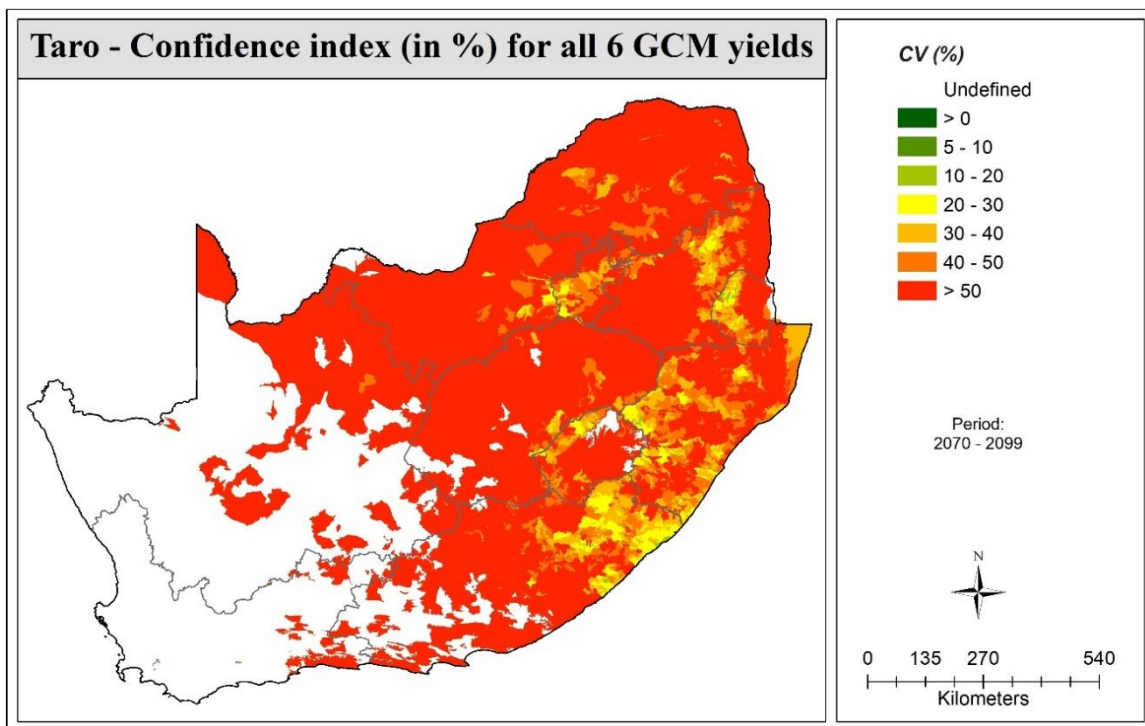
(a)



(b)



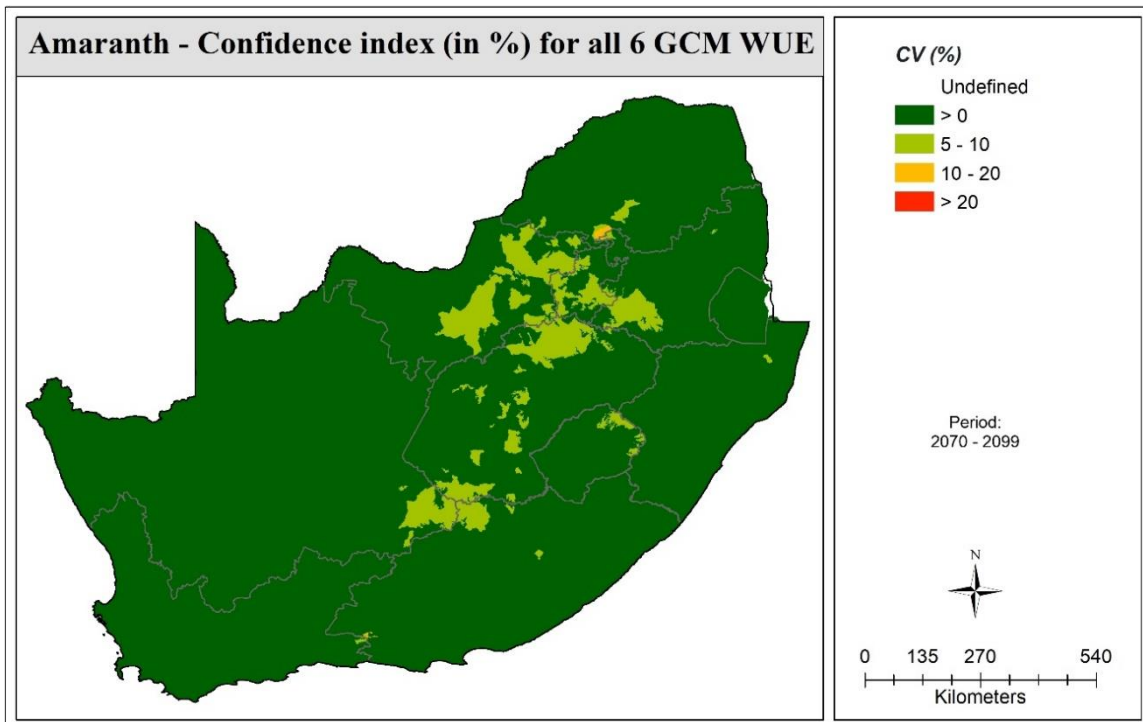
(c)



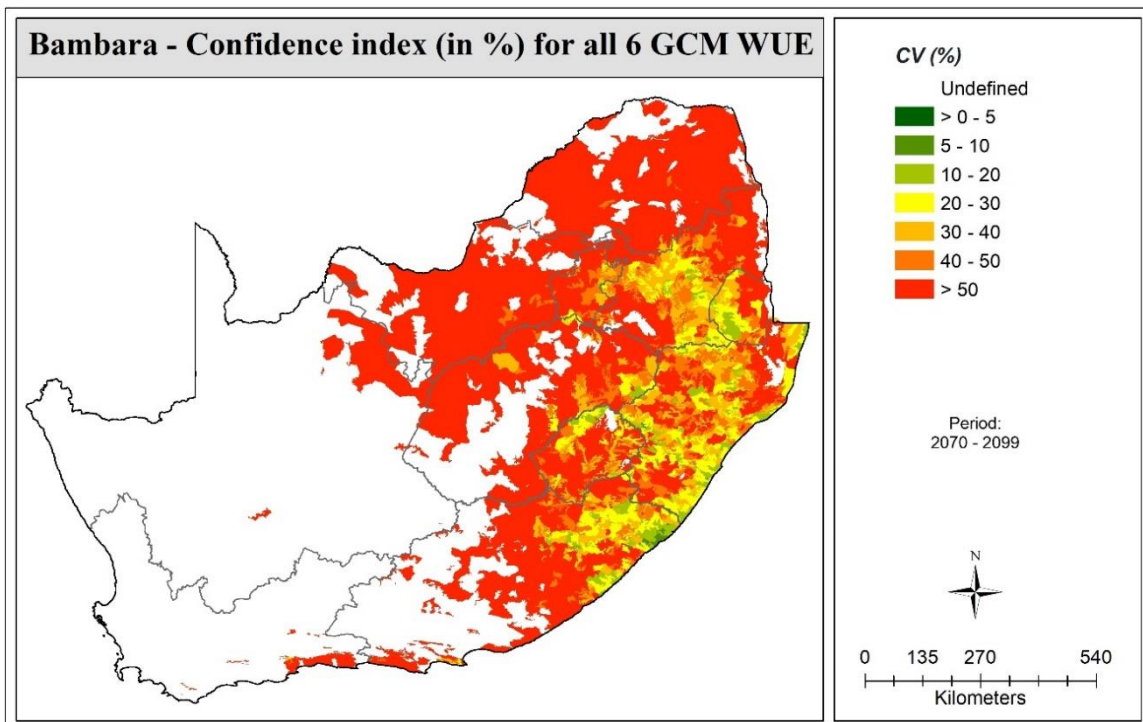
(d)

Figure 12.1 Coefficient of variation (CV in %) in distant future yield obtained from the six GCMs for (a) amaranth, (b) bambara groundnut, (c) sorghum, and (d) taro

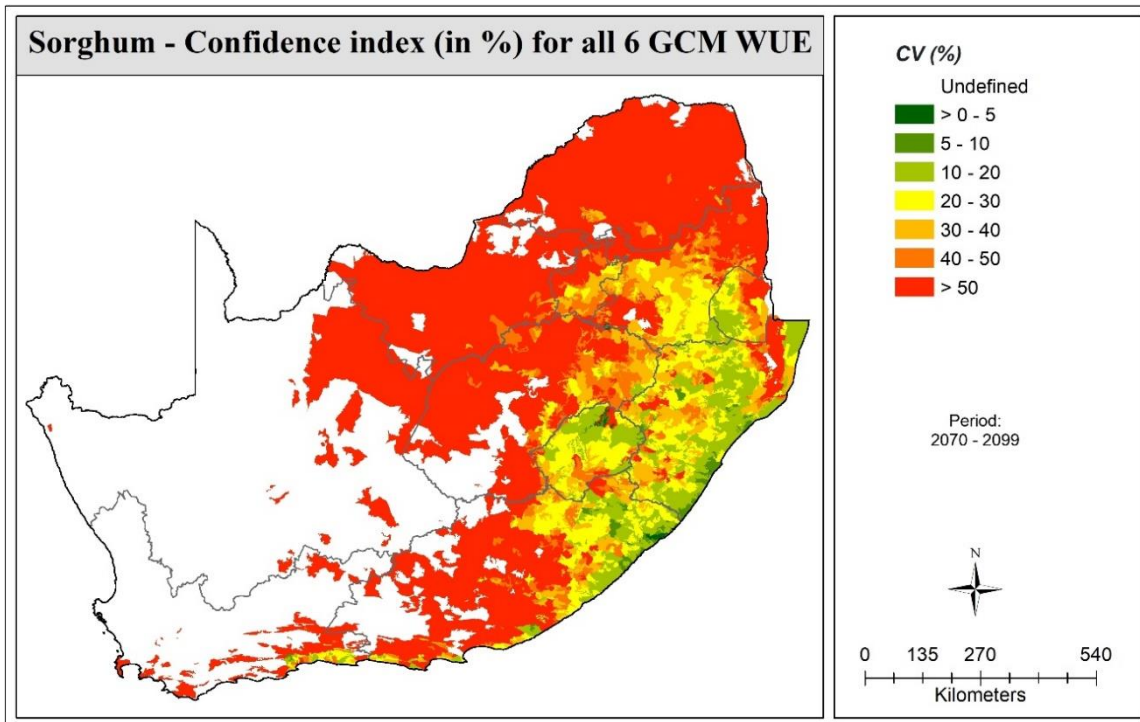
13 APPENDIX E2: VARIATION IN DISTANT FUTURE WUE BETWEEN THE GCMS



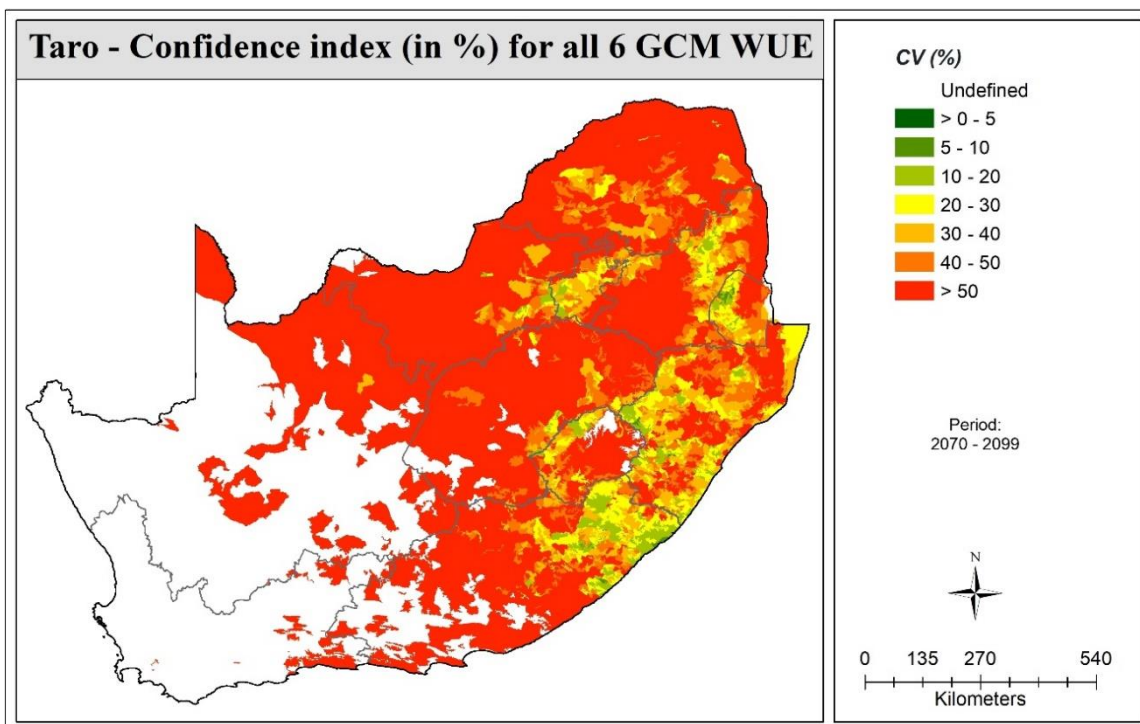
(a)



(b)



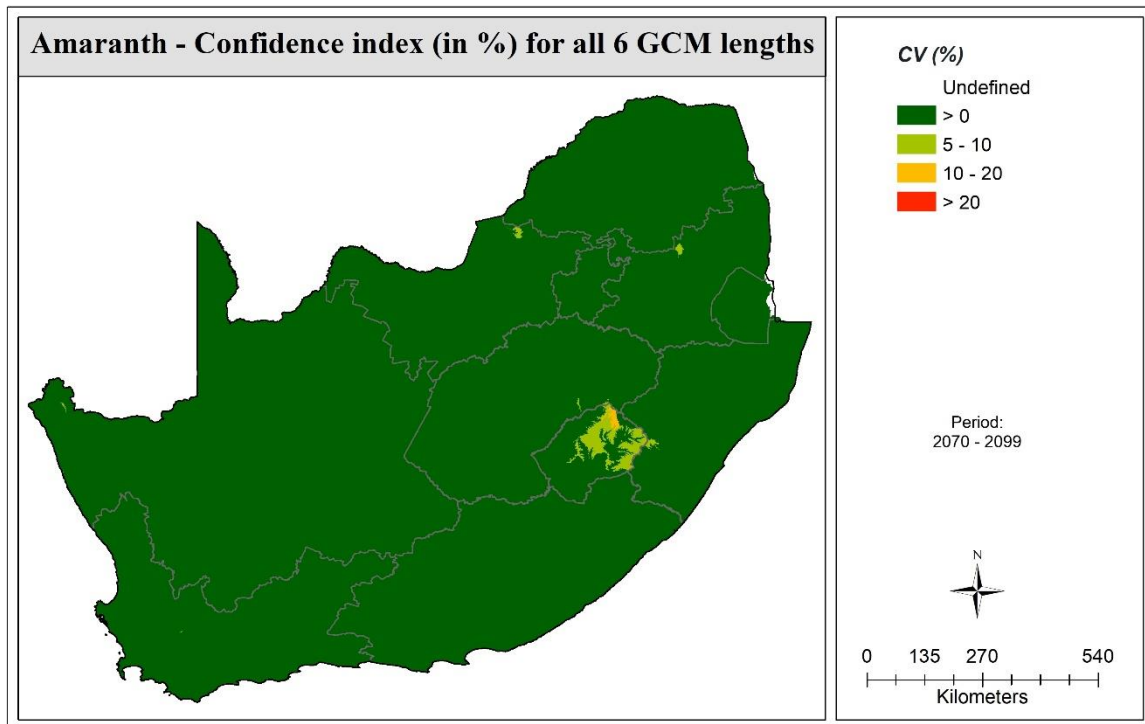
(c)



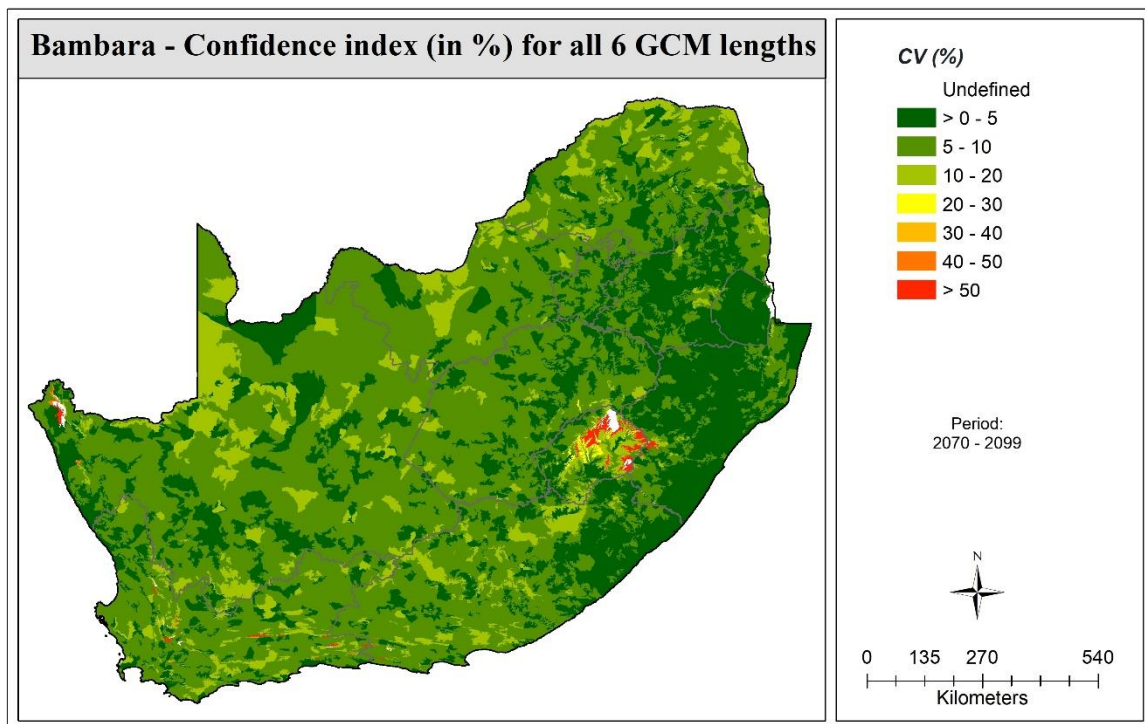
(d)

Figure 13.1 Coefficient of variation (CV in %) in distant future water use efficiency (WUE) obtained from the six GCMs for (a) amaranth, (b) bambara groundnut, (c) sorghum, and (d) taro

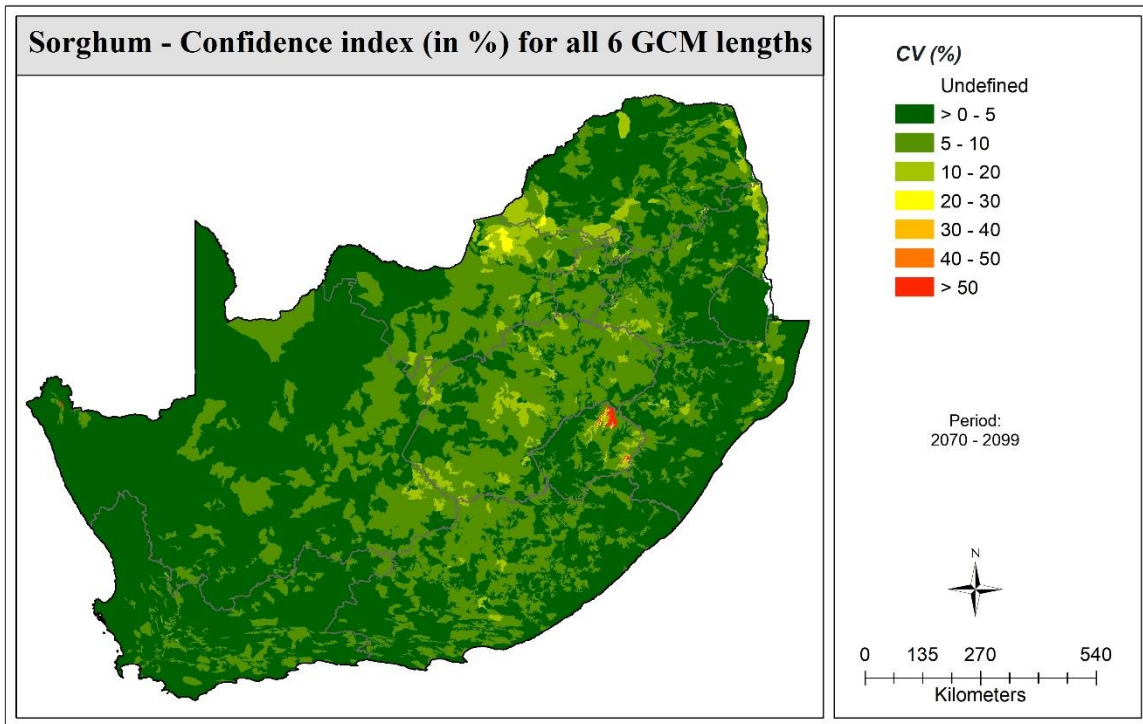
14 APPENDIX E3: VARIATION IN DISTANT FUTURE SEASON LENGTH BETWEEN THE GCMS



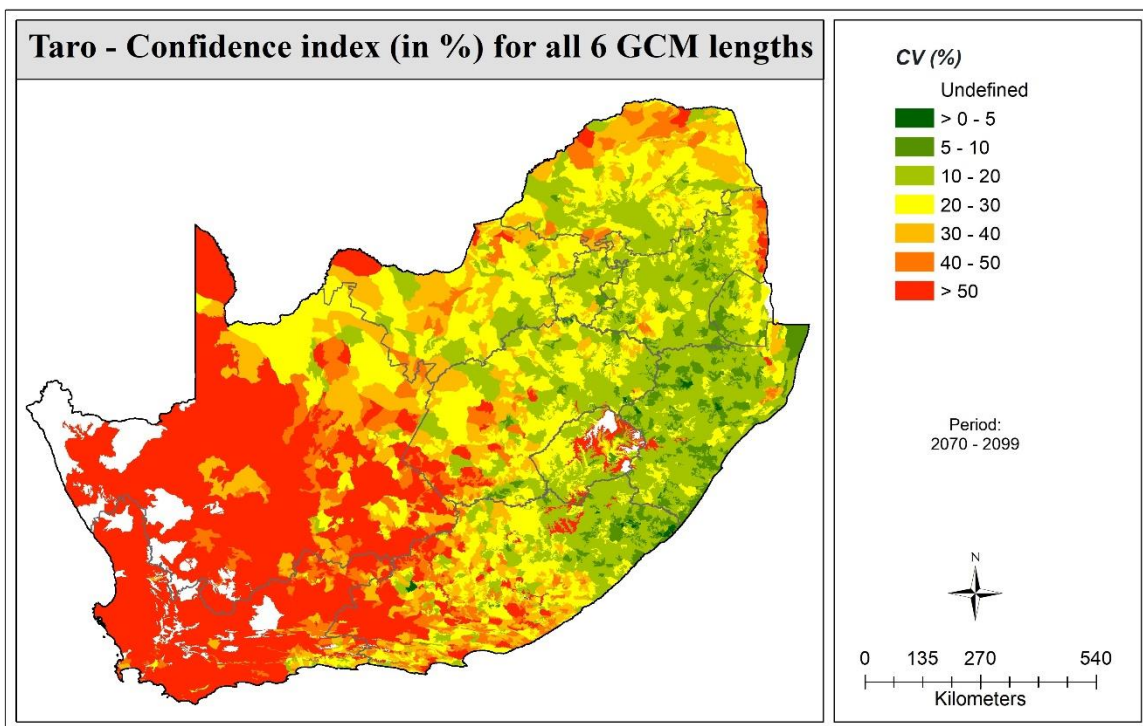
(a)



(b)



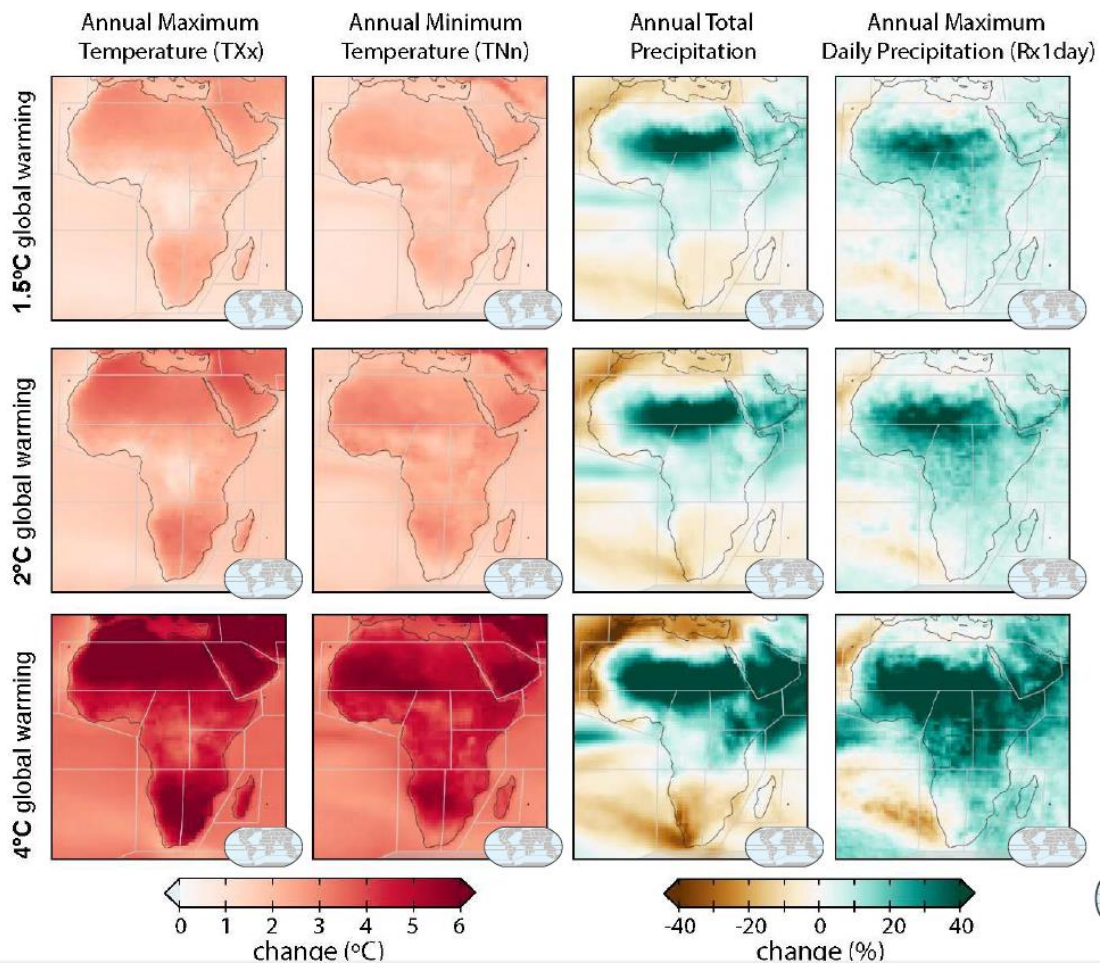
(c)



(d)

Figure 14.1 Coefficient of variation (CV in %) in distant future season length obtained from the six GCMs for (a) amaranth, (b) bambara groundnut, (c) sorghum, and (d) taro

15 APPENDIX F: CMIP6-BASED CLIMATE PROJECTIONS



Source:

[https://www.ipcc.ch/report/ar6/wg1/downloads/factsheets/IPCC AR6 WGI Regional Fact Sheet Africa.pdf](https://www.ipcc.ch/report/ar6/wg1/downloads/factsheets/IPCC_AR6_WGI_Regional_Fact_Sheet_Africa.pdf)

Figure 15.1 Projected changes in annual maximum (TXx) and minimum (TNn) temperatures, total annual precipitation and maximum daily precipitation (Rx1day) at 1.5, 2 and 4°C of global warming compared to 1851-1900, based on CMIP6 multi-model ensemble means